Modelling soil evolution to assess soil system behaviour under global change

Emmanuel Opolot

Promoter: Prof. Dr. Peter Finke

UNIVERSITEIT GENT

Thesis submitted in fulfilment of the requirements for the degree of Doctor (PhD) of Science: Geology

May 2016

Faculteit Wetenschappen

Cover picture: Soil evolution from the SoilGen model perspective. Soil development starts from an unconsolidated material (bottom left circle) and through the action of physical, geochemical and biological processes (listed in the two bottom circles) over time, and driven by external factors (such as climate and vegetation) a soil profile (intersection) is formed.

With the financial and logistical support of the following institutions:

Belgian Science Policy Office

Interuniversity Attraction Poles

Ghent University

Copyright: Emmanuel Opolot 2016
Department of Soil Management
Coupure Links 653, 9000 Gent
Belgium

Citation: Opolot E., 2016: Modelling soil evolution to assess soil system behaviour under global change. PhD thesis, Ghent University, Gent, Belgium.

Faculteit Wetenshappen

Modelling soil evolution to assess soil system behaviour under global change

Modellering van bodemevolutie ter inschatting van bodemsysteemgedrag in een veranderende wereld

Emmanuel Opolot

Promoter

Prof. Dr. Peter Finke (Department of Soil Management, Ghent University, Belgium)

Examination Committee

Prof. Dr. Stephen Louwye (Department of Geology, Ghent University, Belgium; **Chair**)

Prof. Dr. Ir. Steven Sleutel (Department of Soil Management, Ghent University, Belgium; **Secretary**)

Prof. Dr. Daniela Sauer (Department of Physical Geography, University of Göttingen, Germany)

Prof. Dr. Veerle Vanacker (Department of Geography, University of Louvain, Belgium)

Prof. Dr. Geert Baert (Department of Applied Biosciences, Ghent University, Belgium)

Em. Prof. Dr. Eric Van Ranst (Department of Geology, Ghent University, Belgium)

Acknowledgments

I would like to utilize the next few pages to salute all the people who contributed in one way or the other to this PhD journey. First and foremost I would like to send my sincere thanks to my promoter, Prof. Dr. Peter Finke. You did not only entrust me with the opportunity to do my PhD research under your supervision, but also you always made it a priority to attend to me whenever I needed your input. I always counted myself lucky to have you as a promoter becuase you were not only knowledgeable and inspiring as a supervisor, but you were also a parent to me and my family. You and Brit ensured that I and my family were as comfortable as possible. The surprising bouquet of flowers you brought to welcome my wife Suzan and my son Benjamin from Uganda, the time you spent in the hospital when we were welcoming our second son, Ethan; the series of luncheons that you always hosted us to and your presence in the first birth day party of Ethan are just among the many examples I would point out. In a few words, you are simply the best!

This PhD research was funded by the Belgian Science Policy Office (BELSPO) under the research project "Soils under Global Change (SOGLO)". I am grateful to BELSPO for the financial support and to the entire SOGLO team for the interactive and constructive discussions that we always had. I particularly enjoyed the field work we had in Porto Alegre, Brazil in the summer of 2014. Although we narrowly missed the world cup, working and eating together coupled with "*chimarrao*" drinking always made me feel at home. At this point, I would also like to extend my sincere thanks Prof. Jean Minella (Federal University of Santa Maria, RS, Brazil) for the great assistance that you rendered to me right from my visa application to the entire stay in Porto Alegre. I also thank the farmers of Arvorezinha and Ilopolis, who would not get tired of hosting us for "*chimarrao*" and barbecue parties.

I would like to extend my sincere gratitude to Prof. Dr. Stephen Louwye for chairing the examination committee of this thesis. I thank all the jury members; Em. Prof. Dr. Eric Van Ranst, Prof. Dr. Daniela Sauer, Prof. Dr. Veerle Vanacker, Prof. Dr. Geert Baert and Prof. Dr. Ir. Steven Sleutel for their time to read, critic and evaluate this thesis. I must say your valuable comments greatly improved the quality of this manuscript.

Chapters 3 and 4 of this thesis benefited from the discussion that I had with Yves Godderis (CNRS-Université de Toulouse, France) and Sophie Cornu (INRA, Aix, France) at the Université de Toulouse, France. I am therefore indebted to these individuals for their time and ideas.

I spent most of my PhD time in the Laboratory of Soil Science and I would like to say special thanks to all my colleagues in this lab: Dr. Basile Mujinya, Dr. Ann Zwertvaegher and Dr Stephen Mureithi, I only started when you were finalizing your work but most importantly, you advised me to see the end from the beginning. Surely the end is now here and I would like to say thanks a bunch for your advice and encouragement. To my fellow colleagues: Drs. Mathijs Dumon, Dr. Hans Erens, Dr. Ingrid Smet, Drs. Willemijn Quaijtaal, Drs. Thanh Thuy Doan and Eline Depelsmaeker, I would like to say thanks for the joyous interactions and the coffee breaks we always had. I was also privileged to interact with Prof. Em. Eric Van Ranst, Prof. Dr. Geert Baert, Dr. Liming Ye, Dr. Mary Ann del Marmol and Prof. Dr. ir. Ann Verdoodt, and for this I say great thanks. Special thanks also go to Prof. Em. Eric Van Ranst for the New Year receptions that you always organized. Many times I received technical and administrative assistance from Hilde Luyckx (R.I.P), Mieke Tanghe and Kurt Blom and I am truly grateful for that.

I moved to the Department of Soil Management in the final year of my PhD and I would like to say thank you to all the colleagues in this department. I enjoyed nice, fruitful and interactive lunch moments with the following colleagues: Saba Keyvanshokouhi, Mojtaba Zeraatpishe, Dr. Mesfin Tsegaye Gebremikael, Jeroen De Waele, Jones Yengwe, Meisam Rezaei, Bashar Al-Barri, Darren Bouwer, Nguyen Min Phoung, Jan De Pue and Mojtaba Pakparvar, I am truly happy for that.

Colleagues from Makerere University; Dr. Alice Amoding, Dr. Giregon Olupot, Dr. Peter Ebanyat ; from National Agricultural Research Laboratories , Kawanda; Dr. Everline Komutunga and Dr. Wasige John and my uncle Charles Okei, you all stood by me and kept encouraging me throughout, great thanks.

Outside the academic arena, I am indebted to so many groups and friends! Ugandans@gent, Ugandans@obsg, my home away from home: OBSG and OBSG staff; I must say I always enjoyed nice and refreshing moments and big ups to you all. I and my family have enjoyed the company of and assistance from many families for which we are truly grateful. On behalf of my family, I would like to

say great thanks to the families of Peter Finke / Brit, Genesis Chevure / Jestinah, Simon De Meulemeester / Haliima, Nash Julius / Meryl and Peter Olaki Ochom / Betty.

Friends; Deborah Amulen, Ismael Ongole, Simon Byarugaba, Ronald Kabbiri, Jackie Epila, Moses Chemurot, Sophie Komujuni, Walter Odongo, Mrisho Malipula, Deo Kawalya, Jane Alexander, Jude Aleu, Joseph Abongosi, Nathan Emuron, David Omomgot, Luke Obilakol, Lawrence Munjonji, Dr. Alfred Obia, Dr. Joseph Birundu Mogendi, Mulugeta Damie Watabaji, Joanita Kataike, Joshua Wesana and Martin Makyeme, you all remained in touch and followed my journey through, thanks a lot.

I reserved part of this page to express my sincere gratitude to my parents; Romans Susuje Opedun and Loyce Among; for your unfailing love and for the struggles that you endured to see me through to this level, may the almighty God bless you abundantly! To my brothers; Tom Okelloto and Sam Opedun and to my Sisters; Florence Ikiria, Naume Kongai, Esther Amuge and Christine Akanya, I would like to say thanks a bunch for your relentless support especially for the 6 years I have been away from you. Special thanks to Tom for not only taking care of the whole family but also for standing in for me whenever I asked to. In a special way, I acknowledge the great support and inspiration that I received from my uncle Ben Ilukor (R.I.P). You were always proud of me and I am sure you will be satisfied with this achievement wherever you are. Great thanks also go to my parents-in-law; Peter Omongin (R.I.P) and Merab Amongin, my brothers' in-law; Albert Olinga and Emmanuel Omongin and my sisters' in-law; Deborah Kiyai, Monica Aido and Eunice Amongin.

Last but most importantly, my heartfelt gratitude goes to my wife Suzan and my sons Benjamin and Ethan. Your everyday smiles have kept me strong all through. Suzan I cannot thank you enough for your emotional support, for your unconditional love and for taking care of our sons while I was away working on this thesis!

Above all, the glory goes to the Almighty God for the unfailing love and care, *Ituritete ijo Yesu!*

Table of Contents

Summary

Soil is a cornerstone to many ecosystem services such as water purification, food, wood and fibre production, nutrient cycling, climate regulation and physical support to human infrastructures. Unfortunately, the sustainability of this important resource is under many threats arising from human interventions and climate change. The soil system processes are therefore significantly changing soil properties even at shorter time scales. Tools capable of assessing such changes are currently needed to be able to guide the sustainable use of the soil resource. Mechanistic soil evolution models are increasingly becoming such invaluable tools to facilitate an improved understanding and prediction of soil evolution. Such information is needed to provide answers to many environmental questions including soil sustainability, soils and climate change interactions, food security and provision of ecosystem services. However modelling of the soil system as a whole, both at profile and landscape scales remains a big challenge. Although modelling of soil and landscape evolution has progressed rapidly over the last decade, emphasis has been on parallel scales rather than integral scales. Therefore, there are models capable of modelling landscape evolution but lack detailed vertical soil forming processes defined in profile scale models and viceversa. It is becoming inevitable to integrate these two approaches in order to have models capable of simulating soil development and global change feedbacks. However such integration is only feasible after addressing challenges such as process coverage, model calibration and verification, and model result quality.

The objectives of this study were to contribute to the state of art overview of soil modelling especially at pedon scale, adapt an existing soil evolution model (the SoilGen model) and extend its chemical weathering and biogeochemical modules such that the fate of a wide range of minerals and elements can be simulated, and to apply the SoilGen model to assess the sensitivity of soil processes and properties to global change (i.e., change in model boundary conditions such as climate, vegetation and soil use). From an overview study, we could conclude that the strengths of the SoilGen soil evolution model included its ability to simulate the integrated effect of biological, geochemical and physical soil processes moreover at a millennium time scale. However some of the processes such as chemical weathering were simplified and needed to be extended. In this study therefore, we formulated an extended chemical weathering mechanism that includes the weathering of primary and secondary minerals and the precipitation of secondary minerals. The approach also takes into account the effect of physical weathering on chemical weathering through its effect on mineral

specific surface areas over time. The chemical module of the SoilGen model was also reformulated to include the cycling of Fe and Si in addition to the already simulated elements (i.e., Na, K, H, Mg, CA and Al).

Furthermore, the SoilGen model was applied in two case studies. In the first case study, the model was applied to test the hypothesis that the relationships between soil properties (e.g., soil horizon depth) and landscape position that were surprisingly absent (based on field measurements) could be explained by the variation in local factors such as tree falls. Two model scenarios of soil development (i.e., with and without tree uprooting events) were defined. The same boundary conditions (climate, vegetation) were used in both scenarios and the SoilGen model simulations (in terms of profiles of a.o. organic carbon, clay percentage) were first converted to horizon depth before being confronted with measured horizon depth. In total, 108 soil profiles (from Meerdaal forest, Belgium) were simulated and the results from the model with treefall events exhibited the same trends as the observed data. The conclusion was drawn that bioturbation due to treefalls could be an explanation for the lack of correlation between landscape properties and soil horizon depths as observed in the field.

In the second case study, the extended SoilGen model was applied to explain the sensitivity of silicate mineral dissolution rates to physical weathering. Our working hypothesis was that physical weathering affects the magnitude of chemical weathering and this could partly explain the systematic deviations between laboratory and field silicate mineral dissolution rates. We tested the hypothesis on the forested loess soil, in the Zinnia forest, Belgium (50°46’31”N, 4°24’9”E). Climate and vegetation evolution over the last 15000 years of model simulation period were reconstructed and were readily available for this site. Our results demonstrated a dominant role of pH and an indirect but substantial effect of physical weathering on silicate mineral dissolution rates. Furthermore, clay migration and plant nutrient recycling processes influenced the pH and thus the dissolution rates. SoilGen simulated silicate dissolution rates were between laboratory and field measured rates. Results from this study demonstrated the necessity to couple different soil-forming processes in mechanistic soil models in order to explain the differences between lab and field dissolution rates.

In general, we could conclude that the SoilGen model is capable of modelling soil processes under different scenarios of climate and land use change. Given field measurements, it is also possible to

verify most of the processes defined in the model. However, a number of challenges need to be addressed (e.g., computation time, process coverage) and more model tests in other environments are required before the model can be integrated into the landscape evolution and other interdisciplinary models.

Samenvatting

De bodem is een sleutelfactor in veel ecosysteemdiensten zoals de zuivering van water, de productie van voedsel, hout en vezels, in nutriëntenkringlopen, klimaatregulering en de fysieke basis van infrastructurele werken. Helaas wordt de duurzaamheid van deze belangrijke hulpbron bedreigd door menselijke interventies en klimaatsverandering. Processen in het bodemsysteem veranderen daarom bodemeigenschappen in belangrijke mate, ook op korte tijdschalen. Er is een actuele nood aan gereedschappen om deze veranderingen te kunnen inschatten en daarmee het duurzaam gebruik van de bodem te kunnen sturen. Mechanistische bodemevolutiemodellen ontwikkelen zich in toenemende mate tot dergelijke waardevolle gereedschappen waarmee de bodemevolutie kan worden begrepen en voorspeld. De hiermee verkregen informatie is noodzakelijk om antwoorden te geven op omgevingsvraagstukken zoals duurzaamheid, de interacties tussen bodem en klimaatverandering, voedselzekerheid en de levering van ecosysteemdiensten door de bodem. Echter, de modellering van het totale bodemsysteem, zowel op de schaal van het profiel als van het landschap blijft een grote uitdaging. Alhoewel de modellering van bodem- en landschapsevolutie sterke progressie heeft geboekt de laatste decade, was dit eerder parallel dan geïntegreerd. Als gevolg zijn er nu modellen die de landschapsontwikkeling kunnen simuleren, maar slechts weinig oog hebben voor verticale bodemvormende processen zoals die zijn gedefinieerd in profiel-modellen, en vice versa. Het is daarom onvermijdelijk dat beide benaderingen worden geïntegreerd om modellen te verkrijgen die in staat zijn bodemontwikkeling zowel als landschapsveranderingen te koppelen aan “global change”. Deze integratie moet echter worden voorafgegaan nadat uitdagingen bij beide modelbenaderingen zijn aangegaan, zoals verbetering van de procesbedekking, modelkalibratie en –verificatie en optimalisatie van de kwaliteit van de modelresultaten.

De objectieven van deze studie waren om een bijdrage te leveren aan de toestandsbeschrijving van de bodemmodellering, vooral op de profielschaal, om aan een bestaand bodemontwikkelingsmodel (SoilGen) de modules betreffende verwering en de biogeochemie zo uit te breiden dat het lot van een groter aantal mineralen en elementen kan worden gesimuleerd, en om de gevoeligheid in te schatten van de bodemvormende processen en bodemkenmerken voor “global change” (d.w.z. veranderingen in modelrandvoorwaarden zoals klimaat, vegetatie en bodemgebruik). In een overzichtsstudie concludeerden we dat de sterktes van het SoilGen model o.a. betreffen het vermogen om het

geïntegreerde effect te simuleren van biologische, geochemische en fysische bodemvormingsprocessen, dit op een tijdschaal van millennia. Echter, sommige processen zoals de chemische verwering waren sterk vereenvoudigd en dienden te worden uitgebreid. Daarom werd in deze studie een uitgebreid verweringsmechanisme geformuleerd dat de verwering van primaire en secondaire mineralen omvat alsook de nieuwvorming van secondaire mineralen. De benadering omvat tevens het effect van fysische verwering met de tijd op de chemische verwering via de verandering van het specifiek oppervlak van mineralen. De chemische module van het SoilGen model werd opnieuw geformuleerd om de kringloop van Fe en Si te beschrijven in aanvulling op de reeds gesimuleerde elementen (Na, K, H, Mg, Ca en Al).

Voorts werd het SoilGen model toegepast in twee gevalstudies. In de eerste studie werd het model toegepast om de hypothese te testen dat de afwezigheid van een duidelijke relatie tussen in het veld gemeten bodemeigenschappen (de aanvangsdieptes van bodemhorizonten) en de landschapspositie kon worden verklaard door een variatie in lokale factoren zoals windvallen. Hiertoe werden twee modelscenario's voor bodemontwikkeling gedefinieerd: mèt en zonder windvallen. Dezelfde modelrandvoorwaarden (klimaat, vegetatie) werden gebruikt in beide scenario's, en de SoilGen modelresultaten (o.a. profielen van organische koolstof, kleigehalte) werden geconverteerd naar horizontdiepte alvorens te worden geconfronteerd met gemeten horizontdiepte. In totaal 108 bodemprofielen (in het Meerdaalwoud, België) werden doorgerekend, en de resultaten van het model mèt windvallen vertoonden dezelfde trends als de observaties in het veld. De conclusie was, dat bioturbatie ten gevolge van windvallen een verklaring kan zijn voor de gebrekkige relatie tussen gemeten horizontdieptes en landschapspositie.

In de tweede gevalstudie werd het uitgebreide SoilGen model gebruikt om de gevoeligheid van de oplossingssnelheid van silicaatmineralen voor fysische verwering te onderzoeken. Onze werkhypothese was dat fysische verwering de mate van chemische verwering beïnvloedt, en dat dit een gedeeltelijke verklaring kan zijn voor de systematische verschillen tussen oplossingssnelheden van silicaatmineralen in het laboratorium en in veldproeven. We testten de hypothese op de lössbodem onder bos van het Zoniënwoud in België (50°46'31"N, 4°24'9"O). De evolutie van klimaat en vegetatie over de laatste 15000 jaar werd reeds gereconstrueerd en was beschikbaar voor deze locatie. Onze resultaten lieten een dominant effect van de pH, en een indirect maar substantieel

effect van fysische verwering zien op oplossingssnelheden van silicaatmineralen. Hierbij beïnvloedden kleimigratie en plant-gerelateerde nutriëntencycli de pH en dus de oplossingssnelheden. De door SoilGen gesimuleerde silicaat-oplossingssnelheden lagen tussen laboratorium- en veldmetingen. Resultaten van deze studie demonstreerden de noodzaak om verschillende bodemvormende processen in mechanistische bodemmodellen te koppelen om de verschillen tussen laboratorium- en veld-oplossingssnelheden te kunnen verklaren.

In het algemeen konden we concluderen dat het SoilGen model in staat is om bodemvormende processen te simuleren onder verschillende scenario's van veranderend klimaat en landgebruik. Bij beschikbaarheid van veldmetingen is het mogelijk de meeste in het model gepresenteerde processen te verifiëren. Echter, een aantal uitdagingen moeten nog worden aangegaan (bijvoorbeeld de rekentijd en de procesdekking) en aanvullende modeltests in andere omgevingen zijn noodzakelijk alvorens het model kan worden geïntegreerd in landschapsevolutiemodellen en andere interdisciplinaire modellen.

Chapter 1 : General Introduction, Problem Statement and Objectives

"When we try to pick out anything by itself, we find it hitched to everything else in the universe." ***- John Muir***

1.1 General background – Soil functions and emerging issues

Soil is one of the most valuable resources supporting life on earth (Carlson et al., 2011). Soils are central in providing many ecosystem functions and services (Fig 1.1). The major ecosystem services provided by soils include (i) provisioning services (e.g., provision of food, wood and fibre, provision of habitat to biodiversity, and provision of support to human infrastructure), (ii) regulating services (e.g., water purification, wastes recycling, carbon sequestration and flood control), (iii) cultural services such as spiritual and aesthetic values, and (iv) supporting services such as soil formation, primary production, photosynthesis and, water and nutrient cycling, (Dominati et al., 2010; FAO and ITPS, 2015; MEA, 2005). Soils therefore play a critical role not only in food security but also in environmental and human health security (Brevik and Sauer, 2015; SSSA, 2015; Zanella et al., 2015). Despite the numerous functions of soils, focus given to this important resource even within earth science remains wanting (Minasny et al., 2015). In addition, global change due to population increase and associated competing needs ranging from industrialization, urbanization, mining to food production threaten the sustainability of soils to provide their crucial ecosystem functions and services (Amundson et al., 2015; FAO and ITPS, 2015). Consequently, there are existing knowledge gaps on the interplay between the soil and other systems (e.g. hydrosphere, biosphere, lithosphere), on the quantification of soil biogeochemical processes particularly under global change and on the prediction of soil evolution at both profile and landscape scales (Frossard, 2006).

Particularly, there is an urgent need for improved understanding and prediction of soil evolution in order to provide answers to many environmental questions including soil sustainability, soils and climate change interactions, food security and provision of ecosystem services (Lin, 2011). Understanding soil processes requires not only laboratory experiments and long term monitoring but also the use of process based models capable of simulating the complexity of the soil system (Brevik et al., 2016; Kirk, 2006; Lin, 2011; Samouëlian and Cornu, 2008; Samouëlian et al., 2012). Challenges in quantifying and understanding soil processes are briefly discussed in the subsequent section.

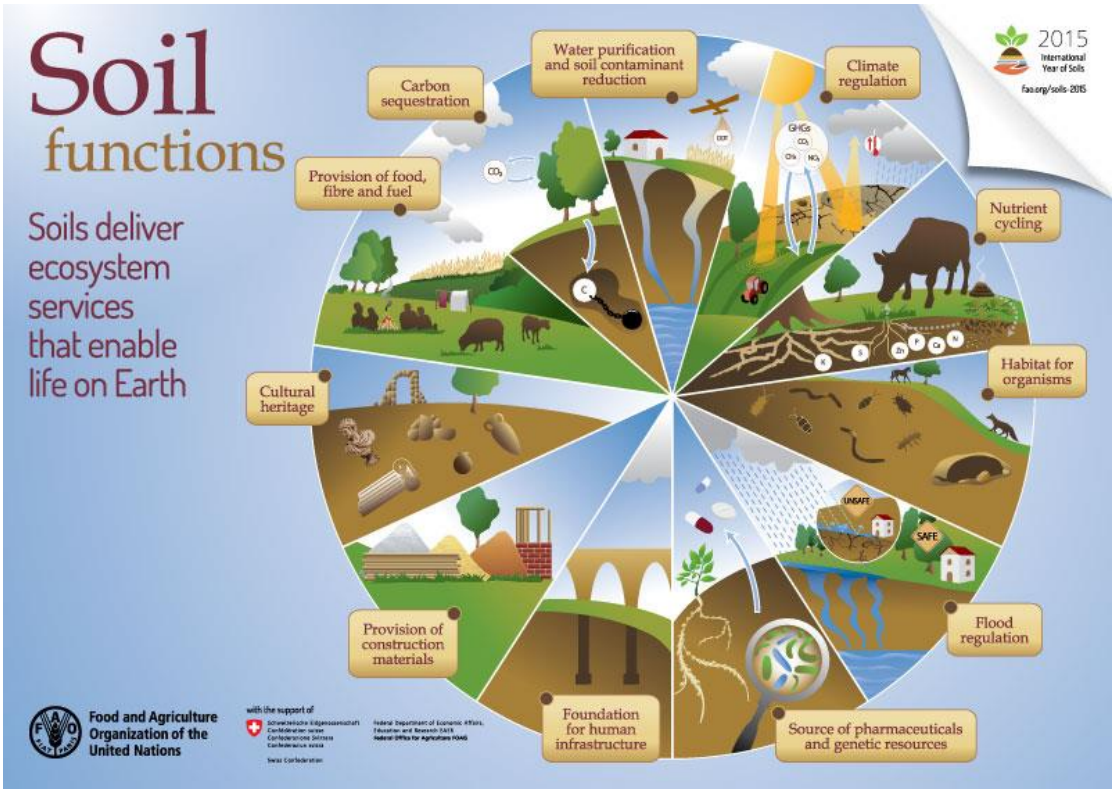

Figure 1.1. Schematic presentation of soil functions and ecosystem services (Source: http://www.fao.org/resources/infographics/infographics-details/en/c/284478).

1.2 Quantifying soil processes and associated challenges

Methodologies and techniques to study soils have evolved over time ranging from just observations on nature in the early civilization period to profile and landscape description coupled with the use of more advanced analytical techniques and field experiments designed to test theories (Brevik and Hartemink, 2010). In the same period, the development of mechanistic soil models has been active though it is still at its infancy (Minasny and McBratney, 2006). To understand the processes behind the formation of a given soil, a pedologist not only needs to describe a soil profile, take soil samples and analyse in the laboratory, but also needs to understand the complexity of the environment within which these soils are formed. This is because soil is the result of the complex interaction with other systems (i.e., lithosphere, biosphere, hydrosphere, and atmosphere; Fig 1.2) and is therefore difficult to study without considering external environmental factors. Soil can be best described by the words of the famous naturalist (John Muin) that *"when we try to pick out anything by itself, we find it*

hitched to everything else in the universe." Dokuchaev (1886) therefore found it important to understand soil formation as a function of not only parent material but also other factors like climate and organisms. This understanding was later useful to Jenny (1941) to formulate a factorial model relating soil properties to factors of soil formation (Eq 1.1).

$$\text{Soil properties} = f(cl, o, r, p, t \ldots) \quad \text{(Eq. 1.1)}$$

where cl is Climate, o represents Organisms, r is Relief, p is the Parent material, t is Time and the three dots at the end were included to represent any additional factors that may influence soil formation.

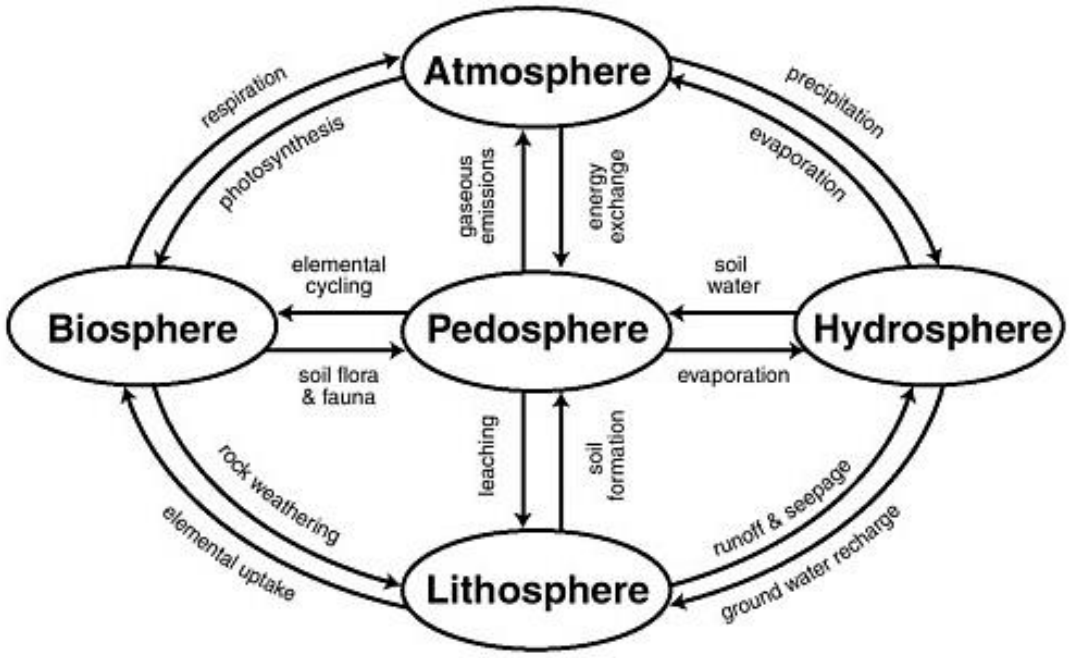

Figure 1.2. Interaction among the pedosphere (soil), atmosphere, hydrosphere, lithosphere and biosphere systems (Source: Lal et al., 1997).

In general, the real soil system is so complex that certain simplifications and assumptions are unavoidable when studying soils, either in a laboratory experiment or when using models (Dijkerman, 1974; van Breemen and Buurman, 2002). In line with these, soil complexity is often reduced by studying (i) climo-sequences (all other factors are assumed constant and only climate is varying), (ii)

topo-sequences (except for topographic position, all other soil-forming factors are constant within the given landscape, (iii) chrono-sequences (the soils are only different with respect to their age; Harden, 1987) and (iv) anthropo-sequences which is rather a recent category (Richter and Yaalon, 2012; Richter et al., 2011) that aims to emphasize the role of human activity in soil formation and therefore the soils are assumed to be different only with respect to human intervention (i.e., land use and management) and its history. From such studies, pedologists have been able to develop empirical models, conceptual models and consequently mechanistic soil models that are capable of describing the interaction of some soil processes (Minasny et al., 2008). However modelling of the soil system as a whole, both at profile and landscape scales remains a big challenge in pedology (Minasny et al., 2008, 2015; Samouëlian et al., 2012; Samouëlian and Cornu, 2008). The history of soil model development and the need for mechanistic soil models in soil studies is presented in the subsequent sections.

1.3 Quantitative mechanistic soil models, history and current knowledge gaps

1.3.1 Why is modelling soil evolution important?

A model is a simplified form of reality that can be used as a tool (Bethke, 2008). A soil model is thus a simple formulation of the soil system that is useful as a tool to describe and or quantify the impact of complex factors and processes on soil formation. Soil models have become indispensable tools to understand the complexity of soil systems (Stockmann et al., 2011). Soil models provide with an opportunity to quantify long term effect of human activities and climate change on soils and landscapes, and give better understanding of the relationships between soils and landscapes (Minasny and McBratney, 2006; Salvador-Blanes et al., 2007). Furthermore, mechanistic soil models are valuable tools to quantify the effects of pedogenetic factors (i.e., “clorpt” factors in Eq 1.1; Jenny, 1941) on the soil forming processes (Finke, 2012; Goddéris et al., 2010; McBratney et al., 2003; Minasny and McBratney, 2006). In addition, soil models are generally useful tools to interpolate in time the soil properties for different applications e.g. in landscape reconstruction and archaeological land evaluation (Zwertvaegher et al., 2010) and to test if reconstructed soils would develop into the soils that we observe at present (Finke, 2012). Last but not least, factorial soil models enable the soil

scientists to predict soil properties in time and space and are therefore are very important tools in soil surveys, classification and soil mapping (Brevik et al., 2016).

1.3.2 A brief history of soil evolution modelling

The history of soil modelling dates back to over a century ago when Dokuchaev (1886) recognized that soil formation was a function of several factors and these ideas were translated into a factorial model (Eq. 1.1) relating the depth distribution of soil properties to soil forming factors (Jenny, 1941; Jenny, 1961). The detailed review of soil models has been presented elsewhere (Bevrik et al., 2016; Hoosbeek and Bryant, 1994; Minasny et al., 2008, 2015; Samouëlian and Cornu, 2008; Samouëlian et al., 2012; Stockmann et al., 2011). In this section, only a summary of these models distinguished either as functional or mechanistic is presented (Fig 1.3).

Functional soil models include factorial and mass balance approaches. These models are quantitative and are mainly based on empirical equations (e.g., Brimhall and Dietrich, 1987; McBratney et al., 2003; Phillips, 1993). Mass balance soil models are based on the principle of mass conservation within the soil profile (Samouëlian and Cornu, 2008). These models have been widely employed in many geochemical studies to quantify the redistribution of elements and matter in soil profiles (e.g., Anderson et al., 2002; Brimhall and Dietrich, 1987; Chadwick et al., 1990; Schoonejans et al., 2016; Yoo et al., 2007). In addition, mass balance approaches have also been important in the development of some mechanistic models (e.g., Dietrich et al., 1995; Kirkby, 1977, 1985; Minasny and McBratney, 1999, 2001; Yoo et al., 2007). However, the application of mass balance approaches is mainly limited to soils developed from homogeneous parent material (Samouëlian and Cornu, 2008). Furthermore, water flow is only implicitly considered in these formulations (Samouëlian and Cornu, 2008; Samouëlian et al., 2012; Minasny et al., 2015).

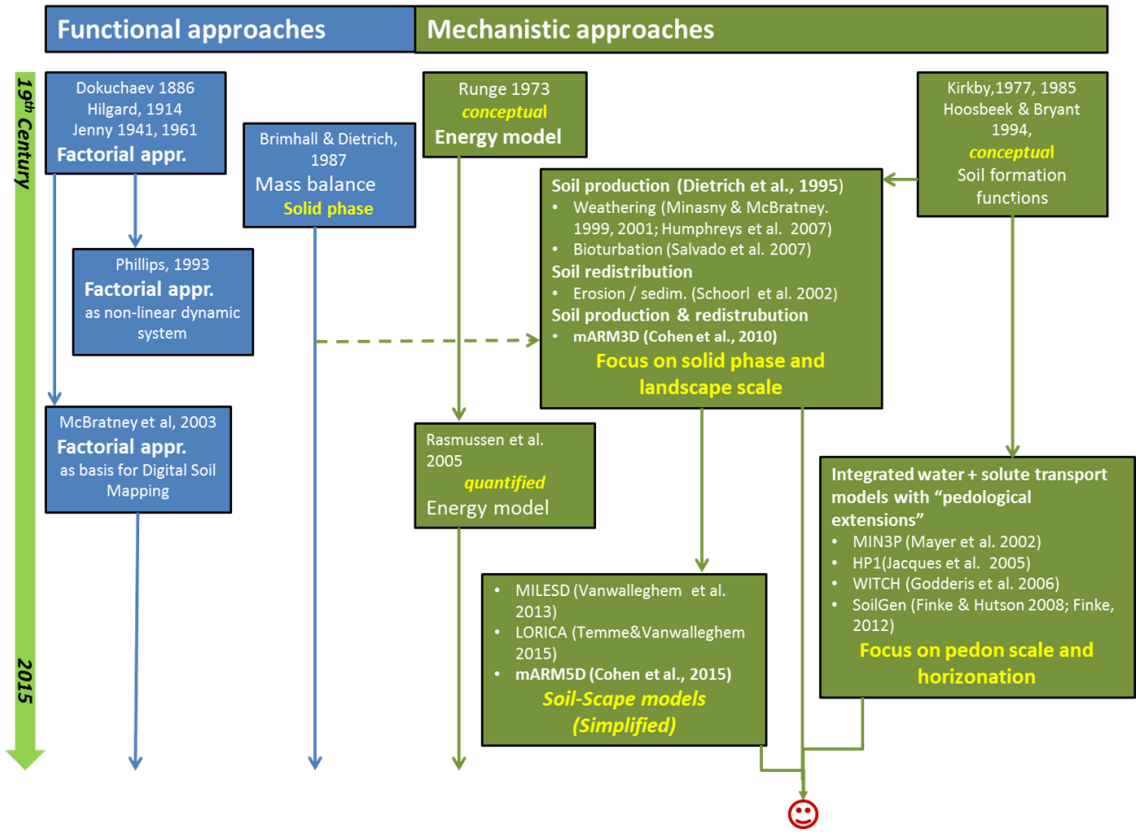

Figure 1.3. Schematic presentation of the history and evolution of soil models. The dashed arrow indicates the integration of mass balance approach into mechanistic models. The smiley represents the current discussion focusing on integrating mechanistic landscape and pedon scale models for improved understanding of the feedbacks between the soil system and other systems cited in Figure 1.2.

Mechanistic soil models on the other hand are process-based and mathematically formulated models to quantify the effects of pedogenetic factors and processes on soil properties. Mechanistic modelling already started in the 1970's and the resulting models were formulated to quantify the evolution of soil in relation to cumulative energy inputs and losses (Runge, 1973) or as a result of interaction among many processes including mineral weathering and, water and solute transport (Kirkby, 1977; 1985; Hoosbeek and Bryant, 1994). From then onwards progress in mechanistic soil model development has been made (e.g., Cohen et al., 2010; Dietrich et al., 1995; Finke, 2012; Finke and Hutson, 2008; Goddéris et al., 2006; Mayer et al., 2002; Minasny and McBratney, 1999, 2001; Schoorl

et al., 2002; Samouëlian and Cornu, 2008; Sommer et al., 2008; Temme and Vanwalleghem., 2015; Vanwalleghem et al., 2013) as shown in Fig. 1.3.

Mechanistic soil models can further be divided into three groups; (i) those that focus on landscape scale and mainly on solid phase (e.g., Salvado et al., 2007, Cohen et al., 2010), (ii) those that focus on profile scale and, integrate water and solute transport (e.g., WITCH model by Godderis et al., 2006, 2010; SoilGen model by Finke and Hutson, 2008 and Finke (2012), and (iii) the recent developments that aim at integrating landscape models and pedon scale soil models in what is termed as soil-scape models (e.g., MILESD by Vanwalleghem et al. (2013); LORICA by Temme and Vanwalleghem (2015); and mARM5D by Cohen et al. (2015). The major aim of these soil-scape models is to bridge the gaps that exist when dealing with only landscape scale (e.g., vertical processes such as clay migration are often missing) or with only profile scale (e.g., lateral processes such as erosion and their feedbacks to the soil profile properties are often missing). Soil-scape models like MILESD (Vanwalleghem et al., 2013) and it's successor, LORICA (Temme and Vanwalleghem, 2015) are therefore formulated with capabilities to simulate the coupling between physical erosion rates and chemical weathering rates at landscape scale, and at the same time keep track of the evolution of soil properties (e.g., texture, bulk density) at the profile scale as influenced by processes such as bioturbation, clay migration and physical weathering. The soil-scape model, mARM5D (Cohen et al., 2015) on the other hand integrates processes such as weathering, sediment transport, aeolian deposition and surface armouring, and assesses both the spatial and temporal evolution of soil properties like partical size distribution and soil depth as affected by these processes. However, these soil-scape models (i.e., MILESD, LORICA and mARM5D) do not explicitly integrate soil solution and soil chemistry in their calculations. Consequently, all soil forming processes may have to be calibrated on a site-specific basis (Minasny et al., 2015).

1.3.3 Knowledge gaps in soil evolution modelling

Most of the mechanistic models (Fig. 1.3) focus on the solid part of the soil and water flow is often missing. However, water flow is an important soil forming process as it governs the redistribution of soluble matter in the soil profile and the landscape (Lin, 2011; Samouëlian et al.,2012; Minasny et al.,

2015). In addition, some models are based on short time scales (Schaetzl and Schwenner, 2006) while some approaches focus on selected individual soil forming processes (e.g., solute transport, soil acidification, heat transport and mineral dissolution) rather than the simultaneous occurrence and interactions among various soil processes (Salvador-Blanes et al., 2007; Samouëlian et al., 2012). Minasny et al. (2015) evaluated the process coverage of mechanistic models using the soil-forming processes defined in Bockheim and Gennadiyev (2000) and reported a higher process coverage in pedon scale soil models than in the landscape scale soil models, but still incomplete coverage in both cases. Furthermore, most pedogenesis models lack causal relations to the soil forming factors in their formulations and are therefore not suitable for simulating the effects of global change (Minasny et al., 2008).

There is therefore need for mechanistic soil models that are based on a whole system approach and comprise physical, geochemical and biological processes (Samouëlian and Cornu, 2008; Samouëlian et al., 2012). Such models are necessary in order to address knowledge gaps regarding soil and global change feedbacks thus contributing to the necessary policy and decision making for sustainable use and management of the soil resource (Lin, 2011). Such models will also facilitate the communication between soil science and society. Vanwalleghem et al. (2013) and, Temme and Vanwalleghem (2015) are among the first attempts (though too simplified) to combine soil vertical forming processes (pedogenetic processes) with the lateral soil forming processes (geomorphologic processes) such as erosion and sedimentation. Such approaches are required to bridge the gaps arising from simplifications made in pedogenesis models and landscape evolution models (Minasny et al., 2015; Opolot et al., 2015). However, there is a need to further improve certain process definitions in pedogenesis models as well as in landscape soil evolution models before such integration could be made. This study addresses some of these knowledge gaps and its objectives are presented in the subsequent section.

1.4 Focus of this thesis

1.4.1 The soil system under global change

This PhD research was part of the consortium “soils under global change (SOGLO)”. The working hypothesis of this research consortium was that “soil-forming processes as well as soil properties are

now influenced even at decadal scales as a result of human interventions (e.g., land use and management, deforestation) on the soil system" (*https://sites.google.com/site/**soglo**project*). The overall objective of SOGLO was therefore "to contribute to the general understanding and quantification of the feedbacks between the soil system and its environment, in the form of sediment, nutrient, water and carbon fluxes as affected by anthropogenic activities over short and long timescales". Attaining this objective involves using different approaches ranging from short and long term field experiments, laboratory experiments and, development and use of mechanistic models. Results from such studies would later be integrated and used to quantify the long term changes in ecosystem services in response to climate and land use change. Eight work packages (WPs) were created within this research consortium to work on different specific objectives (Fig. 1.4). The PhD research presented here focused on work package five (WP5) whose overall objective was to contribute to the further development and testing of an already existing mechanistic soil profile model. Specific objectives and organization of this PhD research are discussed in the subsequent sections.

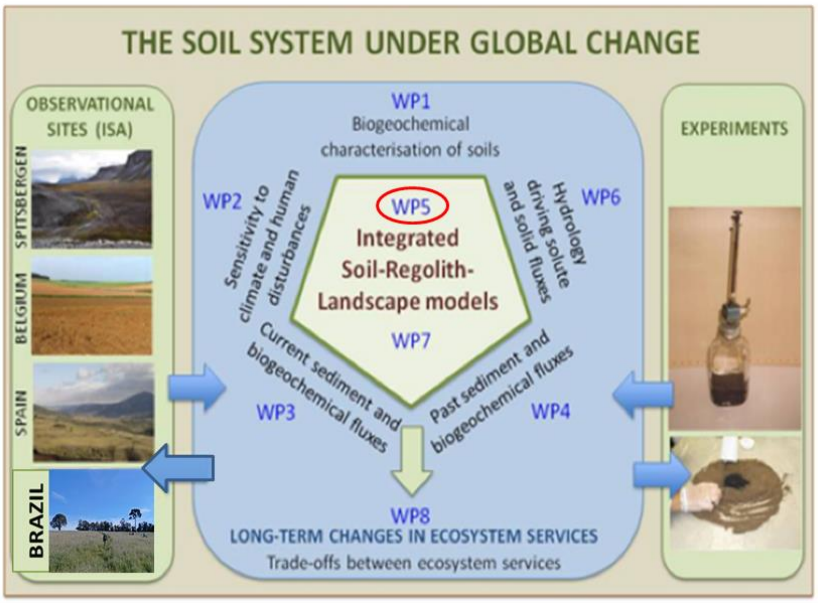

Figure 1.4. Work packages identified in the soil system under global change research consortium (Source: Modified from: https://sites.google.com/site/sogloproject/home/research-themes). The current study focuses on work package 5 (WP5).

1.4.2 Specific objectives and research questions

As pointed out in the previous section, the overall objective of this study was to contribute to the further extension and testing of an existing soil mechanistic model. The SoilGen model (explained in details in chapter 2) is one of the few mechanistic soil models with a high coverage of soil-forming processes and it is capable of simulating the evolution of soils at the soil profile scale (Samouëlian et al.,2012; Minasny et al., 2015). The model integrates detailed processes of water flow, clay migration, physical weathering and carbon cycling among others and had already been tested in several prior studies, giving results comparable with field and laboratory measurements. However most of its application was restricted to some environments (particularly in the loess soils) and therefore required further development (of some processes) and testing before it could be applied to different environments. For example, the chemical weathering module in the SoilGen model simulates weathering of few primary minerals (anorthite, chlorite, microcline, albite) and consequently release of few elements (Ca, Mg, K, Na and Al) during chemical weathering. There was therefore need to extend the weathering and chemical modules of SoilGen in order to simulate the weathering of more primary minerals and release of more element species like silicon (Si) and iron (Fe). These elements have strong influence on soil properties during soil formation (Sposito, 1989; Struyf et al., 2009). The implementation of such an extended weathering mechanism and the inclusion of Si and Fe oxides would also enhance the use of the SoilGen model output in assessing the degree of weathering, through the use of weathering indices.

Therefore the **specific objectives** addressed in this study include:

1. To contribute to the on-going discussion of process definition of soil mechanistic models, achievements and challenges, and on the possibility to integrate pedon scale models and landscape evolution models (Chapter 2; ***Opolot et al., 2015***).
2. To extend the description of the chemical weathering of primary minerals to accommodate release of more chemical species by various types of primary minerals, and implement such a mechanism in the SoilGen model (Chapter 3)
3. To evaluate the necessity and possibility to include the formation of major secondary minerals and implement such a mechanism in the SoilGen model (Chapter 3)
4. To implement the output of varying weathering indices to allow better comparison of model results with field and literature data (Chapter 3)

5. To extend the chemical sub model of the SoilGen model to include more species than at present (notably adding Si and Fe species) (Chapter 4)
6. To assess the evolution of soil propeties as a function of global change (i.e., changing climate, vegetation / land use) using the SoilGen model and based on different sensitivity and calibration case studies (Chapters: 5 and 6: ***Finke et al., 2013***; ***Opolot and Finke, 2015***).

In summary, this study is designed to answer the following four research questions:

1. What is the current status of soil mechanistic models and what processes need to be described in such models in order to be able to simulate the soil evolution under global change?
2. How can the weathering of other primary minerals and formation of major secondary minerals be modelled in the SoilGen model?
3. How can inclusion of more chemical elements such as Si and Fe in the chemical module of the SoilGen model be realized?
4. What kind of studies can the SoilGen model be used for and how do simulated results compare with the respective field or laboratory measurements?

1.4.3 Scope of this PhD research

This thesis mainly focuses on the development and application of a soil mechanistic model at the pedon scale. Emphasis was on proposing and formulating an extended weathering system for implemention into the SoilGen soil model. This work also contributed to the extension of the number of chemical elements simulated in the chemistry module from currently 5 elements (Ca, Mg, K, Na and Al) to 7 elements (i.e., Ca, Mg, K, Na ,Al , Fe, Si) and calculation of various weathering indices. Focus was also given to the calibration, testing and application of the model through sensitivity and test case studies. The test case studies are intended to assess the evolution of soil properties in response to global change. Throughout this thesis, the terminology “global change” is defined as a change in the model boundary conditions (i.e., climate, vegetation / land use, bioturbation) along the simulation period (which usually comprises several millenniums). All the case studies (chapter 5 and 6) therefore have defined boundary conditions that reflect global change. However, the effect of the

possible climate or land use change scenarios such as those provided by Intergovernmental Panel on Climate Change (IPCC) is not simulated in this study.

1.4.4 Organization of the thesis

This work has been organized in seven (7) chapters. This introductory chapter presents the state of art, knowledge gaps in soil evolution modelling and objectives of this PhD study. Chapter 2 gives an overview of soil modelling, achievements and challenges, with detailed overview of the SoilGen model, its application range, calibration studies and limitations. Chapter 3 explains the weathering system in the SoilGen model and the improvements resulting from this study while chapter 4 describes the biogeochemical processes in SoilGen together with the resulting developments from this study. Chapters 5 and 6 are case studies on modelling evolution of soil properties as a function of different processes and changing boundary conditions. Chapter 5 describes the application of the SoilGen model to simulate the effect of bioturbation (due to treefalls) on the thickness of soil horizons, and comparing model results with field measurements. In Chapter 6, the SoilGen model is applied to assess the sensitivity of the silicate mineral dissolution rates to physical weathering. The last chapter (Chapter 7) gives summary, general conclusions, recommendations and areas for future research.

Author contribution

This chapter was fully designed, formulated and written by E. Opolot.

References

Amundson, R., Berhe, A. A., Hopmans, J. W., Olson, C., Sztein, A. E. and Sparks, D. L.: Soil and human security in the 21st century, Science (80), 348(6235), 1261071–1261071, doi:10.1126/science.1261071, 2015.

Anderson, S. P., Dietrich, W. E., and Brimhall, G. H.: Weathering profiles, mass-balance analysis, and rates of solute loss: Linkages between weathering and erosion in a small, steep catchment, Geol. Soc. Am. Bull., 1143‐1148, 2002.

Bethke, C.M.: Geochemical and Biogeochemical Reaction Modeling. Cambridge University Press, 547 pp, 2008.

Brevik, E. C., Calzolari, C., Miller, B. A., Pereira, P., Kabala, C., Baumgarten, A. and Jordán, A.: Soil mapping, classification, and pedologic modelling: History and future directions, Geoderma, 264, 256–274, doi:10.1016/j.geoderma.2015.05.017, 2016.

Brevik, E. C. and Sauer, T. J.: The past, present, and future of soils and human health studies, SOIL, 1, 35-46, doi:10.5194/soil-1-35-2015, 2015.

Brimhall, G. H. and Dietrich, W. E.: Constitutive mass balance relations between chemical composition, volume, density, porosity, and strain in metasomatic hydrochemical systems: Results on weathering and pedogenesis, Geochim. Cosmochim. Acta, 51(3), 567–587, doi:10.1016/0016-7037(87)90070-6, 1987.

Carlson, D., Plummer, C., and Hammersley, L.: Physical Geology Earth Revealed, 9th Edition, Published by McGraw-Hill, New York, 670p, 2011.

Chadwick, O. A., Brimhall, G. H. and Hendricks, D. M.: From a black to a gray box - a mass balance interpretation of pedogenesis, Geomorphology, 3(3-4), 369–390, doi:10.1016/0169-555X(90)90012-F, 1990.

Cohen, S., Willgoose, G., Svoray, T., Hancock, G. and Sela, S.: The effects of sediment transport, weathering, and aeolian mechanisms on soil evolution, J. Geophys. Res. Earth Surf., 120, 260–274, doi:10.1002/2014JF003186, 2014.

Cohen, S.,Willgoose, G., Hancock, G.: The mARM3D spatially distributed soil evolution model: Three-dimensional model framework and analysis of hillslope and landform responses. J. Geophys. Res. Earth Surf. 115 (F04013), 2010.

Dietrich, W.E., Reiss, R., Hsu, M.-L., Montgomery, D.R., 1995.A process-based model for colluvial soil depth and shallow landsliding using digital elevation data.Hydrol.Process. 9, 383–400

Dijkerman, J.C.: Pedology as a science: The role of data, models and theories in the study of natural soil systems, Geoderma, 11, 73-93, 1974.

Dokuchaev, V.V., 1883. Russian Chernozem. : Selected works of V.V. Dokuchaev. Volume I (translated in 1967). Israel Program for Scientific Translations, Jerusalem.

Dominati, E., Mackay, A. and Patterson, M.: Modelling the provision of ecosystem services from soil natural capital, 19th World Congr. Soil Sci., (August), 32–35, 2010.

FAO and ITPS.: Status of the World's Soil Resources (SWSR) – Main Report. Food and Agriculture Organization of the United Nations and Intergovernmental Technical Panel on Soils, Rome, Italy, 2015.

Finke, P. A.: Modelling the genesis of Luvisols as a function of topographic position in loess parent material, Quat. Int., 265, 3–17, doi:10.1016/j.quaint.2011.10.016, 2012.

Finke, P. A. and Hutson, J. L.: Modelling soil genesis in calcareous loess, Geoderma, 145(3-4), 462–479, doi:10.1016/j.geoderma.2008.01.017, 2008.

Finke, P. A., Vanwalleghem, T., Opolot, E., Poesen, J. and Deckers, J.: Estimating the effect of tree uprooting on variation of soil horizon depth by confronting pedogenetic simulations to measurements in a Belgian loess area, J. Geophys. Res. Earth Surf., 118(4), 2124–2139, doi:10.1002/jgrf.20153, 2013.

Frossard, E.: The future of soil science: the role of soils for the society and the environment. In.The future of soil science / edited by Alfred E. Hartemink (1964). Wageningen: IUSS International Union of Soil Sciences. 165 pp,2006.

Goddéris, Y., François, L. M., Probst, A., Schott, J., Moncoulon, D., Labat, D. and Viville, D.: Modelling weathering processes at the catchment scale: The WITCH numerical model, Geochim. Cosmochim.Acta, 70(5), 1128–1147, doi:10.1016/j.gca.2005.11.018, 2006.

Goddéris, Y., Williams, J. Z., Schott, J., Pollard, D. and Brantley, S. L.: Time evolution of the mineralogical composition of Mississippi Valley loess over the last 10 kyr: Climate and geochemical modelling, Geochim. Cosmochim.Acta, 74(22), 6357–6374, doi:10.1016/j.gca.2010.08.023, 2010.

Harden, J.W.: Soils developed in granitic alluvium near Merced, California. Bulletin 1590-A. U.S. Geological Survey, 1987

Hilgard, E.W.: Soils: Their Formation, Properties, Composition, and Relations to Climate and Plant Growth in the Humid and Arid Regions. The Macmillan Company, New York, 1914.

Hoosbeek, M.R. and Bryant, R.: Towards the quantitative modeling of pedogenesis—a review, Geoderma, 55(3), 251–265, 1992.

Hoosbeek, M.R. and Bryant, R.B.: Developing and adapting soil process submodels for use in the pedodynamic Orthod model. In: Bryant, R.B., Arnold, R. (Eds.), Quantitative Modelling of Soil

Forming Processes. SSSA Special Publication, ASA, CSSA, and SSSA, Madison, WI, pp. 111–128, 1994.

https://sites.google.com/site/sogloproject/home/research-themes. Accessed on 05-January-2016.

http://www.fao.org/resources/infographics/infographics-details/en/c/284478. Accessed on 04-January-2016.

Humphreys, G.S., Wilkinson, M.T.: The soil production function: a brief history and its rediscovery. Geoderma 139, 73–78, 2007.

Jacques, D., Šimůnek, J., Mallants, D. and van Genuchten, M. T.: Modelling coupled water flow, solute transport and geochemical reactions affecting heavy metal migration in a podzol soil, Geoderma, 145(3-4), 449–461, doi:10.1016/j.geoderma.2008.01.009, 2008.

Jenny, H., 1941. Factors of soil formation. A System of Quantitative Pedology. McGraw-Hill Book Company, New York, London.

Jenny, H., 1961. Derivation of state factor equations of soils and ecosystems. Soil Sci. Soc. Am. Proc. 25, 385–388.

Kirk, G.: Views on the future of soil science. In.The future of soil science / edited by Alfred E. Hartemink (1964). Wageningen: IUSS International Union of Soil Sciences. 165 pp, 2006.

Kirkby, M.J.: A basis for soil profile modelling in a geomorphic context. J. Soil Sci. 36, 97–121, 1985.

Kirkby, M.J.: Soil development models as a component of slope models. Earth Surf.Process.2, 203–230, 1977.

Lal, R., Kimble, J.M., Follett,R.F.: Pedospheric processes and the carbon cycle. Pp. 1-8 in *Soil Processes and the Carbon Cycle*, R. Lal, J. M. Kimble, R. F. Follett, and B. A. Stewart, eds. Boca Raton, FL: CRC Press, 1997.

Lin, H.: Three Principles of Soil Change and Pedogenesis in Time and Space, Soil Sci. Soc. Am. J., 75(6), 2049, doi:10.2136/sssaj2011.0130, 2011.

Mayer, K.U., Frind, E.O., Blowes, D.W.: Multicomponent reactive transport modelling in variably saturated porous media using a generalized formulation for kinetically controlled reactions. Water Resources Research 38, 1174, 2002.

McBratney, A.B., Mendonca Santos, M.L., Minasny, B.: On digital soil mapping. Geoderma 117, 3 - 52, 2003.

MEA.: 'Millennium Ecosystem Assessment: Ecosystems and Human Well-being: Synthesis.' (Island Press: Washington DC), 155pp, 2005.

Minasny, B. and McBratney, A. B.: A rudimentary mechanistic model for soil production and landscape development, Geoderma, 90(1-2), 3–21, doi:10.1016/S0016-7061(98)00115-3, 1999.

Minasny, B. and McBratney, A. B.: A rudimentary mechanistic model for soil formation and landscape development II .A two-dimensional model incorporating chemical weathering, 161–179, 2001.

Minasny, B. and McBratney, A. B.: Mechanistic soil–landscape modelling as an approach to developing pedogenetic classifications, Geoderma, 133(1-2), 138–149, doi:10.1016/j.geoderma.2006.03.042, 2006.

Minasny, B., Finke, P., Stockmann, U., Vanwalleghem, T. and McBratney, A. B.: Resolving the integral connection between pedogenesis and landscape evolution, Earth-Science Rev., 150, 102–120, doi:10.1016/j.earscirev.2015.07.004, 2015.

Minasny, B., McBratney, A. B. and Salvador-Blanes, S.: Quantitative models for pedogenesis — A review, Geoderma, 144(1-2), 140–157, doi:10.1016/j.geoderma.2007.12.013, 2008.

Opolot, E. and Finke, P. A.: Evaluating sensitivity of silicate mineral dissolution rates to physical weathering using a soil evolution model (SoilGen2.25),Biogeosciences, 12, 6791-6808, doi: 10.5194/bg-12-6791-2015, 2015.

Opolot, E., Yu, Y. Y. and Finke, P. A.: Modelling soil genesis at pedon and landscape scales: Achievements and problems, Quat. Int., 34–46, doi:10.1016/j.quaint.2014.02.017, 2015.

Phillips, J. D.: Stability implications of the state factor model of soils as a nonlinear dynamical system, Geoderma, 58(1-2), 1–15, doi:10.1016/0016-7061(93)90082-V, 1993.

Rasmussen, C., Southard, R. J. and Horwath, W. R.: Modelling energy inputs to predict pedogenic environments using regional environmental databases, Soil Sci. Soc. Am. J., 69(4), 1266–1274, doi:10.2136/sssaj2004.0283, 2005.

Richter, D. deB and Yaalon, D. H.: “The Changing Model of Soil” Revisited, Soil Sci. Soc. Am. J., 76(3), 766, doi:10.2136/sssaj2011.0407, 2012.

Richter, D. deB., Bacon, A. R., Megan, L. M., Richardson, C. J., Andrews, S. S., West, L., Wills, S., Billings, S., Cambardella, C. A., Cavallaro, N., DeMeester, J. E., Franzluebbers, A. J., Grandy, A. S.,

Grunwald, S., Gruver, J., Hartshorn, A. S., Janzen, H., Kramer, M. G., Ladha, J. K., Lajtha, K., Liles, G. C., Markewitz, D., Megonigal, P. J., Mermut, A. R., Rasmussen, C., Robinson, D. A., Smith, P., Stiles, C. A., Tate, R. L., Thompson, A., Tugel, A. J., van Es, H., Yaalon, D. and Zobeck, T. M.: Human–Soil Relations are Changing Rapidly: Proposals from SSSA's Cross-Divisional Soil Change Working Group, Soil Sci. Soc. Am. J., 75(6), 2079, doi:10.2136/sssaj2011.0124, 2011.

Runge, E.C.A.: Soil development sequences and energy models. Soil Sci. 115, 183–193, 1973.

Salvador-Blanes, S., Minasny, B. and McBratney, A. B.: Modelling long-term in situ soil profile evolution: application to the genesis of soil profiles containing stone layers, Eur. J. Soil Sci., 58(6), 1535–1548, doi:10.1111/j.1365-2389.2007.00961.x, 2007.

Samouëlian, A. and Cornu, S.: Modelling the formation and evolution of soils, towards an initial synthesis, Geoderma, 145(3-4), 401–409, doi:10.1016/j.geoderma.2008.01.016, 2008.

Samouëlian, Anatja; Finke, Peter; Goddéris, Yves; Cornu, Sophie Hydrologic Information in Pedologic Models. pp. 595–636. In: Lin H. (ed.)., 2012. Hydropedology: Synergistic Integration of Pedology and Hydrology. ISBN 9780123869418

Schoonejans, J., Vanacker, V., Opfergelt, S., Ameijeiras-Mariño, Y., and M. Christl.: Kinetically limited weathering at low denudation rates in semiarid climatic conditions, J. Geophys. Res. Earth Surf., 121, 336‐350, doi:10.1002/ 2015JF003626., 2016.

Schoorl, J. M., Veldkamp, A. and Bouma, J.: Modelling Water and Soil Redistribution in a Dynamic Landscape Context , 1619, 1610–1619, 2002.

Sommer, M., Gerke, H. H. and Deumlich, D.: Modelling soil landscape genesis - A "time split" approach for hummocky agricultural landscapes, Geoderma, 145(3-4), 480–493, doi:10.1016/j.geoderma.2008.01.012, 2008.

SSSA.: Soil Science Scoiety of America. Soils: The Foundation of Human and Environmental Health. Science Policy Office | 900 2nd Street, NE, Suite 205 Washington, DC 20002 | 202.408.5558, 2015

Stockmann, U., Minasny, B. and McBratney, A. B.: Quantifying Processes of Pedogenesis. Advances in Agronomy, Volume 113, 2011.

Temme, A. J. A. M. and Vanwalleghem, T.: LORICA – A new model for linking landscape and soil profile evolution: Development and sensitivity analysis, Comput. Geosci., doi:10.1016/j.cageo.2015.08.004, 2015.

Van Breemen, N. and Buurman, P.: Soil formation, Second Edition, Kluwer Academic Publishers, Doordrecht, The Netherlands, 404 pp, 2002.

Vanwalleghem, T., Stockmann, U., Minasny, B. and McBratney, A. B.: A quantitative model for integrating landscape evolution and soil formation, J. Geophys. Res. Earth Surf., 118(2), 331–347, doi:10.1029/2011JF002296, 2013.

Yoo, K., Amundson, R., Heimsath, A. M., Dietrich, W. E. and Brimhall, G. H.: Integration of geochemical mass balance with sediment transport to calculate rates of soil chemical weathering and transport on hillslopes, J. Geophys. Res. Earth Surf., 112(2), doi:10.1029/2005JF000402, 2007.

Zanella, M. A., Rahmanian, M., Perch, L. N., Callenius, C., Rubio, J. L., Vuningoma, F., Rist, S. and Mapfumo, P.: Discussion: Food security and sustainable food systems: The role of soil, Int. Soil Water Conserv. Res., 3(2), 154–159, doi:10.1016/j.iswcr.2015.06.001, 2015.

Chapter 2 **:** Modelling soil genesis at pedon and landscape scales: Achievements and problems

Based on:

E. Opolot, Y.Y. Yu and P.A. Finke. 2015. Modelling soil genesis at pedon and landscape scales: Achievements and problems. Quat. Int., 376: 34-46, DOI: 10.1016/j.quaint.2014.02.017.

Abstract

Modelling soil evolution is an important step towards understanding the complexity of the soil system and its interaction with the other systems. The major challenge confronted by pedologists until now is the ability to develop models capable of describing the complete complexity of the soil system. This paper presents the state of art overview of such a soil evolution model, SoilGen, its applications and limitations. In addition, the paper gives an overview of how the SoilGen model may be linked to landscape evolution models to model soilscape development. SoilGen is a mechanistic pedogenetic model in which soil processes such as clay migration, decalcification, carbon cycling, bioturbation, physical and chemical weathering coupled with water flow are simulated at multi-millennium time scale. The model has been calibrated and undergone extensive field testing, giving reasonable results at both pedon and landscape scales. However discrepancies between observed and simulated soil properties such as base saturation (BS), cation exchange capacity (CEC) and pH have been reported. These have been attributed partly to simplification of soil forming processes particularly in the weathering and chemical systems. There is therefore a need to extend the description of the chemical module and the chemical weathering system in the SoilGen model. These extensions will not only improve model performance but will also enlarge its application range in simulating the genesis of typical features of more than half of the WRB-Reference Soil Groups. We also note here that although landscape evolution models have been successfully applied to model soil production and distribution, simplified and/or incomplete description of soil forming processes remain major limitations. We therefore add to the voices in scientific literature calling for integration of pedon and landscape scale models. In addition there is critical need for high quality chronosequence, climosequence and toposequence profile datasets to enhance calibration and validation of soil evolution models.

2.1. Introduction

Soil genesis is an important subject linking soil science to other scientific fields. The processes involved in soil formation provide an understanding of the interactions between the atmosphere, hydrosphere, lithosphere and the biosphere. It is the interactions among these systems (termed as foundation for earth system science) that define the existence of life on terrestrial ecosystems as they influence nutrient cycles, energy budgets, hydrological cycle and ecosystem productivity (Noorallah,

1999). Various studies have demonstrated the importance of soil formation processes like mineral weathering in regulating the earth's surface temperature by consuming carbon dioxide (Ferrier et al., 2010; Violette et al., 2010). In addition, these interactions provide a foundation for assessing the influence of human activities on global environmental change (Noorallah, 1999).

Despite the importance of soil genesis, our knowledge of soil evolution remains limited compared to that of plant and animal growth (Stockmann et al., 2011). Nevertheless, the development of soil genesis models (pedogenesis models) has generally enhanced our understanding of soils over the last few decades. As already presented in the previous chapter, the reasons behind the development of pedogenesis models are numerous. Pedogenesis models are useful tools to understand the complexity of soil systems (Stockmann et al., 2011). These models are also indispensable to be able to quantify the response of soil forming processes to the Jenny (1941) pedogenetic factors ("CLORPT") i.e. climate, organisms, relief, parent material and time (McBratney et al., 2003; Goddéris et al., 2010; Finke, 2012). In addition pedogenesis models provide an opportunity to interpolate in time soil characteristics for different applications e.g. in landscape reconstruction and archaeological land evaluation (Zwertvaegher et al., 2010). Other motives for soil evolution models include assessing the effects of global change on ecosystems, to improve our knowledge of soil forming processes (Salvador-Blanes et al., 2007) and to evaluate if reconstructed soils would develop into the soils that we observe in the present time (Finke, 2012).

The above motives have prompted the development of various pedogenesis models. These models have been developed for specific purposes ranging from digital soil mapping, soil production and redistribution studies to biogeochemical studies. The detailed history of development of soil evolution models has been presented in previous studies (Minasny et al., 2008; Samouëlian and Cornu, 2008; Stockmann et al., 2011, Samouëlian et al., 2012) and already summarized in chapter 1 of this thesis (Fig. 1.3). In general, pedogenesis models have been categorized into either functional or mechanistic models. Briefly, functional pedogenetic models are those models that are mainly aimed at describing the net effect of pedogenetic processes without detailing all underlying processes although they can also be based on empirical equations (Stockmann et al., 2011). The development of such models dates back into the 19th century, the most cited one being Jenny (1941) who described soil formation

as a function of "CLORPT" factors. Other functional pedogenesis models are those developed by Brimhall et al. (1985) and Phillips (1993).

As knowledge of soil science improved and was based on the functional approaches, the development of mechanistic models started. Mechanistic pedogenesis models are those that are based on process-describing mechanisms formulated in the form of mathematical equations (Hoosbeek and Bryant, 1992; Stockmann et al., 2011). According to Stockmann et al. (2011), the idea of mechanistic soil modelling at landscape scale was first proposed by Hugget (1975). The first comprehensive mechanistic approach of soil profile development was presented by Kirkby (1977) and later developed by Kirkby (1985). Mechanistic models can be divided into two; those that focus on landscape scales (e.g. Dietrich et al., 1995; Minasny and McBratney, 1999; 2001; Schoorl et al., 2002; Samouëlian and Cornu, 2008) and those that focus on pedon scale (e.g. Mayer et al., 2002; Goddéris et al., 2006; Finke and Hutson, 2008; Sommer et al., 2008; Finke, 2012). The summary of the principles of most of these models is provided in the review by Stockmann et al. (2011).

According to Samouëlian et al. (2012), most of the above modelling approaches do not include water flow yet water flow is key to soil evolution. The other drawback for most of these approaches is that they have mainly focused on individual soil processes (e.g. solute transport, soil acidification, heat transport and mineral dissolution) rather than the simultaneous occurrence and interactions of various soil forming processes (Salvador-Blanes et al., 2007; Samouëlian et al., 2012). The application of most of these models in soil evolution studies has been limited due to their incomplete coverage of soil formation processes and their inability to take into account all the soil forming factors (Finke, 2012). In addition models simulating soil evolution over millennia-time scales are limited (Schaetzl and Scwenner, 2006; Finke, 2012).

The SoilGen model (Finke and Hutson, 2008; Finke, 2012) is one of the most complete soil evolution models identified in a review by Samouëlian et al. (2012). The model in essence couples all the three interacting processes of soil formation i.e. biological, geochemical and physical processes. These three processes have been described in Samouëlian and Cornu (2008) and Samouëlian et al. (2012) as processes that must be included in a model that simulates soil evolution at different climate and land

use scenarios. Furthermore, the SoilGen model is able to simulate soil formation over multi-millennium time scale. The objectives of this study are (1) to provide the state of art overview of the SoilGen model (simulated soil forming processes, model data input), (2) to explain calibration strategies and model quality tests, (3) to discuss field applications and limitations of soil genesis models at pedon and landscape scales, and (4) to contribute to future perspectives of pedon and landscape soil modelling.

2.2. The SoilGen model

SoilGen 2.16 (Finke, 2012) is a pedon scale soil evolution model developed to simulate vertically discretized change in soil properties over millennium time scale. Essentially, SoilGen is a water flow driven, process-based soil model in which factors of soil formation ("CLORPT") are taken into account (Table 2.1). Major soil processes such as clay migration, decalcification, physical/chemical weathering, bioturbation, chemical equilibria and carbon cycling are simulated in SoilGen. In addition, SoilGen simulates the impact of human activity on soil formation by taking into account fertilization and plowing and incorporating the effect of erosion and deposition (Table 2.1). The model has been calibrated and successfully applied in a number of field case studies (Finke, 2012; Sauer et al., 2012; Yu et al., 2013, Finke et al., 2013; Zwertvaegher et al., 2013; Finke et al., 2015; Opolot and Finke, 2015). We describe briefly governing processes in SoilGen 2.16, calibration and application case studies in the subsequent sections. For a detailed description of the SoilGen model, reference is made to Finke and Hutson (2008) and Finke (2012).

2.2.1 SoilGen governing processes

2.2.1.1 Water, solute and heat transfer

Transfer modules should be present in a pedogenesis model if such a model has to predict the impact of land use and climate change on soil formation (Samouëlian et al., 2012). In SoilGen, the transfer of water, solute and heat through the soil profile is simulated following the concepts in the LEACHC code (Hutson, 2003). Unsaturated vertical water flow is described using Richards' equation (Eq 2.1):

$$\frac{\partial h}{\partial t} C(\theta) = \frac{\partial}{\partial Z}\left[K(\theta)\frac{\partial H}{\partial Z}\right] - U(z,t) \quad (2.1)$$

where $C(\theta)$ is the differential water capacity $\frac{\partial \theta}{\partial h}$, θ ($m^3$ m^{-3}) is the volumetric water content, h and H represent the soil water pressure head (Pa.10) and the hydraulic head (Pa.10), respectively. K(θ) ($m.10^{-3}$ d^{-1}) is the hydraulic conductivity and U(z,t) describes the sink term accounting for the water lost at depth z and time t by transpiration. K-θ-h relations are parametrized using the van Genuchten closed form functions (Van Genuchten, 1980). The Hypres pedotransfer function (Wösten et al., 1999) is used at annual time steps to update the Van Genuchten parameters to include the effect of changing OC, texture, bulk density on hydraulic parameters.

The heat flow equation (Eq 2.2) is used to simulate heat and temperature distribution in the soil profile. In case of frozen conditions (soil temperatures below 0 ^{0}C), hydraulic conductivity is reduced by an impedance factor, Ω (Finke and Hutson, 2008).

$$\frac{\partial T}{\partial t} = \frac{\partial}{\partial z}\left[\frac{K_t(\theta)}{\beta} \times \frac{\partial T}{\partial z}\right] \quad (2.2)$$

where T (°C) is the temperature and $K_t(\theta)$ ($J\ m^{-1}\ s^{-1}\ °C^{-1}$) is the thermal conductivity calculated at θ (-) following the method presented in Wierenga et al. (1969). β ($J\ m^{-3}\ °C^{-1}$) represents the volumetric heat capacity and it is calculated as $\beta = \rho_s C_s + \theta C_w \rho_w$, where ρ_s and ρ_w are the bulk densities of solids and water (1000 kg m^{-3}) respectively, C_s is the gravimetric heat capacity of solids (840 J kg^{-1} $°C^{-1}$) and C_w is the gravimetric heat capacity of water (4200 J kg^{-1} $°C^{-1}$).

Table 2.1. Factors of soil formation and their link to soil processes simulated in the SoilGen model.

Factor of soil formation		SoilGen governing processes
Climate	Temperature	Heat flow [1]
	Precipitation: water	Water flow [1]
	Precipitation: solutes	Solute flow [1]
	Evaporation	Evapotranspiration [1]
Organisms	Vegetation	C-cycling [2]
		CO_2 production and diffusion
		Cation uptake and release
		Root distribution
	Fauna	Bioturbation
	Human influence	Fertilization [1]
		Plowing/tillage
Relief	Slope	Runoff [1]
	Erosion/sedimentation	Removal or addition of top layers
	Local variants of T, P, and E	Heat/water/solute flow with P and E as f(exposition)
Parent material	Texture	Dissolution/precipitation [1]
		Bioturbation
		C-cycling
		Physical weathering
		Clay migration
		CEC as a f(clay, OC)
	Mineralogy	Cation release from chemical weathering [3]
	Solute and exchange chemistry of Ca, Al, Mg, Na	Chemical equilibria [1]
		Cation exchange equilibria [1]
		Arrhenius temperature correction
		Al-Gibbsite equilibrium, Exchangeable acidity
		Base saturation
Time	Change of boundary conditions	

T, P and E are Temperature, precipitation, and evapotranspiration, respectively.

Source: Adapted from Finke and Hutson (2008) and Finke (2012)

[1] Based on LEACHC code (Hutson, 2003),

[2] Based on RothC 26.3 (Coleman and Jenkinson, 2005)

[3] Based on NUCSAM (Kros, 2002)

Transfer of solutes is described using the convection–dispersion equation (CDE; Eq 2.3). In addition, the diffusive flow of CO_2 is simulated using a gas regime equation (Eq. 2.4). Detailed description of how these equations are solved in the model is given in the SoilGen user manual (Finke, 2011).

$$\frac{\partial(\theta C)}{\partial t} = \frac{\partial}{\partial Z}[\theta D(\theta, q) - qC] \pm \Phi \quad (2.3)$$

where C (kg m^{-3}) is the solute concentration, $D(\theta, q)$ (mm^2 d^{-1}) is the dispersion coefficient representing the combined effect of mechanical dispersion and aqueous diffusion, q (mm d^{-1}) is the water flux and Φ (kg m^{-3} d^{-1}) is a source or sink term accounting for plant uptake or release by decomposition of organic matter.

$$\varepsilon.\frac{\partial c}{\partial t} = D(T)_{gs}.\frac{\partial^2}{\partial z^2} + P(z,t) \quad (2.4)$$

where ε is dimensionless and represents the air-filled porosity, c and P(z,t), respectively are the CO_2 partial pressure in the soil air and the CO_2 production in each soil compartment. $\mathrm{D(T)_{gs}}$ (m^2 s^{-1}) is the gas diffusion coefficient in soil and its estimated by Moldrup et al. (2000) as described in (Eq 2.5):

$$D(T)_{gs} = D(T)_0.(2\varepsilon_{100}^3 + 0.04\varepsilon_{100}).\left(\frac{\varepsilon}{\varepsilon_{100}}\right)^{2+3/b} \quad (2.5)$$

where ε_{100} is the air-filled porosity at -1m pressure head and b is the Campbell soil water retention parameter (estimated from the Van Genuchten parameters following Sommer and Stöckle (2010)). $D(T)_0$ is the gas diffusion coefficient in free air and it is calculated from equation 2.6, assuming a constant pressure of 101.3 kPa.

$$D(T)_0 = 1.39 \times 10^{-5}.\left(\frac{T+273.16}{273.16}\right)^{1.75} \quad (2.6)$$

where T (°C) is the soil temperature.

2.2.1.2 Weathering processes

The SoilGen model describes two weathering processes (physical and chemical) as primary mechanisms by which soil is formed from the parent material/saprolite. Properties (e.g., texture, carbon percentage, mineralogy) of the parent material (C-horizon) are assumed as initial conditions at the start of the simulations. These properties will evolve over time as influenced by different soil processes (e.g weathering) and factors ("CLORPT"). Physical weathering is modelled as a function of temperature and it leads to the reduction in grain size consequently producing clay sized material that can be moved by processes such as clay migration. Reduction in particle size also increases surface area thus enhancing dissolution of minerals (chemical weathering). Chemical weathering of primary minerals in the model represents the major source of cations in non-agricultural soils. This process therefore influences soil solution concentrations and equilibrium reactions. Pools of cations (amounts of primary minerals) reduce over time as weathering continues. Physical and chemical weathering processes are described below. For detailed descriptions of these processes, reference is made to Finke and Hutson (2008) and Finke (2012).

Physical weathering

Finke (2012) describes physical weathering as the process "that breaks up soil particles due to strain caused by temperature gradients usually associated with fluctuations in thermal expansion inside the particle, by ice growth or growth of other crystals of larger size than the porosity permits". The net effect of the physical weathering process is a reduction in grain size, consequently producing material in the clay fraction that may be moved by clay migration.

As in Salvador-Blanes et al. (2007), physical weathering in SoilGen is modelled as a probabilistic process with a clear connection to soil temperature gradients in the SoilGen approach. The fine earth fraction is divided into particle size classes with boundaries at 2048-1024-512-256-128-64-32-16-8-4-2 µm (i.e. class boundaries are powers of 2). The major assumption is that all particles are cubes with an edge size halfway between the class limits: 1536, 768, 384, 192, 96, 48, 24, 12, 6, 3, and 1 µm. Therefore, each particle needs to be split in half up to 7 times to obtain 8 equally sized particles in the

next smaller particle size class. The splitting probability of a particle, P_s is assumed to follow Bernoulli process and it depends on the temperature gradient over a certain time interval, dt (Finke, 2012):

$$P_s = \begin{cases} P_{s,max} & if\ \frac{dT}{dt} > B \\ \frac{P_{s,max} \times \frac{dT}{dt}}{B} & if\ \frac{dT}{dt} \leq B \end{cases} \quad (2.7)$$

where, $P_{s,max}$ is the maximal split probability. B is a threshold temperature gradient over dt where $P_{s,max}$ becomes maximal, T is the temperature and $\frac{dT}{dt}$ is also a function of depth (see Eq 2.2). In the study by Finke (2012), $P_{s,max}$ was subjected to calibration while B was fixed to a value of 1 $^{\circ}C\ h^{-1}$.

The expected number E (N) of the potential splitting events required to achieve successful splits, m (i.e., m = 7) are assumed to follow the negative binomial distribution and are described as:

$$\mathrm{E(N)} = \frac{\mathrm{m}}{\mathrm{P_s}} \quad (2.8)$$

Therefore, the number of grains S, in any particle size class i that is split in time dt is calculated as:

$$\mathrm{S_{i,dt}} = \min\left(\mathrm{k_{i,t-dt}}, \mathrm{k_{i,t-dt}/E(N)}\right) \quad (2.9)$$

where, $k_{i,t\text{-}dt}$ represents the number of grains in particle size class at the start of dt and $k_{i,t}$ is described as:

$$\mathrm{k_{i,t}} = \mathrm{k_{i,t-dt}} - \mathrm{a} \times \mathrm{S_{i,dt}} + \mathrm{b} \times 8 \times \mathrm{S_{i-1,dt}} \quad (2.10)$$

where, a = 0 for clay fraction (i = 11) and a = 1 else; b = 0 for the coarsest sand fraction (i = 1) and b = 1 else (Finke, 2012).

The breakup of bedrock (e.g. by plant roots) and the splitting of gravel-sized particles is not yet included in the description of physical weathering, this currently limits application of the SoilGen model to unconsolidated, non-gravelly deposits.

Chemical weathering of primary minerals

In SoilGen, anorthite, chlorite, microcline and albite primary minerals are taken as major pools of Ca, Mg, K, and Na, respectively. The weathering flux, FX ($mol_c ha^{-1} y^{-1}$) of cation X from the primary mineral into the soil solution is described as in (Kros, 2002):

$$FX = \rho \times T \times kX \times (\theta cH)^{\alpha(X)} \times cX \quad (2.11)$$

where ρ is dry soil bulk density (kg m^{-3}), T is soil compartment thickness (m), kX is a weathering rate constant (m^3 mol_c^{-1} y^{-1}) for cation X, cH is the hydrogen concentration (mol_c m^{-3}), θ is water content (m^3 water m^{-3} soil), a modification introduced in SoilGen to convert hydrogen concentration to volume basis (i.e. mol_c H m^{-3} soil), α(X) is dimensionless and it is a parameter describing the effect of pH on weathering rate, and cX is the content of element X in the primary mineral (mol_c kg^{-1}).

Congruent weathering of anorthite, chlorite, microcline and albite is used to model the weathering flux of Al (FAI) from primary minerals (Kros, 2002; Finke, 2012):

$$FAl = 3FCa + 0.6\,FMg + 3FK + 3FNa \quad (2.12)$$

2.2.1.3 Clay migration

The clay migration process is described by detachment, dispersion, transportation and filtering sub-processes. The process is initiated at the surface by splash detachment that brings part of the clay in the top soil compartment in the transportable state. Mechanical impact and low solute concentration of raindrops both bring clay in a transportable state at the soil surface. At any depth in the soil, clay can be dispersed when the solute concentration falls below a threshold value, and then also enters a transportable state. Thus, the clay migration process starts at the surface, but it can occur at any depth of the soil profile depending on the solute concentration (Finke, 2012). Splash detachment is modelled based on the approach of Jarvis et al. (1999) but modified by Finke (2012) to include the reducing effect of a humus profile and a vegetation cover on splash detachment and the effect of bioturbation on redistribution of clay.

Thus, at the surface the mass balance of dispersible particles is computed as:

$$\frac{dA_s}{dt} = -D + P \tag{2.13}$$

where, A_s is the mass of dispersible particles at the soil surface (g m^{-2}), D and P represent the splash detachment rate (g m^{-2} h^{-1}) and the replenishment rate (g m^{-2} h^{-1}), respectively.

A_s is a function of cation exchange capacity (CEC), clay fraction and organic carbon (OC), (Equation 2.14). The maximal dispersible clay, DC_{max} (%), is first calculated based on the regression equations of Brubaker et al. (1992):

$$DC_{max} = \begin{cases} 0.635 \times clay \;\; if \;\; (CEC - 3 \times OC)/clay \leq 0.4 \\ 0.340 \times clay \;\; if \;\; (CEC - 3 \times OC)/clay > 0.4 \end{cases} \tag{2.14}$$

The parameter $A_s$is finally calculated as:

$$A_s = DC_s \times \; \rho \times 0.01 \tag{2.15}$$

where, DC_s (g g^{-1} soil) is the amount of readily available dispersible particles at the soil surface (1 mm) with its initial value set equal to DC_{max}, ρ is the dry soil bulk density (Kg m^{-3}) and 0.01 is the unit conversion factor.

The parameter, D in equation 2.13 is computed for each rainfall event as follows:

$$D = k_d \times E \times R \times (1 - sc) \times \; DC_s \tag{2.16}$$

where k_d is the soil detachability coefficient (g J^{-1}) and it was set to the value of 15 by Jarvis et al. (1999) during calibration. sc is the dimensionless parameter accounting for the fraction of the soil surface that is covered by vegetation or the humus profile. R (mm h^{-1}) is rainfall intensity, and E (J m^{-2} mm^{-1}) is kinetic energy of the rainfall obtained from relation described in the revised universal soil loss equation (Brown and Foster, 1987):

$$E = 29 \times \{1 - 0.72 \times \exp(-0.05 \times R)\} \tag{2.17}$$

The replenishment rate, P in equation 2.13 is estimated following the procedure of Jarvis et al. (1999):

$$P = k_r \times \left(1 - \frac{DC_s}{DC_{max}}\right) \quad (2.18)$$

where k_r is the replenishment rate coefficient (g m^{-2} h^{-1}) set to the value 0.1 as calibrated by Jarvis et al. (1999). In SoilGen, the value of P is restricted such that it does not exceed the amount present in the surface 1 mm layer after bioturbation (Finke, 2012).

The proportion of clay that is in a transportable dispersed state, fDC in every soil compartment is a function of the total electrolyte concentration, SC ($mmol_c$ dm^{-3} water) and critical salt concentration, CSC ($mmol_c$ dm^{-3} water) at which soil clay mixtures stay flocculated. SC and CSC are computed each time step and their threshold values are evaluated. The transportable dispersed clay then follows the CDE that is modified to include filtering as an additional sink term:

$$fDC = \{1 - (\mathrm{SC}/\mathrm{CSC})\} \times \theta_{macro} \times fVC \quad (2.19)$$

where, θ_{macro} is the volumetric water fraction (m^3m^{-3}) in macro-pores and it is estimated from the water retention curve at pressure head h (hPa) near saturation. fVC is the fraction of soil volume taken by clay. The parameter SC is estimated by the model every time step and CSC (Eq. 2.20) is determined by the model (Finke, 2012) using simulated soil parameters (Sodium adsorption ratio, SAR and pH), and a regression relation (based on the experimental data (measured CSC at various levels of measured SAR, pH and clay mineralogy composition) from Goldberg and Foster (1990).

$$CSC = [b_1 \times (M + I) + b_2 \times SAR + b_3] \times exp\,[b_4 \times (b_5 \times M + b_6 - pH)^2] \quad (2.20)$$

where, $b_1,\ b_2, \ldots . b_6$ are non-linear regression coefficients and, M and I are proportions (%) of montmorillonite and illite minerals, repectively. In the SoilGen model, except for SAR and pH which are recalculated each timestep, all the regression parameters in Eq. 2.20 are given to the model as constants (Finke, 2012).

The filtering process (e.g. entrapment of clay particles in small pores) is modelled based on calculated pore water velocities using the equation given in Jarvis et al. (1999):

$$F = f_{ref} \times v_{ref}^{n} \times v^{1-n} \times c \times \theta \quad (2.21)$$

where, f_{ref} (m^{-1}) is a reference filter coefficient, v_{ref} (m h^{-1}) is the pore water velocity at which f_{ref} is measured of which values of 2 m^{-1} at 0.1 m h^{-1} were taken from Jarvis et al. (1999) and used in SoilGen. The parameter *v* is the current pore water velocity and, *c* and *n* represent the particle concentration (g m^{-3} water) and an empirical exponent, respectively. In SoilGen, *c* is a vector containing the dispersible and transportable clay calculated using equation 13. This parameter also contains the associated exchangeable cations i.e., Ca, Mg, Na, K, H and Al (Finke, 2012).

2.2.1.4 Cation exchange capacity

The dynamics in soil cation exchange capacity (CEC) (e.g. due to clay migration and variation in organic matter content) is simulated using a 2-domain CEC model. The initial total CEC is partitioned into two: (1) portion attributed to the mineral fraction and (2) portion attributed to the initial soil organic carbon, OC (i.e., the amount of carbon in the parent material at the start of the simulation). The regression equation by Foth and Ellis (1996) based on the 12000 data sets, is used to determine the percentage contributions of OC (%) and clay (%) to the total CEC ($mmol^{+}$ kg^{-1}):

$$CEC = f \times (32 + 36.7 \times OC + 1.96 \times Clay) \quad (2.22)$$

where f is a factor matching the empirical CEC after Foth and Ellis (1996)to the initial CEC in the simulated pedon. The intercept (32 $mmol^{+}$ kg^{-1}) in the regression equation accounts for cation exchange sites at particles larger than 2 µm, and may be also due to the choice of a linear regression model by Foth and Ellis (1996). Equation (2.22) is based on analytical data collected by Foth and Ellis (1996), where clay is defined as the fraction less than 2 µm. However, grain sizes slightly larger than 2 µm may still contribute to the CEC because there are exchange sites on the mineral surface, but will not be correlated to clay (%) and thus become part of the intercept of the regression equation. Additionally, the intercept may be the result of analytical errors or values of clay and OC near the

laboratory detection limit. According to Finke (2012), this approach is a simplification of reality as the possible effect of pH change on CEC is not accounted for.

2.2.1.5 Soil chemical system and chemical equilibria

Five phases (i.e. solution, precipitated, exchange, organic and unweathered phases) are categorized in the SoilGen model chemical system (Figure 2.1). Dissolution of primary minerals (unweathered phase), decomposition of organic matter, atmospheric depositions and addition through fertilizers are considered as major processes through which ions are released into the soil solution. Uptake by plants, leaching and precipitation are processes through which these species leave the soil solution phase.

The soil solution phase is brought into equilibrium with precipitated and exchange phases by satisfying various solubility laws and rate constants that include: (1) Henry's Law constant for CO_2, (2) the dissociation constant of H_2CO_3, (3) the dissociation constant of H_2O, (4) the solubility constants of gypsum, calcite and gibbsite, (5) ion pair stabilities constants of different species in the soil solution and (6) Gapon selectivity constants for exchange/solution phase equilibriums for Ca-Mg-Na-K-H-Al. Instantaneous equilibrium is assumed because calculations are repeated at small time steps (usually a fraction of a day), with small water fluxes during those time steps, and so changes in chemical composition are expected to be gradual. Generally, the equilibration is done repetitively in 4 steps as described in detail by Finke and Hutson (2008), taking into account Arrhenius' temperature correction of all chemical constants.

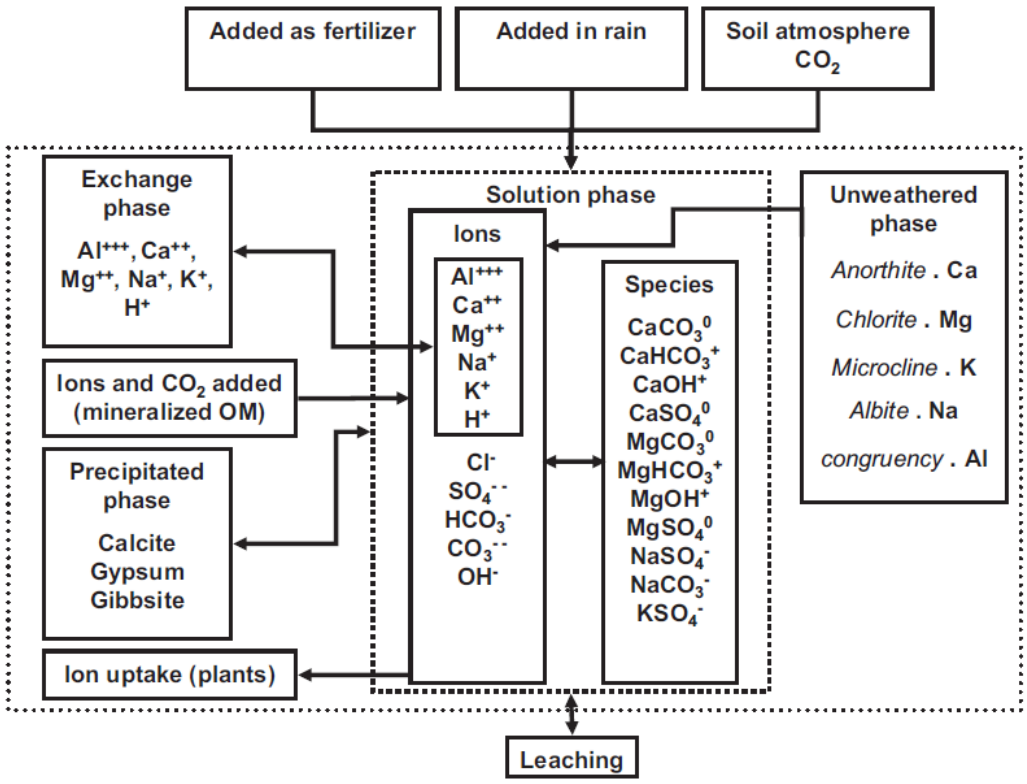

Figure 2.1. Soil chemical system simulated by SoilGen (Source: Finke, 2012)

2.2.1.6 Vegetation, carbon cycling and plant uptake processes

The interaction between the soil and the vegetation in SoilGen, occurs mainly through annual litter input, carbon cycling and ion uptake (Figure 2.2), and these depend on the vegetation type. Four vegetation types are distinguished (grass/scrub, agriculture, conifers and deciduous wood). Each of these vegetation types is characterized by a unique rooting density function, cation uptake, carbon decomposition rates and annual leaf and root litter input (Finke and Hutson, 2008).

Carbon cycling is simulated following the concepts of the RothC 26.3 model (Jenkinson and Coleman, 1994) where dead plant material is split into leaf litter and root litter. The root litter is further subdivided into resistant plant material (RPM) and decomposable plant material (DPM) (Figure 2.2). Both RPM and DPM fractions degrade into microbial biomass (BIO), humus (HUM) and CO_2 at rates determined by the fraction that is decomposing as well as environmental factors like soil temperature, soil moisture deficit, soil cover fraction and the time increment (Finke and Hutson,

2008). The CO_2 produced at each time step (i.e. daily in SoilGen) enters into the gas regime equation (Eq. 2.4). The distribution of CO_2 in the soil profile at the end of each day gives values of partial CO_2 (pCO_2) for the chemical equilibria of that day. Additionally, ions taken up by the plants follow the same decomposition pathways and are eventually released again in the solution phase (Finke and Hutson, 2008).

Cation (Al, Ca, Mg, Na, and K) uptake by vegetation is assumed to occur via the transpiration stream by preferential uptake to reflect the relative fractions of those elements measured in the plant. Therefore, each vegetation is characterized by a target content of these cations. Relative concentrations of Al, Ca, Mg, Na, and K for four vegetation types considered in SoilGen have been published (Finke, 2012, Table 2). The computation of cation and anion uptake in each soil compartment then follows a step by step procedure described in Finke and Hutson (2008).

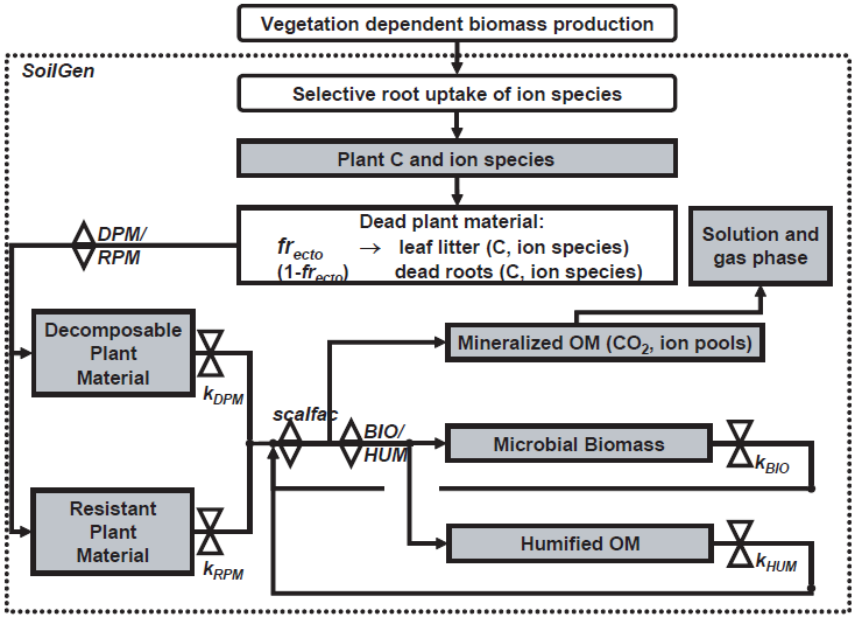

Figure 2.2. Carbon cycling process as described in SoilGen (Source: Yu et al., 2013). Grey boxes represent carbon pools, ⧗ and ◊ indicate rate and distribution factors, respectively. The dotted line represents the process boundary.

2.2.1.7 Soil phases redistribution processes

In addition to physical weathering and clay migration processes described earlier, SoilGen considers bioturbation, tillage, erosion, sedimentation and, dissolution and precipitation of calcite and gypsum as other processes that lead to redistribution of soil phases (solid and liquid) in the soil profile. When simulating these redistribution processes, the central assumption of constant volume of each compartment with time is made. This is a simplification of reality because soil volume may increase in response to biological processes like burrowing of animals or collapse as a result of processes like decalcification and clay migration. In the terminology of Brimhall and Dietrich (1987) collapse corresponds to a strain of <0 and expansion to a strain >0, and the SoilGen model assumes a strain = 0. The errors introduced by this simplification may not directly affect the calculated mass percentages, but may have influence on some soil physical properties such as bulk density (Finke and Hutson, 2008).

Bioturbation is described as an incomplete mixing process. First, the fraction of the mass subject to vertical redistribution by soil meso- and macro-fauna in each compartment is determined. This fraction is an input in SoilGen and it is made to vary over time with respect to vegetation, climate and soil depth (Finke and Hutson, 2008). The input mass fraction is used to vertically mix and redistribute soil masses to the bioturbated soil compartments (each compartment thickness is set to 50 mm). Secondly, the resulting mass in each compartment, consisting partly of a bioturbated mixture and partly of the original content, is horizontally (1x1 m area) mixed within the same compartment. This gives a new set of soil properties per soil compartment (Finke and Hutson, 2008). In addition, the effect of tillage is considered as an extreme form of bioturbation, where the mass fraction involved in the turbation is set to 50% over the plowing depth as determined by Ullrich and Vork (2009).

Erosion and sedimentation processes are currently implemented as inputs to the SoilGen model. In essence erosion and sedimentation processes respectively remove and add entire soil compartments at the surface of the soil profile. Rates (Mg ha^{-1} y^{-1}) of erosion or deposition are needed as input to the model and this holds also for the composition of the added sediment.

2.2.1.8 Coupling the effect of slope/exposition on precipitation and evapotranspiration

To model the effect of relief ('R' factor) on soil formation, precipitation and evaporation inputs are corrected for slope and exposition in SoilGen. First the wind speed in the direction of the slope, V_2 (m s^{-1}) is calculated (Eq 2.23) based on the approach by Mauersberger (2001). V_2 together with the mean fall velocity of raindrops, v_r (set to 5 m s^{-1} in SoilGen: Finke, 2012) are used to calculate the diversion angle, β (degrees) from the vertical rainfall induced by wind (Eq 2.24). Finally, the net amount of rainfall, R_2 (mm) on a unit sloped area is obtained by correcting the precipitation at the horizontal plane for slope angle, diversion angle and the bearings of these two angles (Equation 2.25) (Finke, 2012).

$$V_2 = V_1 \times \cos(\delta - \gamma) \tag{2.23}$$

where, V_1 is the wind speed in wind direction, δ and ϒ are the upslope bearing and the wind bearing (in degrees), respectively.

$$\beta = \mathrm{abs}\left(\arctan\left(\frac{V_2}{v_r}\right)\right) \tag{2.24}$$

$$R_2 = R_1(1 + \tan(\beta) \times \tan(\alpha)) \times \cos(\delta - \gamma) \tag{2.25}$$

where, R_1(mm) is the precipitation at the horizontal plane.

Net potential evapotranspiration PE_{net} is obtained by correcting the measured potential evapotranspiration PE_m for latitude, slope angle and slope azimuth. This is done with the assumption that potential evapotranspiration responds linearly to differences in incoming radiation for different slopes. The correction factor is therefore the ratio between the potential solar radiation on a horizontal surface at given latitude, summarized for one year, and the potential solar radiation on a slope with upslope bearing converted to map area for the same period (Finke, 2012). This ratio is calculated with an implementation of an algorithm developed by Swift (1976).

2.2.1.9 Process order and temporal scales

The SoilGen model simulates soil forming processes over a multi-millennium timescale (up to 15000 years). However different soil forming processes operate at different time scales ranging from

milliseconds (e.g., transport processes) to thousands of years (e.g., weathering) and this has to be taken care of. The process order and temporal scale as simulated in the SoilGen model are summarized in (Figure 2.3). Heat flow and physical weathering are calculated at hourly time steps. Chemical and transport processes are calculated at time steps of milliseconds to hours, while mineral weathering and organic matter accumulation are calculated at daily time steps. Events such as bioturbation, erosion/sedimentation and fertilization are incorporated in the model at yearly time steps. All the outputs are however reported after every one year. More description of the SoilGen model temporal scales and processes time steps is given in Finke and Hutson (2008) and Finke (2012).

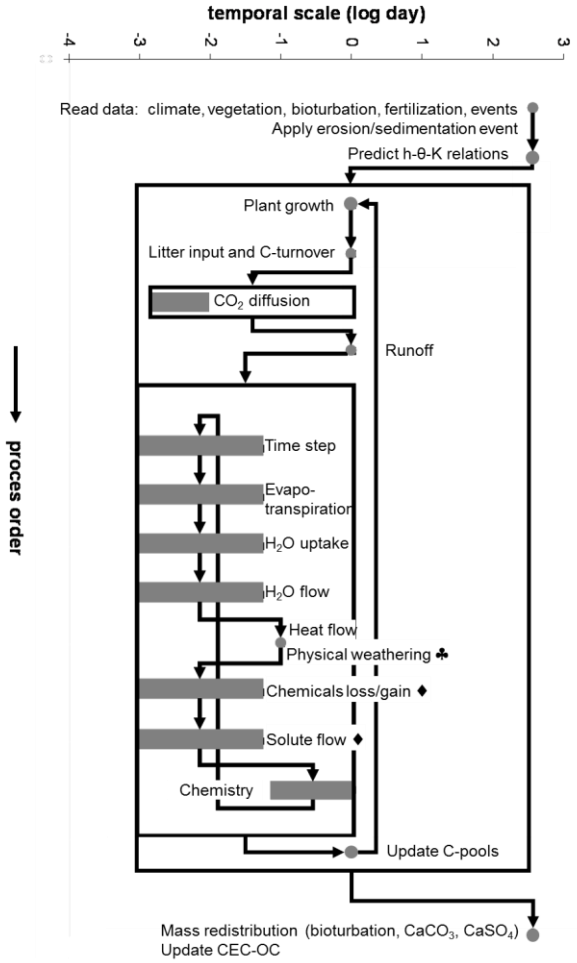

Figure 2.3. Process order and temporal scales (solid boxes or dots) of the sub-processes as simulated in SoilGen2 within each year. Open boxes represents processes repeated daily during each year. (Source: Finke, 2011; Finke, 2012).

2.2.2 SoilGen data input

Factors of soil formation ('CLORPT') are linked to SoilGen as input parameters (Table 2.2). These inputs can be introduced as initial conditions (IC) or boundary conditions (BC). Some of these inputs (e.g. soil temperature, texture, OC) are also simulated/updated (SIM) within the model for use in the next time steps (Table 2.2). Initial conditions specify the soil (or sediment) at the start of the simulations, and properties are usually taken from C-horizons of analysed soils. Properties at the end of the simulations can be compared to soil analysis for model calibration or validation. Slope and wind direction are input to assess the effect of local topography on precipitation and potential evapotranspiration. The other data input (e.g. bioturbation, erosion and sedimentation) is required if the effects of such factors are to be investigated. These are therefore not mandatory and may not be introduced to the model. The factor time ('T', not shown in the table) is captured in the model by constant updating of all the other input parameters based on the time steps. We summarize in Table 2.2, the basic data input to the SoilGen model, indicating whether it is mandatory or not. Temperature and potential evaporation are introduced into the model as weekly averages while daily values are needed for precipitation. Vegetation type, litter/manure, bioturbation, erosion and sedimentation are all annual inputs to the model. In addition, other detailed soil profile information (e.g. soil texture, bulk density, pCO_2, BS, CEC, moisture content) is necessary for model calibration and validation. Furthermore, additional constants need to be provided to complete the description of some processes (Table 2.3). These constants are currently given as default values in SoilGen and are only adjusted during calibration. The user may change these values whenever necessary.

2.2.3 SoilGen model calibration and quality tests

Calibrating a model entails a systematic process of modifying the input parameters to a model until the best match between model simulations and observations is obtained (Yu et al., 2013). The calibration process can also be done by reproducing observed values already observed in literature. The usual way to calibrate the model is to identify sensitive parameters (sensitivity analysis) as a first step. Due to large runtimes and many processes described, calibration in SoilGen has followed a step by step procedure in which processes have been calibrated independently. Processes that have been calibrated in SoilGen include physical weathering in combination with clay migration (Finke, 2012),

decalcification (Finke and Hutson, 2008; Finke, 2012; Zwertvaegher et al., 2013) and carbon cycling (Yu et al., 2013). In most cases, calibration compared the simulated final state of the soil to present measurements. Calibration focused on process parameters and not on the initial conditions or boundary conditions along the time line, although these are also associated with uncertainty. We briefly describe each of the approaches followed in calibrating these processes.

Table 2.2. Basic data input to the SoilGen model. IC = initial condition, BC = boundary condition and SIM = simulated input.

Soil forming factor	Input parameter	Units	Condition	Mandatory
Climate	Air temperature	°C	BC, SIM	Yes
	Precipitation	mm y^{-1}	BC	Yes
	Potential evapotranspiration	mm y^{-1}	BC	Yes
Organisms	Vegetation type	-	BC	Yes
	C-input (litter, organic manure)	1000 kg ha^{-1} y^{-1}	IC	Yes
	Bioturbation	1000 kg ha^{-1} y^{-1}	BC	No
	Erosion/Sedimentation	1000 kg ha^{-1} y^{-1}	BC	No
Relief	Slope	°	IC	Yes
	Slope exposition	°	IC	Yes
	Wind direction	°	IC	Yes
Parent material	Clay/Silt/Sand	Mass %	IC, SIM	Yes
	OC	Mass %	IC, SIM	Yes
	Ca, Mg, Na, K, Al, SO4, Cl, Alkalinity in solution	mmol dm^{-3}	IC, SIM	Yes
	Ca, Mg, Na, K, Al, H on exchange complex and CEC	mmol^{+} kg^{-1}	IC, SIM	Yes
	$CaCO_3$ / $CaSO_4$	Mass %	IC, SIM	Yes
	Gapon exchange coefficients	mol dm^{-3}	IC, SIM	Yes
	Ca, Mg, Na, K, Al in primary minerals	mol^{+} kg^{-1}	IC, SIM	Yes
	Release rate of cations (Ca, Mg, Na, K, Al) from mineral weathering	m^3 $molc^{-1}$ y^{-1}	IC	Yes
	Parameter describing effect of pH on mineral chemical weathering rate	-	IC	Yes

Table 2.3. Additional input parameters required to describe some soil processes in SoilGen. DPM and RPM = decomposable and resistant plant material, respectively. BIO = microbial biomass and HUM = humus

Soil process	Input parameter	Units
C-cycling	DPM/RPM ratio	-
	Fraction of litter that is from leaf (per vegetation type)	-
	Fraction of litter that is from root (per vegetation type)	-
	Fraction of precipitation that is intercepted (per vegetation type)	-
	Decomposition rate constants of DPM, RPM, BIO and HUM	h^{-1}
	Distribution ratios (BIO/HUM and CO_2 / (BIO+HUM))	-
Physical weathering	Maximum splitting probability	-
	Temperature gradient where splitting probability becomes maximal	$°C\ h^{-1}$
Clay migration	Soil detachability coefficient	$g\ J^{-1}$
	Replenishment rate coefficient	$g\ m^{-2}\ h^{-1}$
	Pressure head at which macro-pores are empty	hPa
	Filtering coefficient	-
	Reference filter coefficient, fref	m^{-1}
	Pore water velocity at which fref is measured	$m\ h^{-1}$
	Bulk density of ectorganic layers	$kg\ dm^{-3}$
	Thickness of ectorganic layer at which no splash occurs	mm
	Montmorillonite content in clay fraction	%
	2:1 clay mineral content	%

2.2.3.1 Physical weathering and clay migration

The maximal physical weathering factor (P_s), filtering factor (n) and hydraulic head at which macro-pores empty (h) were the parameters identified for calibration of the physical weathering and clay migration processes. The calibration was done by adjusting these parameters to match the profile texture distribution (Finke, 2012). The test model runs were first done to identify the possible range of each of the 3 parameters. The model was run for 14 different combinations of P_s, n and h parameters. Each time the model outputs were confronted with the observations to quantify accuracy of the simulations. Then, a polynomial function was fitted that predicts the simulation

accuracy as a function of the parameter values of P_s, n and h. The position in parameter space with optimal simulation was predicted by analysing the partial derivatives of the fitted polynomial function. The found parameter combination is then tested with one more simulation to check if this combination does give the best results. According to Yu et al. (2013), this approach is suitable for long runtime models like SoilGen, but it may not find the true optimal parameter set. Calibration tests (Figure 2.4 a) showed that clay percentage distribution over depth was quite well reproduced. The model however underestimated clay percentage (i.e. predicted very strong clay eluviation) at the top layer (0 – 40 cm). This mismatch was attributed to the probable underestimation of physical weathering (Finke, 2012).

2.2.3.2 Carbon cycling

The SoilGen carbon module was calibrated for the Belgian loess soils under permanent deciduous forests and for the Chinese loess soils under secondary deciduous forests (Yu et al., 2013). Prior to calibration, Yu et al. (2013) performed a sensitivity analysis (SA) following Morris (1991) method. They identified decomposition rate factors of humus (k_{Hum}) and RPM (k_{RPM}), and the fraction of incoming plant material in form of leaf litter (fr_{ecto}) as the three most sensitive parameters. Because of long runtime, Yu et al. (2013) preferred another approach of minimizing the difference between measurements and simulations. Their calibration method involved calibrating each of the three identified sensitive parameters step by step starting with the most sensitive parameter. A possible range for each parameter was determined during SA and parallel tests were done. For each test, simulated results were confronted with measurements and evaluated based on model quality indicators like root mean square error (RMSE), mean difference (MD) and dissimilarity (DIS). The calibration of a given parameter was completed whenever the best result was < 5% better than the second best. Their calibration results were consistent with previous studies and indicated that the calibrated SoilGen carbon module was able to reproduce measured carbon vertical distribution over time (Figure 2.4 b).

2.2.3.3 Decalcification rate

The decalcification process influences a number of soil properties including porosity, bulk density, cation content, pH and indirectly also water flow. It is therefore an important process that should be accurately constrained to minimize uncertainty in model results. Previous studies (Finke and Hutson, 2008; Finke, 2012; Zwertvaegher et al., 2013) have followed a similar calibration approach in which the dissolution constant of calcium carbonate (k_{SO}) was adjusted to match the decalcification speed values reported in Egli and Fitze (2001) based on an extensive field data set. In principal, the number of years needed to decalcify the upper 1100 mm of standard loess soil were calculated and compared with the value based on the study of Egli and Fitze (2001). The comparison was repeated for different values of k_{SO} and at a precipitation surplus of 472 mm yr^{-1} (Finke, 2012) or 247 mm yr^{-1} (Zwertvaegher et al., 2013). The k_{SO} with the best comparison was selected and then checked against values from Egli and Fitze (2001) for different precipitation surpluses. Calibration test results (Zwertvaegher et al., 2013) indicated that the SoilGen model reproduced the decalcification process with good accuracy at high and extremely very high precipitation surpluses but overestimation of decalcification was observed at low precipitation surpluses. This is partly based on the fact that the Egli and Fitze (2001) data set includes few low precipitation surpluses. Finke and Hutson (2008) and Finke (2012) also reported good agreement between Egli and Fitze (2001) results and SoilGen simulations (Figure 2.4 c). Best $\log_{10}$ k_{SO} values of –9.2 (Zwertvaegher et al., 2013) and -8.36 (Finke, 2012) were reported for precipitation surpluses of 247 mm yr^{-1} and 472 mm yr^{-1}, respectively (in sandy and silt loam soils, respectively).

2.2.3.4 Degree of leaching

In calibrating the degree of leaching, the fraction of rain intercepted by vegetation (P_{int}) was considered as the main factor influencing water percolation. The calibration approach involved adjusting P_{int} to match the measured values of base saturation (BS %), CEC and pH (Finke, 2012). Results showed fairly good estimation of CEC (Figure 2.4 d) but base saturation, BS % (Figure 2.4 e) and pH (Figure 2.4 f) were poorly estimated.

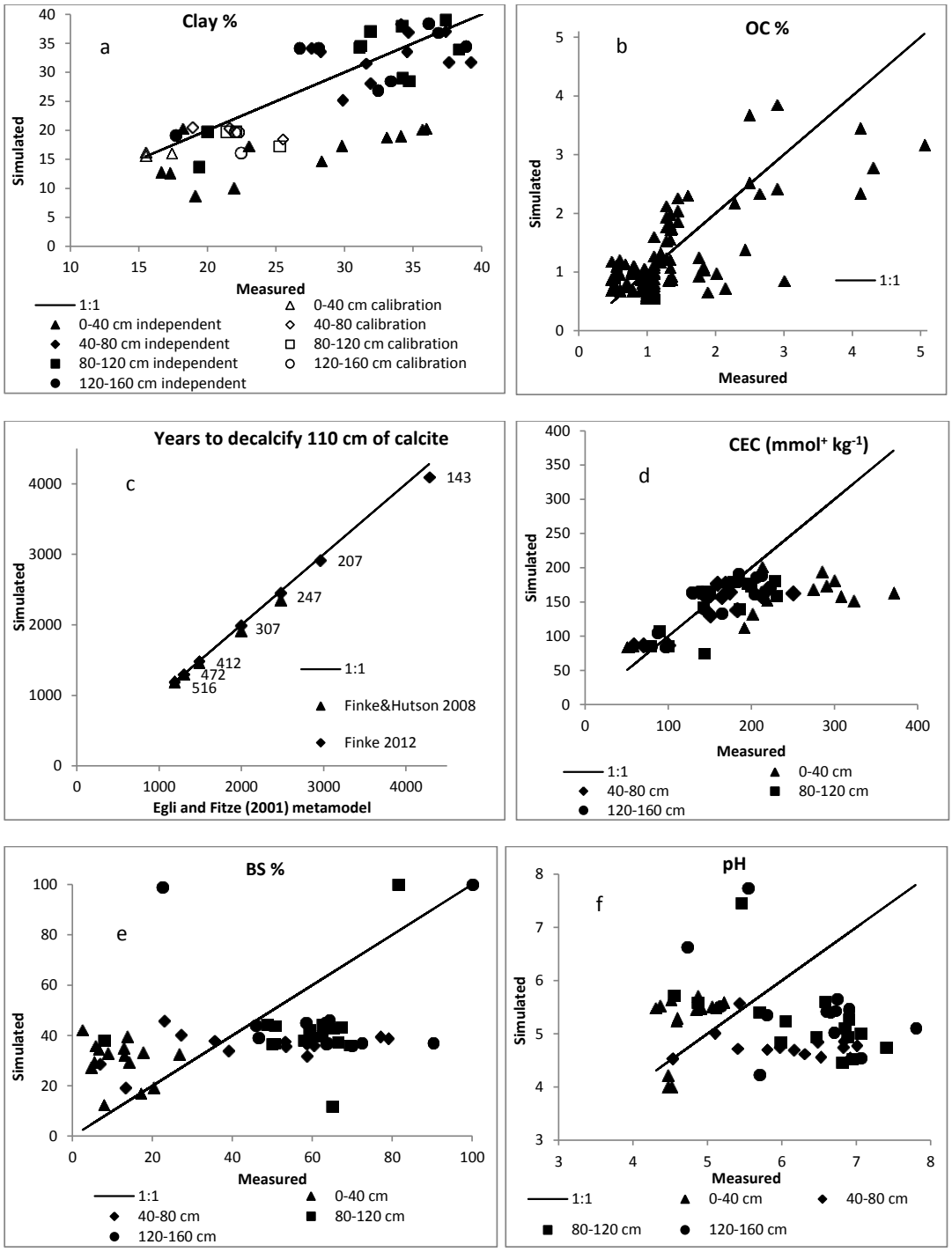

Figure 2.4. SoilGen calibration tests for (a) clay migration (b) carbon cycling (c) decalcification and (d, e, f) degree of leaching. Measurements of OC were obtained from 6 different locations with sampling done at 5 cm interval for a depth 0 – 100 cm. Notice quite good simulations for clay percentage, carbon percentage, decalcification rate and CEC but poor results for BS and pH.

2.2.4 SoilGen model field applications, limitations and future perspectives

2.2.4.1 Pedon scale applications

Finke and Hutson (2008) applied SoilGen to study the effect of varying climate on the formation of calcareous loess soils in Belgium and Hungary. The effects of bioturbation, vegetation and agriculture on soil formation from uniform calcareous loess parent material were also tested for the two areas. Calibration of decalcification rate was done prior to model application. Simulated soil properties included OC, calcite content, bulk density, clay dispersion indicator and pH. Results from this study demonstrated that decarbonisation of the upper 1.2 m was completed in less than 2000 years under the Belgian leaching climate compared to the drier climate of Hungary in which decarbonisation process was slow. In addition the clay migration process was more pronounced in the leaching climate of Belgium as compared to Hungary. Bioturbation slowed down the decarbonisation processes by bringing sufficient calcite to the soil surface while keeping the pH high (Finke and Hutson, 2008). Agriculture through liming increased the calcite content in the soil, increased the soil pH and slowed down the clay migration process. Vegetation type influenced the distribution of exchangeable cations (e.g. K). Furthermore, Finke and Hutson (2008) observed that cations concentrated in the topsoil when deciduous wood vegetation persisted but leached quickly when agriculture started. In general, their study demonstrated that the SoilGen model can be used to simulate the effect of climate, vegetation and organisms on soil formation processes and properties.

An independent SoilGen model quality test was done by Sauer et al. (2012). Their study was aimed at testing how well soil development would be described by the SoilGen model. Against this background, observed soil properties from two chronosequences (12 soil profiles in total) in marine sediments of Southern Norway were compared with SoilGen simulated soil properties. Results from this study indicated that the SoilGen model simulated clay content and particle size distribution reasonably well. For example, deviation of modelled clay content from measured clay content from 12 soil profiles was between -8 % to 4%. However, there was underestimation of OC, CEC, BS and pH, and over estimation of clay depletion especially in the upper part of the soil profiles as reported in Sauer et al. (2012: Table 6). The overestimation of leaching in the topsoil was explained by the fact that formation of preferential flow structures (e.g. due to ripening) is unaccounted for by SoilGen. Overall, Sauer et

al. (2012) concluded that the SoilGen model was capable of simulating soil development as a function of time.

Finke (2012) has applied SoilGen to model soil formation as a function of relief. The studied soil profiles were taken from 3 topographic positions of soil loess cover in the Zonian forest (Belgium). Input parameters to the model were the same for 3 topographic positions except for precipitation and evapotranspiration that had to be corrected for exposition and slope. Calcite dissolution rate, clay migration and physical weathering processes were first calibrated following procedures described in the earlier sections. The model simulations after 15000 years before present were confronted with field measurements of 3 topographic points. Results show that, the model was able to reproduce measured soil properties such as OC %, sand % and CEC. The model was also able to estimate the development of A, E and Bt horizons in response to sedimentation, bioturbation, physical weathering and clay migration soil forming processes. Base saturation and calcite content were however generally over estimated by the model most likely due to poor estimates of surplus precipitation, non-homogeneous initial calcite content and variations in initial bulk density (Finke, 2012).

Application domain: World Reference Base - Reference Soil groups

Table 2.4 shows which diagnostic horizons, properties and materials according to the World Reference Base (WRB; IUSS Working Group WRB, 2006) can be identified using the soil properties simulated by SoilGen2.16. As a consequence, Table 2.5 shows the application domain of SoilGen in simulating the genesis of typical features (excluding morphological features) of World Reference Base - Reference Soil groups (RSG). With the processes and chemistry currently described in SoilGen (i.e. clay migration, texture, CEC, BS, Al-chemistry), the millennium-scale genesis of typical features of 15 RSG can be simulated (Table 2.5). By extending the weathering and chemical systems of SoilGen (e.g. adding Fe and Si, mineralogy), the genesis of typical features of 9 more RSG can be simulated (Table 2.5). In total, SoilGen has a potential to simulate soil forming processes of up to 24 out of 32 RSG. Simulating the genesis of typical features of the remaining 8 RSG however remains a challenge due to the complexity of the processes involved. For example, simulation of Podzolisation process (Podzol RSG) requires describing the Al, Fe and OC complexation process, leaching of these complexes and the effects of soil micro- and mesofauna on humus breakdown (Table 2.5), which is currently difficult to

implement in SoilGen. Technosols have a wide range of chemical and physical properties e.g. the effects of stoniness that currently cannot be simulated by SoilGen. Worthy to note here is that the model is not designed for application in acid sulphate soils as well as stony/gravely soils and thus RSG with such features may not be simulated.

Table 2.4. Diagnostic horizons, properties and materials that can be inferred from SoilGen2.16 outputs. Morph=morphological properties; w.m.=weatherable minerals; min.=mineralogy; "waived" indicates those properties that matter for classification but are not essential. Petro* = petrocalcic, petroduric, petrogypsic and petroplinthic

Diagnostic horizons		Diagnostic properties	
Inferable (waived)	Not inferable (cause)	Inferable (waived)	Not inferable (cause)
Anthric	Albic (color)	Abrupt textural change	Albeluvic tonguing (morph)
Argic	Anthraquic (morph)	Aridic properties (color)	Andic (min.)
Calcic	Cambic (color, structure)	Ferralic properties	Continuous hard rock
Cryic	Duric (Si)	Secondary carbonates	Geric (δpH, ECEC)
Folic	Ferralic (w.m.)		Gleyic color pattern (morph)
Gypsic	Ferric (color)		Reducing conditions (Fe, morph)
Histic	Fragic (slaking)		Stagnic color pattern (morph)
Irragric	Fulvic (min.)		Vertic (COLE, morph)
Mollic (color)	Hortic (P)		Vitric (min.)
Natric (structure)	Hydragric (Fe, Mn)		
Plaggic	Melanic (min.)	Diagnostic materials	
Salic	Nitic (Fe)	Not inferable (cause)	Not inferable (cause)
Umbric (color)	Petro*	Gypsiric material	Artefacts
	(Piso)plinthic (Fe, morph)	Mineral material	Colluvic material (morph)
	Sombric (color)	Organic material	Fluvic material (morph)
	Spodic (color, Fe)		Limnic material
	Takyric		Ornithogenic material (P)
	Terric (morph)		Sulphidic material (S)
	Thionic (S, min.)		Technic hard rock
	Vertic (morph)		Tephric material (min.)

Table 2.5. World Reference Base - Reference Soil Groups (RSG) that can (not) be simulated in SoilGen

RSG-simulation, few limitations	Soil forming process [1]	Limitations (not simulated)
Cryosols	cryoturbation	cryoturbation morphology
Solonetz	solonization, solodization	columnar structure
Solonchaks	salinization	S and non-halite minerals
Chernozems	melanization	color
Kastanozem	melanization, calcification	color
Phaeozems	melanization (argilluviation)	color
Gypsisols	calcification	cementation
Calcisols	calcification	cementation
Alisols	argilluviation, base cation leaching	clay neo-formation
Acrisols	argilluviation, ferrallitization	clay neo-formation (simulation time)
Luvisols	argilluviation, biological enrichment of base cations	clay neo-formation
Lixisols	argilluviation, biological enrichment of base cations	clay neo-formation (simulation time)
Umbrisols	melanization	
Arenosols	very weak soil formation	
Regosols	very weak soil formation	
RSG- simulation feasible		Processes /chemistry to include (limitations)
Anthrosols	anthrosolization	P, Fe, Mn
Leptosols	very weak soil formation	soil production from hardrock
Fluvisols	very weak soil formation	physical ripening
Nitisols	argilluviation, ferrallitization	Fe, weathering and clay newformation (structure, simulation time)
Ferralsols	ferrallitization	Fe, Al, weathering and clay newformation (simulation time)
Planosols	gleization, argilluviation	Fe, redox (ferrolysis)
Stagnosols	gleization	Fe (stagnogley morphology)
Durisols	silicification	Si (cementation)
Cambisols	weak soil formation	Fe, weathering (structure)
RSG-simulation difficult		Causes
Histosols	paludization	peat growth and decomposition
Technosols		artefacts, rock and highly varied mineralogy
Vertisols	vertization	argilloturbation process
Gleysols	gleization	gley morphology, Mn
Andosols	andisolization	allophane chemistry
Podzols	podzolization	Al-Fe-OC complexation, migration and biobreakdown
Plinthosols	gleization, podzolization	plinthite morphology and consistence
Retisols	argilluviation	Albeluvic tonguing

[1] Terminology of Bockheim and Gennadiyev (2000)

2.2.4.2 Landscape scale applications

The potential application of the SoilGen model at landscape scale has been demonstrated in recent studies by Zwertvaegher et al. (2013) and Finke et al. (2013). In Zwertvaegher et al. (2013), SoilGen was applied to different point locations (96 profiles) distributed over an area of 584 km^2 in sandy Flanders (Belgium) to reconstruct soil characteristics such as texture, bulk density, OC %, calcite and pH. Calibration of calcite dissolution rate was done as discussed earlier (section 2.2.2.4). The predicted variables were confronted with measurements and generally showed good agreement. Predicted point soil characteristics were then used to produce full cover soil maps at a given period of time using regression kriging techniques. The soil map produced was used in combination with hydrological model, digital elevation model (DEM) and land evaluation model for application in landscape reconstruction and archaeological land evaluation.

Finke et al. (2013) have applied the SoilGen model to simulate variation of soil characteristics (e.g. OC, calcite content and clay content) and soil horizons at landscape scale in the presence and absence of tree uprootings. In their study, they formulated a probabilistic approach to predict the occurrence of tree uprooting in a certain year at pedon scale. Simulations were done at 108 locations for two scenarios: one in which soil formation occurs without the influence of tree uprootings and one with the influence of tree uprootings. To compare with the observed horizons, simulated soil characteristics at present year were converted to horizon thicknesses following a protocol developed using measured and simulated soil data (Finke et al., 2013). Regression kriging was then used to produce spatial soil-landscape relationship using an approach similar to that of Vanwalleghem et al. (2010). Their findings indicate that including tree uprooting events in the SoilGen model better explains spatial patterns of horizon thicknesses. In addition, the model simulations showed that the relation between the starting depth of some horizons (e.g. Bt) and terrain properties was lost due to the homogenizing effect of treefalls. This was consistent with the observations in the field by Vanwalleghem et al. (2010).

2.2.4.3 SoilGen model limitations

The aforementioned studies clearly demonstrate the potential field applications of SoilGen both at pedon scale and at landscape scale. However, results from these studies have also reported some cases of major discrepancies between model predictions and measurements. These discrepancies can be partly attributed to (1) incomplete process descriptions, (2) incorrect estimates of initial data inputs and (3) incorrect values of variables that describe boundary conditions (Finke, 2012). Furthermore, heterogeneity within the soil profile is only partly captured as the model assumes a homogeneous initial mineralogical composition. There are also issues of process simplifications such as constant volume of each compartment with time.

According to Vanwalleghem et al. (2013), the major limitation of the SoilGen model especially for application at landscape scale is its inability to take into account spatial patterns and links between individual profiles. At landscape scale, data requirement and simulation time also increase. In addition, verification of pedon-landscape linked models becomes very difficult if not impossible especially when dealing with human-affected landscapes because the land use history is often imprecisely known at the level of model input parameters.

2.2.4.4 Future priorities

In its current state, the SoilGen chemical weathering module describes only four primary minerals (Anorthite, Chlorite, Microcline, Albite) as major pools for Ca, Mg, K and Na, respectively. This means that the fate of a wide range of primary minerals and elements may not be simulated. In addition, formation of major secondary minerals is not taken into account in SoilGen weathering and chemical systems. Formation and presence of these secondary clay minerals is important as they influence CEC. CEC together with clay content and OC are used in the SoilGen model (clay migration module) to simulate the amount of dispersible clay. Therefore there is need to explore the possibility of extending the description of SoilGen chemical weathering module such that it can accommodate the weathering of more primary minerals, release of more elements as well as the formation of major secondary minerals.

SoilGen chemical module also needs to be extended to allow simulation of more chemical species such as Si and Fe. These species have pronounced effects on most soil processes and soil properties. For example Si in form of phytoliths has been shown to influence the decomposition rates of organic matter (Song et al., 2012, 2014) while Fe may cause cementation and influences the composition of the exchange complex. If Si, Fe and Al fate is simulated, weathering indices can be calculated as well, which enlarges the possibility to compare model results with field studies reported in literature. The chemical module therefore needs to be developed in such a way that it is flexible and allows interactions among chemical elements. Well-developed weathering and chemical systems will probably improve simulations of soil chemical properties such as BS, CEC and pH.

Furthermore, the interaction between the soil and the vegetation in SoilGen is currently described through ion uptake and annual litter input. However, the changes in the annual litter input in response to soil conditions such as soil moisture and temperature are not captured. To capture these interactions and feedbacks, there is need to implement the concepts of soil-vegetation interactions usually described in vegetation models.

Inclusion of the above processes will improve the description of the weathering and chemical systems in the SoilGen model. In addition, these inclusions will enhance the SoilGen model flexibility so that it can be applied to different parent materials and simulation of genesis of typical features of at least half of the WRB-RSG. Capturing interactions and feedbacks between the soil and vegetation system will also enhance the sensitivity of the SoilGen model to global change.

2.3. Soil genesis in landscape evolution models

2.3.1 Current capabilities of landscape evolution models

Landscape evolution models are those in which soil production and soil redistribution over time is simulated at a landscape scale. In contrast to pedon scale models which are mainly based on pedology and geochemistry, landscape evolution models are mainly based on geomorphology and soil is simulated as a single layer of regolith (Minasny et al., 2008). Major soil forming processes considered include physical weathering, chemical weathering, erosion and deposition (Minasny and McBratney, 2001). These models (e.g. Dietrich et al., 1995; Minasny and McBratney, 1999; 2006) and

notably the LAPSUS-model by Schoorl et al., 2002 and the MILESD-model by Vanwalleghem et al. (2013) have successfully been applied to simulate soil thickness over time as influenced by weathering and erosion processes. The limitations of these approaches are that, they consider only the solid phase of the soil and thus the impact of water flow on soil formation is not accounted for. This means that such models cannot be used to simulate soil formation under varying climate and land use (Samouëlian and Cornu, 2008; Samouëlian et al., 2012). In addition these approaches assume a closed system within the landscape such that, apart from soil production by weathering there is no soil either lost from the landscape or brought into the landscape from areas outside the model, e.g. by loess deposition or alluvial inputs, thus simplifying reality. There is also no clear horizonation of the soil when applying these models (Samouëlian and Cornu, 2008). According to Vanwalleghem et al. (2013) most landscape models do not explicitly consider soil forming processes and thus observed differences may only result from sediment sorting by erosion and deposition processes. Practically, it is also very difficult to verify these models under field conditions.

To address some of these limitations, there is a need to work towards an integrated system (Vanwalleghem et al., 2013) in which fully tested pedon scale models are integrated or linked to landscape models, thus producing soilscape genesis models.

2.3.2. Towards modelling of soilscape genesis

Probably the simplest case of soilscape development modelling is when soil redistribution across the landscape is negligible and water fluxes are mainly vertical. In that case, spatially distributed modelling with a pedon-scale model in combination with geostatistical mapping methods will suffice to produce maps of soil properties for desired points in time. Such approach has shown promising results. Zwertvaegher et al. (2013) did multiple point simulations with SoilGen in a relatively flat cover sand area for the period from the Younger Dryas up till recently, and interpolated pedon-scale results (e.g., base saturation in the topsoil) to full coverage maps for desired points in time by a regression kriging technique. Finke et al. (2013) did likewise in a forest-covered landscape without much erosion in loess parent material.

When soil redistribution through erosion and sedimentation processes occurs, but water fluxes are still mainly vertical, a 1-D pedon soil genesis model may be linked to landscape evolution models. The pedon model runs for several geographic position in the landscape and communicates with the landscape model at meaningful time intervals. In this case, the landscape evolution model provides boundary inputs to the pedon model: the amount of soil material lost by erosion or added by sedimentation at the surface boundary during a time interval. SoilGen is able to handle surface loss by erosion or addition of soil material of known composition. This requires that the transported material is characterized in terms of all the soil properties that are used in the pedon model, such as texture, OC percentage and element composition. The pedon model can return the topsoil composition to the landscape model to update the erodibility and infiltrability and their spatial distributions. Such model linkage is feasible, but the large computing time probably limits the amount of pedon scale models that can be linked to the landscape model. As in case of the spatially distributed modelling, geostatistics can be of value to obtain complete coverage of the landscape with pedogenetic data. When erosion processes are known to be dominant over soil formation processes in a particular period, a time-split approach as proposed by Sommer et al. (2008) may be applied to use either a distributed soil formation model or a soil redistribution model in such period, thus saving computing effort.

The most complex case is when soil redistribution takes place and water flow is not strictly vertical. Ideally, in this case a 3-D soilscape model is developed that integrates surface soil redistribution processes, a 3-D water and solute transport model and additional model components that cover the soil formation processes. Such a model is not known to exist today, and is expected to be computationally demanding.

A general problem with modelling of soilscape genesis is that various boundary inputs must be assessed for all positions in the landscape and also over time, in particular this concerns the type of vegetation and its coverage and agricultural land use. Such reconstructions are highly complex and the resulting boundary inputs are associated with uncertainty.

In summary, the major issues to be solved in the modelling of soilscape genesis are computation time and data demand. These issues may render simplification of some process descriptions unavoidable. Part of the solution points to the development of complete and tested pedon scale models that are at a later stage simplified and tuned to reproduce the detailed pedon models. For such testing, there is need for high quality profile datasets (e.g. chronosequences, climosequences and toposequences).

2.4. Conclusions

Models for soil evolution are increasingly becoming invaluable tools to provide soil information required for hydrological, land evaluation, biogeochemical and global change studies. Although still limited, such models are progressively being developed. We demonstrate here that the SoilGen model is one of such models with capabilities to simulate soil formation over multi-millennia time scale. Simple calibration approaches have been developed and used to calibrate the SoilGen model. The model has undergone extensive field testing and satisfactory results at both pedon and landscape scales have been reported. Its ability to take into account complex physical, geochemical and biological processes coupled with water flow makes it such a unique and versatile soil evolution model. However there is still need to further develop it for application in different environmental scenarios and for a larger variety in parent materials. Particularly the chemical and weathering systems need to be extended in a flexible way. This PhD work contributed to the further development of the weathering and chemical modules of the SoilGen model, and these extensions are presented in chapters 3 and 4, respectively.

We also note here that landscape evolution models are valuable to simulate soil production and distribution over time at landscape scale. The major drawback of these models is that only soil solid phases are considered and a limited number of soil forming processes (i.e. only physical/chemical weathering, erosion and deposition) are considered. Working towards an integrated system of pedon and landscape models presents a better approach to improve modelling of landscape evolution. However, increased data requirement and computation time (discussed in detail in chapter 7) remain a major challenge. There is critical need for high quality chronosequence, climosequence and toposequence profile datasets. This type of dataset would surely provide a good test for soil evolution

models. Pedologists also need to strengthen links with other disciplines such as palaeopedologists, Critical Zone and climate research communities. Such links will undoubtedly facilitate better understanding of soil formation through collaboration and sharing of quality data, technology and experiences.

Author contribution

This chapter was developed and written by the first author (E. Opolot) based on a conference contribution by the third author (Peter Finke) and some contribution from the second author (Y.Y.Yu).

Acknowledgements

This work is part of the PhD project funded by the Belgian Science Policy Office (project BELSPO/IUAP p7/24).

References

Bockheim, A.N., Gennadiyev, A.N., 2000. The role of soil-forming processes in the definition of taxa in Soil Taxonomy and the World Soil Reference Base. Geoderma 95, 53–72.

Brimhall, G.H., Alpers, C.N., Cunningham, A.B., 1985. Analysis of supergene ore-forming processes and ground water solute transport using mass balance principles. Economic Geolology 80, 1227–1256

Brimhall, G.H., Dietrich,W., 1987. Constitutive mass balance relations between chemical composition, volume, density,porosity, and strain in metasomatic hydrochemical systems: Results on weathering and pedogenesis. Geochimica et Cosmochimica Acta 51, 567–587

Brown, L.C., Foster, G.R., 1987. Storm erosivity using idealized intensity distributions. Transactions of the American Society of Agricultural Engineers 30, 379-386.

Brubaker, S.D., Holzhey, C.S., Brasher, B.R., 1992. Estimating the water-dispersible clay content of soils. Soil Science Society of America 56, 1227-1232.

Coleman K, Jenkinson D.S., 2005. RothC-26.3 A Model for the Turnover of Carbon in Soil. November 1999 issue (modified April 2005). http://www.rothamsted.

Dietrich, W.E., Reiss, R., Hsu, M., Montgomery, D.R., 1995.A process-based model for colluvial soil depth and shallow landsliding using digital elevation data. Hydrological Processes 9, 383–400.

Egli, M., Fitze, P., 2001.Quantitative aspects of carbonate leaching of soils with differing ages and climates.Catena 46, 35-62.

Ferrier K.L, Kirchner J.W, Riebe C.S, Finkel R.C., 2010. Mineral-specific chemical weathering rates over millennial time scales: Mesasurements ar Rio Icacos, Puerto Rico. Chemical Geology 277, 101-114

Finke P.A, Hutson J.L., 2008. Modelling soil genesis in calcareous löss. Geoderma 145, 462-479.

Finke P.A. 2012. Modelling the genesis of Luvisols as a function of topographic position in loess parent material. Quaternary International 265, 3-17

Finke P.A., 2011. SOILGEN: A simulation model for soil development in various parent materials. User Manual for SoilGen2.16, 43 pp, Ghent University, Belgium.

Finke, P. A., Samouëlian, A., Suarez-Bonnet, M., Laroche, B. and Cornu, S. S. 2015. Assessing the usage potential of SoilGen2 to predict clay translocation under forest and agricultural land uses, Eur. J. Soil Sci., 66(1), 194–205.

Finke, P.A., Vanwalleghem, T., Opolot, E., Poesen, J., Deckers, J. 2013. Estimating the effect of tree uprooting on variation of soil horizon depth by confronting pedogenetic simulations to measurements in a Belgian loess area.Journal of Geophysical Research-Earth Surface 118(4), 2124–2139, doi:10.1002/jgrf.20153.

Foth, H.D., Ellis, B.G., 1996. Soil Fertility, second ed. CRC press, Lewis, ISBN 1-56670- 243-7, 304 pp.

Goddéris, Y., Francois, L.M., Probst, A., Schott, J., Moncoulon, D., Labat, D., Viville, D., 2006. Modelling weathering processes at the catchment scale: The WITCH numerical model. Geochimica et Cosmochimica Acta 70, 1128-1147.

Godderis, Y., Williams, J.Z ., Schott, J., Pollard, D., Brantley, S.L., 2010. Time evolution of the mineralogical composition of Mississippi Valley loess over the last 10 kyr: Climate and geochemical modelling. Geochimica et Cosmochimica Acta 74, 6357–6374.

Goldberg, S., Forster, H.S., 1990. Flocculation of reference clays and arid-zone soil clays. Soil Science Society of America Journal 54, 714-718.

Hoosbeek, M. R., Bryant, R.B., 1992. Towards the quantitative modelling of pedogenesis-A review. Geoderma 55, 183–210.

Huggett, R. J., 1975. Soil landscape systems: A model of soil genesis. Geoderma 13, 1–22

Hutson, J.L., 2003. LEACHM - A process-based model of water and solute movement, transformations, plant uptake and chemical reactions in the unsaturated zone. Version 4. Research Series No R03-1 (Dept. of Crop and Soil Sciences, Cornell University, Ithaca, NY). Journal of Soil Science. 36, 97–121

IUSS Working Group WRB. 2006. World reference Base for soil resources 2006, 2nd edition. World Soil Resources Reports No. 103. FAO, Rome.

Jarvis, N.J., Villholth, K.G., Ulén, B., 1999. Modelling particle mobilization and leaching in macroporous soil. European Journal of Soil Science 50, 621-632.

Jenkinson, D.S., Coleman, K., 1994. Calculating the annual input of organic matter to soil from measurements of total organic carbon and radiocarbon. European Journal of Soil Science 45, 167-174.

Jenny, H., 1941. Factors of Soil Formation.A System of Quantitative Pedology. McGraw-Hill Book Company, New York, London

Kirkby, M. J., 1985. A basis for soil profile modelling in a geomorphic context. Journal of Soil Science 36 (1): 97-121.

Kirkby, M. J.,1977. Soil development models as a component of slope models. Volume 145 Working paper. University of Leeds.School of Geography.

Kros, J., 2002. Evaluation of biogeochemical models at local and regional scale.PhD thesis Wageningen University, Wageningen, Netherlands, 284 p. ISBN 90-3270-313-7.

Mauersberger, F., 2001. Modellrechnungen zum Einfluss des Aufprallwinkels der Regentropfen auf die Mobilisierung und den Transport von Bodenpartikeln. Diploma thesis Technical University Freiburg.

Mayer, K.U., Frind, E.O., Blowes, D.W., 2002. Multicomponent reactive transport modelling in variably saturated porous media using a generalized formulation for kinetically controlled reactions. Water Resources Research 38, 1174

McBratney, A.B., Mendonça-Santos, M.L., Minasny, B., 2003.On digital soil mapping. Geoderma 117, 3-52.

Minasny, B., McBratney, A.B., 1999. A rudimentary mechanistic model for soil production and landscape development. Geoderma 90, 3-21.

Minasny, B., McBratney, A.B., 2001. A rudimentary mechanistic model for soil production and landscape development II.A two-dimensional model incorporating chemical weathering. Geoderma 103, 161-179.

Minasny, B., McBratney, A.B., 2006. Mechanistic soil-landscape modelling as an approach to developing pedogenetic classifications. Geoderma 133 (1-2), 138-149.

Minasny, B., McBratney, A.B., Salvador-Blanes, S., 2008. Quantitative models for pedogenesis: a review. Geoderma 144, 140-157.

Moldrup P., T. Olesen, P. Schjonning, T. Yamaguchi and D.E. Rolston., 2000.Predicting the gas diffusion coefficient in undisturbed soils from soil water characteristics. Soil Sci. Soc. Am. J. 64: 94-100.

Morris, M. D., 1991. Factorial sampling plans for preliminary computational experiments, Technometrics 33, 161–174.

Noorallah, J.G., 1999. Pedosphere and Its Dynamics Book Series: Introduction to Soil Science and Soil Resources. Salman Productions Inc publishers. ISBN: 1-896263-10-0.

Opolot, E. and Finke, P. A., 2015. Evaluating sensitivity of silicate mineral dissolution rates to physical weathering using a soil evolution model (SoilGen2.25), Biogeosciences, 12, 6791-6808.

Phillips, J.D., 1993. Stability implications of the state factor model of soils as a nonlinear dynamical system. Geoderma 58, 1–15.

Salvador-Blanes, S., Minasny, B., McBratney, A.B., 2007.Modelling long-term *in situ* soil profile evolution: application to the genesis of soil profiles containing stone layers. European Journal of Soil Science 58, 1535-1548.

Samouëlian, A., Cornu, S., 2008.Modelling the formation and evolution of soils, towards an initial synthesis.Geoderma 145 (3-4), 401- 409.

Samouëlian, A., Finke, P., Goddéris, Y., Cornu, S., 2012.Hydrologic Information in Pedologic Models. In: Lin, H. (Ed.), Hydropedology: Synergistic Integration of Soil Science and Hydrology. Academic Press, Elsevier B.V., pp. 595–636. ISBN: 9780123869418

Sauer, D., Finke, P.A., Schülli-Maurer, I., Sperstad, R., Sørensen, R., Høeg, H.I., Stahr, K., 2012.Testing a soil development model against southern Norway soil chronosequences. Quaternary International 265, 18-31

Schaetzl, R.J., Schwenner, C., 2006. An application of the Runge "Energy Model" of soil development in Michigan's upper peninsula. Soil Science 171/2, 152–166.

Schoorl, J.M., Veldkamp, A., Bouma, J., 2002. Modelling water and soil redistribution in a dynamic landscape context. Soil Science Society of America Journal 66, 1610-1619.

Sommer, M., Gerke, H.H., and Deumlich, D., 2008. Modelling soil landscape genesis- A "time split" approach for hummocky agricultural landscapes. Geoderma 145, 480–493.

Sommer, R., and Stöckle, C., 2010. Correspondence between the Campbell and van Genuchten Soil-Water-Retention models. Journal of irrigation and drainage engineering, 2010: 559-562.

Song, Z., Müller, K. and Wang, H., 2014. Biogeochemical silicon cycle and carbon sequestration in agricultural ecosystems, Earth-Science Rev., 139, 268–278, doi:10.1016/j.earscirev.2014.09.009

Song, Z., Wang, H., Strong, P. J., Li, Z. and Jiang, P., 2012. Plant impact on the coupled terrestrial biogeochemical cycles of silicon and carbon: Implications for biogeochemical carbon sequestration, Earth-Science Rev., 115(4), 319–331, doi:10.1016/j.earscirev.2012.09.006.

Stockmann, U., Minasny, B., McBratney, A.B., 2011. Quantifying pedogenesis processes. Advances in Agronomy, Volume 113, p.2-67.

Swift Jr, L.W., 1976. Algorithm for solar radiation on mountain slopes. Water Resources Research 12 (1), 108-112. doi:10.1029/WR012i001p00108.

Ullrich, A., Volk, M., 2009. Application of the soil and water assessment tool (SWAT) to predict the impact of alternative management practices on water quality and quantity. Agricultural Water Management 96 (8), 1207-1217.

Vanwalleghem, T., Poesen, J., McBratney, A., Deckers, J., 2010. Spatial variability of soil horizon depth in natural loess-derived soils. Geoderma 157, 37-45.

Vanwalleghem, T., Stockmann, U., Minasny, B., McBratney, A. B. 2013. A quantitative model for integrating landscape evolution and soil formation. Journal of Geophysical Research: Earth Surface 118(2), 331-347

Violette, A., Goddéris, Y., Maréchal, J.C., Riotte, J., Oliva, P., Mohan Kumar, M.S., Sekhar, M., Braun, J.J., 2010.Modelling the chemical weathering fluxes at the watershed scale in the Tropics (Mule Hole, South India): Relative contribution of the smectite/kaolinite assemblage versus primary minerals.Chemical Geology 277, 42–60.

Wierenga, P.J., D.R. Nielsen and R.M. Hagan., 1969. Thermal properties of a soil based upon field and laboratory measurements. Soil Sci. Soc. Amer. Proc. 33:354-360.

Wosten, J.H.M., Lilly, A., Nemes, A. and Le Bas, C.,1999. Development and use of a database of hydraulic properties of European soils. Geoderma, 90, 169–185

Yu, Y.Y., Finke, P.A, Guo, Z.T, Wu H.B., 2013. Sensitivity analysis and calibration of a soil carbon model (SoilGen2) in two contrasting loess forest soils.Geoscientific Model Development 6, 29-44.

Zwertvaegher, A., Finke, P., De Smedt, P., Gelorini, V., Van Meirvenne, M., Bats, M., De Reu, J., Antrop, M., Bourgeois, J., De Maeyer, P., Verniers, J., Crombe, P., 2013. Spatio- temporal modelling of soil characteristics for soilscape reconstruction. Geoderma 207-208, 166-179

Zwertvaegher, A., Werbrouck, I., Finke, P.A., De Reu, J., Crombé, Ph., Bats, M., Antrop, M., Bourgeois, J., Court-Picon, M., De Maeyer, Ph., De Smedt, Ph., Sergant, J., Van Meirvenne, M., Verniers, J., 2010. On the use of integrated process models to reconstruct prehistoric occupation with examples from Sandy Flanders, Belgium. Geoarchaeology 25 (6), 784-814.

Chapter 3 **:** Chemical Weathering- Redesigning the kinetics of mineral dissolution and precipitation of the SoilGen Model

3.1 Introduction

Chemical weathering is the process through which rock minerals at the earth's surface are chemically altered to constituent solutes and solid residues (van Breemen and Buurman, 2002; Carlson et al., 2011). The major forms of chemical weathering include hydrolysis, redox-reactions and carbonation. Chemical weathering is one of the major soil-forming processes and plays a central role in many key environmental processes such as nutrient cycling, carbon sequestration and neutralization of acid precipitation (Goddéris et al., 2006; Stendahl et al., 2013; White and Brantley, 2003). However the spatial variability of soil and the complex interaction of factors affecting chemical weathering (i.e., climate, parent material, organisms and relief), make it difficult to directly calculate field weathering rates based on the laboratory determined rates. Therefore process-based models are necessary to upscale laboratory rates to field scale (Holmqvist, 2001). Such models are also necessary to be able to assess the effect of global change on soil biogeochemical processes and properties. The aim of this chapter is to propose and discuss an extended chemical weathering mechanism that is implemented in the SoilGen model.

3.1.1 Background and Objectives

As already mentioned in chapters 1 and 2 of this thesis, only four common primary minerals (albite, anorthite, chlorite, microcline) are considered in the SoilGen2.16 (Finke et al., 2013) and SoilGen2.24 (Finke et al., 2015) versions of the SoilGen model. These four minerals act as pools for Ca, Mg, K and Na, respectively. This means that the fate of a wide range of primary minerals and elements may not be simulated. In addition, formation of major secondary minerals is not taken into account in SoilGen, yet secondary mineral precipitation is one important factor determining the dissolution rates of primary minerals (Ganor et al., 2007; Goddéris et al., 2006; Zhu et al., 2010). Therefore one of the objectives of this thesis research (Chapter 1) was to explore the possibility of extending the SoilGen weathering module such that it can accommodate the weathering of more primary minerals as well as the formation of major secondary minerals. Such an extension would ensure the flexibility of the SoilGen model and its applicability to different study sites with different primary and secondary minerals. In addition, different concepts of weathering indices are implemented to enhance the use of SoilGen to explicitly describe the degree of soil formation. In summary, the specific objectives addressed in this section include:

1. To extend the description of the weathering of primary minerals to accommodate release of more chemical species by various minerals.
2. To evaluate the necessity and possibility to include the formation of secondary minerals and implement such a mechanism in the SoilGen model.
3. To implement the calculation of varying weathering indices to allow better comparison of model results with field and literature data.

3.2 Primary minerals

In a geological context, a primary mineral is defined as a mineral that is formed at high temperature and pressure, at the same time as its parent rock and retains its original structure and chemical compostion. The properties of a primary mineral are therefore very much dictated by the conditions under which the parent material was formed (van Breemen and Buurman, 2002). In pedology, a primary mineral is a mineral inherited from the parent material. Generally, primary minerals are mainly characterised by structures consisting of configurations dominated by silica and oxygen atoms (van Breemen and Buurman, 2002). The current chemical weathering module (unweathered phase) of SoilGen considers four most common primary minerals (Anorthite, Chlorite, Microcline, Albite) that respectively release Ca, Mg, K, and Na. Congruent weathering of Anorthite, Chlorite, Microcline and Albite releases Al. The detailed mechanism has already been presented in chapter 2 (section 2.2.1.2: Weathering processes; Eqs 2.11 and 2.12). In general the approach assumes that the parent material is homogeneous. In addition, the approach is based on the acidification models and only a few minerals are considered. There was need to extend this module to allow simulation of chemical weathering of a wider range of primary minerals such that more chemical species may be simulated (Opolot et al., 2015).

In the subsequent sections, we present the implemented mechanism capable of simulating the dissolution kinetics of the commonly occurring primary minerals (Carlson et al., 2011) and, the proposed mechanism for dissolution and precipitation of selected secondary minerals. Table 3.1 summarises the list of primary and secondary minerals incorporated in the chemical weathering module of the SoilGen model. Table 3.1 also shows dissolution reactions, enthalpies of these reactions and equilibrium constants of each of the minerals based on values reported in the

PHREEQC.dat database (Parkhurst and Appelo, 1999), unless otherwise mentioned. These values are based on laboratory batch experiments aimed at measuring the reaction kinetics of minerals at defined pressures, temperature and pH.

3.3 Secondary minerals

During dissolution of primary minerals and depending on the prevailing soil conditions (pH, organic matter, oxygen concentration, temperature) precipitation of secondary minerals takes place (Madé et al., 1994; Schroeder et al., 2000). As mentioned in the previous sections, formation and presence of these secondary minerals is very important as they influence cation exchange capacity (CEC), and other chemical processes such as weathering of primary minerals (Maher et al., 2009). Cation exchange capacity together with clay content and organic carbon content is used in the SoilGen model (Clay migration module; Chapter 2: Eq 2.14) to simulate the amount of dispersible clay. It is therefore necessary to define and implement a mechanism that allows precipitation of secondary minerals once the soil solution is saturated with respect to such minerals. The list of minerals provided in Table 3.1 is certainly not exhaustive of all the secondary minerals. Generally, 3 groups of secondary minerals were considered (1) Phyllosilicates (2) Fe oxides and Al hydroxides (Mn is not described in the SoilGen chemical system and therefore Mn hydroxides are not included) and (3) Poorly crystalline alumino-silicates (e.g., Imogolite). Lastly, we have also considered other common secondary precipitates such as calcite, dolomite and gypsum.

What about other minerals not listed in Table 3.1?

The list of minerals given in Table 3.1 is certainly not exhaustive of all primary and secondary minerals. Nevertheless at the moment up to two extra minerals not defined in Table 3.1 can be introduced into the model through extra input files defining these minerals as “otherite” and “amorphite”. These two minerals are treated exactly the same in the model and for both minerals, dissolution rate parameters (see Table 3.2 for an example) and geochemical composition have to be provided as input. The name “amorphite” is reserved for those minerals whose structure may not easily be identified through XRD (e.g., allophane) and have to be introduced into the model through the bulk geochemical composition. The name “otherite” on the other hand is used to define a mineral with easily identifiable structural composition (based on XRD) but not listed in Table 3.1 (e.g., diopside). Like minerals listed in Table 3.1, “otherite” and “amorphite” are weathered as a function of pH and surface area following the weathering mechanism described in section 3.4.

Table 3.1. Reaction equations and equilibrium constants (Log K_{eq}) of primary and secondary minerals implemented in the SoilGen model. Values reported are based on the PHREEQC.DAT database (input data to PHREEQC geochemical software containing thermodynamic data for aqueous species and mineral phases; Parkhurst and Appelo, 1999). ΔH_R is the enthalpy of reaction (energy change in the system when one mole of matter is transformed by a chemical reaction). The dash sign (-) means missing data.

Mineral	**Reaction**	**ΔH_R** ($kJmol^{-1}$)	**Log K_{eq}** ($T = 25^oC$)
Primary minerals			
Albite	$NaAlSi_3O_8 + 4H_2O + 4H^+ = Na^+ + Al^{3+} + 3H_4SiO_4$	108.35	-18.00
Anorthite	$CaAl_2Si_2O_8 + 8H^+ = Ca^{2+} + 2Al^{3+} + 2H_4SiO_4$	48.45	-19.71
Augite	$FeSiO_3 + 2H^+ + H_2O = Fe^{2+} + H_4SiO_4$	-	-
Biotite	$KMg_{1.5}Fe_{1.5}AlSi_3O_{10}(OH)_2 + 10H^+ = K^+ + 1.5Mg^{2+} + 1.5Fe + Al^{3+} + 3H_4SiO_4$	-55.60	-32.87[1]
Chlorite	$Mg_5Al_2Si_3O_{10}(OH)_8 + 16H^+ = 5Mg^{2+} + 2Al^{3+} + 3H_4SiO_4 + 6H_2O$	-633.85	68.38
Fayalite	$Fe_2SiO_4 + 4H^+ = 2Fe^{2+} + H_4SiO_4$	-	19.11[2]
Forsterite	$Mg_2SiO_4 + 4H^+ = 2Mg^{2+} + H_4SiO_4$	-203.25	-28.31[2]
Hornblende	$Ca_2Mg_4AlSi_{6.7}AlO_{22.4} + 4.4H_2O + 18H^+ = 2Ca^{2+} + 4Mg^{2+} + Al^{3+} + 6.7H_4SiO_4$	-	-
Illite	$K_{0.6}Mg_{0.25}Al_{2.3}Si_{3.5}O_{10}(OH)_2 + 11.2H_2O = 0.6K^+ + 0.25Mg^{+2} + 2.3Al(OH)_4^- + 3.5H_4SiO_4 + 1.2H^+$	228.80	-40.27
Muscovite	$KAl_3Si_3O_{10}(OH)_2 + 10H^+ = K^+ + 3Al^{3+} + 3H_4SiO_4$	-248.40	12.70
K-feldspar	$KAlSi_3O_8 + 4H_2O + 4H^+ = K^+ + Al^{3+} + 3H_4SiO_4$	128.95	-20.57
Quartz	$SiO_2 + 2H_2O = H_4SiO_4$	25.06	-3.98
Secondary minerals			
Calcite	$CaCO_3 = CO_3^{-2} + Ca^{+2}$	9.61	-8.48
Dolomite	$CaMg(CO_3)_2 = Ca^{2+} + Mg^{2+} + 2CO_3^{2-}$	-39.48	-17.09
Gibbsite	$Al(OH)_3 + 3H^+ = Al^{3+} + 3H_2O$	-95.40	8.11
Goethite	$FeOOH + 3H^+ = Fe^{3+} + 2H_2O$	-60.58	-1.00
Gypsum	$CaSO_4{:}2H_2O = Ca^{2+} + SO_4^{2-} + 2H_2O$	-0.46	-4.58
Hematite	$Fe_2O_3 + 6H^+ = 2Fe^{3+} + 3H_2O$	-129.01	-4.01
Imogolite	$HOSiO_3Al_2(OH)_3 + 6H^+ = 2Al^{3+} + H_4SiO_4 + 3H_2O$	-99.00	6.60[3]
Kaolinite	$Al_2Si_2O_5(OH)_4 + 6H^+ = H_2O + 2H_4SiO_4 + 2Al^{3+}$	-147.70	7.44
Montmorillonite	$Ca_{0.04125}Mg_{0.04125}Na_{0.0825}K_{0.0825}Al_{1.67}Si_4O_{10}(OH)_2 + 4H_2O + 6H^+ = 0.04125Ca^{2+} + 0.04125Mg^{2+} + 0.0825Na^+ + 0.0825K^+ + 1.67\,Al^{3+} + 4H_4SiO_4$	-78.11	-2.46[1]
Siderite	$FeCO_3 = Fe^{2+} + CO_3^{2-}$	-10.38	-10.89

[1]Data as reported in Godderis et al., 2006. Values for montmorillonite are average values from all montimorillonte minerals reported in Godderis et al., 2006; [2] Data from Sugimori et al., 2012; [3]Data for imogolite as reported in Gustafsson et al., 2001.

3.4 Modelling chemical weathering of primary and secondary minerals

Quantitative modelling of kinetics of mineral and water interactions started more than three decades ago (e.g., Helgeson and Murphy, 1983; Madé et al., 1994; Parkhurst et al., 1980; Sverdrup and Warfvinge, 1993, 1995; Wolery, 1979). These early approaches employed kinetic rate laws to simulate the speed of mineral-water interactions and the establishment of solution equilibrium. However such models were not coupled with other soil-forming processes such as solute transport (Madé et al., 1994; Steefel and Lasaga, 1994). The application of such geochemical models was therefore limited to the closed systems such as batch reactors (Steefel and Lasaga, 1994). Since then progress has been made on developing geochemical models capable of linking kinetics of mineral-water reactions with transport processes (e.g., PHREEQC- Parkhurst and Appelo, 1999; CrunchFlow- Steefel et al., 2005; Steefel, 2008; NANOKIN code - Fritz et al., 2009; WITCH- Godderis et al., 2006; CRONO code - Novoselov and Souza Filho, 2013). Detailed comparison of different geochemical models has been presented elsewhere (e.g., Bethke, 2008; Steefel et al., 2014; Nordstrom, 2003) and it is outside the scope of this thesis. However it is important to note that most modelling studies focusing on quantifying chemical weathering rates (e.g., Goddéris et al., 2006, 2010; Gudbrandsson et al., 2011, 2014; Koptsik et al., 1999; Koseva et al., 2010; Maher et al., 2009; Pham et al., 2011, 2012; Phelan et al., 2014; Roelandt et al., 2010; Stendahl et al., 2013; Violette et al., 2010; Whitfield et al., 2010) have either directly used or adapted some of the geochemical codes mentioned above, to solve geochemical equilibrium reactions. Most of these geochemical models assume steady state (i.e. the composition of the ion exchange complex does not change over time) when simulating mineral dissolution and precipitation processes (e.g., PROFILE model; WITCH model). Therefore processes such as chemical weathering are assumed to proceed at a constant rate (Holmqvist, 2001), and soil properties such as mineral surface area and soil texture are usually assumed constant. Such steady state assumptions may be valid when looking at short time scales but not at pedogenetic time scales (Holmqvist, 2001).

In the subsequent subsections, we propose and discuss the chemical weathering rate mechanism that is adapted and implemented in the extended chemical weathering module of the SoilGen model. The discussion will mainly focus on the two key parameters (i.e., reactive surface area and mineral

dissolution rate) in quantifying the amount of cations released during the dissolution of primary and secondary minerals, and precipitation of secondary minerals.

3.4.1 Proposed mechanism of cation release rate during mineral dissolution and precipitation

Similar to the equations applied in previous geochemical studies (e.g., Godderis et al., 2006; Gudbrandsson et al., 2011), the release rate of cation i ($r_{i,k}$; mol m^{-2} s^{-1}) from all k minerals can be computed as in (Eq 3.1):

$$r_{i,k} = \sum_{k=1}^{N} A_k v_{i,k} r_k m_k T \quad (3.1)$$

where A_k (m^2 mol^{-1}) is the reactive surface area of the k^{th} mineral (see section 3.4.1.1), $v_{i,k}$ (-) is the stoichiometric number of the i^{th} element in mineral k and r_k (mol m^{-2} s^{-1}) is the dissolution rate of the k^{th} mineral (see section 3.4.1.2). m_k is the amount of the k^{th} mineral (mol m^{-3} soil) in the parent material (see section 3.4.1.3) and T (m) is the thickness of the soil compartment.

3.4.1.1 Quantifying the mineral reactive surface area, A_k

Accurate estimation of mineral reactive area, particularly at field scale, remains a big challenge and a subject of major discussion (Brantley et al., 2008). The observed differences within laboratory measurements and between laboratory and field weathering rates are also partly attributed to the uncertainty of this parameter (Brantley et al., 2008; White et al., 1996). The principal methods for estimation of reactive surface area at the laboratory scale include (i) Brunauer-Emmet-Taylor (BET-N_2 adsorption) method, (ii) Ethylene Glycol Monoethyl Ether (EGME) method and (iii) water vapour adsorption method. Detailed principles of each of these methods are not discussed here. Each of these methods has its own strengths and limitations. For example the BET-N_2 method is a reliable and widely used method for estimating external mineral area but it is always associated with underestimation of total surface area since it does not consider the internal surface area (Heister, 2014). On the other hand, the EGME method gives better estimates of the total mineral surface area but it is tiresome and time consuming (Arthur et al., 2013).

For geochemical modelling purposes, the BET-N_2 measured surface areas have mainly been used when extrapolating laboratory weathering rates to field weathering rates. However, different laboratory procedures may lead to either underestimation or overestimation of the actual BET-N_2 surface area. For example, removing organic matter prior to BET-N_2 analysis is associated with an increase in BET-N_2 area, as coated surfaces finally become available for reaction. This is especially true for soils with organic carbon content greater than 3% (Theng et al., 1999). On the other hand, not removing these coatings may lead to underestimation of the BET-N_2 area as organic molecules may clog the pores and consequently hinder the penetration of N_2 into the mineral surface (Heister, 2014). Moreover, increase in surface area after removal of organic matter and Fe and Al-(hydr) oxides has also been linked to decomposition and heat-induced transformation of minerals (e.g. during oxidation with H_2O_2) rather than just removal of organic matter (Heister, 2014).

In addition, due to the time and resources needed for such laboratory approaches, it would be preferable that the mineral surface area is estimated from more readily measured soil properties such as particle size (Hodson et al., 1998). One of the first and the most widely used approach to estimate mineral surface area is that described in Sverdrup and Warfvinge (1993; 1995). This approach was first used in the PROFILE model (Sverdrup and Warfvinge, 1993; 1995) to calculate the surface area from an empirical equation (Eq 3.2) relating soil texture to measured BET surface areas. According to Sverdrup and Warfvinge (1995), Eq 3.2 is derived from about 100 Swedish soil samples though it is not clear if organic matter and, iron and aluminium sesquioxides were removed these samples prior to the BET-N_2 surface area analysis (Hodson et al., 1997). The approach is based on the assumptions that all the particle size fractions (i.e., coarse sand, sand, silt and clay) add up to 1 (Sverdrup and Warfvinge, 1995) and that all the particle grains exhibit the same shape. This approach is simple and it is advantageous especially for pedogenetic models since it allows the evolution of surface area as a function of the soil particle size. However the use of this approach has received critical evaluations (e.g., Hodson, 2002; Hodson et al., 1997). According to Hodson (2002), Eq 3.2 imposes the artificial limits on soil mineral surface area since the equation is limited to only soils with less than 20% clay fraction. In addition, Hodson et al. (1998) reported a low coefficient of determination (r^2 = 0.12) between measured BET surface area and mineral surface area calculated using Eq 3.2.

$$A_j = 8\,x_{clay} + 2.2\,x_{silt} + 0.3\,x_{sand} + 0_{xcoarse} \quad (3.2)$$

where A_j ($m^2\ g^{-1}$) is the total mineral specific surface area, x denotes a given particle size fraction and coefficients 8, 2.2 and 0.3 represent the specific surface areas ($m^2\ g^{-1}$) of clay, silt and sand sized particles, respectively. These coefficients can be subjected to calibration (Salm, 2001).

Nonetheless, using Eq 3.2 remains a simple way to model mineral surface area and it is widely used in most geochemical modelling studies (Goddéris et al., 2006; Gudbrandsson et al., 2011; Koptsik et al., 1999; Koseva et al., 2010; Phelan et al., 2014; Stendahl et al., 2013; Violette et al., 2010; Whitfield et al., 2010). Additionally, we chose to use this approach since it suits the setup of our model, and the coupling between physical weathering and chemical weathering soil-forming processes can easily be made. The physical weathering process (see chapter 2 section 2.2.1.2) is already implemented in the SoilGen model; it is sensitive to temperature fluctuations and results to the splitting up of soil particles into finer particles (Finke, 2012). Consequently, the sand, silt and clay fractions in Eq 3.2 are dynamic and are updated each time step. The coupling of equation 3.2 with physical weathering therefore allows us to estimate the change in mineral surface area over time. Change in mineral surface area with time is an important aspect that has hardly been considered in modelling mineral dissolution and precipitation mechanisms (Brantley et al., 2008). However, we make an assumption that all minerals physically weather at the same rate (i.e., all minerals respond to temperature gradients and break apart at the same rate) which is not always true in reality. Therefore the rate of physical weathering for hard minerals like quartz may be overestimated.

In summary, we calculate the reactive mineral surface area of the k^{th} mineral (A_k, $m^2\ mol^{-1}$) as a product of the fraction of the k^{th} mineral in the soil matrix, k_{comp}(-) and the total surface area of the soil, A_j ($m^2\ g^{-1}$) estimated from Eq 3.2. A_k is again multiplied by the relative formula mass of the mineral (k_{RFM}, $g\ mol^{-1}$) to give each mineral surface area, A_k in $m^2\ mol^{-1}$ (Eq 3.3):

$$A_k = A_j \times k_{comp} \times k_{RFM} \quad (3.3)$$

Dealing with the initial reactive surface area of secondary minerals initially not present

The challenge to simulating precipitation of secondary minerals especially those initially not present is the determination of initial surface area (Godderis et al., 2006; 2010; Marty et al., 2015; Pham et al., 2011; Zhu et al., 2010). As such Godderis et al. (2006) considered only secondary minerals initially present as the ones that will precipitate. Although it is a simplification of reality, the authors justified the assumption as reasonable especially for their study which assumed that the catchment was close to steady-state conditions. Other studies have solved this problem by assuming an initial surface area of each mineral that is likely to precipitate. In this study, a common approach in geochemistry (Zhu et al., 2010) is followed, and the initial surface area of the mineral to precipitate is assumed to be equal to its BET-N_2 measured surface area (these values are given in Table 3.2). This value is then multiplied by the respective mineral molecular weight to give area in m^2 mol^{-1}. The reactive surface area of the respective secondary mineral is then the product of the BET-N_2 area (m^2 mol^{-1}) and the weight composition of the secondary mineral. The initial value of the latter is set to a very small value close to zero. Once the mineral starts precipitating, its new weight composition is used together with total mineral surface area obtained from the particle size distribution function (Eq 3.2) to calculate the new mineral reactive surface area using Eq 3.3.

3.4.1.2 Mineral dissolution and precipitation mechanisms

One of the common approaches to modelling both dissolution and precipitation rate of minerals involves the use of kinetic laws derived from the transition state theory, TST (Eyring, 1935; Lasaga, 1981; Aagaard and Helgeson, 1982) in combination with parameters derived from laboratory experiments (Godderis et al., 2006; Marty et al., 2015). According to the TST, the rate at which an elementary reaction proceeds depends on the concentration of the activated complex (transition state) and the frequency at which this activated complex crosses the energy barrier between the reactants and products (Samouëlian et al., 2012). The transition state in this case is an intermediate stage involving two reacting molecules before the actual formation of the product molecule(s). At this transitional stage, the reacting molecules combine to form what is referred to as an activated complex. Aagaard and Helgeson (1982) define an activated complex as an aggregation of atoms similar to an ordinary molecule but with a stronger affinity to dissociate. One of the basic assumptions

of the TST is that the reacting mineral is in some sort of quasi-equilibrium with the activated complex during this transition state (Aagaard and Helgeson, 1982). Thus, assuming H^+, H_2O and OH^- as the only aqueous species involved in the formation of the activated complex with the mineral, the dissolution or precipitation of a mineral promoted by these species can be expressed as in Eq. 3.4. Although the linear-TST approach (Eq 3.4) is general and benefits from existing large database of rate parameters (Marty et al., 2015), the approach has been shown to overestimate mineral growth rates especially for common carbonates (Hellevang and Aagaard, 2013; Pham et al., 2011).

$$r_{TST} = kA(1 - \Omega^s) \tag{3.4}$$

where, r_{TST} (mol s^{-1}) is the dissolution or precipation rate of a given mineral according to transition state theory, A (m^2) is the mineral surface area, $k = k_H a_{H^+}^n + k_{H_2O} + k_{OH} a_{OH^-}^m$, is an empirical dissolution rate constant (mol m^{-2} s^{-1}) at acid, neutral and basic conditions and corrected for temperature (see Eqs 3.7 – 3.10 for details). The part in brackets is usually referred to as the chemical affinity term. The parameter Ω is the saturation term (Eq 3.12) and the superscript s (usually set equal to 1) is a factor used to describe the stoichiometry of the reaction after the activated complex is formed (Aagaard and Helgeson, 1982).

Some studies have therefore opted to use TST-based approach only for estimating mineral dissolution rates and a different model to simulate mineral growth in a separate equation (Equation 3.5). Such approaches have been shown to improve estimation of mineral growth rates but are limited by the unavailability of data on growth rate constants for most minerals, and the difficulty in estimating initial reactive surface areas of growing minerals (Pham et al., 2011; Hellenvang and Aagaard, 2013). To solve the problem of initial mineral surface area, recent mechanisms for simulating secondary mineral nucleation and growth (Fritz et al., 2009; Noguera et al., 2011; Pham et al., 2011) have integrated the nucleation rate term that allows the nucleation of the initial surface area (Pham et al., 2011; Hellenvang and Aagaard, 2013) with the growth rates. Pham et al.(2011) for example, have formulated an approach that still describes mineral dissolution based on the TST theory but applies a

modified growth model combining both growth and nucleation rate term (Nucleation-Growth model) to simulate secondary mineral formation rates (Eq 3.6).

$$r_{Gk} = k_G A(1-\Omega)^2 \quad (3.5)$$

where r_{Gk} is growth rate of mineral k (mol s^{-1}) and k_G is the growth rate constant (mol m^{-2} s^{-1}). A (m^2) is the mineral surface area and Ω is the saturation term (see Eq 3.12)

$$r_{NGk} = -r_{Gk} - k_N \times \exp\left\{-\tau\left(\frac{1}{(T)^{3/2}\mathrm{In}\Omega}\right)^2\right\} \quad (3.6)$$

where r_{NGk} (mol s^{-1}) is the nucleation and growth rate of the k^{th} mineral, k_N (mole s^{-1}) is the nucleation rate term derived from classical nucleation rate theory, and τ is the parameter lumping together the effect of surface tension, molar volume and geometric shape of the surface on the nucleation rate (Hellenvang and Aagaard, 2013; Pham et al., 2011).

The major challenge in applying equations 3.5 and 3.6 is lack of data on growth and nucleation rate constants for most minerals (Marty et al., 2015; Zhu et al., 2010). Hellenvang and Aagaard (2013) compared results from near- and far- from equilibrium experimental studies and demonstrated that the mineral growth rate constant, k_G (from near-equilibrium experiments) can be orders of magnitude lower compared to the dissolution rate constants, k (Eq 3.4) normally obtained far from equilibrium experiments (equation 3.7). They therefore estimated k_G for minerals with missing growth rate constants as equal to two orders lower than their respective k values. Data on nucleation rate term, k_N for most minerals is also lacking and a wide range of these values (10^{10} - 10^{30} nuclei per second per kg of water) have been reported in literature (Fritz et al., 2009; Pham et al., 2011; Steefel and Van Cappellen, 1990). Pham et al. (2011) chose an intermediate value of ($k_N = 10^{22}$ nuclei s^{-1}kg water^{-1}) and recalculated as (k_N = 1 mole s^{-1}) assuming 1 nm spherical nuclei, a density of 2.7 gcm^{-3} and a molar mass of 100 g mol^{-1}. In the same study they set (k_N = 1 mole s^{-1}) for all minerals as varying this term by as much as 3 orders (i.e $1x10^{-3}$, 1 and $1x10^3$ mole s^{-1}) did not significantly influence the timing and the amount of secondary minerals that formed (Pham et al., 2011). Similarly, (Fritz et al., 2009; Noguera et al., 2011) in another modelling approach using the NANOKIN code (Fritz et al., 2009) showed that mineral precipitation rates were not qualitatively

affected by the nucleation rate pre-factor, k_N. τ values for all secondary minerals ranged from $2x10^{10}$ for faster growing minerals to $4x10^{10}$ for slow growing minerals (Pham et al., 2011).

In summary, the lack of sufficient data on rate parameters used in growth and nucleation models (equation 3.5 and 3.6) for most minerals as well as the wider uncertainty for some known parameters, was key for us in our choice to apply the TST based mechanism (equation 3.4) to simulate both mineral dissolution (when $\Omega < 1$) and precipitation (when $\Omega > 1$). Moreover some studies (Schott et al., 2012 and references there in) have shown that both dissolution and precipitation of hydroxides, hydroxyl-carbonates and clays with high BET surface areas and roughness (e.g., Kaolinite) are well described by the TST rate laws indicating a linear relationship between dissolution / precipitation and solution saturation state (Ω). While some experimental findings (Gautier et al., 1994; Oelkers et al., 1994) demonstrated that albite and K-feldspar followed a TST-based approach, other findings (e.g., Hellmann and Tisserand, 2006) reported a sigmoidal relationship between dissolution and growth with the solution saturation state. According to Schott et al. (2012), the differences reported in literature could be explained by the different experimental protocols followed in the laboratory such as fluid flow rates used. Based on Schott et al. (2012) conclusions, minerals with low surface areas and consequently fewer sites for dissolution and growth (e.g quartz, albite, K-feldspar, magnesite), may exhibit a wide range (linear to highly non-linear) of rates of dissolution and precipitation dependency on solution saturation state.

Implemented mechanism for the mineral dissolution rate, r_k

Brantley et al. (2008) have provided an extensive review of mineral dissolution rate mechanisms. In general, the dissolution rate mechanism depends on the group in which the mineral belongs (i.e., feldspars, oxides or carbonates). Similar to the mechanisms described elsewhere (Godderis et al., 2006; Maher et al., 2009; Violette et al., 2010), we calculate the dissolution rate of each mineral at far from equilibrium conditions, as a function of pH (Brantley et al. (2008); Eq. 3.7). The affinity term and the inhibition factor are added to equation 3.7 to account for the reactions at near-equilibrium conditions and the effect of dissolved ions (Godderis et al., 2006; Violette et al., 2010), respectively on the mineral dissolution rate (Eq. 3.8). The mineral precipitates when the affinity term is negative

(Godderis et al., 2006). Different mechanisms (Eq 3.13) and (Eq 3.14) are however defined for dolomite and calcite. Table 3.2 presents input data of dissolution rate constants, activation energies and reaction orders required for simulation of H^+ (k_H) and OH^- (k_{OH}) promoted dissolution / precipitation rates of minerals proposed for implementation to the SoilGen model.

$$r_k = k_H a_{H^+}^n + k_{H_2O} + k_{OH} a_{OH^-}^m \quad (3.7)$$

$$r_k = \left(k_H a_{H^+}^n + k_{H_2O} + k_{OH} a_{OH^-}^m\right) \times f_{inh} \times (1 - \Omega^s) \quad (3.8)$$

where k_H and k_{OH} are mineral dissolution rate constants at acidic and basic conditions, respectively. The parameters k_H and k_{OH} have to be corrected for temperature (Eqs. 3.9 and 3.10). $a_{H^+}$and a_{OH^-} are activities of H^+ and OH^-, respectively and superscripts n and m denote the reaction orders. k_{H_2O} is a parameter describing the dissolution rate at neutral pH and was not considered in the implementation because at neutral conditions the dissolution rate of silicates is so slow that this term makes an insignificant contribution to the overall silicate dissolution rate (Brantley, 2004). f_{inh} (see next next page for more explanation) is the aluminium inhibition factor calculated as a function of total aluminium activity in solution (Oelkers et al.,1994; Oelkers and Schott, 1995) as described in (Eq. 3.11), Ω is the saturation ratio of the mineral calculated as in (Eq 3.12) and superscript s is set equal to 1.

$$\frac{k_H}{k_{H25}} = exp\left[\frac{E_a H}{R}\left(\frac{1}{298.15} - \frac{1}{T}\right)\right] \quad (3.9)$$

$$\frac{k_{OH}}{k_{OH25}} = exp\left[\frac{E_a OH}{R}\left(\frac{1}{298.15} - \frac{1}{T}\right)\right] \quad (3.10)$$

where k_{H25} and k_{OH25} are measured dissolution rate constants at 25°C (298.15 K), $E_a H$, $E_a OH$ (KJ mol $^{-1}$ K $^{-1}$) are the activation energies of a kth mineral at acidic and basic conditions, respectively and

R is a gas constant (0.00831446 KJ mol $^{-1}$ K $^{-1}$). T is absolute soil temperature (K) and it is simulated in the model.

Accounting for the inhibition of mineral dissolution by aqueous species

The inhibition of dissolution of minerals by aqueous species has been explored in a number of studies (e.g., Biber et al., 1994; Ganor and Lasaga, 1998; Gautier et al., 1994; Oelkers et al., 1994; Stumm and Wollast, 1990). According to Ganor and Lasaga (1998), the retarding of mineral dissolution rate by the inhibiting aqueous species (e.g., Al^{3+}) can be explained by two mechanisms: (i) the competition of the inhibitor (e.g., Al^{3+}) with the dissolution catalyst (e.g., H^+ and OH^-) for the same mineral surface adsorption sites and (ii) the independent adsorption of the inhibitor on to the mineral surface sites. During such reactions, the inhibitor (particulary at higher concentration) may limit the contact between the mineral surface and the catalyst, consequently retarding the dissolution process (Biber et al., 1994; Ganor and Lasaga., 1998; Stumm and Wollast, 1990). According to Oelkers et al. (1994), the dissolution rate of alkali feldspars is inhibited by high aluminium solution concentration. These authors reported a linear decrease of log-transformed dissolution rates of kaolinite and albite minerals with increase in log-transformed aluminium solution concentration. Gautier et al. (1994) found a similar relationship between aluminium solution concentration and K-feldspar dissolution rates. Unlike for other species (e.g., Na^+ and K^+), the inhibition of dissolution by Al solution concentration is well studied and seems to be the most important (e.g., Biber et al., 1994; Ganor and Lasaga., 1998; Gautier et al., 1994; Godderis et al., 2006; Oelkers et al.,1994; Oelkers and Schott, 1995; Roeland et al., 2010). Therefore, the total aluminium solution concentration is considered here (see Eq 3.8) as the only inhibiting aqueous species and it is described by the inhibition factor, f_{inh}. This f_{inh} factor (Eq 3.11) is described in Roelandt et al. (2010) and is derived from experimental results on dissolution rates of aluminosilicates (e.g., Oelkers et al.,1994; Oelkers and Schott, 1995).

$$f_{inh} = \left[\frac{10^{-7}}{10^{-7}+\sum Al}\right]^{0.33} \quad (3.11)$$

where $\sum Al$ is the sum of all dissolved Al-species (mol L^{-1}).

$$\Omega = {}^{IAP}/_{K_{eq}} \quad (3.12)$$

where IAP is the ion activity product expressed as the ratio of product activities to reactant activities. IAP therefore takes the same form as equilibrium constant (K_{eq}) but describes the activities of reactants and products for a solution that may not be in the state of equilibrium. Log K_{eq} values for the implemented minerals are given in Table 3.1. Based on Eq. 3.12, a given mineral is precipitated when $\Omega > 1$ i.e., when its IAP value is higher than its respective K_{eq} value.

In addition to pH, the dissolution kinetics of calcite and dolomite (equations 3.13 and 3.14) are influenced by the activities of Ca^{2+} and CO_3^{2-} ions in the soil solution. The dissolution and precipitation rates of these minerals are therefore modelled differently as in (Alkattan et al., 1998; Goddéris et al., 2010; Pokrovsky et al., 2009; Violette et al., 2010):

$$r_{calcite} = \left[k_H a_{H^+} + \frac{k_0}{1\times10^{-5} + a_{CO_3{}^{2-}}}\right] \times (1 - \Omega^s) \quad (3.13)$$

where $k_H = 1 \times 10^{-0.659}$ mol m^{-2} s^{-1} and $k_0 = 1 \times 10^{-11}$ mol m^{-2} s^{-1} at 25 ^oC (Wollast, 1990). Pokrovsky et al. (2009) set the activation energies for k_H and k_0 equal to 8.5 and 30 kJ mol^{-1}, respectively. s is set equal to 1 for calcite (Goddéris et al., 2010; Violette et al., 2010).

$$r_{dol} = \left[k_H a_{H^+}^{0.75} + k_{Mg} * \left(\frac{1.575*10^{-9}}{1.575*10^{-9}+3.5*10^{-5}+ a_{CO_3} * a_{Ca}}\right)\right] \times (1 - \Omega^{1.9}) \quad (3.14)$$

where $k_H = 1 \times 10^{-3}$ mol m^{-2} s^{-1} and $k_{Mg} = 1 \times 10^{-8.2}$ mol m^{-2} s^{-1}, at 25 ^oC (Pokrovsky et al., 1999). The activation energies for k_H and k_{Mg} are given as 40 and 60 kJ/mol, respectively (Goddéris et al., 2010; Pokrovsky et al., 1999).

Table 3.2 Summary of input data for calculation of mineral dissolution and precipitation rate, r_k (Eq 3.8). $k_{H\ and}$ k_{OH} are mineral kinetic dissolution rate constants at 25°C (Mol m^{-2} s^{-1}) promoted by H^+ and OH^- species, respectively. E_aH and E_aOH denote the activation energies (KJ mol^{-1} K^{-1}) during reactions promoted by H^+ and OH^-, respectively. n and m indicate reaction orders with respect to H^+ and and OH^- promoted dissolution.

	k_H			**k_{OH}**				Surface
Mineral, k	Log k_{H25} Mol m^{-2} s^{-1}	E_aH KJ mol^{-1} K^{-1}	n (-)	Logk_{OH25} Mol m^{-2} s^{-1}	E_aOH KJ mol^{-1} K^{-1}	m (-)	Source	Area (m^2 g^{-1})
Primary minerals								
Albite	-9.70	66.9	0.50	-9.95	60	0.50	[1]	0.17[5]
Anorthite	-5.90	79.5	0.90	No effect			[1]	0.43[6]
Augite	-6.82	78.0	0.70	No effect			[2]	0.24
Biotite	-10.88	35.0	0.32	No effect			[3]	1.66[5]
Chlorite	-10.02	40.0	0.50	-11.8	40	0.20	[3]	1.35[5]
Fayalite	-4.80	94.4	0.69	No effect			[2]	0.08[6]
Forsterite	-6.85	67.2	0.47	No effect			[2]	0.08[6]
Hornblende	-10.20	50.0	0.55	No effect			[3]	0.18[6]
Illite	-11.47	46.0	0.60	-12.3	67	0.60	[1]	41.00[7]
K-feldspar	-9.90	50.2	0.40	-10.7	50	0.30	[1]	0.11[6]
Muscovite	-11.8	54.4	0.14	-11.7	22	0.16	[1]	0.68[6]
Quartz	No effect			-11.0	85	0.25	[3]	0.07[5]
Secondary minerals								
Calcite	-0.3	14.4	1.00	-3.48	35.4	1.00	[2]	0.70[5]
Dolomite	-3.19	36.1	0.50	-5.11	34.8	0.50	[2]	0.12[5]
Gibbsite	-7.65	47.5	0.99	-16.65	80.1	-0.78	[2]	1.28[5]
Goethite	-	-	-	-	-	-		41.50[8]
Gypsum	-	-	-	-	-	-		-
Hematite	-9.39	66.2	1.00	No effect			[2]	311.00[8]
Imogolite	-	-	-	-	-	-		133.00[9]
Kaolinite	-12.45	50.0	0.28	-10.74	40.0	0.73	[1]	11.22[5]
Montmorillonite	-9.8	48.0	0.38	No effect			[1]	71.00[7]
Siderite	-5.23	56.0	0.60	No effect			[4]	3.30[5]

[1]Goddéris et al., 2006; [2] Data as reported in Palandri and Kharaka, 2004 (T=25 °C; pH= 0);[3]Violette et al., 2010; [4]Leal et al., 2015. Dashes (-) imply no data reported at acid and basic conditions. [5]Average of the range of BET-SSA values for minerals based on database reported in Marty et al., 2015 and available at https://www.thermochimie-tdb.com/pages/kinetic_models.php; [6]Average of the range of BET-N_2 specific surface area (SSA) values for minerals based on database compiled by Bandstra et al.,2008; [7]SSA of Illite and Montmorillonite as reported in Macht et al., 2011; [8]SSA of Hematite and Goethite as reported in Villacís-García et al., 2015; [9]SSA of Imogolite as reported in Gustafsson et al., 1998.

Steps for tracking precipitation of secondary minerals in SoilGen

Schematic representation of the steps that are followed when incorporating precipitation of secondary minerals into SoilGen weathering module is shown in Figure 3.1. These steps are as follows:

1. Based on the given set of secondary minerals (shown in Table 3.1), and based on their composition in the soil solution, minerals likely to precipitate can be determined. The likelihood of a mineral precipitating depends on the values of equilibrium constants and saturation term
2. Therefore for each secondary mineral k, saturation ratio, Ω_k (Eq 3.12) is calculated (assuming congruent reactions; Table 3.1) at every time step.
3. If at that time step, $\Omega_k > 1$, then that mineral will precipitate and the moles used up to form a precipitate are calculated following Eq 3.8. A negative sign will however be added to this equation indicating removal of moles from the soil solution. Whatever is precipitated is added into the precipitated phase (Figure 3.1).
4. Otherwise if $\Omega_k < 1$, then that secondary mineral will dissolve contributing to element fluxes with moles calculated following equation 3.8 but with positive sign indicating addition of moles into the soil solution.
5. Or else there is an equilibrium situation, and at that time step the mineral will neither dissolve nor precipitate. The precipitation of primary silicate minerals is not allowed and this is ensured by setting their dissolution rates equal to zero whenever there is there is saturation (i.e., $\Omega_k > 1$) with respect to these minerals (Godderis et al., 2010).

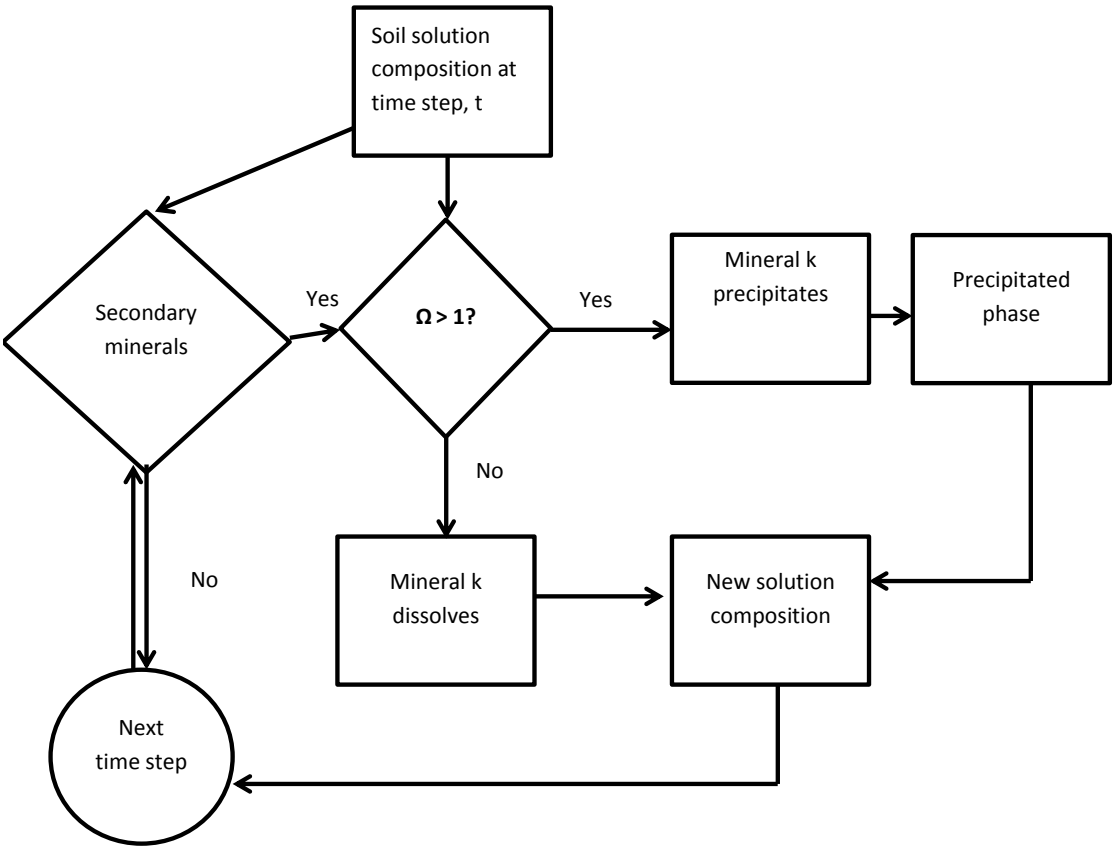

Figure 3.1. Flow chart showing the steps to incorporate the precipitation of minerals into the biogeochemical system implemented in the SoilGen model. Ω = $^{IAP}/_{K_{eq}}$ where IAP = ion activity and K_{eq} is the equilibrium constant.

Other related dissolution mechanisms

In addition to the dissolution and precipitation mechanisms described above, the soil solution composition of Iron (Fe) and Silicon (Si) are influenced by redox processes and phytolith dissolution, respectively. The detailed terrestrial cycling of these two elements is presented in chapter 4. In this section, we proposed to add phytoliths (defined in chapter 4) dissolution mechanism (Eq 3.15) and redox processes (Eqs 3.17 and 3.19) as additional mechanisms controlling the soil solution composition of Si and Fe, respectively.

The release rate of Si from the dissolution of phytoliths presented here is based on the empirical equation (Eq 3.15) defined in Fraysse et al. (2009). Phytoliths have been identified as a major pool of Si in the soil (Fraysse et al., 2009; Gérard et al., 2008) and are therefore important to take into account when modelling Si cycling.

$$\mathrm{r_{Siphyto}}\left(\frac{mol}{m^2 s}\right) = 6 \times 10^{-12} \times a_{H+} + 5 \times 10^{-14} + 3.5 \times 10^{-9} \times a_{OH-}^{0.33} \quad (3.15)$$

$$\mathrm{Si}_{phyto} = \mathrm{r_{Siphyto}} \times \mathrm{A_{phyto}} \times m_{\mathrm{phyto}} \quad (3.16)$$

where Si_{phyto} (mol m^{-2} s^{-1}) is the moles of Si released from phytolith dissolution, $\mathrm{r_{Siphyto}}$ is the dissolution rate of phytoliths, and A_{phyto} (m^2 g^{-1}) is the specific surface area of phytolith. m_{phyto} (g m^{-2}) is the mass content of phytoliths in the soil which depends on the vegetation type and the total above ground net primary productivity (NPP). For example, Song et al. (2013) reported an average phytoliths content of 1.71 % (for forest species) while Song et al. (2012) estimated an average of 3.3 % (for grass species) of the total above ground net primary productivity (NPP).

Oxidation rate of Fe^{2+} to Fe^{3+} ($\mathrm{r}_{Fe^{2+}_{oxid}}, mol\ L^{-1} min^{-1}$) has been given in (Stumm and Lee, 1961) and modelled as in Eq 3.17 while reduction rate of Fe^{3+} to Fe^{2+} in natural environments is described in (Eq 3.19) following concepts described in Stumm and Sulzberger (1992) and Roden and Urrutia (1999).

$$\mathrm{r}_{Fe^{2+}_{oxid}} = \mathrm{k}_{oxd} \times \mathrm{a}_{Fe^{2+}} \times pO_2 \times \mathrm{a}_{OH^-}{}^2 \quad (3.17)$$

where k_{oxd} = 1.5 x 10^{-13} L^2 Mol^{-2} atm^{-1} min^{-1} (Stumm and Lee, 1961), $\mathrm{a}_{Fe^{2+}}$ and a_{OH^-} are the activities of Fe^{2+} and OH^- ions in the soil solution, respectively. pO_2 (the partial pressure of oxygen; atmospheres) in the soil can be related to pCO_2 (already simulated in SoilGen as a function of decomposition of organic matter and diffuse gas transport in the soil). Assuming that the partial

pressure of nitrogen gas (pN_2) is constant, a relationship between pO_2 and pCO_2 in the atmosphere (equation 3.18) can be used to calculate pO_2 as:

$$\mathrm{pO_2} + \mathrm{pCO_2} = 0.21035 \text{ (i.e., 0.21 + 0.00035)} \quad (3.18)$$

To prevent negative values of pO_2, a function $pO_2 = \max(0,\ 0.21035 - 0.00035)$ is included.

Iron (III) reduction rate is modelled from first order rate equation (Eq 3.19) and is directly proportional to the activity of Fe^{3+} in the soil solution.

$$\mathrm{r}_{Fe^{3+}_{red}} = \mathrm{k}_{red} \times \mathrm{a}_{Fe^{3+}} \quad (3.19)$$

where k (day^{-1}) is the reduction rate constant. Roden and Urrutia (1999) estimated k value at 0.453 day^{-1} after fitting the regression equation of measured Fe^{3+} reduction rates versus the initial concentration of free surface sites.

3.4.1.3 Estimating the initial amount of the mineral, m_k

The initial total mass of all the minerals in the parent material, M in each soil compartment is corrected for organic matter (f_{rOM}) and estimated as follows:

$$M = \rho \times (1 - f_{rOM}) \quad (3.20)$$

where ρ (kg m^{-3}) is the bulk density of the soil and f_{rOM} is calculated from organic carbon content (%OC) and it represents the fraction of soil matrix occupied by organic matter.

The initial amount of individual mineral, m_k (needed in Eq 3.2) is obtained by multiplying the weight fraction of each k^{th} mineral in the parent material, $f_{j,k}$ by the fraction of the parent material in the soil layer, f_j with the total mineral mass M (equation 3.20) as:

$$m_k = f_{j,k} \times f_j \times M \quad (3.21)$$

3.5 Weathering indices

A weathering index is a proxy of chemical weathering intensity usually calculated by comparing the molecular amounts of elemental oxides in a weathered material with their respective composition in the original un-weathered material (Le Blond et al., 2015; Fiantis et al., 2010; Price and Velbel, 2003). One of the objectives (Chapter 1) was to incorporate the calculation of weathering indices in the SoilGen model. Incorporating calculation of weathering indices in the SoilGen model not only widens the application of the model outputs (e.g. in evaluating soil fertility) but also enhances comparison of model results with field data and literature findings. Specifically, calculating such indices using the simulated elemental composition of soils over time will help in answering several questions such as (i) whether the weathering-related processes in the model are adequately defined, (ii) whether the past and present fluxes at the model boundary are sufficiently known; and (iii) how the future global change will affect chemical weathering rates.

Weathering indices (WIs) have long been used in assessing the degree of chemical weathering and as well as soil development (e.g., Le Blond et al., 2015; Buggle et al., 2011; Harnois, 1988; Price and Velbel, 2003; Zhang et al., 2007). Previous studies have also demonstrated the use of some WIs in climatic studies (e.g., Nesbitt and Young, 1982; Adams et al., 2011; Goldberg and Humayun, 2010), in assessing soil fertility (e.g., Delvaux et al., 1989; Fiantis et al., 2010) and in geochemical and environmental studies (e.g., Gallagher and Sheldon, 2013; Lee et al., 2008).

Examples of the WIs commonly found in literature include; chemical index of alteration (CIA), chemical index of weathering (CIW), plagioclase index of alteration (CPA), index B, weathering index (WI), weathering index of Parker (WIP), Ruxton ratio (R) and chemical proxy of alteration (CPA). Table 3.3 summarizes commonly applied weathering indices (Buggle et al., 2011) together with their formulas and comments on their strengths and potential limitations. Evaluation of most of these WIs for their application in assessing degree of chemical weathering has been presented in previous studies (Hranois, 1988; Duzgoren-Aydin et al., 2002; Price and Veldel, 2003; Zhang et al., 2007; Buggle et al., 2011; Shao et al, 2012). According to Price and Veldel (2003), whether a weathering index is applicable or not for a given situation can be evaluated by observing the trends and comparing with independent measures of weathering such as bulk density. Therefore WIs whose values increase with

intensity of weathering (e.g. CIA, CIW and CPA) should increase as bulk density decreases. Burke et al. (2006) also showed that weathering intensity increases with decreasing pH. Thus WIs that increase with intensity of weathering should increase with decreasing pH while the opposite trends should be observed for the WIs that decrease with increasing weathering intensity (e.g. Index B, R, WIP). In addition, weathering intensity should generally decrease with increasing profile depths.

3.5.1 Weathering indices implemented in the SoilGen model

The outputs of SoilGen model at each simulation year include concentrations of cations (Ca, Mg, Na, K, Al) in solution, as precipitates, in the exchange phase and in organic matter, pH, bulk density, cation exchange capacity (CEC), calcite, organic carbon (OC) and texture (sand %, clay %, silt %). Calculation of various WIs, which requires the total concentration of mobile elements (Ca, Mg, Na, K) and immobile elements (Al) is therefore feasible in the model. The weathering indices that are already calculated in the SoilGen model include (CPA, CIA, CIW, PIA, Index B and WI). It was possible to calculate these indices based on the simple chemistry already described in the SoilGen model (chapter 2: Fig 2.1). Calculation of other weathering indices (e.g., Sa and Saf; Table 3.3) is feasible after the full implementation and testing of the extended chemical weathering mechanism (described above) and the inclusion of more chemical elements (described in chapter 4).

In general, the weathering indices were computed by summing up respective element concentrations from different pools (i.e., mineral, exchange and solution phases, organic pools and precipitated pools; see Fig 2.1 in chapter 2) at each time step (yearly). This approach mimics laboratory protocols such as in Fiantis et al. (2011) that are applied on the entire soil. These total concentrations were converted to molecular proportions needed in the calculation of WIs using respective oxide molecular weights (RFM). Figure 3.2 summarises the steps followed in the calculation of the weathering indices in the SoilGen model.

Table 3.3. Overview of weathering indices commonly reported in chemical weathering studies

Weathering index	Formula	Strength	Weakness	Reference
Chemical proxy of alteration (CPA)	$[Al_2O_3/(Al_2O_3+Na_2O)]$ x100	Na is very mobile and suitable in carbonate rich parent material Al forms insoluble hydrolyzate, thus suitable as immobile element	May not to be suitable for carbon free parent materials	Buggle et al., 2011
Chemical index of alteration (CIA)	$[Al_2O_3/(Al_2O_3+Na_2O+CaO^*+K_2O)]$x100		Less sensitive for weak pedogenic alteration: K becomes immobile as it becomes adsorbed	Nesbitt & Young, 1982
Index B	$(CaO^*+Na_2O+K_2O)/(Al_2O_3+CaO^*+Na_2O+K_2O)$			Kronberg & Nesbitt, 1981
Chemical index of weathering (CIW)	$[Al_2O_3/(Al_2O_3+Na_2O+CaO^*)]$x100		Indices relying on Ca and Mg tend not to reflect true weathering and leaching intensity of a palaeosol due to postpedogenic formation of secondary carbonates (Buggle et al., 2011)	Harnois, 1988
Plagioclase index of alteration (PIA)	$[(Al_2O_3- K_2O)/(Al_2O_3+ CaO^*+ Na_2O - K_2O)]$x100			Fedo et al., 1995
Silcon- Aluminium ratio (Sa)	SiO_2/Al_2O_3		Could not adequately express sequential weathering degree of the chronosequence	
Silcon- Aluminium-iron ratio (Saf)	$SiO_2/(Al_2O_3 + Fe_2O_3)$			Zhang et al., 2007
Weathering index (WI)	$R_{sample}/R_{reference}$, where R = $Al_2O_3/(CaO+Na_2O)$, underlying rock is used as reference	Gives good relationship with age (Zhang et al., 2007)	Also relies on Ca, and so tend not to reflect true weathering &leaching due to 2^o carbonate formation	Price et al., 1991
Ba/ Nb	Ba/ Nb		Lost under intense weathering	Zhang et al., 2007
Rare Earth Elements	REE	Excellent linear relationship with soil age was obtained		Zhang et al., 2007 Price et al., 1991

CaO* is Calcium from only silicate minerals, it is measured with assumption that molar ratio of CaO/Na_2O from carbonate free silicate material does not exceed 1 (Buggle et al., 2011).

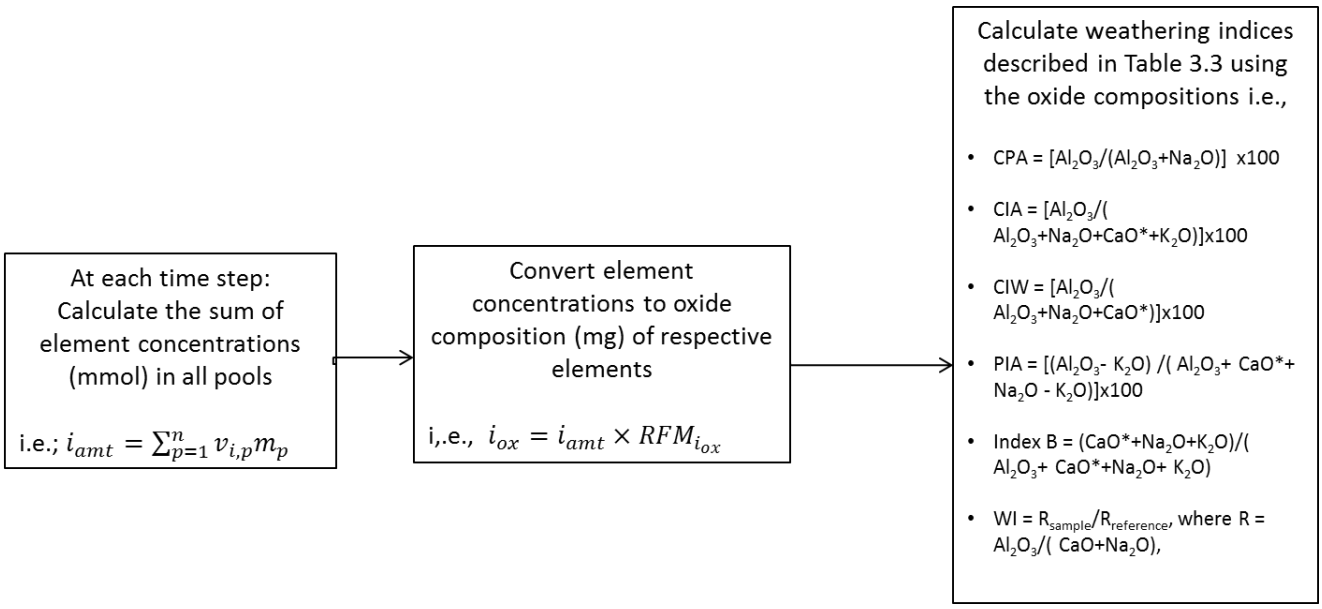

Figure 3.2. Steps followed in calculating weathering indices in the SoilGen model. $\boldsymbol{v_{i,p}}$ is the stoichiometric number of cation i in pool p, $\boldsymbol{m_p}$ is the total mmoles of pool p at a given time step, n is the total number of pools, $\boldsymbol{i_{amt}}$ is the amount of a given element (mmol) remaining at each timestep during weathering. $\boldsymbol{i_{ox}}$ is the elemental oxide composition (mg) and $\boldsymbol{RFM_{i_{ox}}}$ is the corresponding relative formular mass (g mol^{-1}) of the oxide (e.g., if i = Na; then $\boldsymbol{RFM_{i_{ox}} = RFM_{Na_2O} = 2 \times 23 + 16 = 62\ g\ mol^{-1}}$)

3.5.2 Preliminary tests on weathering indices implemented in the SoilGen model

Test model simulations were carried out on a toposequence in Belgian loess soils (50°46'31"N, 4°24'9"E). The evolution of six implemented WIs (Fig 3.2) was simulated for three profiles located in 3 different topo-sequence positions (i.e.; Plateau, North and South facing slopes; Finke, 2012). These soils were characterized mineralogically and chemically as well (Van Ranst, 1981; Finke, 2012). Example results from these test simulations are presented in Fig. 3.3.

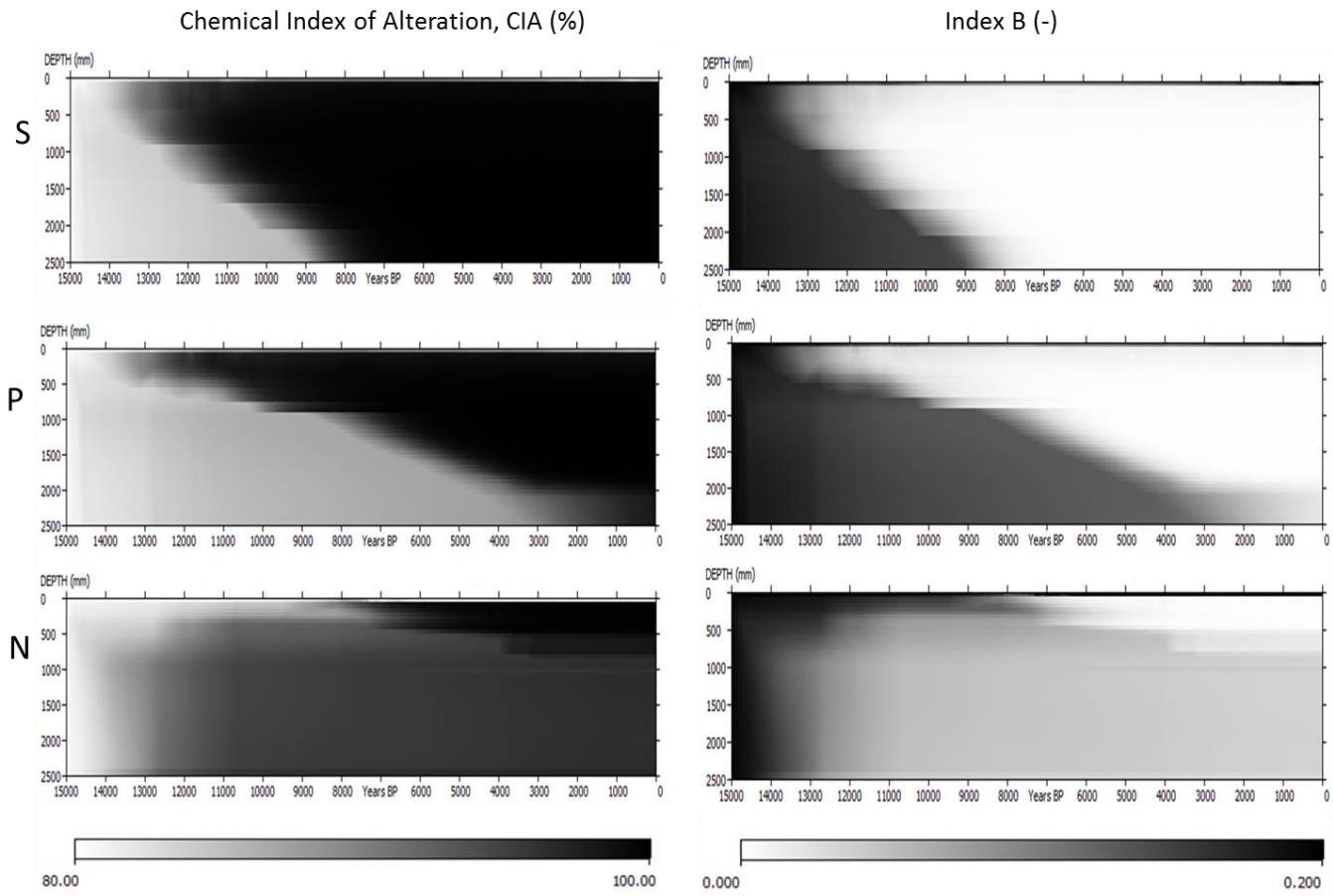

Figure 3.3. An example output of the evolution of weathering indices over depth (mm) and time (15000 years) as chemical weathering progresses. S, P and N represent three profiles at different topo-sequence positions: South, Plateau and North facing profiles, respectively. Notice that weathering intensity is differently represented by two indices i.e., Chemical Index of Alteration (CIA) values increase with time but Index B values decrease with time. Therefore higher values of CIA indicate stronger weathering whereas lower values of Index B indicate stronger weathering.

Time-depth diagrams of the weathering indices over 15000 years (Figure 3.3) showed a plausible development over time and depth. In addition, results showed a consistent relation between the topographic position, the amount of percolation and consequently the chemical weathering intensity (Figure 3.3). In general, all weathering indices indicated that chemical weathering was more intensive at the South facing slope, which receives more rain and solar radiation compared to the North facing

slope, receiving relatively lower net precipitation and radiation due to its exposition (Finke, 2012). However, the weathering indices indicated that the loess is highly depleted in mobile elements. As an example, simulated CIA-values are up to 94% after 15000 years of soil development (Figure 6.3). Such high CIA values indicate the dominance of kaolinite mineral (Nesbitt and Young, 1982). Confrontation of simulated weathering indices to those calculated from analytical data (see Table 3.4) also showed a systematic model overestimation of the indices across all the three profiles (CIA: 20 to 30% higher; CIW: 10 – 15% higher and PIA: 13- 20% higher). Thus, the simulated weathering is probably too strong or the initial pool size was underestimated. It should also be noted that the calculation of these indices was based on the simple chemical weathering system (Chapter 2, Fig 2.1) in which newformation of secondary minerals is not yet included. These results are therefore preliminary and are not discussed further in this thesis.

Table 3.4. Comparison of selected simulated and calculated weathering indices

Profile	Depth (m)	Index	*Calculated (%)	Simulated (%)	Difference (%)
P	1.7	CIA	75.99	98.48	-22.49
		CIW	88.01	98.78	-10.77
		PIA	85.73	98.74	-13.01
S	1.7	CIA	68.35	97.98	-29.63
		CIW	83.12	98.04	-14.92
		PIA	78.43	98.16	-19.73
N	1.7	CIA	69.43	94.45	-25.02
		CIW	83.40	95.35	-11.95
		PIA	79.21	95.00	-15.79

* Weathering indices were calculated based on the total geochemical analysis results presented in van Ranst, 1981, pg 57. P, S and N are plateau, south facing and north facing profiles respectively. Slope orientation is the main difference among these profiles with the South facing profile directly facing the direction of rain, while north facing profile is shaded off. Both calculated and simulated weathering indices are weighted averages over the profile depth of 1.7 m.

3.6 Summary

In this chapter, an extended chemical weathering mechanism based on laboratory kinetic laws and previous studies, has been formulated and implemented in the SoilGen model. The proposed weathering mechanism includes both the dissolution of primary and secondary minerals and the precipitation of secondary minerals. The formulated chemical weathering routine simulates the release of cation species (Ca, Mg, K , Na Fe, Al and Si) from each mineral as a function of the mineral reactive surface area, the mineral dissolution / precipitation rate, the weight composition of the mineral and the stoichiometric coefficient of that cation in the mineral (Eq 3.1). The two key parameters in this formulation include (i) the mineral surface area and (ii) the mineral dissolution / precipitation rate. We adapted the approach by Sverdrup and Warfvinge (1993; 1995) to calculate the total mineral surface area from soil texture (i.e., fractions of sand, clay and silt) and individual mineral reactive surface area is calculated as the product of the total area and individual mineral weight composition. Our approach is unique in that the change in mineral surface area over time is calculated by coupling physical weathering and chemical weathering processes. The mineral dissolution or precipitation rate is formulated based on the transition state theory and soil pH is a driving parameter. Sensitivity results of the coupling of physical and chemical weathering processes (Eqs 3.2, 3.3) using far-from equilibrium mineral dissolution rate mechanism (Eq 3.7) are presented in Opolot and Finke, 2015 (Chapter 6 of this thesis). Implementation of near-equilibrium mineral dissolution rate mechanism (Eq 3.8) into the SoilGen model is still underway and therefore such test case studies are not presented in this thesis. Finally, calculation of six weathering indices was implemented in the SoilGen model. A test case study was done on the soil profiles in the Zonian forest, Belgium and preliminary results showed that weathering intensity was overestimated by the model.

Author contribution

This chapter was designed, developed and written by E. Opolot. Peter Finke had a significant contribution through reviewing, introducing flexibility through “amorphite” and “otherite” minerals and programming the extended weathering code into the SoilGen code.

References

Aagaard, P., Helgeson, H.C., 1982. Thermodynamic and kinetic constraints on reaction rates among minerals and aqueous solutions: I. Theoretical considerations. American Journal of Science 282 (3), 237–285.

Adams, J. S., Kraus, M. J. and Wing, S. L.: Evaluating the use of weathering indices for determining mean annual precipitation in the ancient stratigraphic record, Palaeogeogr. Palaeoclimatol.Palaeoecol., 309(3-4), 358–366, doi:10.1016/j.palaeo.2011.07.004, 2011.

Alkattan, M.: An experimental study of calcite and limestone dissolution rates as a function of pH from −1 to 3 and temperature from 25 to 80°C, Chem. Geol., 151(1-4), 199–214, doi:10.1016/S0009-2541(98)00080-1, 1998.

Arthur, E., Tuller, M., Moldrup, P., Resurreccion, A. C., Meding, M. S., Kawamoto, K., Komatsu, T. and de Jonge, L. W.: Soil Specific Surface Area and Non-Singularity of Soil-Water Retention at Low Saturations, Soil Sci. Soc. Am. J., 77(1), 43, doi:10.2136/sssaj2012.0262, 2013.

Bandstra J. Z., Buss H. L., Campen R. K., Moore J., Hausrath E. M., Liermann L. J., Navarre A. K., Jang J. and Brantley S. L.: Compilation of mineral dissolution rates. In Kinetics of Water Rock Interactions (eds. S. L. Brantley and J. D. K. A. F. White). Springer, New York, 2008.

Biber, M. V., Afonso, M. D. and Stumm, W.: the Coordination Chemistry of Weathering .4. Inhibition of the Dissolution of Oxide Minerals, Geochim. Cosmochim. Acta, 58(9), 1999–2010, doi:10.1016/0016-7037(94)90280-1, 1994.

Brantley, S. L.: Reaction kinetics of primary rock-forming minerals under ambient conditions. In Treatise on Geochemistry (Surface and ground water, weathering, and soils) (ed. J. I. Drever). Elsevier Pergamon, San Diego, CA. pp. 73–118. 2004.

Brantley, S. L., Kubicki, J. D. and White, A. F.: Kinetics of Water-Rock Interaction. Springer Science+Business Media, LLC. 2008.

Buggle, B., Glaser, B., Hambach, U., Gerasimenko, N. and Marković, S.: An evaluation of geochemical weathering indices in loess–paleosol studies, Quat. Int., 240(1-2), 12–21, doi:10.1016/j.quaint.2010.07.019, 2011.

Burke, B.C., Heimsath, M.A. and White, A.F.: Coupling chemical weathering with soil production across soil-mantled landscapes, Earth Surf. Process. Landforms, DOI: 10.1002/esp.1443, 2006.

Carlson, D., Plummer, C., and Hammersley, L.: Physical Geology Earth Revealed, 9th Edition, Published by McGraw-Hill, New York, 670p, 2011.

Delvaux, B., Herbillon, A. J. and Vielvoye, L.: Characterization of a weathering sequence of soils derived from volcanic ash in Cameroon. Taxonomic, mineralogical and agronomic implications, Geoderma, 45(3-4), 375–388, doi:10.1016/0016-7061(89)90017-7, 1989.

Duzgoren-Ayden, NS, Ayden, A, Malpas, J.: Reassessment of chemical weathering indices: case study on pyroclastic rocks of Hong Kong. Engineering Geology 63: 99–119, 2002.

Eyring, H.: The activated complex in chemical reactions. J. Chem. Phys. 3, 107–115, 1935.

Fedo C.M, Nesbitt H.W, Young G.M.: Unraveling the effects of potassium metasomatism in sedimentary rocks and paleosols, with implications for paleoweathering conditions and provenance. Geology 23: 921-924, 1995.

Fiantis, D., Nelson, M., Shamshuddin, J., Goh, T. B. and Van Ranst, E.: Determination of the geochemical weathering indices and trace elements content of new volcanic ash deposits from Mt. Talang (West Sumatra) Indonesia, Eurasian Soil Sci., 43(13), 1477–1485, doi:10.1134/S1064229310130077, 2010.

Fiantis, D., Nelson, M., Shamshuddin, J., Goh, T. B. and Van Ranst, E.: Changes in the chemical and mineralogical properties of Mt. Talang volcanic ash in West Sumatra during the initial weathering phase, Communications in Soil Science and Plant Analysis 42, 569-585, doi:10.1080/00103624.2011.546928, 2011.

Finke, P. A.: Modeling the genesis of luvisols as a function of topographic position in loess parent material, Quat. Int., 265, 3–17, doi:10.1016/j.quaint.2011.10.016, 2012.

Fraysse, F., Pokrovsky, O. S., Schott, J. and Meunier, J.-D.: Surface chemistry and reactivity of plant phytoliths in aqueous solutions, Chem. Geol., 258(3-4), 197–206, doi:10.1016/j.chemgeo.2008.10.003, 2009.

Fritz, B., Clément, a., Amal, Y. and Noguera, C.: Simulation of the nucleation and growth of simple clay minerals in weathering processes: The NANOKIN code, Geochim. Cosmochim. Acta, 73(5), 1340–1358, doi:10.1016/j.gca.2008.11.043, 2009.

Gallagher, T. M. and Sheldon, N. D.: A new paleothermometer for forest paleosols and its implications for Cenozoic climate, Geology, 41(6), 647–650, doi:10.1130/G34074.1, 2013.

Ganor, J. and Lasaga, A. C.: Simple mechanistic models for inhibition of a dissolution reaction, Geochim. Cosmochim. Acta, 62(8), 1295–1306, doi:10.1016/S0016-7037(98)00036-2, 1998.

Ganor, J., Lu, P., Zheng, Z. and Zhu, C.: Bridging the gap between laboratory measurements and field estimations of silicate weathering using simple calculations, Environ. Geol., 53(3), 599–610, doi:10.1007/s00254-007-0675-0, 2007.

Gautier, J.-M., Oelkers, E. H. and Schott, J.: Experimental study of K-feldspar dissolution rates as a function of chemical affinity at 150°C and pH 9, Geochim. Cosmochim. Acta, 58(21), 4549–4560, doi:10.1016/0016-7037(94)90190-2, 1994.

Gérard, F., Mayer, K. U., Hodson, M. J. and Ranger, J.: Modelling the biogeochemical cycle of silicon in soils: Application to a temperate forest ecosystem, Geochim. Cosmochim.Acta, 72(3), 741–758, doi:10.1016/j.gca.2007.11.010, 2008.

Goddéris, Y., François, L. M., Probst, A., Schott, J., Moncoulon, D., Labat, D. and Viville, D.: Modelling weathering processes at the catchment scale: The WITCH numerical model, Geochim. Cosmochim.Acta, 70(5), 1128–1147, doi:10.1016/j.gca.2005.11.018, 2006.

Goddéris, Y., Williams, J. Z., Schott, J., Pollard, D. and Brantley, S. L.: Time evolution of the mineralogical composition of Mississippi Valley loess over the last 10kyr: Climate and

geochemical modeling, Geochim. Cosmochim.Acta, 74(22), 6357–6374, doi:10.1016/j.gca.2010.08.023, 2010.

Goldberg, K. and Humayun, M.: The applicability of the Chemical Index of Alteration as a paleoclimatic indicator: An example from the Permian of the Paraná Basin, Brazil, Palaeogeogr. Palaeoclimatol.Palaeoecol., 293(1-2), 175–183, doi:10.1016/j.palaeo.2010.05.015, 2010.

Gudbrandsson, S., Wolff-Boenisch, D., Gislason, S. R. and Oelkers, E. H.: An experimental study of crystalline basalt dissolution from 2⩽pH⩽11 and temperatures from 5 to 75°C, Geochim. Cosmochim.Acta, 75(19), 5496–5509, doi:10.1016/j.gca.2011.06.035, 2011.

Gudbrandsson, S., Wolff-Boenisch, D., Gislason, S. R. and Oelkers, E. H.: Experimental determination of plagioclase dissolution rates as a function of its composition and pH at 22°C, Geochim. Cosmochim.Acta, 139, 154–172, doi:10.1016/j.gca.2014.04.028, 2014.

Gustafsson, J.P., Berggren, D., Simonsson, M., Zysset, M., and Mulder, J.: Aluminium solubility mechanisms in moderately acid Bs horizons of podzolized soils, European Journal of Soil Science, 52, 655 -665, 2001.

Gustafsson, J.P., Karltun, E., and Bhattacharya, P.: Allophane and imogolite in Swedish soils. Research Report TRITA-AMI 3046, Division of Land and Water Resources, Royal Institute of Technology (KTH), Stockholm, Sweden. 33pp, 1998.

Harnois, L.: The CIW index: A new chemical index of weathering, Sediment. Geol., 55(3-4), 319–322, doi:10.1016/0037-0738(88)90137-6, 1988.

Heister, K.: The measurement of the specific surface area of soils by gas and polar liquid adsorption methods-limitations and potentials, Geoderma, 216, 75–87, doi:10.1016/j.geoderma.2013.10.015, 2014.

Helgeson, H. C., and Murphy, W. M., Calculation of mass transfer among minerals and aqueous solutions as a function of time and surface area in geochemical processes. I. Computational approach: Jour. Math. Geology, v. 15, no. 1, 109-130, 1983.

Hellevang, H. and Aagaard, P.: Can the long-term potential for carbonatization and safe long-term CO2 storage in sedimentary formations be predicted?, Appl. Geochemistry, 39, 108–118, doi:10.1016/j.apgeochem.2013.09.012, 2013.

Hellevang, H., Aagaard, P., 2010. On the use of Transition-State-Theory (TST) to predict the potential for carbonate growth in sedimentary basins. GSA, Denver, CO,USA.

Hellevang, H., Pham, V. T. H., and Aagaard, P.: Kinetic modelling of CO2–water–rock interactions. *International Journal of Greenhouse Gas Control*, *15*, 3–15. doi:10.1016/j.ijggc.2013.01.027, 2013.

Hellmann, R. and Tisserand, D.: Dissolution kinetics as a function of the Gibbs free energy of reaction: An experimental study based on albite feldspar, Geochim. Cosmochim.Acta, 70(2), 364–383, doi:10.1016/j.gca.2005.10.007, 2006.

Hodson, M. : Comments on “Calculations of weathering rate and soil solution chemistry for forest soils in the Norwegian–Russian border area with the PROFILE model” by G. Koptsik, S. Tevedal, D.

Aamlid and K. Venn, Appl. Geochemistry, 17(2), 117–121, doi:10.1016/S0883-2927(01)00096-8, 2002.

Hodson, M. E., Langan, S. J., Kennedy, F. M. and Bain, D. C.: Variation in soil surface area in a chronosequence of soils from Glen Feshie, Scotland and its implications for mineral weathering rate calculations, Geoderma, 85(1), 1–18, doi:10.1016/S0016-7061(98)00013-5, 1998.

Hodson, M.E., Langan S.J. and Wilson, M.: A critical evaluation of the use of the PROFILE model in calculating mineral weathering rates. Water, Air, and Soil Pollution 98: 79-104, 1997.

Holmqvist, J.: Modelling Chemical Weathering in Different Scales. Doctoral thesis, Lund University, Sweden, 98p, 2001.

Koptsik, G., Teveldal, S., Aamlid, D. and Venn, K.: Calculations of weathering rate and soil solution chemistry for forest soils in the Norwegian-Russian border area with the PROFILE model, Appl. Geochemistry, 14(2), 173–185, doi:10.1016/S0883-2927(98)00048-1, 1999.

Koseva, I. S., Watmough, S. A. and Aherne, J.: Estimating base cation weathering rates in Canadian forest soils using a simple texture-based model, Biogeochemistry, 101(1-3), 183–196, doi:10.1007/s10533-010-9506-6, 2010.

Kronberg B.I, Nesbitt H.W.: Quantification of weathering, soil geochemistry and soil fertility. Journal of Soil Science 32: 453-459, 1981.

Lasaga, A.C., 1981. Transition state theory. Reviews in Mineralogy and Geochemistry 8 (1), 135–168.

Le Blond, J. S., Cuadros, J., Molla, Y. B., Berhanu, T., Umer, M., Baxter, P. J. and Davey, G.: Weathering of the Ethiopian volcanic province: A new weathering index to characterize and compare soils, Am. Mineral., 100(11-12), 2518–2532, doi:10.2138/am-2015-5168CCBY, 2015.

Leal, A. M. M., Blunt, M. J. and LaForce, T. C.: A chemical kinetics algorithm for geochemical modelling, Appl. Geochemistry, 55, 46–61, doi:10.1016/j.apgeochem.2014.09.020, 2015.

Lee, C.-T. A., Morton, D. M., Little, M. G., Kistler, R., Horodyskyj, U. N., Leeman, W. P. and Agranier, A.: Regulating continent growth and composition by chemical weathering., Proc. Natl. Acad. Sci. U. S. A., 105(13), 4981–6, doi:10.1073/pnas.0711143105, 2008.

Macht, F., Eusterhues, K., Pronk, G. J. and Totsche, K. U.: Specific surface area of clay minerals: Comparison between atomic force microscopy measurements and bulk-gas (N2) and -liquid (EGME) adsorption methods, Appl. Clay Sci., 53(1), 20–26, doi:10.1016/j.clay.2011.04.006, 2011.

Madé, B., Clément, A. and Fritz, B.: Modeling mineral/solution interactions: the thermodynamic and kinetic code KINDISP, Comput. Geosci., 20(9), 1347–1363, 1994.

Maher, K., Steefel, C. I., White, A. F. and Stonestrom, D. A.: The role of reaction affinity and secondary minerals in regulating chemical weathering rates at the Santa Cruz Soil Chronosequence, California, Geochim. Cosmochim.Acta, 73(10), 2804–2831, doi:10.1016/j.gca.2009.01.030, 2009.

Marty, N. C. M., Claret, F., Lassin, A., Tremosa, J., Blanc, P., Madé, B., Giffaut, E., Cochepin, B. and Tournassat, C.: A database of dissolution and precipitation rates for clay-rocks minerals, Appl. Geochemistry, 55, 108–118, doi:10.1016/j.apgeochem.2014.10.012, 2015.

Nesbitt Y.W, Young G.M.: Early Proterozoic climates and plate motions inferred from major element chemistry of lutites. Nature 299: 715-717, 1982.

Noguera, C., Fritz, B. and Clément, A.: Simulation of the nucleation and growth of clay minerals coupled with cation exchange, Geochim. Cosmochim.Acta, 75(12), 3402–3418, doi:10.1016/j.gca.2011.03.016, 2011.

Novoselov, A. A. and Souza Filho, C. R.: CRONO—A code for the simulation of chemical weathering, Comput. Geosci., 60, 168–175, doi:10.1016/j.cageo.2013.07.007, 2013.

Oelkers, E. H. and Schott, J.: Experimental study of anorthite dissolution and the relative mechanism of feldspar hydrolysis, Geochim. Cosmochim. Acta, 59(24), 5039–5053, doi:10.1016/0016-7037(95)00326-6, 1995.

Oelkers, E. H., Schott, J. and Devidal, J.-L.: The effect of aluminum, pH, and chemical affinity on the rates of aluminosilicate dissolution reactions, Geochim. Cosmochim. Acta, 58(9), 2011–2024, doi:10.1016/0016-7037(94)90281-X, 1994.

Opolot, E. and Finke, P. A.: Evaluating sensitivity of silicate mineral dissolution rates to physical weathering using a soil evolution model (SoilGen2.25), Biogeosciences, 12, 6791-6808, doi: 10.5194/bg-12-6791-2015, 2015.

Opolot, E., Yu, Y. Y. and Finke, P. A.: Modeling soil genesis at pedon and landscape scales: Achievements and problems, Quat. Int., 376, 1–13, doi:10.1016/j.quaint.2014.02.017, 2014.

Palandri, J. L. and Kharaka, Y. K.: A compilation of rate parameters of water-mineral interaction kinetics for application to geochemical modelling, : U.S. Geol. Survey, Open File Report 2004-1068, 70p, 2004.

Parkhurst D. L. and Appello C. A. J.: User's Guide to PHREEQC (Version 2). A Computer Program for Speciation, Batch-reaction, One-dimensional Transport, and Inverse Geochemical Calucations. U.S. Geological Survey Water-Resources Investigations, Report 99-4259, 312 pp, 1999.

Parkhurst, D. L., Thorestenton, D., and Plummer, L. N., PHREEQE: a computer program for geochemical calculations: U.S. Geol. Survey, Water Resources Invest. Rept. 80--96, 193 p, 1980.

Pham, V. T. H., Lu, P., Aagaard, P., Zhu, C. and Hellevang, H.: On the potential of CO2–water–rock interactions for CO2 storage using a modified kinetic model, Int. J. Greenh. Gas Control, 5(4), 1002–1015, doi:10.1016/j.ijggc.2010.12.002, 2011.

Pham, V. T. H., Lu, P., Aagaard, P., Zhu, C., & Hellevang, H. (2011).On the potential of CO2–water–rock interactions for CO2 storage using a modified kinetic model. International Journal of Greenhouse Gas Control, 5(4), 1002–1015. doi:10.1016/j.ijggc.2010.12.002

Phelan, J., Belyazid, S., Kurz, D., Guthrie, S., Cajka, J., Sverdrup, H. and Waite, R.: Estimation of Soil Base Cation Weathering Rates with the PROFILE Model to Determine Critical Loads of Acidity for Forested Ecosystems in Pennsylvania, USA: Pilot Application of a Potential National Methodology, Water, Air, Soil Pollut., 225(9), 2109, doi:10.1007/s11270-014-2109-4, 2014.

Pokrovsky, O. S., Schott, J. and Thomas, F.: Dolomite surface speciation and reactivity in aquatic systems, Geochim. Cosmochim. Acta, 63(19), 3133–3143, doi:10.1016/S0016-7037(99)00240-9, 1999.

Pokrovsky, O. S., Golubev, S. V., Schott, J. and Castillo, A.: Calcite, dolomite and magnesite dissolution kinetics in aqueous solutions at acid to circumneutral pH, 25 to 150 °C and 1 to 55 atm pCO2: New constraints on CO2 sequestration in sedimentary basins, Chem. Geol., 260(3-4), 317–329, doi:10.1016/j.chemgeo.2009.01.013, 2009.

Price R.C, Gray C.M, Wilson R.E.: The effect of weathering on rare-earth element, Y and Ba abundances in tertiary basalts from Southeastern Australia. Chemical Geology, 93:245-265, 1991.

Price, J. R. and Velbel, M. A.: Chemical weathering indices applied to weathering profiles developed on heterogeneous felsic metamorphic parent rocks, Chem. Geol., 202(3-4), 397–416, doi:10.1016/j.chemgeo.2002.11.001, 2003.

RAISIN.: International Workshop "Rates of Soil Forming Processes in Mediterranean Climate" 24-28 September 2013, University of Calabria in Arcavacata di Rende (near Cosenza), 2013.

Roden, E. E. and Urrutia, M. M.: Ferrous iron removal promotes microbial reduction of crystalline iron(III) oxides, Environ. Sci. Technol., 33(11), 1847–1853, doi:10.1021/es9809859, 1999.

Roelandt, C., Goddéris, Y., Bonnet, M.-P.and Sondag, F.: Coupled modeling of biospheric and chemical weathering processes at the continental scale, Global Biogeochem. Cycles, 24(2), n/a–n/a, doi:10.1029/2008GB003420, 2010.

Salm, C. Van Der, Köhlenberg, L. and Vries, W. De: Assessment of weathering rates in Dutch loess and river-clay soils at pH 3.5, using laboratory experiments, Geoderma, 41–62, 1998.

Samouëlian, A., Finke, P., Goddéris, Y., Cornu, S.: Hydrologic Information in Pedologic Models. In: Lin, H. (Ed.), Hydropedology: Synergistic Integration of Soil Science and Hydrology. Academic Press, Elsevier B.V., pp. 595–636. ISBN: 9780123869418, 2012.

Schott, J., Oelkers, E. H., Bénézeth, P., Goddéris, Y. and François, L.: Can accurate kinetic laws be created to describe chemical weathering?, Comptes Rendus Geosci., 344(11-12), 568–585, doi:10.1016/j.crte.2012.10.005, 2012.

Schroeder, P. A., Melear, N. D., West, L. T. and Hamilton, D. A.: Meta-gabbro weathering in the Georgia Piedmont, USA: implications for global silicate weathering rates, Chem. Geol., 163(1-4), 235–245, doi:10.1016/S0009-2541(99)00129-1, 2000.

Shao, J., Yang, S. and Li, C.: Chemical indices (CIA and WIP) as proxies for integrated chemical weathering in China: Inferences from analysis of fluvial sediments, Sediment. Geol., 265-266, 110–120, doi:10.1016/j.sedgeo.2012.03.020, 2012.

Song, Z., Liu, H., Si, Y. and Yin, Y.: The production of phytoliths in China's grasslands: implications to the biogeochemical sequestration of atmospheric CO 2, Glob. Chang.Biol., 18(12), 3647–3653, doi:10.1111/gcb.12017, 2012.

Song, Z., Liu, H., Li, B. and Yang, X.: The production of phytolith-occluded carbon in China's forests: implications to biogeochemical carbon sequestration., Glob. Chang.Biol., 19(9), 2907–15, doi:10.1111/gcb.12275, 2013.

Steefel C. L.: CrunchFlow. Software for Modeling Multicomponent Reactive Flow and Transport. User's Manual. Available from: <http://www.csteefel.com/CrunchPublic/WebCrunch. html>. 2008.

Steefel, C. I., Appelo, C. A. J., Arora, B., Jacques, D., Kalbacher, T., Kolditz, O., Lagneau, V., Lichtner, P. C., Mayer, K. U., Meeussen, J. C. L., Molins, S., Moulton, D., Shao, H., Šimůnek, J., Spycher, N., Yabusaki, S. B. and Yeh, G. T.: Reactive transport codes for subsurface environmental simulation, Comput Geosci, DOI 10.1007/s10596-014-9443-x, 2014.

Steefel, C., Depaolo, D. and Lichtner, P.: Reactive transport modeling: An essential tool and a new research approach for the Earth sciences, Earth Planet. Sci. Lett., 240(3-4), 539–558, doi:10.1016/j.epsl.2005.09.017, 2005.

Steefel, C.I., Lasaga, A.C.: A coupled model for transport of multiple chemical species and kinetic precipitation/ dissolution reactions with application to reactive flow in single phase hydrothermal systems. Am. J. Sci. 294, 529–592, 1994

Steefel, C. I. and Van Cappellen, P.: A new kinetic approach to modeling water-rock interaction: The role of nucleation, precursors, and Ostwald ripening, Geochim. Cosmochim. Acta, 54(10), 2657–2677, doi:10.1016/0016-7037(90)90003-4, 1990.

Stendahl, J., Akselsson, C., Melkerud, P.-A. and Belyazid, S.: Pedon-scale silicate weathering: comparison of the PROFILE model and the depletion method at 16 forest sites in Sweden, Geoderma, 211-212, 65–74, doi:10.1016/j.geoderma.2013.07.005, 2013.

Stumm, W. and Lee, G. F.: Oxygenation of Ferrous Iron, 53(February), 143–146, 1961.

Stumm, W. and Sulzberger, B.: The cycling of iron in natural environments: Considerations based on laboratory studies of heterogeneous redox processes, Geochim. Cosmochim. Acta, 56(8), 3233–3257, doi:10.1016/0016-7037(92)90301-X, 1992.

Stumm W. and Wollast R.: Coordination chemistry of weathering: Kinetics of surface-controlled dissolution of oxide minerals. Rev. Geophys. 28, 53–69, 1990.

Sugimori, H., Kanzaki, Y. and Murakami, T.: Relationships between Fe redistribution and PO2 during mineral dissolution under low O2 conditions, Geochim. Cosmochim.Acta, 84, 29–46, doi:10.1016/j.gca.2012.01.001, 2012.

Sverdrup, H. and Warfvinge, P.: Calculating field weathering rates using a mechanistic geochemical model PROFILE, Appl. Geochemistry, 8, 273–283, doi:10.1016/0883-2927(93)90042-F, 1993.

Sverdrup, H. and Warfvinge, P.: Estimating field weathering rates using laboratory kinetics. In: White, A., Brantley, S. Eds.., Weathering Kinetics of Silicate Minerals. Reviews in Mineralogy 31. Min. Soc. of America, 485–542, 1995.

Theng, B. K. G., Ristori, G. G., Santi, C. A. and Percival, H. J.: An improved method for determining the specific surface areas of topsoils with varied organic matter content, texture and clay mineral composition, Eur. J. Soil Sci., 50(June), 309–316, 1999.

Van Breemen N, Buurman P.: Soil Formation. Second Edition.Kluwer Academic Publishers, 404 pp, 2002.

Van Ranst, E.: Genesis and properties of silty forest soils in central Belgium and the Ardennes. Unpublished PhD-thesis, Ghent University, Belgium, 349 pp., 1981 (in Dutch)

Villacís-García, M., Ugalde-Arzate, M., Vaca-Escobar, K., Villalobos, M., Zanella, R. and Martínez-Villegas, N.: Laboratory synthesis of goethite and ferrihydrite of controlled particle sizes, Bol. la Soc. Geol. Mex., 67(3), 433–446, 2015.

Violette, A., Goddéris, Y., Maréchal, J.-C., Riotte, J., Oliva, P., Kumar, M. S. M., Sekhar, M. and Braun, J.-J.: Modelling the chemical weathering fluxes at the watershed scale in the Tropics (Mule Hole, South India): Relative contribution of the smectite/kaolinite assemblage versus primary minerals, Chem. Geol., 277(1-2), 42–60, doi:10.1016/j.chemgeo.2010.07.009, 2010.

White, A. F. and Brantley, S. L.: The effect of time on the weathering of silicate minerals: why do weathering rates differ in the laboratory and field?, Chem. Geol., 202(3-4), 479–506, doi:10.1016/j.chemgeo.2003.03.001, 2003.

White, A. R. T. F., Blum, A. E., Schulz, M. S., Bullen, T. O. M. D., Harden, J. W., Peterson, M. L., Survey, U. S. G. and Park, M.: Chemical weathering rates of a soil chronosequence on granitic alluvium : I . Quantification of mineralogical and surface area changes and calculation of primary silicate reaction rates , 60(14), 2533–2550, 1996.

Whitfield, C. J., Aherne, J., Watmough, S. A. and Mcdonald, M.: Estimating the sensitivity of forest soils to acid deposition in the Athabasca Oil Sands Region , Alberta, , 69(2004), 201–208, doi:10.3274/JL10-69-S1-20, 2010.

Wolery, T. J.: Calculation of chemical equilibrium between aqueous solution and minerals: the EQ3/6 software package: Technical Info. Dept., Lawrence Livermore Lab., UCRL 52658, Univ. California, 41p, 1979

Wollast, R.: Rate and mechanism of dissolution of carbonates in the system CaCO3-MgCO3, in Stumm, W., editor, Aquatic Chemical Kinetics: Reaction Rates of Processes in Natural Waters: New York, J. Wiley & Sons, p. 431–445, 1990.

Zhang, G. L., Pan, J. H., Huang, C. M. and Gong, Z. T.: Geochemical features of a soil chronosequence developed on basalt in Hainan Island, China, Rev. Mex. Ciencias Geol., 24(2), 261–269, 2007.

Zhu, C., Lu, P., Zheng, Z. and Ganor, J.: Coupled alkali feldspar dissolution and secondary mineral precipitation in batch systems: 4. Numerical modelling of kinetic reaction paths, Geochim. Cosmochim.Acta, 74(14), 3963–3983, doi:10.1016/j.gca.2010.04.012, 2010.

Chapter 4 : Biogeochemical cycling- Extending the biogeochemical module of the SoilGen Model to include more element species

4.1 Biogeochemical cycling in the SoilGen model

A biogeochemical cycle is defined here as the process-based movement and transformation of elements through four main pools (i.e., biological pool, geological pool, chemical pool and atmospheric pool). The biogeochemical model that is explained here is based on the processes presented in chapter 2 (Fig 2.1). Atmospheric deposition, organic matter decomposition, chemical weathering, leaching, and plant uptake are the major processes that control the soil solution composition of each element in each soil compartment (= 5 cm in the SoilGen). Atmospheric deposition includes both wet (through precipitation) and dry (through dust input) depositions and the amounts of each element deposited are provided as an input to the model. Organic matter decomposition and carbon cycling process (explained in Chapter 2; Figure 2.2) represent the major biological pools through which elements are released into the soil solution. In addition, the elemental composition in the soil solution is influenced by the plant uptake process. Plant uptake of cations (i.e., Al^{3+}, Ca^{2+}, Mg^{2+}, Na^{+} and K^{+}) is vegetation dependent, occurs via the transpiration stream and is described by preferential uptake based on the relative concentrations of each of these elements in the plant (Finke and Hutson, 2008). Chemical weathering (described in Chapter 3) is the main process representing the cycling of elements from the geological pool while the soil solution and exchange phases are the major components of the chemical pool. Elements in the soil solution may be moved down the soil profile from one soil compartment to another through the leaching process.

4.1.1 Objectives

Major element species considered in the previous biogeochemical system (Chapter2; Fig 2.1) include (H^{+}, K^{+}, Na^{+}, Ca^{2+}, Mg^{2+}, Al^{3+}, SO_4^{2-}). Iron (Fe^{2+}, Fe^{3+}) species and Silicon species (H_4SiO_4) were not included in the previous system. Iron and Silicon are considered as major elements influencing soil-formation (e.g., Gerard et al., 2008; Sposito, 1989). The main objective of this chapter was to extend the biogeochemical module of the SoilGen model such that the cycling of Iron and Silicon elements can be realised. First a review of Si and Fe elemental cycling, and conceptual models of how these elements might be incorporated into the SoilGen model are presented. Including Si and Fe elemental cycling required rebuilding the biogeochemical system (Chapter 2; Fig 2.1) of the SoilGen model. Therefore independent reactions, mass action equations, mass balance equations and charge balance

equations for each element species were rewritten. These equations and the steps followed in solving for the geochemical system equilibrium are presented after process definitions of Silicon and Iron cycles.

4.1.1.1 Silicon in the soil

Silicon (Si) constitutes 28.8% by mass of the earth's crust, making it the second most abundant element after oxygen (Umemura and Takenaka, 2014). Silicon cycle is very important from the environmental point of view as it influences removal of CO_2 from the atmosphere, through processes such as enhanced silicate mineral weathering and phytolith occlusion of carbon (Song et al., 2012, 2014; Conley, 2002; Struyf et al., 2009). It is also very important in biogeochemical processes such as chemical weathering, soil development and plant growth (Gérard et al., 2008). However several studies (Clymans et al., 2011; Conley, 2002; Struyf and Conley, 2011; Struyf et al., 2009) have shown a significant influence of human activity on the Si cycle through land use and management. Such human impact could be simulated using the SoilGen model for different study sites once Si cycling is included in the SoilGen biogeochemical module. According to Conley (2002), research on the global Si cycle has mainly focused on the cycling of Si in the oceans and less attention has been paid to the terrestrial Si cycle. Furthermore, biogeochemical models have hardly incorporated Si cycling in the simulation of soil-forming processes. Part of this chapter is dedicated to defining Si cycling mechanism that is subsequently incorporated into the SoilGen model. Phytoliths dissolution which is an important source Si in the soil solution (Clymans et al., 2011; Conley, 2002; Fraysse et al., 2009; Gérard et al., 2008; Struyf and Conley, 2011; Struyf et al., 2010) is also included in the mechanism.

Terrestrial Silicon cycle

Silicon in the soil exists in three main phases (liquid phase, adsorbed phase and solid phase). In the liquid and adsorbed phases, silicon may exist as monosilic acid, in organo-silicon compounds or in organic and inorganic complexes (Sauer et al., 2006). Within the solid phase, Si may be present in different forms including amorphous form (e.g., phytoliths), poorly crystalline form (e.g., allophane and imogolite) and crystalline form such as quartz, feldspar and mica minerals (Sauer et al., 2006). Here, we assume that Si movement in the soil is governed by three important pools (Alexandre et al., 1997); mineralogical pools (primary and secondary minerals), dissolved Si in soil solution (chemical

pool) and Si in the biogenic pool (Fig 4.1). The arrows in Fig 4.1 demonstrate Si movement and interaction among the three pools. Silicon (mainly in the form H_4SiO_4) is released into the soil solution through mineral weathering (based on the mechanism described in Chapter 3), organic matter decomposition, phytoliths dissolution (see Chapter 3; Eq 3.15 -3.16) and atmospheric deposition (Sommer et al., 2006). Silicon may be removed from the soil solution through mineral precipitation, plant uptake and leaching processes (Fig 4.1). Previous studies have shown that temperature is the most important factor governing the concentration of Si in the soil solution (e.g., Gérard et al., 2008). Equilibrium concentration of Si doubles when the temperature rises from 5 to 25 $^{\circ}$C. Soil pH in the range of 2.5 to 8.5 has negligible influence on Si concentration but above this, higher pH values increase concentration of dissolved Si. Other factors that influence the amount of dissolved Si in the soil solution include pore residence time and the presence of Fe and Al (Struyf et al., 2009).

Once in the soil solution, Si (H_4SiO_4) may be taken up by plants and re-deposited as a solid amorphous Si in plant roots, stems and plant cells (Conley, 2002). Part of the Si present in the plant cells forms what is known as phytoliths. Phytoliths are silicified structures formed following a bio-mineralisation process within plants (Parr and Sullivan, 2005). Several studies (Parr and Sullivan, 2005, 2010; Parr et al., 2009; Song et al., 2012; Zuo and Lü, 2011) have demonstrated the potential of plant phytoliths in sequestering carbon. This is explained by the high resistance of carbon occluded within phytoliths to decomposition compared to other organic carbon pools (Parr and Sullivan, 2005). The concentration of phytoliths in plants depends on the vegetation species and it is reported to be in the range of 0.5% in dicotyledonous plants to about 15% of plant dry biomass in wetland species (Song et al., 2012). Global average plant concentration of Si is reported to be in the range of 1 to 3% per unit dry weight (Conley, 2002). Once in the phytoliths some of the Si is labile (about 92.5%) while 7.5% is locked up in the phytoliths (Alexandre et al., 1997). According to Alexandre et al. (1997), phytoliths dissolution contributes twice as much Si than that from silicate mineral weathering. These findings emphasize the importance of phytoliths dissolution on the cycling of Si in the soil.

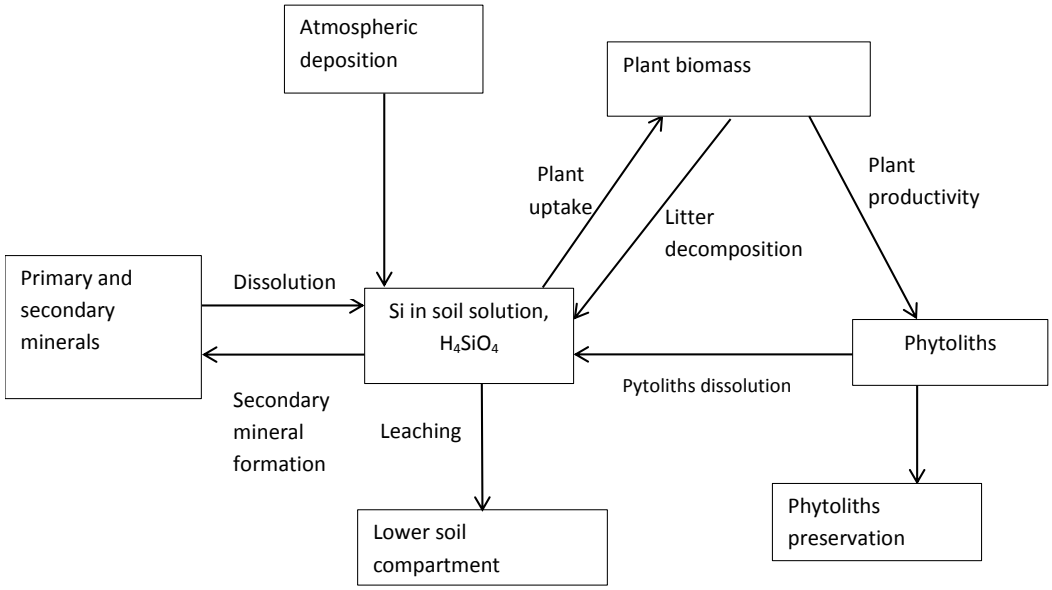

Figure 4.1. Biogeochemical cycling of Si proposed for implementation in the SoilGen model (cited in Alexandre et al., 1997 and modified here to include atmospheric deposition).

4.1.1.2 Iron in the soil

Iron (Fe) is the fourth most abundant element after oxygen, silicon and aluminium. It is an important element in pedology as it can be used as measure of the degree of weathering (e.g., ratio of DCB extractable iron to total iron should increase with weathering intensity). In addition iron oxides in the soil have strong influence on soil properties such as color, redox behavior, surface adsorption as well as soil aggregation (Sposito, 1989). Iron naturally occurs in silicate minerals such as biotite, hornblende and fayalite (e.g., Chapter 3; Table 3.1). Once exposed to an aerobic environment, Fe^{2+} is readily oxidized to Fe^{3+} and Fe^{3+} in common pH range will hydrolyze to form sparingly soluble iron (iii) oxides (Sposito, 1989). Other sources of Iron in the soil solution include atmospheric deposition (wet and dry), organic matter decomposition and fertilizers.

Describing Iron cycling in the SoilGen model

A schematic representation of Fe movement in the soil as proposed for the biogeochemical module of SoilGen is given in Fig. 4.2. Generally iron inputs include primary and secondary mineral dissolution, atmospheric deposition and organic matter decomposition. Once in soil solution plants will take up Fe mainly in Fe^{2+} form. Iron (III) is soluble only at very low pH (< 4) and in highly aerated conditions. Aerated conditions directly relate to the amount of oxygen. Simulation of oxygen was previously not

included in SoilGen and therefore a relationship (see Eq 3.17 in Chapter 3) is assumed to link aerated conditions to the presence of CO_2. This will mean that the higher the CO_2 production and the lower the removal of CO_2 from a soil layer by gas diffusion, the less aerated the conditions are. In general, the redox processes and their effect on Fe^{2+} and Fe^{3+} concentrations in the soil solution are modelled based on the equations presented by Stumm and Lee (1961) as described already in chapter 3 (see Eqs 3.17 and 3.19).

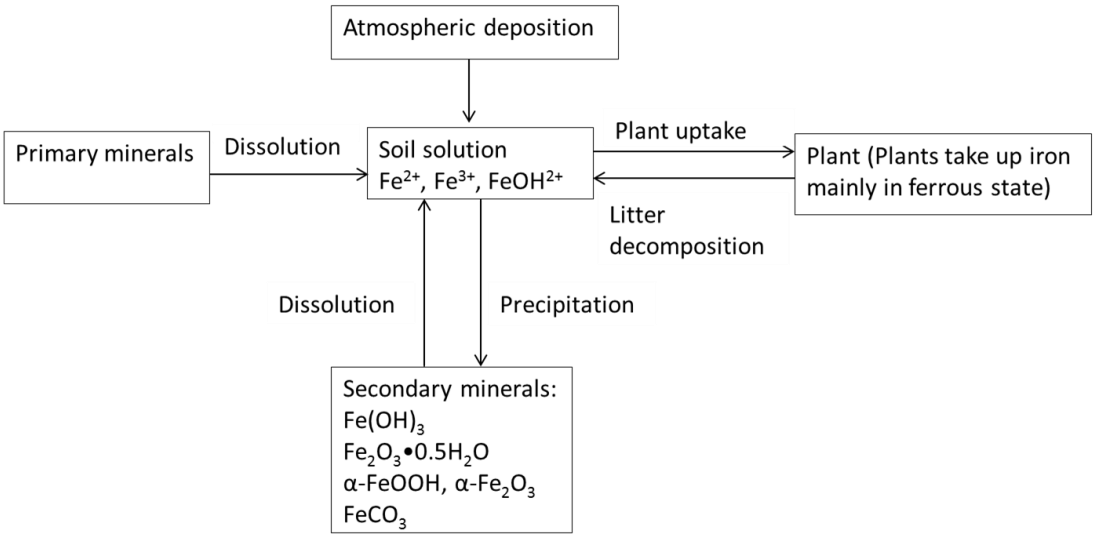

Figure 4.2. Schematic representation of iron cycling in the soil as proposed for implementation into the SoilGen biogeochemical module

Depending on the soil conditions (pH, redox potential, organic matter, microbial activity, mineral type and the crystal size) iron will be precipitated in form of oxides, hydroxides, carbonates and sulphates. In most soil conditions, Goethite (α-FeOOH), Hematite (α-Fe_2O_3) and ferrihydrite (Fe_2O_3•$0.5H_2O$) are the common precipitates of Fe (Sposito, 1989; van Breemen and Buurman, 2002). Iron carbonate (i.e., Siderite: $FeCO_3$) is also included in the mechanism (Fig 4.1) although it occurs under very reduced conditions (pe < 0) and high pH (> 8), that may not be common in most soils (van Breemen and Buurman, 2002).

It should be noted that, in addition to mineral dissolution (section 3.4.1, chapter 3) and the oxido-reduction mechanisms of iron (Eqs 3.17 and 3.19), the reductive dissolution of ferric iron oxides is an important process controlling the total concentration of iron in the soil solution (Sposito, 1989; Frohne et al., 2011; Husson, 2013). Biotic reduction of ferric iron oxides is mainly driven by redox potential (Eh). At low Eh, Fe^{3+} is reduced to Fe^{2+} while at high Eh, Fe^{2+} is oxidized to Fe^{3+} (Sposito, 1989; Husson, 2013). However, Eh mechanism is not yet simulated in the SoilGen model, making it impractical to simulate biotic reduction of ferric oxides at this stage. The simple redox processes proposed (in chapter 3) may therefore underestimate the dissolution as well as the precipitation rates of iron oxides especially in soil conditions where biotic reductive dissolution may be a predominant process (e.g., high organic matter supply and reducing conditions). At the same time, studies focusing on measurement of Eh are limited mainly due to difficulty in measurement of Eh particulary in aerobic environments, and due to the high temporal and spatial variability of this property (Husson, 2013). Simulating and constraining such a process in the SoilGen model therefore remains unexplored.

4.2 Building a biogeochemical model

Conceptualizing the geochemical system to be modelled forms the most important and critical stage in developing a geochemical model (Bethke, 2008). The system in this case is the soil and within this system it is important to define the processes of interest and the extent of the system. At this stage then comes the need to define the components of the system and the equilibrium of such a system. The biogeochemical conceptual model (Fig 4.3) that is explained in the subsequent sections is an extension of the already existing biogeochemical model (conceptualized in Chapter 2; Figure 2.1). The primary species considered in the system include (H^+, K^+, Na^+, Ca^{2+}, Mg^{2+}, Fe^{2+}, Fe^{3+}, Al^{3+}, Si^{4+}, SO_4^{2-}, Cl^-, CO_3^{2-}, HCO_3^- and OH^-) and the composition of each of these primary species and secondary species in the soil solution is influenced by processes such as cation exchange, leaching, plant uptake, atmospheric deposition, mineral dissolution/precipitation and organic matter decomposition (Fig 4.3). Independent reactions, mass action equations and mass balance equations for each master species are defined in the subsequent subsections. In addition, charge balance equations are derived for each element species and then solved for system equilibrium using the bisection method.

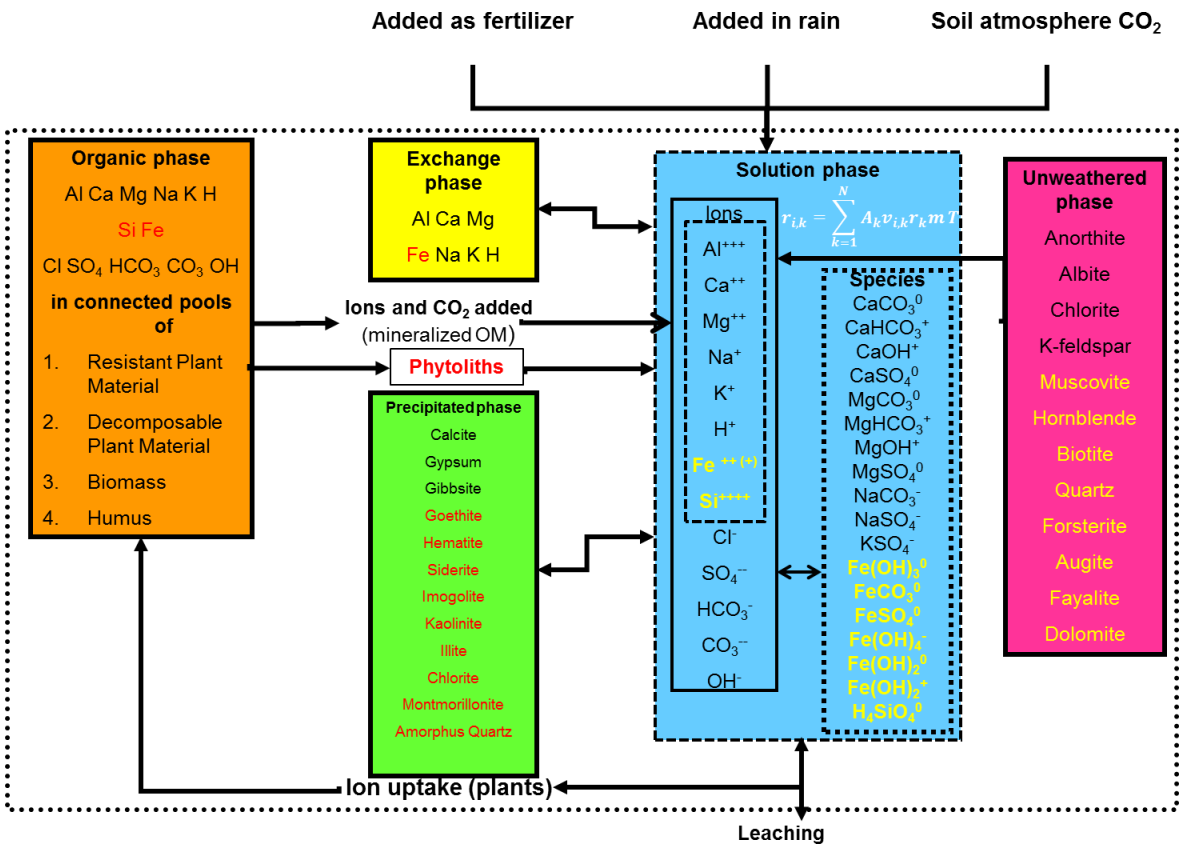

Figure 4.3. Conceptualization of the biogeochemical system as proposed for the SoilGen model. Governing processes that influence the element soil solution concentration include organic matter decomposition, mineral dissolution / precipitation, deposition, ion exchange and leaching. Coloured text refers to the additions (on to Fig 2.1; Chapter 2) resulting from this thesis.

4.2.1 Independent reactions, mass action, mass balance and charge balance equations

Independent reactions (reactions between secondary species and master species) that can occur among species, minerals and gases in the system need to be written as these form a basis for deriving mass action equations and consequently mass balance equations (Bethke, 2008). For simplicity, we assume our chemical system to consist of primarily two components; the aqueous component (hereafter denoted as: A_i) and the mineral component (hereafter denoted as: A_k). In all our calculations, we have also assumed that the activity of water is equal to 1.

For each secondary species, A_j an independent reaction is written in the form of equation (4.1):

$$A_j = \sum_1^j v_{ij} A_i + \sum_1^k v_{kj} A_k \quad (4.1)$$

Where v_{ij} and v_{kj} are reaction coefficients of A_i and A_k, respectively.

Mass action equations describe the chemical equilibrium among aqueous species and minerals. They are simply the expression of equilibrium constant for secondary species, K_j of each independent reaction (Eq 4.2), rearranged to give the molarity of secondary species, m_j (Eq 4.3) and thus reducing the number of independent variables (Bethke, 2008).

$$K_j = \frac{\prod_1^i (\Upsilon_i m_i)^{vij} \times \prod_1^k a_k^{vkj}}{\Upsilon_j m_j} \quad (4.2)$$

$$m_j = \frac{1}{K_j \Upsilon_j} \left[\prod_1^i (\Upsilon_i m_i)^{vij} \times \prod_1^k a_k^{vkj} \right] \quad (4.3)$$

where m_i is the molarity of aqueous master species and $a_k$is the activity of mineral species, respectively. Υ_i and Υ_j are the activity coefficients of aqueous master species and secondary species, respectively.

Mass balance equations are used as book keeping strategy and they express conservation of moles in terms of the master species. Each master species has its moles distributed among different aqueous species and minerals that make up the whole geochemical system (Bethke, 2008). Taking a system presented in Fig 4.3 and Ca^{2+} as an example master species, the total moles of Ca in the system includes Ca that is in the calcium-bearing minerals, calcite, gypsum, calcium bi-carbonate, free calcium ion in the solution (Ca^{2+}), exchange phase Ca^{2+} and Ca^{2+} in the organic phase. The total moles of master species i (M_i) in the aqueous system, A_i can therefore be written as:

$$M_i = m_i + \sum_j v_{ij} m_j \quad (4.4)$$

where m_i and m_j respectively, are the molarities of the master species, i and secondary species, j.

Charge balance equations: when solving for solution equilibrium we deal with charge balance rather than mass balance as shown in Eq. 4.4. Therefore, charge balance equation is derived by summing the charge of each primary species, $z_i m_i$ and the charge of its corresponding secondary species, $z_j m_j$ (where $z_j = v_{ij} z_i$). Consequently, the total charge (m_c) of each species component is calculated from both primary and secondary species as:

$$m_c = \sum_i z_i \left(m_i + \sum_j v_{ij} m_j\right) \quad (4.5)$$

By comparing Eq 4.4 with Eq 4.5, it can be seen that the term in parentheses in Eq 4.5 is actually M_i. Thus the overall charge balance M_c in the solution is calculated as:

$$M_c = \sum_i^n Z_i M_i \quad (4.6)$$

where n is number of species, Z_i is charge of species i and M_i is the total moles of master species i in the soil solution.

The total number of moles of each mineral in the mineral component system M_k is the sum of moles of the mineral corresponding to the component, n_k and the amount required to form the dissolved secondary species, m_j (Bethke, 2008). Therefore the mass balance equation for each mineral in the geochemical system can be written as:

$$M_k = n_k + \sum_j v_{kj} m_j \quad (4.7)$$

4.2.2 The equilibrium state of a geochemical system

At this stage, all the mass action equations have been written for each independent reaction and all the mass balance equations have been derived, showing the distribution of moles of each component among the aqueous master species, m_i and secondary species formed in the system, m_j. Remember that at equilibrium, m_j is described as in Eq 4.3. Therefore substituting the expression for m_j in each of the sets of mass balance equations (4.4 and 4.7), gives a set of governing equations (4.8 and 4.9) that are used to describe the geochemical system equilibrium state. Note that Eq 4.8 has to be written for each aqueous master species in the system while Eq 4.9 is written for each mineral considered in Fig 4.3. Table 4.1 shows a summary of the chemical species, reactions and their respective equilibrium equations.

$$M_i = m_i + \sum_j \frac{v_{ij}}{K_j \Upsilon_j} \left[\prod_1^i (\Upsilon_i m_i)^{vij} \times \prod_1^k a_k^{vkj} \right] \quad (4.8)$$

$$M_k = n_k + \sum_j \frac{v_{kj}}{K_j \Upsilon_j} \left[\prod_1^i (\Upsilon_i m_i)^{vij} \times \prod_1^k a_k^{vkj} \right] \quad (4.9)$$

4.2.3 Finding the equilibrium state of the geochemical system

Finding the equilibrium state of the defined geochemical system is no more than finding the solutions (roots) of the system governing equations (i.e., Eq 4.8 and 4.9). As can be noticed, these governing equations are non-linear as they involve products and powers of unknown parameters. Unlike linear form equations that can easily be solved using linear algebra, solving non-linear equations requires indirect methods that involve iterating a set of values until a solution is found (Bethke, 2008). Newton-Raphson method is one of the most powerful techniques to solve non-linear equations (Bethke, 2008; Press et al., 1989; Steefel et al., 2014). However the method can be unreliable for some functions (e.g., functions whose derivatives are equal to zero) and convergence may not be guaranteed (Press et al., 1989). Here, a bisection method already implemented in the SoilGen is

employed to solve for the geochemical system equilibrium. A bisection method is a simple and robust method of finding roots of non-linear functions. The method starts with bisecting an initial interval (two points within which a solution to the function lies), and subsequently calculating the sub-intervals from the initial interval until a solution is found (Press et al., 1989). Although the bisection method is slower than Newton-Raphson method, convergence is always guaranteed once the two starting points are known (Press et al., 1989) under the condition that the non-linear function is monotonously decreasing or increasing. Steps followed in executing the bisection method are described below.

4.2.3.1 Bisection iteration approach

The Bisection iteration procedure is executed in the following steps:

- First the initial concentration (Mol L^{-1}) of each master species (identified in Table 4.1) in the soil solution is calculated by summing up inputs from all pools (see Figure 4.3).
- The next step is to define a set of non-linear equations making sure that the complexity of the problem is reduced by reserving the equations that can be solved linearly. This is important in minimising the amount of computing time. Taking a look at the governing equations 4.8 and 4.9, the complexity could be reduced by conserving Eq 4.9 since mineral moles, n_k is linear to the total moles, M_k. In this case, only equation 4.8 (written for each aqueous species) remains to be solved.
- Once complexity has been reduced, the next step is to compute the residual functions of each non-linear equation. Residual functions are used to measure how well the guess is. In this case it is simply derived by equating charge balance equation (Eq 4.6) to zero (i.e., $\sum_i^n Z_i\, M_i = 0$) or rather to the lowest tolerable difference called residual, R_i. Therefore the residual function for the electroneutrality in the system is written as:

$$R_i = \sum_i^n Z_i\, M_i \tag{4.10}$$

4.2.3.2 Implementation of the extended biogeochemical module into the SoilGen model

With the geochemical system clearly schematized in Figure 4.3 and, mass balance and charge balance equations for each primary species written, the time is then ripe to implement such a system. As stated earlier, only non-linear equations for master species in the soil solution (Table 4.1) are solved with bisection iteration procedure in order to minimise the computing time. Therefore the moles of each mineral component in the system, n_k is constrained. Once convergence has been reached for master species in the solution (i.e., $\sum_i^n Z_i\, M_i \approx 0$), the total number of moles of each mineral in the system, M_k is calculated from Eq 4.9. Using the bisection method, the iteration is done for a range of pH values until a pH value for which ($\sum_i^n Z_i\, M_i \approx 0$) is obtained. As presented in Chapter 2 (section 2.2.1.5), the calculations are repeated until all the various solubility laws and rate constants (presented by reaction equations in Table 4.1) have been satisfied. Steps followed in implementing the biogeochemical system (schematized in Fig 4.3) are summarized in Fig 4.4 and include the following:

Step 1. Determine the initial soil solution

Each step starts with a given initial soil solution composition with contributions from all processes described in Fig 4.3.

- At the iteration step = 1; the initial solution composition contains total concentrations of each species (i.e., TAl, TSi, TFe2, TFe3, TMg, TCa, TK, TNa, TOH, TH, TCO3, THCO3, TSO4, TCL) from different pools (see Fig. 4.3) e.g., deposition, weathering and organic matter decomposition.
- All necessary unit conversions are performed at this stage (i.e., all elemental concentrations in the soil solution should be in MOL L^{-1})

Step 2. Determine the ionic solution strength (ISS) and activity coefficients (ϒ)

- With the initial solution defined step 1, the ionic solution strength, ISS is computed as:

  $$\mathrm{ISS} = \frac{1}{2}\sum_{i=1}^{i} z_i^2 C_i$$

  Where z_i is the charge of ion i and C_i is the concentration of ion i

Table 4.1. Aqueous species, reaction equations, equilibrium constants and energies of formation. All the data reported in the table was obtained from PhreeqC.dat database (input data to PHREEQC geochemical software containing thermodynamic data for aqueous species and mineral phases; Parkhurst and Appelo, 1999).

Master species	Secondary Species	Reaction	Equilibrium equation, K	Log K	delta Hr (kJ mol^{-1})
H_2O		$H_2O = H^+ + OH^-$	$K_w = [H^+][OH^-]$	-14	55.91
H_2CO_3		$CO_2 + H_2O = H_2CO_3$	$K_h = [H_2CO_3] / [CO_2]$	-1.468	-19.98
HCO_3^-		$H_2CO_3 = H^+ + HCO_3^-$	$Ka_1 = [H^+][HCO_3^-]/ [H_2CO_3]$	-6.352	9.11
CO_3^{2-}		$HCO_3^- = H^+ + CO_3^{2-}$	$Ka_2 = [H^+][CO_3^{2-}]/[HCO_3^-]$	10.329	14.90
H^+					
OH^-					
Al^{3+}	$Al(OH)^{2+}$	$Al^{3+} + H_2O = Al(OH)^{2+} + H^+$	$K_{Al(OH)2+} = [Al(OH)^{2+}][H^+]/[Al^{3+}]$	-4.99	49.79
	$Al(OH)_2^+$	$Al^{3+} + 2H_2O = Al(OH)_2^+ + 2H^+$	$K_{Al(OH)2+} = [Al(OH)_2^+][H^+]^2/[Al^{3+}]$	-10.1	112.55
	$Al(OH)_3$(aq)	$Al^{3+} + 3H_2O = Al(OH)_3 + 3H^+$	$K_{Al(OH)3} = [Al(OH)_3][H^+]^3/[Al^{3+}]$	-16.9	166.90
	$Al(OH)_4^-$	$Al(OH)_4^- + 4H^+ = Al^{3+} + 4H_2O$	$K_{Al(OH)4-} = [Al(OH)_4^-][H^+]^4/[Al^{3+}]$	-22.7	176.98
Ca^{+2}	$CaCO_3$ (aq)	$CaCO_3 = Ca^{2+} + CO_3^{2-}$	$K_{CaCO3} = [Ca^{2+}][CO_3^{2-}]/[CaCO_3]$	-3.22	14.83
	$CaHCO_3^+$	$CaHCO_3^+ = Ca^{2+} + H\,CO_3^-$	$K_{CaHCO3+} = [Ca^{2+}][HCO_3^-]/[CaHCO_3^+]$	11.44	-3.64
	$CaOH^+$	$CaOH^+ = Ca2+ + OH-$	$K_{CaOH+} = [Ca^{2+}][OH^-]/ [CaOH^+]$	-1.30	-8.21
	$CaSO_4$ (aq)	$CaSO_4 = Ca^{2+} + SO_4^{2-}$	$K_{CaSO4} = [Ca^{2+}][SO_4^{2-}]/[CaSO_4]$	-2.30	-6.90
Fe^{+2}	$Fe(OH)_2$ (aq)	$Fe(OH)_2 = Fe^{2+} + 2OH^-$	$K_{Fe(OH)2} = [Fe^{2+}][OH^-]^2/[Fe(OH)_2]$	-20.57	119.52
	$Fe(OH)_3^-$	$Fe(OH)_3^- = Fe^{2+} + 3OH^-$	$K_{Fe(OH)3-} = [Fe^{2+}][OH^-]^3/ [Fe(OH)_3^-]$	-30.99	126.86
	$FeCO_3$	$FeCO_3 = Fe^{2+} + CO_3^{2-}$	$K_{FeCO3} = [Fe^{2+}][CO_3^{2-}]/[FeCO_3]$	-4.38	-27.96[1]
	$FeSO_4$(aq)	$FeSO_4 = Fe^{2+} + SO_4^{2-}$	$K_{FeSO4} = [Fe^{2+}][SO_4^{2-}]/[FeSO_4]$	-2.39	13.52
Fe^{3+}	$Fe(OH)_2^+$	$Fe(OH)_2^+ = Fe^{3+} + 2OH^-$	$K_{Fe(OH)2+} = [Fe^{3+}][OH^-]^2/[Fe(OH)_2^+]$	-5.67	71.59
	$Fe(OH)_3$	$Fe(OH)_3 = Fe^{3+} + 3OH^-$	$K_{Fe(OH)3} = [Fe^{3+}][OH^-]^3/[Fe(OH)_3]$	-12.56	103.83
	$Fe(OH)_4^-$	$Fe(OH)_4^- = Fe^{3+} + 4OH^-$	$K_{Fe(OH)4-} = [Fe^{3+}][OH^-]^4/ [Fe(OH)_4^-]$	-21.6	133.56
Si^{4+}	H_4SiO_4				
	SiO_2(aq)	$SiO_2 + 2H_2O = H_4SiO_4$	$K_{SiO2} = [H_4SiO_4] / [SiO_2]$	-2.71	13.98
K^{+1}	KSO_4^-	$KSO_4^- = K^+ + SO_4^{2-}$	$K_{KSO4-} = [K^+][SO_4^{2-}]/ [KSO_4^-]$	0.85	-9.41
Mg^{+2}	$MgCO_3$ (aq)	$MgCO_3 = Mg^{2+} + CO_3^{2-}$	$K_{MgCO3} = [Mg^{2+}][CO_3^{2-}]/ [MgCO_3]$	-2.98	-11.35
	$MgHCO_3^+$	$MgHCO_3^+ = Mg^{2+} + HCO_3^-$	$K_{MgHCO3+} = [Mg^{2+}][HCO_3^-]/[MgHCO_3^+]$	-1.07	-3.31
	$MgOH^+$	$MgOH^+ = Mg^{2+} + OH^-$	$K_{MgOH+} = [Mg^{2+}][OH^-]/[MgOH^+]$	-2.56	-10.84
	MgSO4 (aq)	$MgSO_4 = Mg^{2+} + SO_4^{2-}$	$K_{MgSO4} = [Mg^{2+}][SO_4^{2-}]/[MgSO_4]$	-2.37	-19.04
Na^{+1}	$NaCO_3^-$	$NaCO_3^- = Na^+ + CO_3^{2-}$	$K_{NaCO3-} = [Na^+][CO_3^{2-}]/ [NaCO_3^-]$	-1.27	-37.28
	$NaSO_4^-$	$NaSO_4^- = Na^+ + SO_4^{2-}$	$K_{NaSO4-} = [Na^+][SO_4^{2-}]/ [NaSO_4^-]$	-0.7	-4.69
Cl^-					
SO_4^{2-}					

[1] Obtained from Fosbøl et al. (2010)

- Activity coefficient, Υ is computed following the Davies' relationship (Stumm and Morgan, 1970): $\Upsilon = -0.509z^2 \times \left(\frac{\sqrt{ISS}}{1+\sqrt{ISS}} - 0.3 \times ISS \right)$

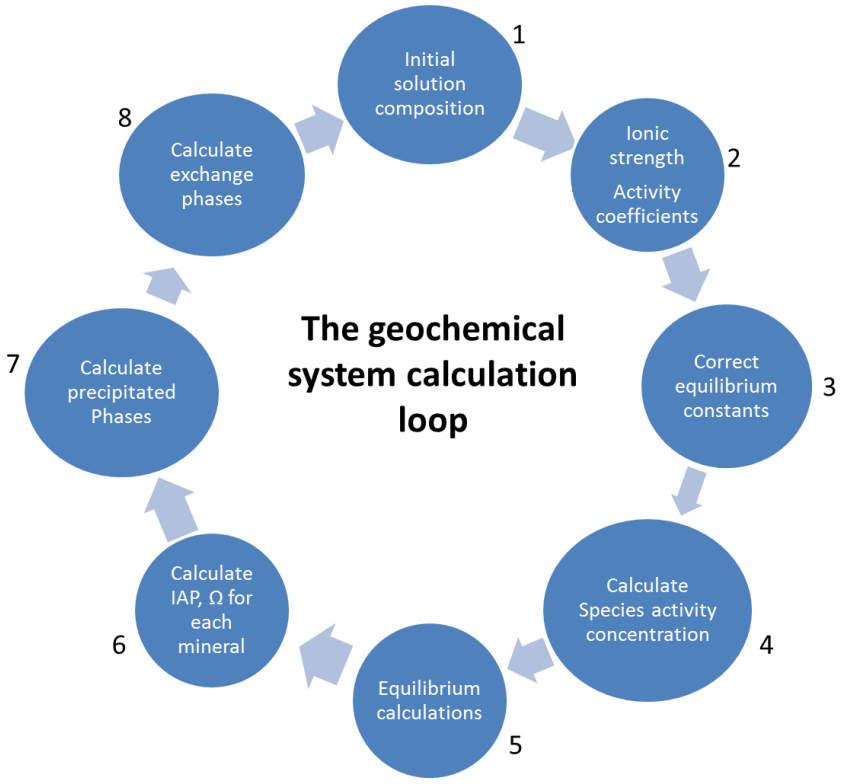

Figure 4.4. Steps followed in solving for the soil solution equilibrium and calculating the precipitated and exchange phases of the biogeochemical system schematized in Fig. 4.3. IAP is the Ionic activity product and Ω is the saturation ratio.

Step 3. Correct thermodynamic equilibrium constants (Log K values given in Table 4.1) for temperature and for activities

- The equilibrium constants of all the species (Table 4.1) are first corrected for temperature, using Arrhenius equation and delta Hr values (Table 4.1) prior to activity correction.
- Using the activity coefficients for each species calculated in step 2 and the equilibrium reactions (Table 4.1), the equilibrium constants (i.e., Log K values in Table 4.1) are corrected

for activities. Taking $MgCO_3^0$ as an example species, the equilibrium constant for this reaction, K_{MgCO3} is written as:

$K_{MgCO3} = [Mg^{2+}][CO_3^{2-}] / [MgCO_3]$

- And the activity corrected equilibrium constant, K_{cMgCO3} is computed as:

  $K_{cMgCO3} = K_{MgCO3} / \frac{\Upsilon_2 \times \Upsilon_2}{1}$,

  where ϒ stands for the activity coefficient of the a given species calculated from ionic strength as described in step 2.

Step 4. Compute the activity and the concentration of each individual chemical species

- Consider the speciation reaction involving $MgCO_3^0$ as described in step 3, the activity of $MgCO_3^0$ in the soil solution can be calculated as:

  $$(MgCO_3) = \frac{\gamma_2[Mg^{2+}]\gamma_2[CO_3^{2-}]}{K_{cMgCO_3}}$$

  And the concentration of $MgCO_3^0$ is calculated as:

  $$[MgCO_3] = \frac{(MgCO_3)}{\gamma_2 \times \gamma_2}$$

- These calculations are done for each species (given in Table 4.1) at each time step

Step 5. Compute the equilibrium of the solution and charge balance

- Based on mass action equation (Eq 4.8); each species (in Table 4.1) is written in form of its respective master species, pH and pCO_2
- Taking an example of total Mg^{2+}: $TMg = Mg^{2+} + MgSO_4^0 + MgCO_3^0 + MgHCO_3^+ + MgOH^+$;
- Equilibrium reaction for each of the above Mg species are as follows;

  $MgSO_4^0 = Mg^{2+} + SO_4^{2-}$; $K_{MgSO4} = [Mg^{2+}][SO_4^{2-}] / [MgSO_4^0]$; $[MgSO_4^0] = [Mg^{2+}][SO_4^{2-}] / K_{MgSO4}$

  $MgCO_3^0 = Mg^{2+} + CO_3^{2-}$; $K_{MgCO3} = [Mg^{2+}][CO_3^{2-}] / [MgCO_3^0]$; $[MgCO_3^0] = [Mg^{2+}][CO_3^{2-}] / K_{MgCO3}$

  $MgHCO_3^+ = Mg^{2+} + HCO_3^-$; $K_{MgHCO3} = [Mg^{2+}][HCO_3^-] / [MgHCO_3^+]$; $[MgHCO_3^+] = [Mg^{2+}][HCO_3^-] / K_{MgHCO3}$

$MgOH = Mg^{2+} + OH^-$; $K_{MgOH} = [Mg^{2+}][OH^-]/ [MgOH^-]$; $[MgOH^-] = [Mg^{2+}][OH^-]/ K_{MgOH}$

Thus total moles of Mg^{2+} is computed as a function of pH and pCO_2 as follows:

$$TMg = Mg^{2+} + [Mg^{2+}] \times [SO_4^{2-}]/ K_{MgSO4} + Mg^{2+} \times K_{a2} \times K_h \times K_{a1} \times pCO_2 / [H^+]^2 / K_{MgCO3}$$

$$+ Mg^{2+} \times K_h \times K_{a1} \times pCO_2 / [H^+] / K_{MgHCO_3^+}] + Mg^{2+} \times (K_w / [H^+]) / K_{MgOH}$$

And thus

$$[Mg^{2+}] = TMg /(1+ [SO_4^{2-}]/K_{MgSO4} + [CO_3^{2-}] / K_{MgCO3} + [HCO_3^-] /K_{MgHCO_3^+} + (K_w / [H^+])/ K_{MgOH})$$

Where $[CO_3^{2-}] = K_{a1} \times K_{a2} \times K_h \times pCO_2/[H^+]^2$, $[HCO_3^-] = K_h \times K_{a1} \times pCO_2 / [H^+]$, K_{a1} and K_{a2} are dissociation constants of H_2CO_3 and HCO_3^-, respectively, K_h is Henry's constant and K_w is water dissociation constant (see Table 4.1)

- The resulting equations are solved for a pH value that satisfies each equilibrium reaction at a fixed pCO_2 (for the current time step) following the bisection procedure described in section 4.2.3.1.
- The pH value satisfying the equilibrium reaction for each species is substituted into each reaction equation in Table 4.1 to get the new species concentration; taking an example of $MgHCO_3^+$ species: New $[MgHCO_3^+]$ is calculated by substituting the pH value in the following equation as;

  $[MgHCO_3^+] = ([Mg^{2+}] \times K_h \times K_{a1} \times pCO_2 / [H^+]) / \times K_{MgHCO_3^+}$
- **Charge balance:** The system at equilibrium should be charge balanced. This is ensured by adjusting pH at each time-step until electroneutrality is achieved. Charge balance occurs if $R_i \approx 0$ (Eq 4.10) i.e., $\sum_i^n Z_i M_i = 0$.
- If no charge balance, steps 1 to 5 are repeated.

Step 6. Compute the Ionic activity product (IAP) and the Saturation ratio (Ω) of each mineral

The Ionic activity product (IAP) for each mineral is calculated using the equilibrium reactions for each mineral (Chapter 3; Table 3.1) and the calculated species activities (step 4). Consider Albite as an example of a mineral whose saturation index (Ω) in the solution is to be calculated.

The equilibrium reaction equation, IAP and Ω, respectively are described as follows:

- $NaAlSi_3O_8 + 4H_2O + 4H^+ = Na^+ + Al^{3+} + 3H_4SiO_4$;
- $IAP_{NaAlSi3O8} = \frac{\Upsilon_1[Na]\times\Upsilon_3[Al]\times\Upsilon_4[Si]^3}{\Upsilon_1\times[H]^4}$; assuming activity of water is equal to 1
- $\Omega_{NaAlSi3O8} = \frac{IAP_{NaAlSi3O8}}{K_{NaAlSi3O8}}$, $K_{NaAlSi3O8}$ has to be corrected for temperature using Gibbs free energy
- **Precipitation or dissolution**: when Ω of a mineral is < 1 then that mineral dissolves, when Ω > 1, then that mineral precipitates, or else the mineral is in equilibrium with the soil solution (see Chapter 3; Fig 3.1 for detailed description)

Step 7. Compute the new rates at which each mineral is dissolving or precipitating at a given time step

- Calculate mineral dissolution / precipitation rates using a mechanism based on the transition state theory (described already in chapter 3; Eq 3.8)

Step 8. Compute the exchange phase

- Calculate the moles of each element adsorbed to the exchange phase using Gapon selectivity coefficients (KG), cation exchange capacity, CEC and cation solution concentrations (calculated in step 4)
- For example an exchange reaction between Mg^{2+} and Ca^{2+} is written as follows:

  $0.5Mg^{2+} + CAX = MGX + 0.5Ca^{2+}$

- And the Gapon coefficient ($K_{Mg/Ca}$) for such a reaction is calculated as:

$K_{Mg/Ca} = (MGX \times CA^{1/2}) / (CAX \times MG^{1/2})$

where MGX and CAX represent exchangeable Mg and Ca , respectively.

- If $K_{Mg/Ca}$ and the CEC are known, then the two equations above can be combined and rewritten for each element such that the only unknowns are MGX and CAX; the total number of

equations (NumEqn) to be solved is calculated as NumEqn = N × 0.5 (N – 1); where N is the number of cations considered in exchange surface

- For example let KGnumber represent exchange reactions between different elements; i.e., KG1 = Mg/Ca; KG2 = Ca/Na; KG3 = Ca/K; KG4= Mg/K; KG5 = Mg/Na; KG6 = K/Na; KG7 = Ca/Al; KG8 = Ca/H; KG9 = Mg/Al; KG10 = K/Al; KG11 = Na/Al; KG12 = Mg/H; KG13 = K/H; KG14 = Na/H; KG15 = Al/H ; KG16 = Fe2+/H ; KG17 = Na/Fe2+ ; KG18 = K/Fe2+ ; KG19 = Mg/Fe2+ ; KG20 = Ca/Fe2+ ; KG21 = Fe2+ /Al
- Then the amount of exchangeable calcium, XCA is calculated by rewriting XCA in terms of gapon coefficients (KG), CEC and all other exchangeable elements such that:

  $XCA = CEC/ (1 + (KG1 \times MG^{1/2})/CA^{1/2} + Na/(KG2 \times CA^{1/2}) + K/(KG3 \times CA^{1/2}) + (AL^{1/3})/(KG7 \times CA^{1/2}) + H/(KG8 \times CA^{1/2} + FE2^{1/2}/(KG20 \times CA^{1/2}))$

  where $CEC = XCA + XMG + XNA + XK + XAL + XH + XFE2$

4.3. Summary

In this chapter, the biogeochemical cycling as proposed for the SoilGen biogeochemical module has been presented. Terrestrial cycling of Iron (Fe) and Silicon (Si) were reviewed and conceptualized prior to their inclusion into the biogeochemical conceptual module of the SoilGen model. These elements play a crucial role in soil formation and should be included in the soil evolution models. The proposed SoilGen biogeochemical module includes iron (Fe^{2+} and Fe^{3+}) and silicon (H_4SiO_4) species. Like the elements already implemented, the cycling of Fe and Si is governed by wet and dry deposition, plant uptake, release through organic matter mineralization and mineral dissolution, and leaching processes. In addition, we included phytoliths as a major pool of Si (H_4SiO_4) in the soil solution and its dissolution rate is modelled as a function of pH similar to the mechanism described in (Fraysse et al., 2009). Iron cycling is also modelled such that redox processes influence the amount of each species in the soil solution. In general, the extended SoilGen biogeochemical module consists of 14 master element species (i.e., Ca^{2+}, Mg^{2+}, K^{+}, H^{+}, Na^{+} Fe^{2+}, Fe^{3+},Al^{3+}, Si^{4+}, Cl^{-}, CO_3^{2-} , HCO_3^{-}, SO_4^{2-} and OH^{-}) and up to 23 other solution species. The implementation of such a geochemical system is accomplished in

about 8 steps (Fig 4.4). We start with a bulk soil solution composition that includes the mass balance calculations involving contributions from all the main biogeochemical processes. Based on the initial soil solution composition, the solution ionic strength (ISS) and the activity coefficients (ϒ) are calculated. The calculated activity coefficients are used to correct the species equilibrium constants. These corrected constants are then used to calculate the species activities which are then used in the solution equilibrium calculation. The bisection procedure is employed to iterate inside a defined pH range until a stable pH (i.e., the pH satisfying the equilibrium conditions for all temperature and activity corrected equilibrium constants) is found. Once a stable pH is found, ionic activity product (IAP) and saturation ratio (Ω) for each mineral is computed and used to decide if a given mineral precipitates or not. The composition of each element in the exchange phase is then calculated using cation exchange capacity, Gapon coefficients and respective element solution concentration. Finally, the mass balancing is done and, the precipitated and exchanged element amounts are subtracted from the solution phase, to form the initial soil solution composition for the next time step.

Author contribution

This chapter was designed, developed and written by E. Opolot. Peter Finke had a significant contribution through reviewing and integrating the extended chemical module into the SoilGen code.

References

Alexandre, A., Meunier, J.-D., Colin, F. and Koud, J.-M.: Plant impact on the biogeochemical cycle of silicon and related weathering processes, Geochim. Cosmochim. Acta, 61(3), 677–682, doi:10.1016/S0016-7037(97)00001-X, 1997.

Bethke, C.M.: Geochemical and Biogeochemical Reaction Modeling. Cambridge University Press, 547 pp, 2008.

Clymans, W., Struyf, E., Govers, G., Vandevenne, F. and Conley, D. J.: Anthropogenic impact on amorphous silica pools in temperate soils, Biogeosciences, 8(8), 2281–2293, doi:10.5194/bg-8-2281-2011, 2011.

Conley, D. J.: Terrestrial ecosystems and the global biogeochemical silica cycle, Global Biogeochem. Cycles, 16(4), 68–1–68–8, doi:10.1029/2002GB001894, 2002.

Finke, P. A. and Hutson, J. L.: Modelling soil genesis in calcareous loess, Geoderma, 145(3-4), 462–479, doi:10.1016/j.geoderma.2008.01.017, 2008.

Fosbøl, P.L., Thomsen, K. and Stenby, E.H.: Review and recommended thermodynamic properties of FeCO3. Corrosion Engineering, Science and Technology, 45 (2), 116-135, 2010.

Fraysse, F., Pokrovsky, O. S., Schott, J. and Meunier, J.-D.: Surface chemistry and reactivity of plant phytoliths in aqueous solutions, Chem. Geol., 258(3-4), 197–206, doi:10.1016/j.chemgeo.2008.10.003, 2009.

Frohne, T., Rinklebe, J., Diaz-Bone, R. A. and Du Laing, G.: Controlled variation of redox conditions in a floodplain soil: Impact on metal mobilization and biomethylation of arsenic and antimony, Geoderma, 160(3-4), 414–424, doi:10.1016/j.geoderma.2010.10.012, 2011.

Gérard, F., Mayer, K. U., Hodson, M. J. and Ranger, J.: Modelling the biogeochemical cycle of silicon in soils: Application to a temperate forest ecosystem, Geochim. Cosmochim.Acta, 72(3), 741–758, doi:10.1016/j.gca.2007.11.010, 2008.

Husson, O.: Redox potential (Eh) and pH as drivers of soil/plant/microorganism systems: A transdisciplinary overview pointing to integrative opportunities for agronomy, Plant Soil, 362(1-2), 389–417, doi:10.1007/s11104-012-1429-7, 2013.

Parkhurst D. L. and Appello C. A. J.: User's Guide to PHREEQC (Version 2). A Computer Program for Speciation, Batch-reaction, One-dimensional Transport, and Inverse Geochemical Calucations. U.S. Geological Survey Water-Resources Investigations, Report 99-4259, 312 pp, 1999.

Parr, J. F. and Sullivan, L. A.: Phytolith occluded carbon and silica variability in wheat cultivars, Plant Soil, 342(1-2), 165–171, doi:10.1007/s11104-010-0680-z, 2010.

Parr, J. F. and Sullivan, L. A.: Soil carbon sequestration in phytoliths, Soil Biol. Biochem., 37(1), 117–124, doi:10.1016/j.soilbio.2004.06.013, 2005.

Parr, J., Sullivan, L. and Quirk, R.: Sugarcane phytoliths: Encapsulation and sequestration of a long-lived carbon fraction, Sugar Tech, 11(1), 17–21, doi:10.1007/s12355-009-0003-y, 2009.

Press, W. H., Flannery, B. P., Teukolsky, S. A., and Vetterling, W. T.: Bracketing and Bisection. In Numerical Recipes in FORTRAN: The art of Scientific Computing. Cambridge, England: Cambridge University Press, pp. 274-278, 1996.

Sauer, D., Saccone, L., Conley, D. J., Herrmann, L. and Sommer, M.: Review of methodologies for extracting plant-available and amorphous Si from soils and aquatic sediments, Biogeochemistry, 80(1), 89–108, doi:10.1007/s10533-005-5879-3, 2006.

Sommer, M., Kaczorek, D., Kuzyakov, Y. and Breuer, J.: Silicon pools and fluxes in soils and landscapes—a review, J. Plant Nutr. Soil Sci., 169(3), 310–329, doi:10.1002/jpln.200521981, 2006.

Song, Z., Liu, H., Si, Y. and Yin, Y.: The production of phytoliths in China's grasslands: implications to the biogeochemical sequestration of atmospheric CO2, Glob. Chang.Biol., 18(12), 3647–3653, doi:10.1111/gcb.12017, 2012.

Song, Z., Müller, K. and Wang, H.: Biogeochemical silicon cycle and carbon sequestration in agricultural ecosystems, Earth-Science Rev., 139, 268–278, doi:10.1016/j.earscirev.2014.09.009, 2014.

Sposito, G.: The Chemistry of Soils (Chaps. 8 and 9). New York: Oxford University Press, 277 pp, 1989.

Steefel, C. I., Appelo, C. A. J., Arora, B., Jacques, D., Kalbacher, T., Kolditz, O., Lagneau, V., Lichtner, P. C., Mayer, K. U., Meeussen, J. C. L., Molins, S., Moulton, D., Shao, H., Šimůnek, J., Spycher, N., Yabusaki, S. B. and Yeh, G. T.: Reactive transport codes for subsurface environmental simulation., 2014.

Struyf, E. and Conley, D. J.: Emerging understanding of the ecosystem silica filter, Biogeochemistry, 107(1-3), 9–18, doi:10.1007/s10533-011-9590-2, 2011.

Struyf, E., Smis, A., Damme, S., Meire, P. and Conley, D. J.: The Global Biogeochemical Silicon Cycle, Silicon, 1(4), 207–213, doi:10.1007/s12633-010-9035-x, 2010.

Struyf, E., Smis, A., Van Damme, S., Meire, P. and Conley, D. J.: The Global Biogeochemical Silicon Cycle, Silicon, 1(4), 207–213, doi:10.1007/s12633-010-9035-x, 2009.

Stumm, W. and Lee, G. F.: Oxygenation of Ferrous Iron, 53, 143–146, 1961.

Stumm, W. and J.J. Morgan.: Aquatic chemistry. Wiley-Interscience, 1970.

Umemura, M. and Takenaka, C.: Biological cycle of silicon in moso bamboo (Phyllostachys pubescens) forests in central Japan, Ecol. Res., 29(3), 501–510, doi:10.1007/s11284-014-1150-5, 2014.

Van Breemen N, Buurman P.: Soil Formation. Second Edition.Kluwer Academic Publishers, 404pp, 2002.

Zuo, X. and Lü, H.: Carbon sequestration within millet phytoliths from dry-farming of crops in China, Chinese Sci. Bull., 56(32), 3451–3456, doi:10.1007/s11434-011-4674-x, 2011.

Chapter 5 : Estimating the effect of tree uprooting on variation of soil horizon depth by confronting pedogenetic simulations to measurements in a Belgian loess area

Based on:

Finke, P.A., T. Vanwalleghem, **E. Opolot**, J. Poesen, J. Deckers. 2013. Estimating the effect of tree uprooting on variation of soil horizon depth by confronting pedogenetic simulations to measurements in a Belgian loess area. Journal of Geophysical Research-Earth Surface, 118 (4), 2124–2139, DOI:10.1002/jgrf.20153.

Abstract

Spatial patterns of soil often do not reflect those of topographic controls. We attempted to identify possible causes of this by comparing observed and simulated soil horizon depths. Observed depths of E, Bt, BC, C1 and C2 horizons in loess-derived soils in Belgium showed a weak to absent relation to terrain attributes in a sloping area. We applied the soil genesis model SoilGen2.16 onto 108 1x1 m^2 locations in a 1329 ha area to find possible causes. Two scenarios were simulated. Model 1 simulated soil development under undisturbed conditions, taking slope, aspect and loess thickness as the only sources of variations. Model 2 additionally included a stochastic submodel to generate tree uprooting events based on the exposure of trees to the wind. Outputs of both models were converted to depths of transitions between horizons, using an algorithm calibrated to horizon depths observed in the field. Model 1 showed strong correlations between terrain attributes and depths for all horizons, although surprisingly regression kriging was not able to model all variations. Model 2 showed a weak to absent correlation for the upper horizons but still a strong correlation for the deeper horizons BC, C1 and C2. For the upper horizons the spatial variation strongly resembled that of the measurements. This is a strong indication that bioturbation in the course of soil formation due to treefalls influences on spatial patterns of horizon depths.

Index terms

Modelling; Soils/pedology; Vadose zone; Geomorphology and weathering

5.1 Introduction

The characterization and prediction of soil properties, such as depth, texture or salinity, is crucial for many ecological, hydrological, geomorphic or agronomic models [*Rantakariet al.*, 2012; *Finke and Bosma*, 1993; *Claessens et al.*, 2007; *Wallach et al.*, 2011]. In agricultural areas, especially on sloping terrain, soil redistribution by erosion has been shown to control the spatial distribution of soil properties like horizon depth, texture, stoniness or soil organic carbon [*Poesen et al.*, 1997; *Li and Lindstrom*, 2001; *Chaplot et al.*, 2009; *Dlugoß et al.*, 2010]. As a result, in such areas there is commonly a strong correlation between topographic attributes such as slope angle or convexity with soil properties. Soil variability patterns are often mapped using digital soil mapping (DSM) methods

[*McBratney et al.*, 2003]. After identifying and employing a statistical relation, DSM allows predicting soil properties or soil type using full-cover ancillary variables. Such ancillary variables are often derived from topographic and land cover attributes. DSM techniques have been applied successfully under a wide range of conditions [*Moore et al.*, 1993; *Gessler et al.*, 2000; *Tesfa et al.*, 2009].

However, the fact that variability patterns can be mapped does not always mean that the causes of variability are known. In other cases soil properties cannot be predicted accurately because the relation between soil properties and ancillary variables is too weak. An example is the study by Vanwalleghem et al. [2010], who were not able to find accurate statistical relations to predict the starting depths of soil horizons from terrain attributes. In their case study in a natural forest area with loess-derived soils they mentioned local soil disturbances such as tree uprootings, and variation in initial soil properties as possible causes that mask soil-landscape relations. In this paper we attempt to explain the poor terrain control on soil horizon depths in the same area by analysing the effects of local disturbances in more detail, and thus focus on loess-derived soils in a Belgian natural forest.

Knowledge of the effect of tree uprooting on spatial soil variability is limited [*Šamonil et al.*, 2010, 2011], but effects on soil genesis (e.g. proxied by soil depth) have been demonstrated. In certain areas, the presence of pit and mound microtopography is visible evidence of natural bioturbation processes. This microtopography is either caused by treefalls, for example in hummocky areas in the European Alps [*Embleton-Hamann*, 2004], or caused by burrowing animals like the mima mounds found in the northwestern US [*Horwath and Johnson*, 2006]. Schaetzl and Follmer [1990] showed this pit and mound topography to be long-lived and found evidence that dated some of these to over 2000 years. Whatever its origin, detailed soil transects have shown that this surface microtopography is reflected in the soil properties [*Embleton-Hamann*, 2004]. Lutz and Griswold [1939], Armson and Fessenden [1973] and Beke and McKeague [1984] mapped the soil profiles of pit and mound features and documented the disruption caused by treefalls, such as an A horizon sandwiched between two B horizons. Langohr [1993] described the importance of treefalls for interpreting soil stratigraphy in a geoarchaeological context. Also in areas without clear topographic evidence, bioturbation processes can control soil properties. Phillips and Marion [2004, 2005] and Phillips [2008] for example observed highly localized soil variability in a National Forest Area in the Ouachita Mountains, Arkansas. They

concluded that biomechanical effects of trees on soil depth were highly significant. Trees may locally deepen the soil by exploring bedrock joints and fractures in bedrock soils. Treefalls then cause uprooting of bedrock material in shallow soils on bedrock or, on unconsolidated sediments like loess or glacial till, resulting in homogenization of soil horizonation. Gabet and Mudd [2010], using a numerical soil redistribution model, showed that this uprooting process resulted in bedrock erosion rates that were consistent with observations in their study area in the Oregon Coast Range. In addition, they suggested that trees might have played a key role in the establishment of soil cover on rocky slopes. Johnson et al. [2005] focused on the effect of burrowing animals, describing how biota create a biomantle, characterized by a distinct zonation between an upper, biologically active and homogenized layer and an underlying layer. Finke [2012] showed in a model study that a combination of clay eluviation and bioturbation can explain the texture contrast between E and Bt horizons, confirming the hypothesis of Phillips [2007]. Kaste et al. [2007] indicated the relevance of bioturbation in contaminant transport, carbon sequestration and landscape evolution at various time scales. Finally, Gabet et al. [2003] reviewed the importance of a wide range of bioturbation processes, from treefalls to the activity of burrowing animals, for sediment flux on hillslopes and soil production. For treefalls on slopes below 20°, they calculated sediment fluxes to be in the order of 10^{-4}-10^{-3} m^3 m^{-1} yr^{-1}, which is typically an order of magnitude lower compared to sediment fluxes caused by soil erosion in agricultural landscapes. A recent study by Hancock et al. [2012] however concluded that the effect of treefalls on sediment fluxes is likely to be negligible as the pit-mound topography acts as sediment traps.

While the above cited studies suggest that bioturbation is significant for soil fluxes and therefore for controlling overall soil depth, the effect of bioturbation processes such as treefalls on soil properties and on the spatial variability of individual soil horizons is largely unknown. Only for a few detailed case-studies has the direct effect between bioturbation and soil horizonation been investigated. A general process-based understanding is largely lacking although this piecewise evidence points to the importance of faunal and floral activity. A recent study by Yoo et al. [2011] explains how the vertical distribution of soil organic carbon in forest soils can be simulated well by a model that contemplates mixing by biota. Finke [2012] demonstrated in a modelling study the importance of bioturbation for the genesis of A, E and Bt-horizons. However, especially at the landscape scale there is a knowledge

gap about the effects of bioturbation on long-term soil formation processes and the resulting spatial soil variability. To a large extent this can be attributed to the seemingly random nature of major bioturbation events like treefalls. We define 'soil formation' as the change in soil properties over time that cause some primary (parent material) properties to disappear (e.g., sedimentary stratification in the topsoil) and secondary properties to develop (e.g., organic carbon content). These effects of soil formation are partly observable in the field as soil horizons.

Initial variability in sediment properties may mask the effect of terrain controls on soil development. Here we focus on loess-mantled landscapes that widely occur in the temperate zone. Loess texture, mineralogy and $CaCO_3$ content at sedimentation time are reported to vary, which may result in soil properties like decalcification depth (the depth to which the calcite has been dissolved due to acidic precipitation) not being related to current terrain properties. Kowalinski et al. [1972] and Pye [1983] identified weak spatial trends in loess texture in north-western Europe and related this to distance to the source. Similar trends were observed in The Netherlands [*Mücher*, 1973] but differences are minor, occur at spatial scales of 100s of kilometres, and may be caused by local soil redistribution as well. At the scale of a forest catchment such as studied by Vanwalleghem et al. [2010], we consider variation in fresh loess sediment composition of minor importance. Little is known on spatial trends in initial calcite content, but C-horizon calcite contents in Weichsel loess have been reported between 2% [*Pye*, 1983] and more than 20% [*Wintle and Brunnacker*, 1982] at exposures across Europe. In summary, spatial variability in texture, mineralogy and calcite content inside small areas is likely not related to the loess sedimentation but to post-depositional sediment and soil transport processes. Additionally, part of the loess may be of older age and already be decalcified at the time of deposition of the Weichsel loess. Both factors are not easy to reconstruct. Thus, exploration of the effect of variability in parent material as a cause of observed soil variability is in most cases only possible in a stochastic way.

These uncertainties about the variability of initial sediment properties and bioturbation lead to the question to what extent soil-landscape relations, detected with DSM-techniques, can be considered a resultant of (1) soil formation processes influenced by terrain position, and (2) local random processes such as major bioturbation events and variability of the parent material properties.

Application of a soil formation model at various locations in a landscape would inform about variability of soil properties caused by those local variations in soil-forming factors that are determined by relief. Inclusion in such a model of stochastic disturbances would inform about their additional effect on variability. We hypothesize that the SoilGen model [*Finke and Hutson*, 2008; *Finke*, 2012] allows the estimation of profile development as a function of local variations in soil forming factors. This assumption is based on Finke [2012], who simulated a clear effect of topographic controls (slope and aspect) on decalcification depth and expression of Bt-horizons, which was supported by soil analytical data. Additionally, this model can be run with stochastic inputs representing for instance the effect of treefalls. Therefore we think the above question can in principle be answered in the setting of a simulation case study. We propose to apply this model in the context of the Vanwalleghem et al. [2010] study to identify the effects of treefalls on spatial variability of horizon depths, while comparing this variability to field observations. The simulation of the effect of variation of parent material properties is not considered for reasons of complexity and computational effort.

The general objective of this work is therefore to analyse the effect of treefalls on soil formation and on the resulting spatial distribution of soil properties at the landscape scale, and to compare results with observed soil variability. Specific objectives are:

1. to apply the soil genesis model SoilGen to simulate soil development in loess-derived soils in a natural forest area in Central Belgium;
2. to convert simulated depth profiles of soil properties into soil horizon profiles;
3. to formulate and apply a partly deterministic, partly stochastic model to generate treefalls along the timeline and convert these to inputs of the SoilGen model; and
4. to analyse the relation between the current terrain, observed and simulated horizon thickness in case of the absence and presence of treefall events.

5.2 Materials and methods

5.2.1 Study area

The study area is a natural, forested area in Central Belgium, called the Meerdaal forest (1329 ha). This area was selected because of the absence of human disturbance on the studied soil profiles. The forest is mentioned in early medieval documents that confirm that the area was forested at least since the mid-12th century. Vanwalleghem et al. [2003, 2005, 2006] showed evidence for a brief period of agricultural land use between the Middle Bronze Age and Roman times. This caused localized gully erosion but left the areas outside largely unaffected. The studied profiles are in these unaffected areas. After Roman times, the area was quickly reforested, as shown by sediment deposits [*Vanwalleghem* et al., 2006]. During Medieval times, the forest was mainly used for hunting. The forest is located in the Belgian loess belt. Local lithology is characterized by Quaternary loess deposits, mostly of Weichselian age [*Gullentops*, 1954], that overlie Tertiary marine sands of Middle to Late Eocene Age (52– 36.6 Ma BP). The thickness of the loess layer is highly variable, ranging between 0 and 8.7 m, with an average thickness of 2.50 m [*Vanwalleghem et al.*, 2010]. The original loess deposits are calcareous. Present-day loess samples reveal an average $CaCO_3$ content of 15 (+/-3) %. The forest is managed as coppiced woodland whereby the larger trees are kept while the smaller undergrowth trees are harvested every 10-15 years. The current management consists of an increase in untouched forest reserve area (to 10% of the total area) and a gradual replacement of exotic species (several pine species) with native species managed in a low-impact silvicultural system. Forest regrowth is largely natural. Only tree species composition has been altered to some extent by silviculture during the last centuries. Current stands are dominated by oak species (*Q. robur L. and Q. petraea L.*) and beech on the loess-derived soils (*Fagus sylvatica L*.) (respectively, 57 and 18% of the area) with pine forest on the sandy outcrops (*Pinus sylvestris, Pinus nigra and Pseudotsuga menziesii*). *Acer pseudoplatanus* is numerous in the understorey of the stands where Quercus is dominating the overstorey. Average stem number is 512 per ha [*De Keersmaeker et al.*, 2009].

5.2.2 Research layout

This research focuses on 108 pedons in the Meerdaal forest. The locations were chosen randomly from a larger number of 258 where the depth to Eocene sands was measured by soil augerings in an

earlier study [*Vanwalleghem et al.*, 2010] and an overlying loess cover was present. Horizon thicknesses have been estimated by these authors in the field. The 108 pedons are a compromise between a sufficient number to perform spatial analyses [*Webster and Oliver*, 1992] and a feasible simulation effort. Two scenarios are simulated for each location (Fig. 5.1): (i) natural soil development, starting at 15000 BP with a parent material consisting of the C-horizon of the loess on top of Eocene marine sand and ending at 0 BP; (ii) natural soil development including occurrences of soil disturbance due to uprooting of trees. With "natural soil development" we mean that direct human influences such as those related to agricultural land use are excluded and a natural vegetation development is assumed. As stated above and in more detail by Vanwalleghem et al. [2010], this is likely the case in the Meerdaal forest with the exception of localized and short-spelled agricultural activities between the Middle Bronze Age and the Roman era. These activities have led to the formation of some gullies in the area but the 108 pedons are all outside these areas.

In order to compare model results with field observations, simulated soil characteristics like organic carbon (OC) and clay content at 0 BP are converted to horizon thickness according to a protocol developed during this study and based on both measured and simulated soil data. Regression kriging is then used to characterize the soil-landscape relationship in an approach similar to Vanwalleghem et al. [2010]. Resulting horizon thicknesses from the 2 simulated scenarios are first correlated to terrain variables using stepwise multiple linear regression techniques to evaluate the effect of tree uprootings on the predictive quality by this digital soil mapping technique. Next, ordinary kriging is used to interpolate the residuals of the regression model and a map would be produced by adding the regression predictions and interpolated residuals. In this case, we are only interested in exploring the spatial correlation in the data by analysing the semivariograms of the residuals.

The spatial differences between the 108 pedons at 0 BP in simulation scenario 1 (hereafter referred to as model 1) can be considered the deterministic response of soil formation processes to initial variation in thickness of loess cover and site aspect only, as all other factors (initial conditions and inputs along the timeline) are kept constant. As such, we expect a strong statistical relation (correlation) between all simulated horizon thicknesses and terrain attributes. The spatial differences in simulation scenario 2 (hereafter referred to as model 2) should be partly attributable to the effect

of tree uprootings over time, which is considered a probabilistic process because there is no mechanistic method to predict uprootings. Therefore we expect a weakened statistical relation (correlation) between simulated horizon thicknesses and terrain attributes. The research layout aims at identifying how much the relation weakens because of treefalls and how this compares to the relations based on measured soil horizon thickness.

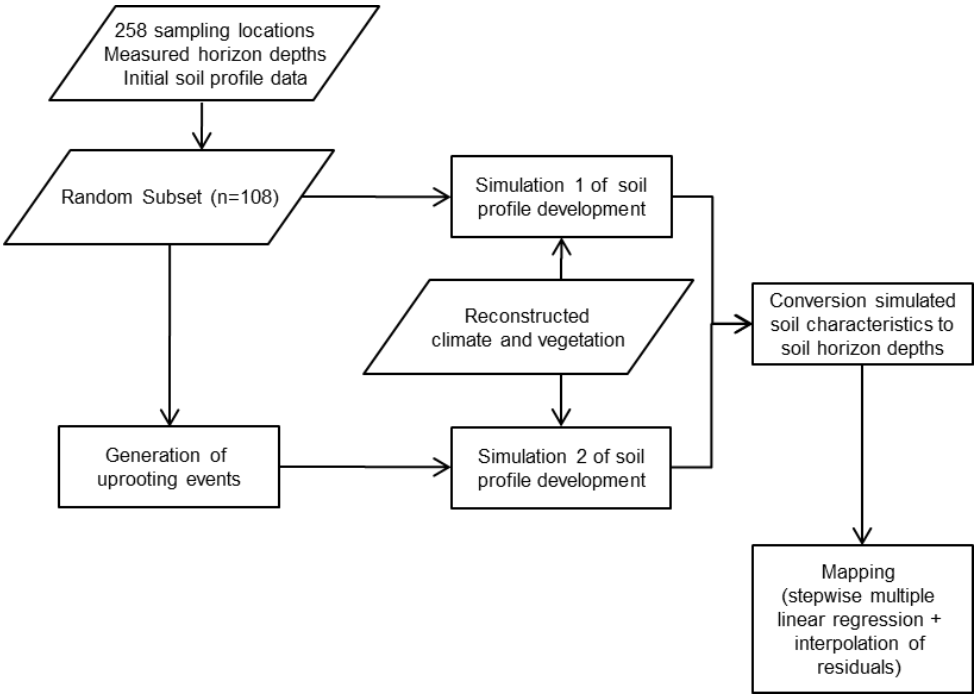

Figure 5.1. Flowchart of simulation and mapping activities (boxes) and used data (rhomboids).

5.2.3 The SoilGen model

The current study was done using SoilGen2.16, documented in Finke [2012] and downloadable from http://users.ugent.be/~pfinke/index_bestanden/SG216.zip. SoilGen is a soil genesis model that describes various soil physical and soil chemical processes such as bioturbation, physical and chemical weathering, clay migration, carbon cycling. It is a 1-D vertical transport model in the sense that it simulates unsaturated water flow by the Richards' equation, solute transport by the Convection-Dispersion Equation and soil temperature by the heat flow equation. Additionally the model is sensitive to soil forming factors such as climate, relief, organisms and parent material making it suitable to answer the objectives of the current study. Detailed description of the SoilGen model including the governing processes and equations is given in Chapter 2 of this thesis.

5.2.4 Model inputs

Each input parameter for SoilGen can either be a process parameter, an initial value or a boundary condition varying in time. We took the process parameters that were calibrated and estimated by Finke [2012] as this preceding study was done on loess-derived soils nearby the Meerdaal forest. Table 5.1 summarizes the parameters and some of their initial values and identifies if time series were reconstructed for boundary inputs along the time line. Figure 5.2 visualizes these boundary inputs. The boundary inputs were assumed spatially constant for all simulated plots, although via the relief and aspect, the inputs precipitation and potential evapotranspiration are corrected at the plot level according to the method described in chapter 2 (section 2.2.1.8).

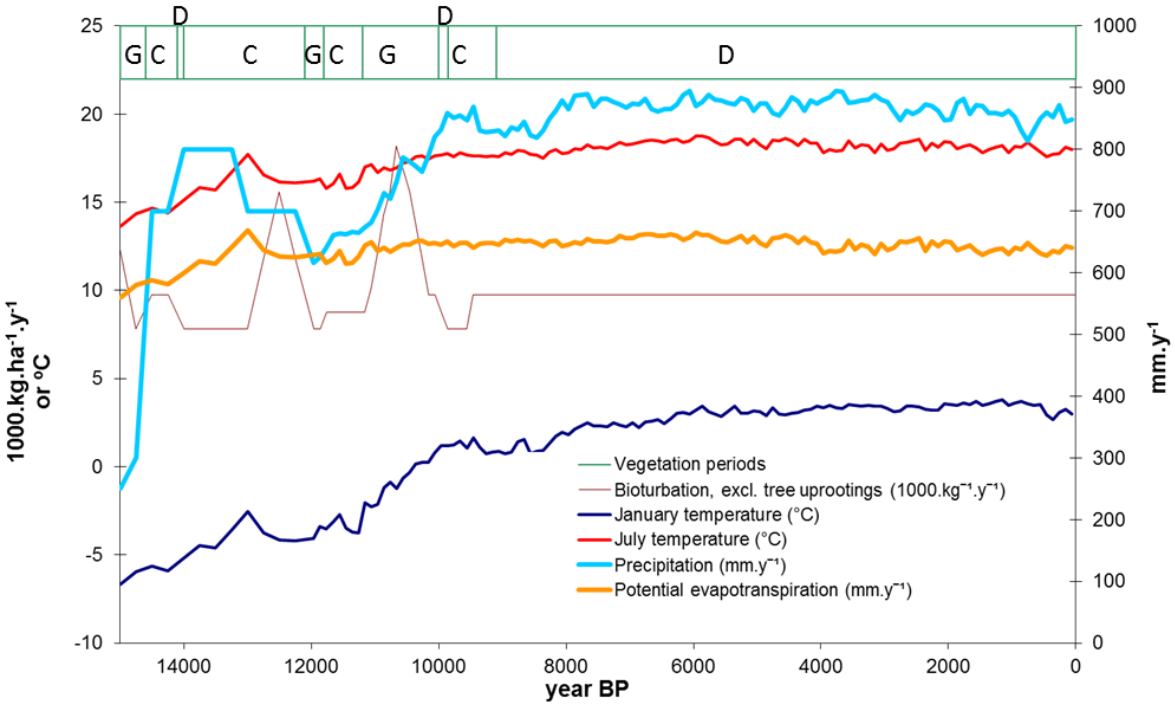

Figure 5.2**.** Boundary conditions for the soil modelling, representing reconstructed climate and vegetation change over the last 15000 years. G=Grassland, C=Coniferous forest, D=Deciduous forest. For data sources see Table 5.1. This data was originally used for Zonian forest (Finke, 2012) but was also assumed valid for Meerdaal forest since the Meerdaal forest is approximately 15 km away from Uccle weather station for which climate and vegetation data reconstruction was based on.

Table 5.1. Inputs for the SoilGen Model and Associated Data Sources.

Group	Input variable or parameter	Dimensions	As initial condition	Time series, in typical year	Time series, annual	Source for data and/or method
Climate	Temperature	°C	Yes	Weekly average and daily amplitude	January and July averages	Davis et al. [2003]; Finke & Hutson [2008]; Godefroid & Koedam [2010]
	Precipitation	mm	-	Daily depth, intensity, chemical composition of rain	Annual sum	Davis et al. [2003]; Finke & Hutson [2008]; Uccle weather data
	Potential evapotranspiration	mm	-	Weekly total	Annual sum	Hargreaves & Samani [1985]; Finke & Hutson [2008]
Organisms	Vegetation type	-	-	-	Vegetation type, rooting depth, C-input as litter	Verbruggen et al. [1996]
	Bioturbation	kg.1000 ha^{-1} y^{-1}	-	-	Yearly depth distribution	Finke [2012]
Relief	Slope angle	°	Yes			DEM; Vanwalleghem et al. [2010]
	Slope aspect	°	Yes			DEM; Vanwalleghem et al. [2010]
	Wind direction	°	Yes			Godefroid & Koedam [2010]
Parent material (for loess and Eocene sand)	Clay/Silt/Sand	Mass %	Yes			Loess: 6.4 / 81.6 / 12.0 % Eocene: 1.4 / 0.6 / 98.0 % Vanwalleghem et al. [2010]
	OC	Mass %	Yes			0.1 % assumed
	Ca, Mg, Na, K, Al, SO_4, Cl, Alkalinity in solution	mmol dm^{-3}	Yes			Unpublished data from analyzed C-horizon in Meerdaal forest
	Ca, Mg, Na, K, Al, H on exchange complex and CEC	$mmol^{+}$ kg^{-1}	Yes			Unpublished data from analyzed C-horizon in Meerdaal forest
	$CaCO_3$ / $CaSO_4$	Mass %	Yes			15 / 0 % Vanwalleghem et al. [2010]
	Gapon exchange coefficients	$(mol\ dm^{-3})^{1/n-1/m}$ *	Yes			De Vries & Posch [2003]
	Ca, Mg, Na, K, Al in primary minerals	mol^{+} kg^{-1}	Yes			Van Ranst [1981]

* n and m are the charges of the ion pair involved

5.2.5 Transforming simulated soil parameters to horizon thickness

During the field inventory by soil augering [*Vanwalleghem et al.*, 2010] the depths of transition between occurring major soil horizons were recorded: A (mineral, humus-rich horizon), E (eluvial horizon, in this case study indicating loss of clay), Bt (illuviation horizon with increased clay content), BC (transitional horizon with limited clay illuviation), C1 (decalcified loess) and C2 (calcareous loess). Also the depth to the underlying Eocene marine sand (C3) was noted and all augerings reached to this depth. A typical horizon sequence is thus: A-E-Bt-BC-C1-C2-C3. Horizon codes were assigned in the field based on soil colour, expert estimations [*FAO*, 2006] of organic matter content and clay content and presence of $CaCO_3$ as shown by effervescence with hydrochloric acid. All profiles were described by the same person. As the SoilGen model calculates soil properties like clay content, carbon content and $CaCO_3$ content at all soil compartments *i*, these values at simulation time 0 BP have to be translated to current horizon codes. Vertical compartment size in SoilGen was set to 5 cm. Horizon codes can be obtained by transforming relevant simulated soil properties to indicators for horizons (or horizon transitions) by comparison to threshold values for these properties. Threshold values for each indicator can iteratively be estimated by minimizing the average difference in horizon depths based on indicator values and the measured depths over all soil profiles that contain the horizon in the field. By calibrating the threshold values (indicated with T) we compensate for unknown bias in the field estimates to identify soil horizons and also for the fact that the SoilGen model was not calibrated for the Meerdaal forest. We propose the following decision rules to obtain indicator values for horizon codes (default values for indicators (I) are 0, for transition depths (D) -999; $\forall$ means "for all"):

- $\forall\ OC_i >= T_{OC} : I_{A,i}=1$, where OC is simulated organic carbon (%) and T_{OC} is a threshold value for OC. This defines all compartments belonging to the A-horizon;

- $\forall(L_i-L_{i-1}) >= T_{Cl} : I_{EBT,i}=1$ (see decision tree in Fig. 5.3), where L is simulated clay (Lutum) percentage and T_{Cl} is a threshold Clay percentage increase; analogous to application of the WRB criteria 1, 2 and 4 [*IUSS Working Group WRB*, 2006; p.13-14] for the *argic* diagnostic horizon. $I_{EBT,i}$ defines the transition depth D_{EBT} between the top of the Bt-horizon and the bottom of the E-horizon. All

compartments between the A-horizon and the top of the Bt-horizon are considered part of the E-horizon;

- $\forall$ $ACDI_i < T_{CDI}$: $I_{BTBC,i}=1$, where $ACDI_i$ is the Average Clay Dispersion Indicator for compartment i over all simulated years. The Clay Dispersion Indicator (CDI) in a compartment at a particular simulation year has the value 0 if there is calcite or gypsum present or if the Electrolyte Concentration (EC)>= Critical Salt Concentration (CSC) as defined in Finke [2012]. In all other cases, the CDI has the value (1-EC/CSC). T_{CDI} is a threshold value for CDI. ACDI indicates the likelihood that clay migration has occurred in a particular compartment over total simulation time. The lower the value of ACDI, the longer the period that flocculating conditions prevailed or the shorter the period of clay dispersion conditions (inhibiting the movement of clay into or out of that compartment). $I_{BtBC,i}$ defines the transition depth (D_{BTBC}) of the Bt-horizon and the BC-horizon.

- $\forall$ $(L_{i,t=T} - L_{i,t=0}) > T_{Ctol}$: $I_{BCC1,i}=1$, where the increase in clay content (L) between 15000 BP (t=0) and present (t=T) is compared to a tolerance threshold clay content T_{Ctol}. $I_{BCC1,i}$ defines the transition depth (D_{BCC1}) between the BC-horizon and the top of the horizon below, usually the decalcified C1-horizon.

- $\forall(Calcite_{i,t=0} - Calcite_{i,t=T}) < T_{calctol}$: $I_{C2,i}=1$, where the initial calcite content at t=0 is based on measurements (Table 5.1). $I_{C2,i}$ identifies all compartments belonging to the (calcareous) C2-horizon. As the decalcification front is very sharp, $T_{calctol}$ can be expected to be close to the initial calcite content. However, because SoilGen is not calibrated to the sites in the Meerdaal forest, there may be systematic differences between simulated and measured depths to the C2 horizon as the annual percolation is uncertain. This is caused by an unknown fraction of the rain that is lost by forest interception [*Finke*, 2012].

- $\forall(i>C3_x)$: $I_{T,I} = 1$. The depth C3 of the Eocene marine sand underlying the loess is known for each location *x*.

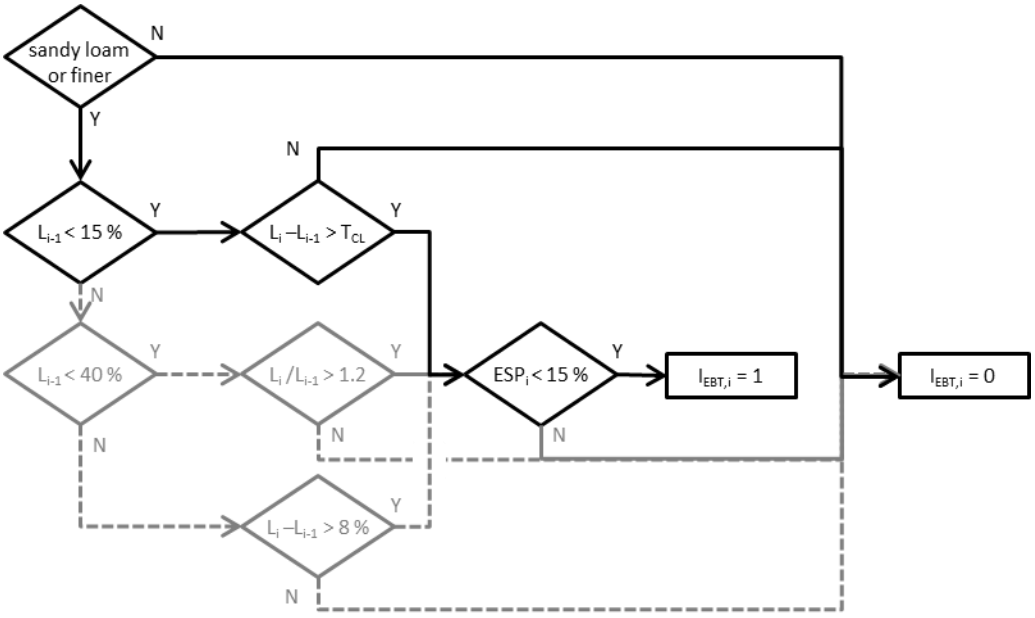

Figure 5.3. Decision tree to decide if a E/Bt horizon transition is present in compartment i, using an indicator value IBT,i based on L (Lutum, clay content, %), ESP (Exchangeable Sodium Percentage) and a threshold value for depth change in clay content (TCI). Solid black lines indicate (simulated) situations occurring in the study area; dashed grey lines indicate non-occurring situations.

After the threshold values T have been obtained by calibration, assignment of horizon codes to soil compartments is straightforward (Fig. 5.4).

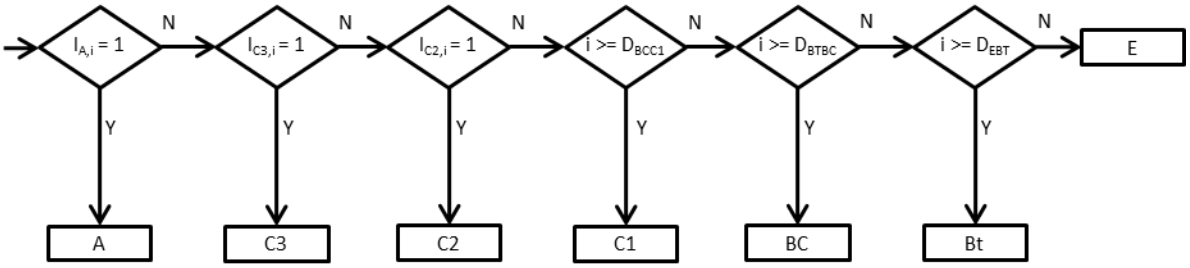

Figure 5.4: Decision tree to decide what horizon occurs at the depth of compartment i. I and D describe the presence of a horizon and transition depth to another horizon respectively. For the derivation of I and D see text. A, C2, C1, BC and Bt are horizon codes [FAO, 2006] and C3 indicates the Eocene marine sand below the loess.

5.2.6 Generating uprooting events

Tree uprooting has long been identified as a factor disturbing the topsoil layers and thus affecting soil genesis [*Schaetzl et al.*, 1988; *Ulanova*, 2000; *Phillips*, 2008]. Various factors have been named as causes for tree uprooting: strong winds, wind exposure, soil wetness and the general condition of the tree as determined by possible disease and age. Empirical studies have identified disturbance cycles (expected number of years between successive treefall events at a location in a forest stand [*Schaetzl et al.*, 1989]) and relation to wind exposure [*Maxwell et al.*, 2010] in case studies. This does not mean that tree uprooting can be predicted with high confidence for individual trees, and thus the likelihood of tree uprooting at the scale of a pedon in a certain year can at best be estimated. We therefore propose a probabilistic approach to predict the occurrence of tree uprooting in a certain year at pedon scale. This probabilistic approach is based on empirical studies worldwide in similar natural forests as were present in the studied loess area in Belgium. Basically, the probability of a treefall is derived from the disturbance cycle (the average time between two tree uprootings in a soil pedon). The disturbance cycle is modified by a factor describing the effect of wind exposure, to obtain a site-specific probability which is subsequently corrected to obtain the probability of treefalls ($P_{treefall}$) that result in uprooting:

- From Schaetzl et al. [1989] we take the disturbance cycle from Illinois of 1730 years, so $P_{treefall} = 1/1730$;

- We calculate the modified treefall probability $P_{treefall,x}$ by multiplying $P_{treefall}$ with a wind exposure factor WE_x at position x;

  A map of the wind exposure factor is obtained by calculating the wind exposure for the DEM of the Meerdaalwoud for all wind directions (at 16 intervals of 22.5°) and associated wind speeds as documented for the nearby Uccle weather station (Fig. 5.5). The SAGA 2.0.8 “wind effect” module from Boehner and Ringeler [2008] and Conrad [2011] is used. An average wind exposure map is then obtained by weighting the resulting 16 maps for the frequency of occurrence of the wind speed.

- Following Maxwell et al. [2010] we assume that 85% of treefalls cause uprooting (15% are broken stems and assumedly do not disturb the soil);

- In any year *y* in which a forest vegetation is present, we decide if a treefall event with uprooting $WU_{y,x}$ occurs at a location *x* by generating a random number R_y [0;1] and applying the rule ($\wedge$ means "as well as"):

  $WU_{y,x} \forall\ R_y<0.85\ P_{treefall,x}\ \wedge$ (no treefall last 70 years) $\wedge$ (forest older than 70 years)

  The last 2 conditions were added because uprootings of young trees (arbitrarily set to younger than 70 years) are assumed not to affect the soil.

- Following Ulanova [2000] we take that the bioturbation in the year of a treefall affects the upper 80 cm. We interpret this as instantaneous near-complete mixing: 95% of the soil mass corresponding to this depth interval is mixed in the year of an uprooting event. As such, we do not take into account that a pit-mound topography may temporarily exist at the location of a treefall, which is gradually levelled but instead assume immediate levelling, which is a simplification of reality.

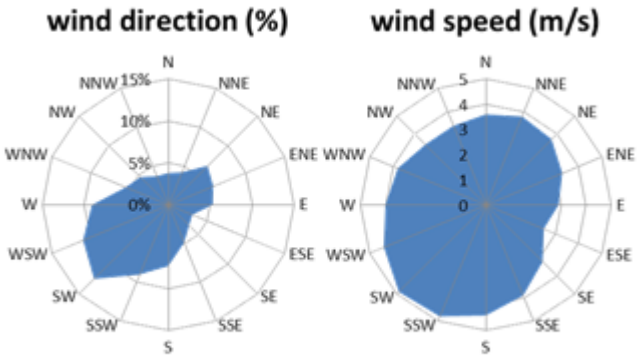

Figure 5.5. Annual distributions of wind direction and wind speed for Uccle, Belgium, used to feed the stochastic tree uprooting model.

5.2.7 Geostatistical analysis

The geostatistical analysis done by Vanwallegem et al. [2010] was repeated for the reduced observation dataset of 108 points (pedons) and for both simulated datasets (model 1 and model 2) at the same locations. Regression kriging was used to produce a spatial prediction model for the thickness of each soil horizon. Regression kriging is a hybrid approach that combines a multiple-linear regression model with ordinary kriging [*Odeh et al.*, 1994]. First, a (multiple) regression model between observed values and (multiple) full-cover environmental variables is fitted. Second, the residuals between the regression predictions and observed values are mapped by ordinary kriging. The full-cover regression predictions and mapped residuals are then added to obtain a full cover map. If no spatial structure is present in the residuals, the model reduces to a simple regression model. If no (multiple) linear statistical relation is present between soil horizon depth and environmental variables, the model reduces to ordinary kriging. Spatial correlation in the observed and simulated soil profiles was assessed by analysis of the semivariogram, which was constructed by using either the residuals, in case a regression model could be established, or else by using the soil horizon depth data directly. Most of the full-cover environmental variables are derived from a DEM. The "wetness index" is equal to the compound topographic index (Eq 5.1) defined by Beven and Kirkby (1979). Statistical analysis was performed with JMP, Version 7. SAS Institute Inc., Cary, NC, 1989-2007. Semivariogram analysis was done with Vesper version 1.6. [*Whelan et al.*, 2001].

$$Wetness\ index = ln(a/tan\beta) \qquad \text{(Eq 5.1)}$$

where a represents the the local upslope area which drains through a given point per unit contour length and β is the slope angle

5.3 Results

5.3.1 Simulated horizon thickness

The results of the calibration of the threshold values to derive depths and thickness of horizons from the model outputs are given in Fig 5.6. The average field thickness of the A-horizon (108 field locations), depth to the boundary between Bt-BC (77 field locations) and BC-C1 (78 field locations)

could be well reproduced by selecting an adequate threshold value. The depth of the E-Bt transition (84 field locations) was best approached by a clay content contrast between E and Bt (T_{Cl}) of 2%, which gives a small (5 cm) bias between average measured and simulated depths that could be bridged by calibration of the model (likely via the depth of bioturbation), but that could equally well be the result of bias because of the augering technique used in the field. The depth to the decalcification front (C1-C2 transition, 68 locations) was coupled to a $T_{calctol}$ of 0.14 (max. 1% of the 15% calcite remaining). The figure shows that for negative values of $T_{calctol}$ the average measured value can be reproduced, but negative values indicate calcite accumulation zones in the C2-horizon, which occurred only in 1 simulation. Choosing $T_{calctol}$ of 0.14 implies a bias of 78.4 cm underestimation of the depth of C1-C2 transition by simulations, which might be bridged by calibration of the model (likely via the fraction of rain intercepted by forest). However, bias in the estimation of absolute horizon depths is not of great importance as it becomes part of the regression constant in the stepwise multiple linear regression with terrain attributes. More important is the spatial structure and the relation with terrain attributes of the simulated soil horizon depths, which is not affected by this bias.

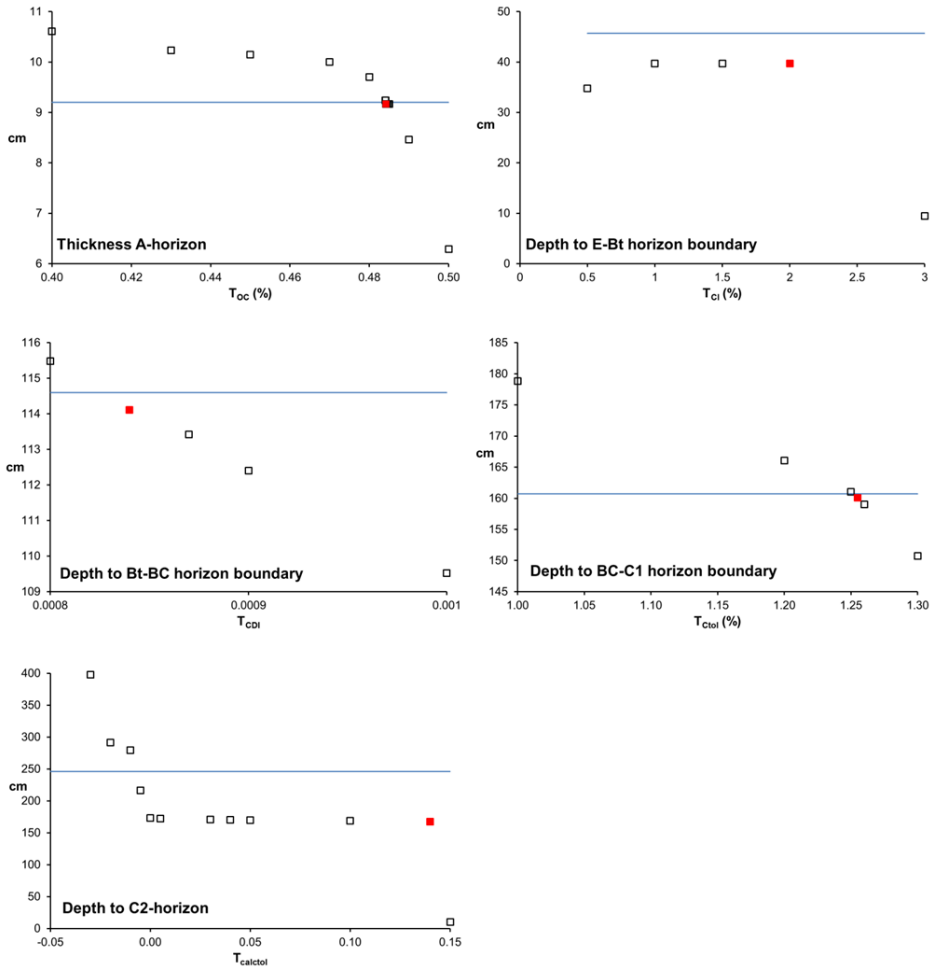

Figure 5.6. Calibration of threshold values (T) of simulated soil properties to match estimated and measured thickness or depth to 5 soil horizons. Solid blue lines indicate average measured values, open symbols indicate average estimated values at various thresholds. Filled red symbols indicate chosen values for T. Note that negative values for Tcalctol indicate calcite accumulations.

5.3.2 Uprooting events

Figure 5.7 shows the total wind exposure over a typical year for the DEM of the Meerdaal forest. Besides the wind exposure of the natural relief, also that of roads and built-up structures is visible, especially to the north. However the simulation locations are always outside the distance of influence of these non-natural relief features. The wind exposure factor over all 108 sites varies between 0.87 and 1.13 for leeward sites and windward sites respectively, with an average of 1.01. The protocol to

calculate tree uprooting events produced a total of 614 uprootings, varying between 1 and 11 uprootings per site (Fig. 5.8) over 12461 years of forest vegetation (see Fig. 5.2; sum of years under coniferous (C) and deciduous (D) forests). This number depended on probability and wind exposure and was equivalent to an average disturbance cycle of 108 ×12641 ×0.85/614 = 1890 years (0.85 is the fraction of treefalls causing uprooting, see section 5.2.6). This number is larger than the assumed disturbance cycle of 1730 years because the forest vegetation period was discontinuous (Fig 5.2), and the protocol assumes that young trees do not uproot, which reduces the period in which tree uprootings can occur.

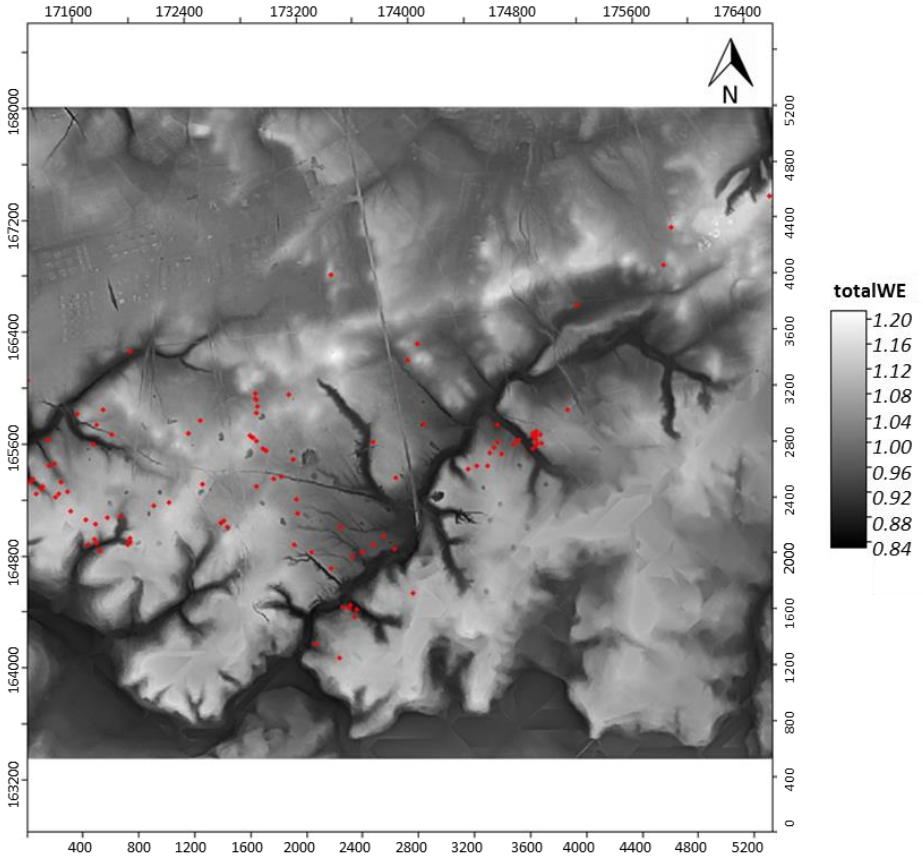

Figure 5.7. Average annual wind exposure (totalWE) for Meerdaal forest and surroundings calculated with distributions of wind direction, wind speed and the DEM. TotalWE values exceeding 1 indicate luff effects (windward slope exposure), those values less than 1 indicate a lee effect. Red dots indicate 108 simulation locations with measured horizon thickness. Axis numbers indicate Lambert-2 coordinates (m).

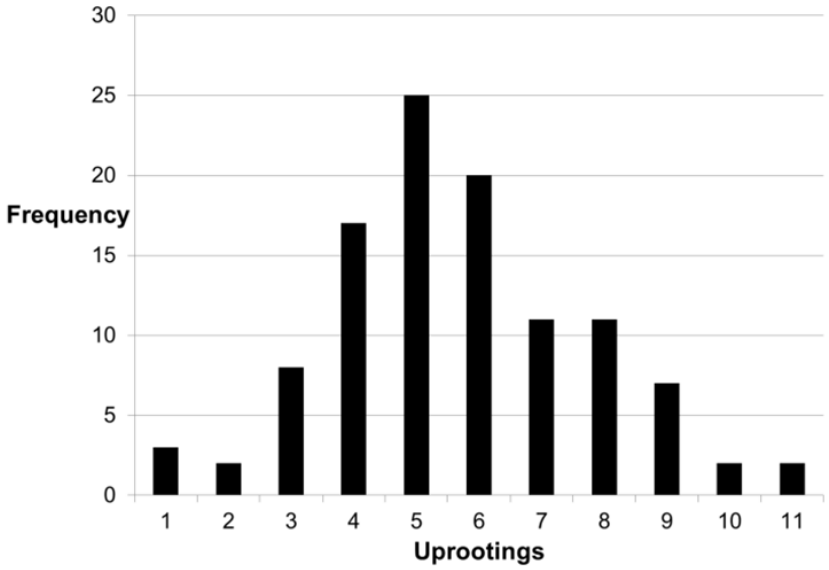

Figure 5.8. Frequency distribution of simulated tree uprootings at 108 locations within Meerdaal forest during the simulation period (15000 – 0 years BP).

5.3.3 Geostatistical analysis and comparison to measured variability

Figure 5.9 shows the evolution of a typical soil profile under both models, without and with treefalls. With model 1, a full profile, that includes all horizons from A to C2, is formed after approximately 5000 years. With model 2, the first treefall at this site occurs after approximately 2000 years (13000 years BP). It can be seen how this event mixes all horizons developed at that time. For a short period, the upper 80 cm classifies into an A horizon according to the protocol. In this example, most of the treefalls occur towards the end of the simulation (0-5000 years BP). Because the lower soil horizons (BC-C1-C2) are then already located below the influence depth of the treefalls, these events no longer cause a full mixing of the soil profile. Nevertheless, the mixing of the upper soil layers still results in the disappearance of the E horizon, under the classification scheme adopted.

The original dataset by Vanwalleghem et al. [2010] showed a very weak correlation between the depth of the different soil horizons and landscape attributes. In particular for the top horizons, E and Bt, no statistically significant relation could be detected. We selected a subset of 108 profiles out of the 399 profiles from the original dataset published by Vanwalleghem et al. [2010], and this led to a slightly different soil-landscape model identified by regression kriging than reported by

Vanwalleghem et al. [2010]. In addition, in this study the variable loess cover thickness was included in the analysis because it was hypothesized that this might have an influence on the simulated soil horizon thickness. However, the main conclusion (that was drawn based on the original data set) that the relation between soil horizon depth and landscape position was weak, still holds. As shown in Table 5.2, for the subset selected in this study, only for the E and C1 horizons, a weak relation was found with wetness index, loess thickness and soil type: r^2 values for the simple linear regression are all below 0.03. Adjusted r^2 values of the multiple regression model are between 0.04 (Bt) and 0.19 (C1). These values are similar to the low explanatory power of the original dataset (n = 300), with adjusted r^2 values between 0.09 and 0.14. The analysis of the experimental semivariograms (Fig. 5.10) shows that the spatial correlation of the observational dataset is low to absent (Fig. 5.10 a to e). All variograms are characterized by a very high to a pure nugget effect, such as for example the E horizon in Fig. 5.10a. The nugget effect is defined as the value of the fitted variogram at distance 0 (*Goovaerts*, 1997). This high nugget effect shows that there is important soil horizon depth variation at the detailed (10 meter) scale.

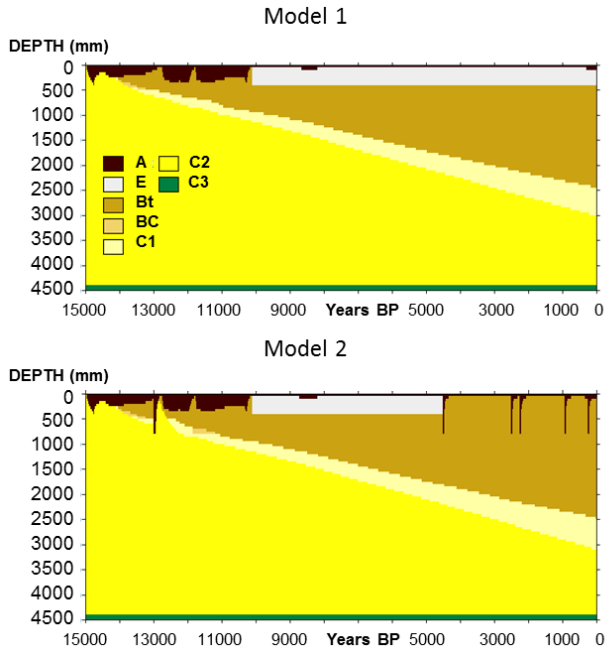

Figure 5.9. Example result of simulated soil horizon (A, E, Bt, BC, C1, C2 and C3) development on loess over time (15000 – 0 years BP) using model 1 (no treefalls) and model 2 (6 treefalls). Note that profile thickness is 4.50 meter.

In contrast to the observed data, the simulated soil horizons by model 1 exhibit a strong correlation with landscape attributes. In this model, which simulates soil formation without disturbance by tree throws, all soil horizons are significantly related to at least one landscape variable and for all cases, a significant multiple linear regression model could be established (Table 5.2). The simulated soil horizon depths correlate with the landscape variables slope angle, wetness index, loess thickness and soil type. The overall prediction capacity of the soil-landscape model is high for the deeper soil horizons, BC, C1 and C2, and explains between 49% (C2) and 73% (BC) of the variance. For the superficial horizons, E and Bt, the model performance is still relatively high, and explains between 38% (E) and 53% (Bt) of the variance. Analysis of the spatial structure of the regression residuals in the data shows a separation of the horizons in two groups. The deeper soil horizons, BC, C1 and C2, are again characterized by an important nugget effect, showing a nearly complete lack of spatial dependence (Fig. 5.10 h to j). The superficial horizons on the other hand are characterized by a sill that is a factor two to three lower than the observed data. The sill is defined as the maximal semivariance of the fitted variogram (*Goovaerts*, 1997). This low sill shows that model 1 underestimates the spatial variation in the data. In addition, the Bt horizon (Fig. 5.10g) does exhibit an increase in semivariance with lag distance.

Finally, the correlation with landscape parameters for model 2, which takes into account treefalls during soil formation, is lower than for model 1, although it is still higher compared to the observed data (Table 5.2). Note that with model 2 no E horizon remains at 0 BP as the parameters used by the algorithm for horizon classification, and specified under section 5.2.5, were not met (Fig. 5.9). Therefore, for the superficial soil horizons, we can only use the Bt horizon for comparison. In contrast with model 1 without disturbance, no significant correlation between Bt horizon depth and landscape parameters was found. For the observed data, the multiple linear regression model had a very low predictive power of only 4% of the variability. This means that for this superficial horizon, model 2 actually predicts a situation similar to the one observed in the field. On the other hand, for the deeper soil horizons BC to C2, soil horizons simulated by model 2 did still exhibit a relation to landscape parameters. While the number of significant relations for the simple linear regression model dropped from 14 under model 1 to 8 under model 2, the overall multiple linear regression model showed a significant relation. The predictive power was in the order of that of model 1, explaining between 44%

and 71% of the variance. Slope aspect appears to show a stronger relation to depths of deeper horizons. Wetness index and loess thickness appear to play a less prominent role than with model 1 (Table 5.2). This corresponds better with the patterns observed in the field. Again, the experimental semivariograms of all soil horizons have a high nugget-to-sill ratio (Fig. 5.10k to n). However, model 2 does represent the spatial variability in the data more accurately as compared to model 1. For all soil horizons, the sill is close to that of the observed data.

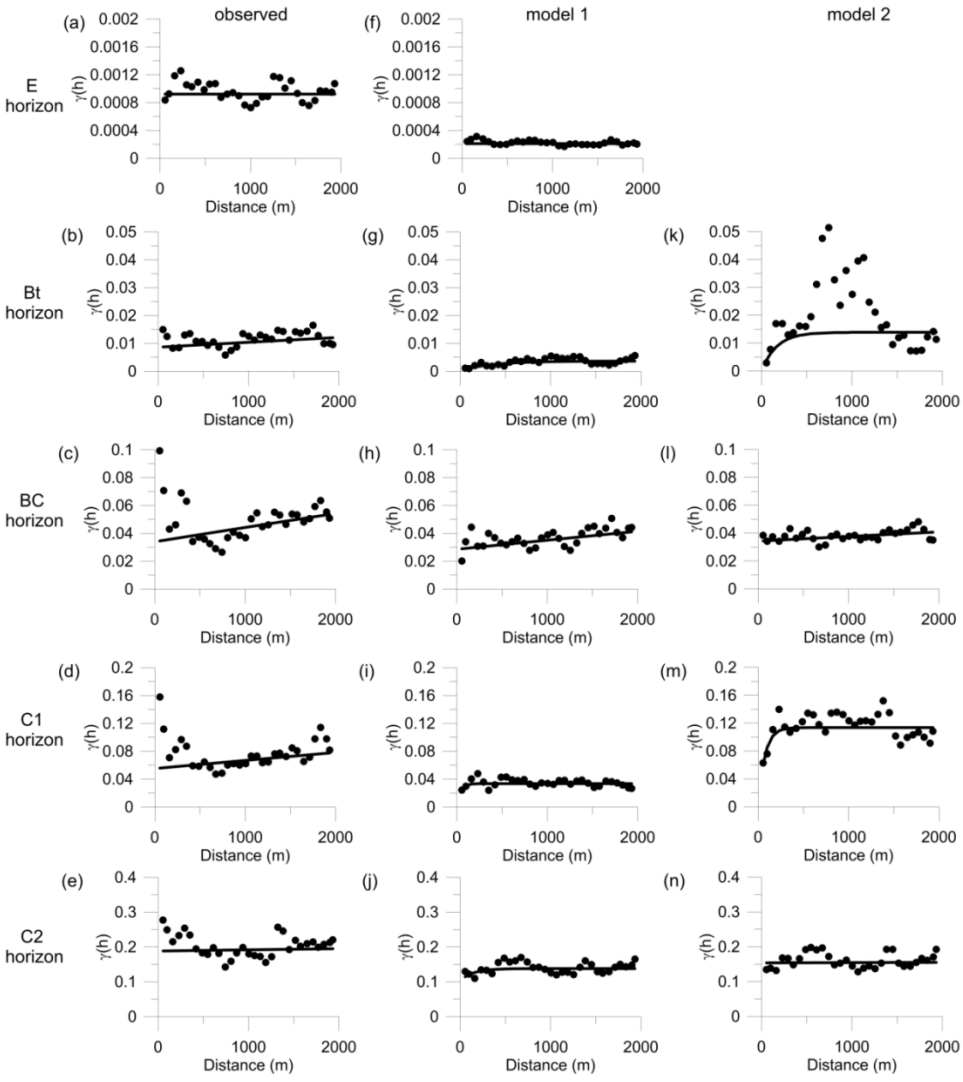

Figure 5.10. Experimental and fitted semivariograms of the observed soil horizon data (a-e), model 1 without tree uprooting (f-j) and model 2 including tree uprooting (k-n). Note that no E horizon remains at present date (0 BP) using model 2.

Table 5.2. Summary statistics for the relations between spatial covariates and observed data, model 1 and model 2.

Regression model	Covariate	Observed data					Model 1 no tree uprooting					Model 2 including tree uprooting				
		Soil horizon					Soil horizon					Soil horizon				
		E	BT	BC	C1	C2	E	BT	BC	C1	C2	E	BT	BC	C1	C2
	n	*70*	*84*	*77*	*77*	*68*	*95*	*105*	*68*	*39*	*108*	*0*	*104*	*47*	*59*	*107*
I - Univariate model [1]																
Landscape attributes	Slope angle	-	-	-	-	-	-	-	0.15 (0.001)	0.24 (0.002)	-	NP	-	-	0.1 (0.02)	-
	Profile curvature	-	-	-	-	-	-	-	-	-	-	NP	-	-	-	-
	Plan curvature	-	-	-	-	-	-	-	-	-	-	NP	-	-	-	-
	Log(Wetness Index)	0.07 (0.02)	-	-	0.08 (0.01)	-	-	-	-	0.21 (0.003)	-	NP	-	-	-	-
	Loess thickness	0.08 (0.02)	-	-	0.06 (0.03)	-	0.18 (<0.001)	0.28 (<0.001)	-	0.16 (0.01)	0.04 (0.03)	NP	-	-	-	0.05 (0.02)
	Soil	-	-	-	0.22 (0.007)	-	0.21 (0.002)	0.45 (<0.001)	-	-	0.15 (0.01)	NP	-	0.23 (0.02)	0.24 (0.02)	0.14 (0.02)
	Landform	-	-	-	-	-	-	-	-	-	-	NP	-	-	-	-
	Aspect	-	-	-	-	-	0.1 (0.019)	-	0.58 (<0.001)	0.3 (0.005)	0.39 (<0.001)	NP	-	0.47 (<0.0001)	0.64 (<0.0001)	0.35 (<0.0001)
II - Multiple regression model [2]																
Intercept		0.15	0.48	1.22	1.69	2.42	0.08	0.24	-297.5	326.9	2.06	NP	-	1.03	1.03	2.14
Landscape attributes [3]	Slope	-	-	-	-	-	-	-	-0.01	0.02	-	NP	-	-	0.02	-
	Profile curvature	-0.0004	-	-	-	-	-	-	-	-	-	NP	-	-	-	-
	Plan curvature	-	-	-	-	-	-	-	-	-	-	NP	-	0.005	-	-
	Log(Wetness Index)	-	-	-	-	-	-	-	21.5	-27.1	-	NP	-	-	-	-
	Loess thickness	-	-	-	-	-	0.004	0.016	-	-	-0.05	NP	-	-	-	-0.06
	Landform: Landf(2&1-3)	-	-0.04	-	-	-	-	-	-	-	-0.12	NP	-	-	-	-
	Landform: Landf(2-3&1)	-	-	-	-	-	-0.004	-	-	-	-	NP	-	-	-	-
	Landform: Landf(1-2&3)	-	-	-	-	-	-	-	-0.08	-	-	NP	-	-	-	-0.12
	Soil: Soil(1&3-2)	-	-	-	-	-	-	-	-	-	-0.44	NP	-	-	-	-0.46
	Soil: Soil(1-5&6)	-	-	-	-	-	-	-	-0.16	-	-	NP	-	-	-	-
	Soil: Soil(4&3&2-1&6&7&5)	-	-	-	-0.17	-	-	-	-	-	-	NP	-	-	-	-
	Soil: Soil(7&4&3&2-1&6)	-	-	-0.11	-	-	-	-	-	-	-	NP	-	-	-	-
	Soil: Soil(3-1&2&4&5&6&7)	-	-	-	-	-	-0.007	-	-	-	-	NP	-	-	-	-

	Soil(1-2&3&4&5&6&7)	-	-	-	-	-	-	-0.09	-0.09	-	-	NP	-	-	-	-
	Soil(4&5&6&7-1&2&3)	-	-	-	-	-	-	-	-	-	-0.33	NP	-	-	-	-0.32
	Soil(1&3-2&4&5&6&7)	-	-	-	-	-0.12	-	-	-	-	-	NP	-	-	-	-
	Soil(1&6&7&3&4-2)	-0.05	-	-	-	-	-	-	-	-	-	NP	-	-	-	-
	Soil(1&6&7-4&3)	-	-	-	-	-	-	-	-	-	-	NP	-	-0.13	-	-
	Soil(1&5&6-7&3&4)	-	-	-	-	-	-	-	-0.14	-	-	NP	-	-	-	-
	Soil(1&5&6-7&4&3&2)	-	-	-	-	-	-	-	-	-	-	NP	-	-	-0.15	-
Aspect	Aspect(1)	-	-	-	-	-	-	-	0.045	-	-	NP	-	-	-	-
	Aspect(2)	-	-	-	-	-	-	-	-0.36	-	-	NP	-	-	-	-
	Aspect(3)	-	-	-	-	-	-	-	-0.031	-	-	NP	-	-	-	-
	Aspect(2-3)	-	-	-	-	-	-	-	-0.17	-	-0.16	NP	-	-0.16	-	-0.13
	Aspect(1-4)	-	-	-	-	-	-	-	-0.17	-	-	NP	-	-0.11	-	-
	Aspect(1&3&4-2)	-0.01	-	-	-	-	-	-	-	-	-	NP	-	-	-	-
	Aspect(4&1-2&3)	-	-	-	-	-	-0.005	-0.01	-	-	-	NP	-	-	-	-
	Aspect(2&3-4&1)	-	-	-	-	-	-	-	-0.19	-0.31	-0.31	NP	-	-	-0.48	-0.3
Model performance[4]	$r^2_{adjusted}$	0.18	0.04	0.07	0.19	0.06	0.38	0.53	0.73	0.60	0.49	NP	-	0.59	0.71	0.44
	Prob > F	0.0036	0.04	0.01	<0.0001	0.05	<0.0001	<0.0001	<0.0001	<0.0001	<0.0001	NP	-	<0.0001	<0.0001	<0.0001

[1] Only significant relations are indicated. The first value is the fraction of the variance explained by the predictor variable. Values between brackets are critical p-values (p*). p* is Prob>t for the linear regression on the continuous variables, p* for the categorical variables is Prob>F in the one-way ANOVA test.

[2] For the multiple regression models, the regression equation coefficients and the total model performance is indicated.

[3] Categorical variables result from the hierarchical approach applied in JMP, Version 7. SAS Institute Inc. and should be interpreted as follows: e.g. Landf(2–3&1&4) combines the levels that are most alike to obtain two groups that are most different (2 versus 1, 3 and 4). In case of landform class = 2, this variable obtains the value + 1, otherwise −1.

[4] Prob>F=significance level associated with the F-statistic.

NP=Not Present (according to protocol)

5.4 Discussion

A process-model SoilGen was used to model change in soil properties over the last 15000 years for 108 locations in a loess parent material. Two scenarios were simulated to assess the effect of treefalls on horizon depths. The horizon classification algorithm allowed us to convert quantitative modelled soil properties (OC, clay content, a clay dispersion indicator and calcite content) into soil horizon depths. Traditionally, as soil surveys split up the soil profile in diagnostic horizons, much of the available soil data is of a discontinuous nature. While the fitting of a continuous soil depth function from discrete soil horizon data has received considerable attention [*Malone et al.,* 2009], the inverse problem has not. The approach proposed here allows us for the first time to explicitly and quantitatively validate our model results with such field data. A calibration to field observations was done to mimic the horizon classification by a soil surveyor. This calibration yielded satisfactory results, but it should be noted that the tuned algorithms are only valid for the test area.

The uprooting model provides acceptable results. The modelled average disturbance cycle of 1890 years is in good agreement with uprooting frequencies found in literature. Phillips and Marion [2004] report a mean uprooting cycle for North American forests between 1000-2000 years. Schaetzl and Follmer [1990] dated tree mounds in Wisconsin and Michigan that were stable somewhat longer, up to 2420 years. In Russia, lower values between 630 – 1000 years have been found [*Vasenev and Targul'yan*, 1995 cited by *Phillips and Marion*, 2004]. The sensitivity of modelled horizon thickness to choices made in the uprooting model was not the subject of study because of the large runtime of the model. We think that the sensitivity to the disturbance cycle will be relatively small, as the number of treefalls during the simulation period is on average fairly high (Fig. 5.8) and only a few treefalls are necessary to mix topsoil horizons (Fig. 5.9). The effect of wind exposition in the current study was relatively limited as indicated by the values of totalWE (Fig. 5.7) between 0.8 and 1.2, but might have been larger in landscapes with more relief. Probably the most sensitive factor was the magnitude and depth of the turbation due to a treefall, which is illustrated by the disappearance of the E-horizon in our simulations (Fig. 5.9). We probably overestimated the degree of mixing and the affected depth by treefalls.

More quantitative research is therefore urgently needed on the importance of bioturbation on soil formation. Large uncertainties are associated with the depth and area affected by single treefalls and with the effect of exposure on uprooting probability. In Belgian loess-derived soils for example, natural soil profiles have been shown to develop a fragipan in the top of the Bt horizon [*Van Vliet and Langohr*, 1981]. Once formed, such a layer would typically affect the soil depth affected by treefalls, as it impedes deep root penetration. It is therefore possible that the constant value of 80 cm for the uprooting depth, as applied in this study, is an overestimation. Also a time-dependent evolution of the uprooting depth would probably be more realistic, as the evolving soil properties themselves will feedback on the soil depth affected by treefalls. However, at present, no further data is available to justify such an approach.

Previous model studies like for example Gabet and Mudd [2010] suggested a prominent effect of biomechanical breaking of rocks on total soil depth. As an analogue to our situation, with soils formed on calcareous loess, we could expect to see an effect of treefalls on the total soil profile thickness. However, mixing of calcareous loess within the upper soil profile by bioturbation did not cause any long-term differences in the decalcification depth when comparing the two model scenarios. During the initial phase of the simulation (between 13 000 and 12 000 BP), when the decalcification border is still above the uprooting depth, there is a short phase where an uprooting event causes clear differences between model 1 and 2 (Fig. 5.9). However, this effect quickly disappears. The main reason is probably that in this study soils are relatively deep with respect to the uprooting depth. In shallow soils formed on bedrock, such as in the Gabet and Mudd [2010] model, uprooting events will affect the whole soil profile throughout the entire model run.

The results do show clearly that including treefalls in the simulation of soil formation has an important effect on the spatial organization of soil profiles in the landscape. Although none of the models reproduces the observed data, which was expected because treefalls were generated via a stochastic process and initial soil properties were assumed uniform across the landscape, it is clear from Table 5.2 and Fig 5.9 that including tree uprooting (model 2) improves the predictions. Especially for the more superficial horizons, model 2 exhibits the same trends as the observed data. The correlation with landscape variables for the Bt horizon disappears as a result of the homogenizing

effect of treefalls, as is observed in the field. In contrast, the simple soil formation model (model 1) exhibits a strong correlation with landscape parameters for all soil horizons, which is not observed in the field. However, model 2 also shows some correlation with landscape variables for the deeper soil horizons while this is not observed in the field data set in Table 5.2. Possible reasons for deviations between model and field estimates of horizon depths may be: (i) The assumption of uniform initial properties of the loess cover was not valid; (ii) Variations in soil microrelief as possible remainders from pit-and-mound topography will influence depth estimates of all soil horizons but were no part of the simulations; (iii) Pit and mound topography will alter soil water fluxes which are not considered in this model; (iv) Field estimated horizon depths may be not without error because of the augering technique (non-perfect vertical precision) and of uncertainties in the field classification. Local heterogeneity of parent material properties was identified by Phillips and Marion [2005] as a cause of soil diversity. Various authors [*Schaetzl and Follmer*, 1990; *Embleton-Hamann*, 2004] have indicated the importance of pit and mound topography on local soil genesis, thus these issues need more study. The first 2 reasons could be the subject of future simulation studies, as the SoilGen model can be run with non-homogeneous parent materials and also with additions or losses of topsoil. Each simulated scenario took 1940 CPU days (1 core), equivalent to 4 months of computing on 4 quad-core computers simultaneously. This large computational demand limited the number of simulated scenarios.

Given the fact that model 1 is fully deterministic and the only factors that determine differences in soil formation are slope angle, slope aspect and thickness of the loess cover, it is surprising that terrain attributes and thickness of loess cover do not fully represent resulting soil horizon variability. Apparently some effective covariates are missing, or there is some noise in the DEM due to measurement errors, or the regression kriging method fails to detect (possibly non-linear) relations between covariates and horizon thicknesses. It may be worthwhile to try out other DSM-methods with the current data set to identify their potential in case that the soil landscape relation is arguably deterministic as in model 1.

5.5 Conclusions

A key challenge in the quantitative modelling of soil formation is to include the effect of bioturbation. While in agricultural areas the spatial pattern of soil properties is largely controlled by soil erosion and redistribution, in natural areas previous work showed that bioturbation by tree uprooting has a large effect on the spatial organization of soil profile depth. We present here the first model that includes this effect in soil evolution. We developed a conversion protocol between simulated soil properties and soil horizon codes and calibrated to field estimates.

A model was developed that generates treefall events as a function of annual distributions of wind direction and wind speed, a DEM and an average disturbance cycle by treefalls.

Application of a process-based simulation model for soil genesis with spatially varying slope angle, slope aspect and loess cover thickness resulted in a spatial distribution of horizon depths that could reasonably well be modelled by a regression kriging approach, however regression kriging was not able to detect and model all soil variation, even while it was fully deterministically linked to slope angle and its aspect.

Application of this model run with simulated treefalls resulted in a spatial distribution of horizon depths that could not well be modelled by a regression kriging approach. As this was also found in the field data the occurrence of treefalls could be an explanation of the lack of spatial structure. In deeper parts of the soil profile, spatial patterns of horizon depths were still well detectable (contrasting to field observations), which may be explained by variations in parent material properties, microrelief and random errors in field estimates.

Author contribution

E.Opolot (third author) contributed to the writing and reviewing of this chapter.

Acknowledgments

Tom Vanwalleghem acknowledges funding by the Spanish Ministry of Economy and Competitiveness (through the Fellowship Ramón y Cajal RYC-2010-07166 and the research project AGL2012-40128-C03-02). Emmanuel Opolot acknowledges funding from the Belgian Science Policy Office (project BELSPO/IUAP p7/24).

References

Armson, K.A. and R.J. Fessenden (1973), Forest windthrows and their influence on soil morphology. Soil Sci. Soc. Am. Proc. 37, 781-783.

Beke, G.J. and J.A. McKeague (1984), Influence of tree windthrow on the properties and classification of selected forested soils from Nova Scotia. Can. J. Soil Sci. 64, 195-207.

Beven, K.J. and M.J. Kirkby (1979), A physically-based variable contributing area model of basin hydrology. Hydrol.Sci. Bull., 24(1-3), 43- 69.

Chaplot, V., B. Bouahom, and C. Valentin (2009), Soil organic carbon stocks in Laos: spatial variations and controlling factors, Glob. Change Biol., 16, 1380–1393.

Claessens, L., A. Knapen, M.G. Kitutu, J. Poesen, and J.A. Deckers (2007), Modelling landslide hazard, soil redistribution and sediment yield of landslides on the Ugandan footslopes of Mount Elgon. Geomorphology 90 (1-2), 23-35. DOI: 10.1016/j.geomorph.2007.01.007

Davis, B.A.S., S. Brewer, A.C. Stevenson, J. Guiot, and Data Contributors (2003), The temperature of Europe during the Holocene reconstructed from pollen data. Quaternary Science Reviews 22, 1701-1716.

De Keersmaeker L., H. Baeté, B. Christiaens, M. Esprit, P. Van de Kerckhove, and K. Vandekerkhove (2009), Bosreservaat Pruikenmakers (Meerdaalwoud): monitoringrapport. Monitoring van de dendrometrische gegevens en de vegetatie in steekproefcirkels en een kernvlakte. Rapporten van het Instituut voor Natuur- en Bosonderzoek 2009 (11). Instituut voor Natuur- en Bosonderzoek, Brussel.

De Vries W. and M. Posch (2003), Derivation of cation exchange constants for sand, loess, clay and peat soils on the basis of field measurements in the Netherlands. Wageningen, Alterra Green World research, Alterra-report 701, 50 pp.

Dlugoß, V., P. Fiener, and K. Schneider (2010), Layer-specific analysis and spatial prediction of soil organic carbon using terrain attributes and erosion modeling. Soil Science Society of America Journal. 74 (3), 922-935.

Embleton-Hamann, C. (2004), Processes Responsible for the Development of a Pit and Mound Microrelief. Catena 57(2), 175-188.

FAO (2006), Guidelines for soil description, 4th edition. FAO, Rome. ISBN 92-5-105521-1

Finke, P.A. (2012), Modeling the genesis of Luvisols as a function of topographic position in loess parent material. Quaternary International 265, 3-17

Finke, P.A. and J.L. Hutson (2008), Modelling soil genesis in calcareous löss. Geoderma 145, 462-479.

Finke, P.A. and W.J.P. Bosma (1993), Obtaining basic simulation data for a heterogeneous field with stratified marine soils. Hydrological Processes 7, 63-75.

Gabet, E., O.J. Reichmann, and E.W. Seabloom (2003), The effects of bioturbation on soil processes and sediment transport. Annu. Rev. Earth Planet. Sci. 31, 249–73.

Gabet, E.J. and S.M. Mudd (2010), Bedrock erosion by root fracture and tree throw: A coupled biogeomorphic model to explore the humped soil production function and the persistence of hillslope soils. Journal of Geophysical Research-Earth Surface 115, F04005, DOI: 10.1029/2009JF001526

Gessler, P.E., O.A.Chadwick, F. Chamron, K. Holmes, and L. Althouse (2000), Modeling soil–landscape and ecosystem properties using terrain attributes. Soil Science Society of America Journal 64, 2046–2056.

Godefroid, S. and N. Koedam (2010). Tree-induced soil compaction in forest ecosystems: myth or reality? Eur J Forest Res 129, 209-217

Goovaerts, P. (1997), Geostatistics for Natural Resources Evaluation. Oxford University Press, New York. ISBN 0-19-511538-4

Gullentops F. (1954), Contribution a la chronologie du Pléistocène et des formes de rélief en Belgique. Mém.Inst. Géol. Univ. Louvain, 18, 123-252.

Horwath, J. L. and D.L. Johnson (2006), Mima-type mounds in southwest Missouri: Expressions of 220 point-centered and locally thickened biomantles. Geomorphology, 77(3-4):308 -319.

Johnson, D.L., J.E.J. Domier, and D.N. Johnson (2005), Reflections on the nature of soil and its biomantle. Annals of the Association of American Geographers 95 (1), 11-31.

Kaste, J.M., A.M. Heimsath, and B.C. Bostick (2007), Short-term soil mixing quantified with fallout radionuclides. Geology 35 (3),243-246.

Kowalinski, S., L.J. Pons, and S. Slager (1972), Micromorphological comparison of three soils derived from loess in different climatic regions. Geoderma 7, 141-158

Langohr, R. (1993), Types of tree windthrow, their impact on the environment and their importance for the understanding of archaeological excavation data. Helinium, XXXIII/1, 36-49.

Li, Y. and M.J. Lindstrom (2001), Evaluating Soil Quality–Soil Redistribution Relationship on Terraces and Steep Hillslope. Soil Sci. Soc. Am. J. 65, 1500–1508.

Lutz, H.J. and F.S. Griswold (1939), The influence of tree roots on soil morphology. Am. J. Sci. 237(6):389–400.

Malone, B.P., A.B. McBratney, B. Minasny, and G.M. Laslett (2009), Mapping continuous depth functions of soil carbon storage and available water capacity. Geoderma 154(1–2), 138-152.

Maxwell, S., D.S. Green, and W. Zhang (2010), Identifying the determinants of windthrow damage in wildlife tree patches in the Boreal White and Black Spruce biogeoclimatic zone of northeastern British Columbia. Journal of Ecosystems and management 10(3), 1-8.

McBratney, A.B., M.L. Mendonça Santos, and B. Minasny (2003), On digital soil mapping. Geoderma 117, 3–52.

Moore, I., P. Gessler, G. Nielsen, and G. Peterson (1993), Soil attribute prediction using terrain analysis.Soil Science Society of America Journal 57, 443–452.

Mücher, H.J. (1973), Enkele aspecten van de loess en zijn noordelijke begrenzing, in het bijzonder in Belgisch en Nederlands Limburg en het daaraangrenzende gebied in Duitsland. K.N.A.G. Geografisch Tijdschrift VII (4), 259-276.

Odeh, I.O.A., A.B. McBratney, and D.J. Chittleborough (1994), Spatial prediction of soil properties from landform attributes derived from a digital terrain model. Geoderma 63, 197–214.

Phillips J.D. and D.A. Marion (2004), Pedological memory in forest soil development. Forest Ecology and Management 188, 363–380.

Phillips, J.D. (2007), Formation of texture contrast soils by a combination of bioturbation and translocation. Catena 70, 92-104.

Phillips, J.D. (2008), Soil system modelling and generation of field hypotheses. Geoderma 145 (3-4), 419-425.

Phillips, J.D. and D.A. Marion (2005), Biomechanical effects, lithological variations, and local pedodiversity in some forest soils of Arkansas. Geoderma 124, 73-89.

Poesen, J., B. van Wesemael, G. Govers, J. Martinez-Fernandez, P. Desmet, K. Vandaele, T. Quine, and G. Degraer (1997), Patterns of rock fragment cover generated by tillage erosion. Geomorphology 18(3-4):183-197.

Pye, K. (1983), Grain surface textures and carbonate content of Late Pleistocene loess from West Germany and Poland. J. Sedimentary Petrology 53 (3), 973-980.

Rantakari, M., A. Lehtonen, T. Linkosalo, M. Tuomi, P. Tamminen, J. Heikkinen, J. Liski, R. Makipaa, H. Ilvesniemi, and R. Sievanen, R. (2012), The Yasso07 soil carbon model - Testing against repeated soil carbon inventory. Forest Ecology and management 286, 137-147. DOI: 10.1016/j.foreco.2012.08.041

Šamonil, P., K. Král, and L. Hort (2010), The role of tree uprooting in soil formation: A critical literature review. Geoderma 157, 65-79.

Šamonil, P., M. Vaitera, S. Bek, B. Sebkova, T. Vrska, and J. Houska (2011), Soil variability through spatial scales in a permanently disturbed natural spruce-fir-beech forest. European Journal of Forest Research 130, 1075-1092.

Schaetzl, R.J. and L. Follmer (1990), Longevity of treethrow microtopography: implications for mass wasting. Geomorphology 3 (2), 113 – 123.

Schaetzl, R.J., D.L. Johnson, S.F. Burns, and T.W. Small (1989), Tree uprooting: review of terminology, process, and environmental implications. Canadian Journal of Forestry Research 19, 1-11.

Tesfa, T.K., D. G. Tarboton, D.G. Chandler, and J.P. McNamara (2009), Modeling soil depth from topographic and land cover attributes, Water Resour. Res., 45, W10438, doi:10.1029/2008WR007474.

Ulanova, N.G. (2000), The effects of windthrow on forests at different spatial scales: a review. Forest Ecology and Management 135, 155-167.

Van Ranst, E. (1981), Vorming en eigenschappen van lemige bosgronden in midden- en hoog België. Unpublished PhD-thesis, Department of Geology and Soil Science, Ghent University, Ghent.

Vanwalleghem, T., H.R. Bork, J. Poesen, M. Dotterweich, G. Schmidtchen, J. Deckers, S. Scheers, and M. Martens (2006), Prehistoric and Roman gullying in the European loess belt: a case study from central Belgium. The Holocene 16 (3), 393–401.

Vanwalleghem, T., J. Poesen, A. McBratney, and J. Deckers (2010), Spatial variability of soil horizon depth in natural loess-derived soils. Geoderma 157, 37-45.

Vanwalleghem, T., J. Poesen, M. Van Den Eeckhaut, J. Nachtergaele, and J. Deckers (2005), Reconstructing rainfall and land use conditions leading to the development of old gullies. Holocene 15, 378–386.

Vanwalleghem, T., M. Van Den Eeckhaut, J. Poesen, J. Deckers, J. Nachtergaele, K. Van Oost, and C. Slenters (2003), Characteristics and controlling factors of old gullies under forest in a temperate humid climate: a case study from the Meerdaal Forest (Central Belgium). Geomorphology 56, 15–29.

Verbruggen, C., L. Denys, and P. Kiden (1996), Belgium. In: Berglund, B.E., H.J.B. Birks, M. Ralska-Jasiewiczowa, H.E. Wright (eds). Palaeoecological events during the last 15000 years.Regional syntheses of Palaeoecological studies of lakes and mires in Europe.Wiley, Chistester.

Wallach, D., S. Buis, P. Lecharpentier, J. Bourges, P. Clastre, M. Launay, J.E. Bergez, M. Guerif, J., Soudais, and E. Justes (2011), A package of parameter estimation methods and implementation for the STICS crop-soil model. Environmental Modelling & Software 26(4), 386-394. DOI: 10.1016/j.envsoft.2010.09.004.

Webster, R., and M. A. Oliver (1992), Sample adequately to estimate variograms of soil properties. Journal of Soil Science 43 (1):177–192.

Whelan, B.M., A.B. McBratney and B. Minasny (2001), Vesper – Spatial prediction software for precision agriculture. In: ECPA 2001. Third European Conference on Precision Agriculture. (G. Grenier, S.Blackmore Eds.) pp. 139-144. Agro Montpellier, Ecole Nationale Agronomique de Montpellier.

Wintle, A.G. and K. Brunnacker (1982), Ages of volcanic tuff in Rhein-Hessen obtained by thermo-luminescence dating of loess. Naturwissenschaften 69, 181-183.

Yoo, K., J. Ji, A. Aufdenkampe, and J. Klaminder (2011), Rates of soil mixing and associated carbon fluxes in a forest versus tilled agricultural field: Implications for modeling the soil carbon cycle. J. Geophys. Res. 116, G01014, doi:10.1029/2010JG001304

Chapter 6 : Evaluating sensitivity of silicate mineral dissolution rates to physical weathering using a soil evolution model (SoilGen2.25)

Based on:

Opolot, E. and Finke, P. A., 2015. Evaluating sensitivity of silicate mineral dissolution rates to physical weathering using a soil evolution model (SoilGen2.25), Biogeosciences, 12, 6791-6808, doi: 10.5194/bg-12-6791-2015.

Abstract

Silicate mineral dissolution rates depend on the interaction of a number of factors categorized either as intrinsic (e.g. mineral surface area, mineral composition) or extrinsic (e.g. climate, hydrology, biological factors, physical weathering). Estimating the integrated effect of these factors on the silicate mineral dissolution rates therefore necessitates the use of fully mechanistic soil evolution models. This study applies a mechanistic soil evolution model (SoilGen) to explore the sensitivity of silicate mineral dissolution rates to the integrated effect of other soil forming processes and factors. The SoilGen soil evolution model is a 1D model developed to simulate the time-depth evolution of soil properties as a function of various soil processes (e.g. water, heat and solute transport, chemical and physical weathering, clay migration and bioturbation) driven by soil forming factors (i.e., climate, organisms, relief, parent material). Results from this study show that although soil solution chemistry (pH) plays a dominant role in determining the silicate mineral dissolution rates, all processes that directly or indirectly influence the soil solution composition equally play an important role in driving silicate mineral dissolution rates. Model results demonstrated a decrease of silicate mineral dissolution rates with time, an obvious effect of texture and an indirect but substantial effect of physical weathering on silicate mineral dissolution rates. Results further indicated that clay migration and plant nutrient recycling processes influence the pH and thus the silicate mineral dissolution rates. Our silicate mineral dissolution rates results fall between field and laboratory rates but were rather high and more close to the laboratory rates owing to the assumption of far from equilibrium reaction used in our dissolution rate mechanism. There is therefore need to include secondary mineral precipitation mechanism in our formulation. In addition, there is need for a more detailed study that is specific to field sites with detailed measurements of silicate mineral dissolution rates, climate, hydrology and mineralogy to enable the calibration and validation of the model. Nevertheless, this study is another important step to demonstrate the critical need to couple different soil forming processes with chemical weathering in order to explain differences observed between laboratory and field measured silicate mineral dissolution rates.

6.1. Introduction

Silicate mineral weathering is the major source of most plant nutrients in soils (Carey et al., 2005; Hartmann et al., 2014) and it is probably the foremost process controlling soil production rates (Anderson et al., 2007; Dixon and von Blanckenburg, 2012). Silicate mineral dissolution rates also have implications on acidification in forest soils (Phelan et al., 2014) and carbon sequestration (Beaulieu et al., 2011; Goddéris et al., 2013; Pham et al., 2011). Quantifying the rates of silicate mineral dissolution is therefore of utmost importance to answer many environmental questions such as the surface and groundwater composition, the supply of macronutrients (e.g. K and Ca) in forests and the neutralization of acid precipitation (Ganor et al., 2007).

Indeed a lot of work has been devoted to quantifying silicate mineral dissolution rates using both laboratory experiments (Blum and Stillings,1995; Chou and Wollast,1985; Knauss and Wolrey, 1986; Lee et al., 1998; Stillings and Susan, 1994; Zhu and Lu 2009) and field experiments (Maher et al., 2009; Parry et al., 2015; White and Brantley, 2003; White et al., 1996; White, 2003, 2002). One common conclusion from most of these studies is that a discrepancy of up to 5 orders of magnitude (Oliva et al., 2003; Parry et al., 2015; White et al., 1996; Zhu, 2005) does exist between laboratory and field weathering rates. There seems to be a general consensus that these differences may be explained by (i) changes in fluid composition (ii) changes in primary mineral surfaces (reactive sites) (iii) the formation of secondary phases (iv) efficiency of solution / mineral contact and, (v) the composition of the soil solution in micro pores. White (2002) grouped these factors into two; intrinsic (e.g. mineral composition, surface area) and extrinsic factors (e.g. solution composition, climate, biological processes). All these five factors could slow field weathering rates compared to laboratory experiments where most of the physical, biological and chemical conditions can be constrained (White and Brantley, 2003). In general the integrated effects of these intrinsic and extrinsic factors are complex and certainly difficult to capture both in the field and in the laboratory experiments. Moreover uncertainty in the extrinsic factors that occurred and varied in the past is difficult to constrain in experiments (Moore et al., 2012; White and Brantley, 2003).

Modelling approaches enhanced by an understanding of silicate kinetic rates and mechanisms from the experimental works are therefore essential to facilitate in the quantification of silicate dissolution

rates (Beaulieu et al., 2011; Goddéris et al., 2006; Hellevang et al., 2013; Roelandt et al., 2010; Stendahl et al., 2013). However, in only a few of these modelling approaches (Goddéris et al., 2006; Maher et al., 2009; Moore et al., 2012) has the integrated effect of some intrinsic and extrinsic factors on silicate mineral dissolution rates been investigated. There is need for mechanistic models capable of simulating the integrated effect of physical, biological and chemical soil forming processes on chemical weathering rates. Such coupling will give the possibilities to determine the role played by intrinsic and extrinsic factors and explain the differences in dissolution rates observed in the laboratory and field experiments (Goddéris et al., 2006; Hartmann et al., 2014; Moore et al., 2012).

The objective of this work is to explore the integrated effect of physical weathering, clay migration and plant uptake processes on the silicate mineral dissolution rates with particular emphasis on physical weathering. The relationship between particle size distribution and chemical mineral weathering is well known. Holding other factors constant (e.g. pH), the smaller the grain size the larger the surface area per unit mass and consequently the higher the rate of chemical weathering (Hartmann et al., 2014). In most cases, a constant grain size distribution has been assumed when estimating weathering rates, this assumption could be invalid especially when looking at longer time scales. Furthermore, recent studies (e.g., Dixon and Von Blanckenburg, 2012; Hilley et al., 2010; Larsen et al., 2014; Schoonejans et al., 2016) have demonstrated that the relationship between physical weathering rates and chemical weathering rates can be either positive or negative depending on the environments under consideration. In weathering regimes where physical weathering rates are high above a certain threshold (as in highly eroding regimes), chemical weathering rates are mainly controlled by reactions kinetics and become negatively correlated with physical weathering rates due to shortened residence time of minerals at the surface (Dixon and Von Blanckenburg, 2012; Gabet, 2007; Hilley et al., 2010; Schoonejans et al., 2016). However, in conditions of minimal to no erosion (as in this study), chemical weathering is limited by the supply of fresh mineral particles and thus it's rates are positively linked to physical weathering rates (Brantley et al., 2007; Larsen et al., 2014). It should however be noted that the effect of physical weathering process (discussed in chapter 2, section 2.2.1.2) in this study is limited to the reduction in mineral particle size due to temperature gradients and the associated increase in mineral surface area. Thus other effects of physical

weathering (e.g., exposure of fresh mineral particles to water and solute flow) on chemical weathering are not explicitly modelled.

In summary, this study addresses the interactive effects of intrinsic and extrinsic factors on chemical weathering, using a mechanistic soil model (SoilGen model: see details in chapter 2). We mainly focused on the effects of physical weathering with the hypothesis that physical weathering positively affects the magnitude of chemical weathering and this could partly be the cause of systematic deviations between laboratory and field approaches to estimate silicate mineral dissolution rates. Specific objectives are to (i) assess the effects of parent material composition on the silicate mineral dissolution rates, (ii) to assess sensitivity of chemical silicate mineral dissolution rates to change in soil texture, (iii) to assess the effect of physical weathering of primary minerals on their dissolution rates, (iv) to assess the effect of interactive soil forming processes on silicate mineral dissolution rates and (v) to compare our modelled silicate mineral dissolution rates to rates reported in literature.

6.2. Materials and methods

6.2.1 Study area

This is a sensitivity test study that is not specific to any location. However choice was made to do this study in the forested loess soils, in the Zonian forest, Belgium (50°46'31"N, 4°24'9"E) primarily because the soil processes (clay migration, physical weathering, decalcification, carbon-cycling) in the model have already been calibrated to this site (Finke and Hutson, 2008; Finke, 2012; Opolot et al., 2014; Yu et al., 2013). In addition, the measured soil data (Finke, 2012; van Ranst, 1981) and other reconstructed model input data (Finke and Hutson, 2008) were readily available for this site.

6.2.2 Research set up

As the objectives (1 and 2) of this study are also to assess the sensitivity of silicate weathering rates to differences in parent material and soil texture, the research set up (Fig 6.1) is such that different initial textures and mineralogy are captured. Therefore rather than using texture and soil mineralogy measurement from the study site, 6 different texture points were randomly selected from the USDA

textural triangle (Soil Survey Division Staff, 1993) to represent the initial soil texture. Three different parent materials (granite, basalt and peridotite) were selected in such a way that slow (felsic igneous rock), moderate (mafic igneous rock) and fast weathering (ultramafic) rocks were taken into account. The geochemical data (oxide weight composition) typical of granite, basalt and peridotite (see Appendix 3.1) was obtained from literature (Blatt and Tracy, 1996; Harris et al., 1967; Hartmann et al., 2013) and the mineralogical compositions (Appendix 3.2) were estimated from these geochemical data using the normative mineralogy calculation method (Cross et al., 1902; Kelsey, 1965). Only primary minerals were considered at this stage and their weight compositions were rescaled to sum up to one (Appendix 3.3).

At this stage two scenarios (with physical weathering, PhyWE and without physical weathering, NoPhyWE) were defined but in two different model setups (Model A and Model B; Fig 6.1). Model setup 1, hereafter referred to as Model A is intended to simulate majorly the effect of change in particle size (due to physical weathering process) on silicate weathering rates. Model A therefore includes all other soil processes simulated in the SoilGen (see chapter 2; Table 2.1) except those that directly affect depth profiles of soil texture (i.e., clay migration, bioturbation). Model setup 2, hereafter referred to as Model B was intended to simulate the interactive effect of all soil processes (listed in chapter 2; Table 2.1) including physical weathering, clay migration, carbon-cycling, plant uptake, bioturbation) on silicate weathering rates. The soil processes included in the SoilGen and input data are discussed in chapter 2. In total, 72 cases were run in the SoilGen model (i.e 2 set ups × 2 scenarios × 6 texture points × 3 parent materials).

The output parameters from the model include soil texture (% mass fraction of clay, silt and sand), pH, base saturation, weathering indices, mass of each mineral remaining, etc. For this study the outputs of interest included pH, clay mass fraction and mineral mass. The mass of each mineral remaining after the simulation period (15000 years) was used to calculate the respective dissolution rates of each mineral and was the basis for the sensitivity analysis as will be explained in the subsequent sections.

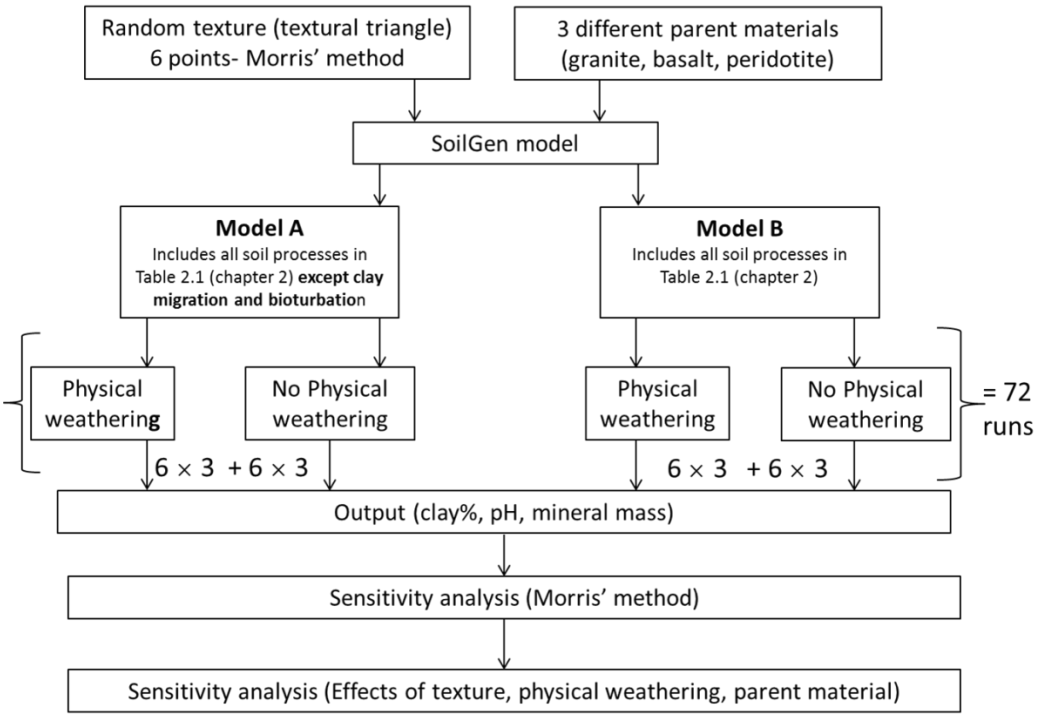

Figure 6.1. Research set up. The difference between Model A and model B is either the inclusion or exclusion of some soil processes. Model A includes all soil processes listed in Table 2.1 (chapter 2) except for clay migration and bioturbation processes that directly affect soil texture. Model B on the other hand is a full SoilGen model and therefore includes all soil processes listed in Table 2.1 (chapter 2). Note that inorder to isolate the effect of physical weathering, both model A and B are run with and without physical weathering. Each model setup included 36 model runs i.e., 6 textures × 3 parent materials × 2 scenarios (with and without physical weathering)

6.2.3 The SoilGen model

The SoilGen model is a 1D model designed to simulate time-depth evolution of soil properties as a function of interactive soil processes (majorly driven by the soil forming factors ('CLORPT'): climate, living organisms, relief, parent material, time). The governing processes in the SoilGen model and input data requirements are presented in (Opolot et al., 2015) and in chapter 2 of this thesis. It should however be noted that this study applies an extended model version (SoilGen2.25) which includes an

extended weathering mechanism (see chapter 3; section 3.4 for details) to simulate kinetics of mineral-water reactions, rather than the weathering mechanism discussed in chapter 2.

6.2.4 Model input data

The SoilGen model was designed keeping in mind the generally accepted paradigm that soil is a function of soil forming factors; 'CLORPT' (Jenny, 1941). Therefore the model uses these factors either as initial conditions (e.g. mineralogy, texture) or boundary conditions (e.g. climate, vegetation, biotubation, slope and exposition). The initial conditions specify to the model the initial soil properties at the beginning of the simulations and are usually assumed to be equal to the soil properties from the analysis of samples taken from the C – horizon. Initial texture and mineralogy used in this study are shown in Table 6.1 and 6.2, respectively. Other initial soil properties (e.g. initial OC %, bulk density, solution and exchange surface chemistry), and boundary conditions (i.e., time series of climate, vegetation and bioturbation) were taken from Finke (2012). Although these initial soil properties (particularly bulk density, solution and exchange surface chemistry) are directly related to parent material, they were kept the same across the three parent materials to be able to isolate the effect of physical weathering. For long run time (as is the case in this study), the initial solution and exchange surface chemistry may pose little effect on to the final silicate dissolutions rates but ignoring differences in bulk density across the 3 different parent materials is a potential limitation of modelled silicate dissolution rates of this study.

Table 6.1. Texture points randomly selected from the USDA textural triangle (Soil Survey Division Staff, 1993) and used as initial soil texture in all the model runs

Texture Number	Sand (%)	Clay (%)	Silt (%)	Textural class
1	63.3	12.0	24.7	Sandy loam
2	41.6	18.7	39.8	Loam
3	5.5	27.4	67.1	Silty Clay Loam
4	86.8	6.1	7.0	Loamy Sand
5	8.7	10.7	80.6	Silt
6	51	4.1	44.9	Sandy Loam

Table 6.2. Primary minerals and their relative weight composition. The oxide weight composition typical of granite, basalt and peridotite was obtained from literature (Blatt and Tracy, 1996; Harris et al., 1967; Hartmann et al., 2013). The mineralogical compositions were estimated from these data using the normative mineralogy calculation method (Cross et al., 1902; Kelsey, 1965). See Appendices 3.1, 3.2 and 3.3 for details of this data.

Parent material type	Primary Silicate Mineral (wt %)			
	Albite	K-feldspar	Quartz	Forsterite
Granite	42.3	26.1	31.6	-
Basalt	32.1	34.5	-	33.4
Peridotite	10.9	0.3	-	88.8

6.2.5 Calculating average silicate dissolution rates

The silicate mineral dissolution rate usually reported in units of mol m^{-2} s^{-1} is defined as the amount of mineral (moles) that is released in form of constituent elements per unit area (e.g., cm^2, m^2 or ha) or volume (cm^3, m^3) over a given period time. Similar to the approach used in White and Brantley (2003), congruent weathering was assumed and the moles of each cation released during silicate mineral dissolution was based on the stoichiometric coefficient of that particular element in the mineral. To calculate the dissolution rate of a given mineral, the amount of mineral (mass per unit volume) remaining after defined simulation period was subtracted from the respective amount of each mineral initially present. This difference was then converted to mol m^{-2} by multiplying with the respective compartment thickness (t) and dividing by the relative formula mass (RFM). The resulting value was again divided by the simulation period to give dissolution rates in mol m^{-2} s^{-1} (Eq. 6.1).

$$k_{diss} = \frac{(m_{kinit} - m_{kfinal}) \times 1000 \times t}{RFM_k \times S.P} \quad (6.1)$$

where k_{diss} (mol m^{-2} s^{-1}) is the dissolution rate of silicate mineral, k, m_{kinit} and m_{kfinal} are the initial and the final mass (kg m^{-3}) of silicate mineral k, RFM_k is the relative formula mass (g mol^{-1}) of mineral k and $S.P$ is the simulation period (s). The number 1000 is the conversion factor from Kg to g of mineral k.

6.2.6 Sensitivity analysis

Morris' sensitivity method (Morris, 1991) was used to assess the sensitivity of average silicate mineral dissolution rates to texture and physical weathering. It is one of the simplest and most widely used sensitivity analysis method (Saltelli et al., 2004). It is computationally cheaper than other sensitivity methods and therefore suitable for especially long run time models such as SoilGen (Finke et al., 2015; Yu et al., 2013). The method basically aims at quantifying the response of model output due to differences in the levels of input parameter (the so called elementary effects). In this study the levels include different textures and whether physical weathering is allowed or not. The output of interest in this case is the amount of mineral (Kg m^{-3}) lost over the simulation period due to chemical weathering which is itself influenced by differences in texture and physical weathering. The elementary effects of differences in texture (u_i) on the amounts of mineral lost were calculated following Eq. (6.2) (Morris, 1991). Sensitivity of each silicate mineral was then evaluated by plotting the mean and the standard deviations of the elementary effects against each other (in the x and y axis, respectively) for both PhyWE and NoPhyWE scenarios and for each parent material.

$$u_i = \frac{Y(x_1, x_2, x_3 \ldots x_i + \Delta x_i) - Y(x_1, x_2, x_3 \ldots x_i)}{\Delta x_i} \quad (6.2)$$

where $x_1, x_2, x_3 \ldots x_i$ are the different levels of input parameter (i.e., different textures, in this study), Δx_i is the variation imposed on the input parameter measured as the Euclidean distance between two points in the textural triangle and Y is the model output in response to each level of input parameter.

6.3. Results and discussion

6.3.1 pH evolution as a function of parent material

The evolution of pH as a function of parent material is shown in Fig. 6.2a (Model A) and Fig. 6.2b for model B. There is erratic behaviour of pH in the beginning of the simulations (between 15000 and 12000 years BP especially under granite. Generally, pH is increasing with depth and decreasing over time across the different parent materials as well as the two different model set ups (i.e, Model A and

Model B). pH is generally higher in basalt and peridotite parent materials than granite but only in the first 5000 years of simulation (i.e., up to 10000 years BP). The trends are however reversed in the subsequent years especially in Model A. There is generally a more gradual evolution of pH under model B compared to model A with a generally lower pH under model A than Model B, when comparing respective parent materials.

The erratic behaviour of pH in the beginning of the simulations (between 15000 and 12000 years BP especially under granite parent material (Figs. 6.2a, 6.2b) could be linked to the sensitivity of dissolution rates to dilution due to variation in precipitation. This period coincides with the drier periods (see Fig.5.2 in chapter 5) with incidences of precipitation deficit in some years. Precipitation deficit means low dilution as well as limited mineral dissolution and release of cations, consequently keeping the pH low. At the current model version, the assumption is that dissolution occurs at far from equilibrium and thus the effect of the formation of secondary mineral formation on pH is not yet accounted for. This is certainly a limitation of this study and work is on-going to incorporate this mechanism into the model. A number of studies (Casey et al., 1993; Goddéris et al., 2006; Maher et al., 2009; Moore et al., 2012; Zhu, 2005; Zhu et al., 2010) have already demonstrated that solute composition and secondary mineral precipitation controls the reaction affinity of primary minerals. The dissolution rates from this study are therefore expected to be faster than they would if secondary mineral precipitation were to be taken into account. The plunge in pH after 10000 years BP for basalt and peridotite (Figs. 6.2a and 6.2b) could be linked to the depletion of Forsterite at that time and thus less release of Mg^{2+}. Comparing Figs. 6.2a and 6.2b, the effect of mineralogical composition on pH appears to become less in Fig. 6.2b (particularly after year 10000 BP; between 500 – 1400 mm) than in Fig. 6.2a. This trend is likely due to the cation exchange capacity (CEC) buffering effect on pH in the zone of clay accumulation (Finke, 2012).

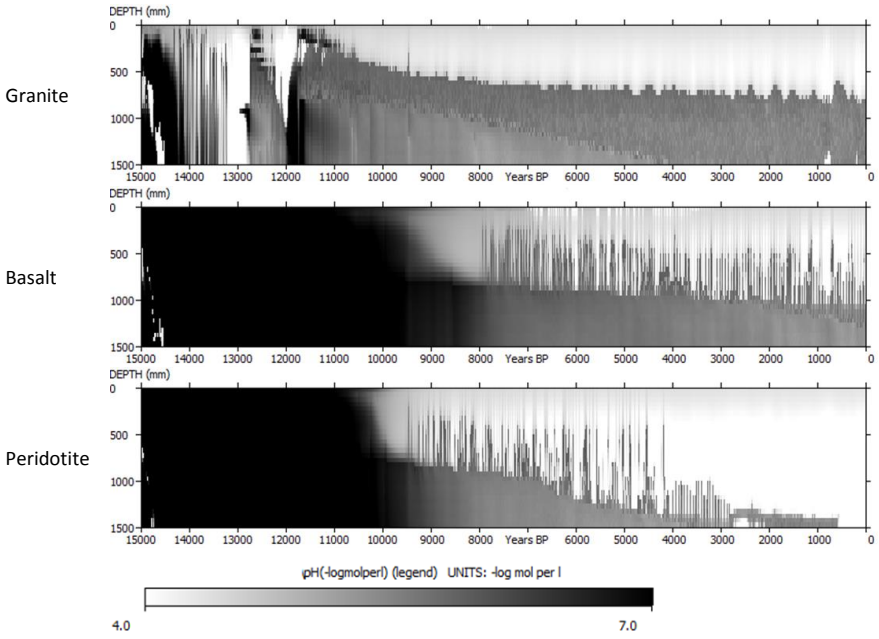

Figure 6.2.a. Time-depth evolution of pH with physical weathering (Model A) for 3 parent materials with texture number 5 (Table 6.1).

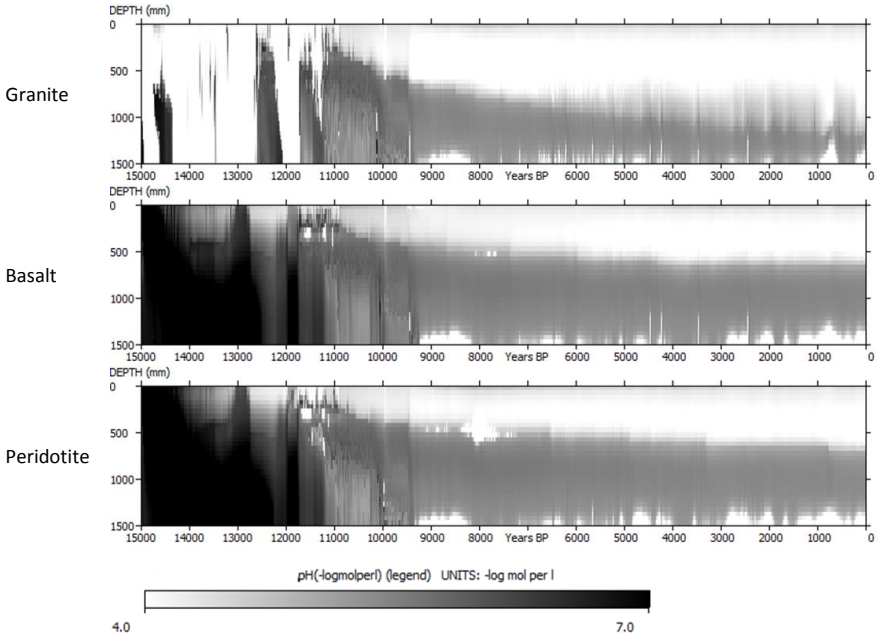

Figure 6.2.b Time - depth evolution of pH with interactive soil processes (Model B) for 3 parent materials with texture number 5 (Table 6.1).

6.3.2 Evolution of clay mass fraction

Figure 6.3 shows the depth distribution of clay mass fraction taken at the final year of simulation (present situation). There is a clear difference between Model A and Model B, with a clear effect of physical weathering (PhyWE; dashed lines) on the amount of clay mass fraction in Model A (particularly in the top 0.3 m depth) where up to 8 % of clay mass is produced due to physical weathering (Fig. 6.3; texture number 3). The effects of other processes notably clay migration on clay mass fraction is clearly visible in model B (Fig. 6.3, right part) with likely formation of an illuvial horizon (Bt horizon). The clay mass that is produced by physical weathering (Fig. 6.3, left panel), is subsequently transported from the top compartments into the lower compartments (through clay migration), forming E and Bt horizons (Fig. 6.3, right panel), respectively (Finke 2012). The complete Bt belly could not be shown by our results probably because of our shallow profile which was considered to reduce the run-time of the model.

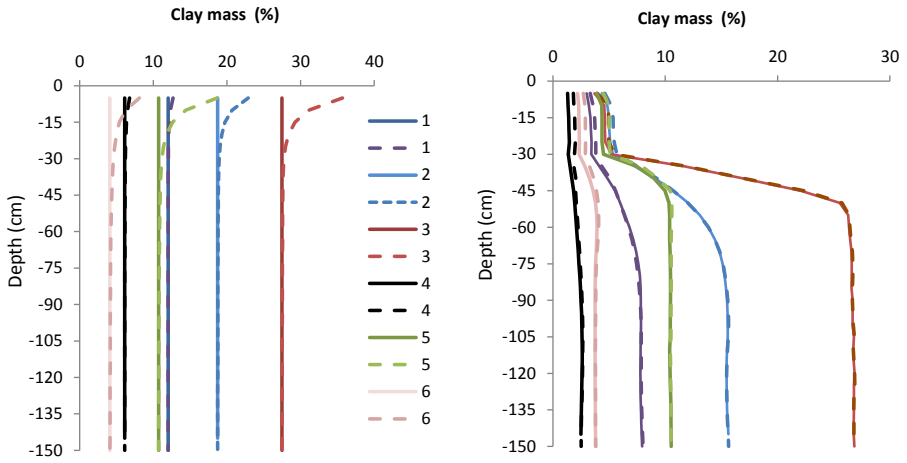

Figure 6.3. Clay mass fraction (%) evolution as a function of physical weathering (Model A, left panel) and as a function of interactive soil processes (Model B, right panel). Roman numerals 1 – 6 represent texture numbers presented in Table 6.1. Solid lines represent no physical weathering while broken lines represent physical weathering. Notice that in Model A (in which clay migration and bioturbation are excluded), with no physical weathering allowed (solid lines), the clay mass fractions do not change whereas in model B (all soil processes included) clay mass fractions change with (dashed lines) or without (solid lines) physical weathering. The changes in clay mass fractions in model B is caused by other processes notably clay migration.

6.3.3 Mineral dissolution rates

6.3.3.1 Effect of parent material composition on dissolution rates

Figure 6.4 shows the effect of parent material composition on the average dissolution rates of K-feldspar, albite, quartz and forsterite over successive time intervals of 500 years. With exception of quartz whose rates were increasing with time, the dissolution rates across the 3 parent materials decrease with time. The dissolution rates of albite and K-feldspar are higher (especially at the beginning of the simulation) under the granite parent material than in basalt and peridotite. Model A dissolution rates across all the minerals are generally higher than the rates from Model B. In granite however, dissolution rates of albite and K-feldspar in Model A between 15000 and 13000 years BP are lower than the respective dissolution rates in Model B. From 13000 years BP until 9000 years the dissolution rates are similar between the two models. In Basalt and peridotite, the dissolution rates of albite and K-feldspar between 13000 and 9000 years BP are higher in model B than in Model A. From 9000 until 0 years BP, the dissolution rates of all minerals (except for quartz) across 3 parent materials are generally higher in model A than in model B.

The properties of the parent material very much influence the chemical weathering rates (Hartmann and Moosdorf, 2011; Navarre-Sitchler and Brantley, 2007; Oliva et al., 2003). Results from this study indicate that the composition of the parent material influences directly the pH of the soil solution in two different ways (i) by the type of cation it releases into the solution (i.e., monovalent, divalent, trivalent) and (ii) by the amount of cations released which is directly related to the amount of mineral that is reacting. Therefore all the trends pointed above and shown in Fig. 6.4 can be explained by the influence that the parent material has on pH (e.g., interpreting Figs. 6.2a for model A and 6.2b for Model B). The higher dissolution rates (especially in the beginning) of albite and K-feldspar observed in granite compared to basalt and peridotite could therefore be due to lower pH observed in granite than in Basalt and Peridotite at that point in time. The Mg^{2+} released from forsterite (which is absent in granite) keeps the pH in the soil solution higher in basalt and peridotite than in granite and thus the lower dissolution rates of albite and K-feldspar in basalt and peridotite. The differences in Model A and B across the parent materials also follow the pH trends. For example in granite, the average pH (at 0.5 m depth) in Model B is generally lower than the pH in Model A between 15000 and 13000

years BP and therefore higher albite and K-feldspar dissolution rates and lower quartz dissolution rates in Model B. In basalt and peridotite, the average pH at this period (between 15000 and 13000 years BP) is more less the same and therefore the same dissolution rates of albite and K-feldspar between for both Model A and Model B. However between 12000 and 9000 years BP, the average pH in basalt and peridotite is lower in Model B than in Model A, thus explaining the observed rise in the dissolution rates of albite and K-feldspar in Model B that are not observed in Model A. From 9000 years BP until 0 years BP, Model A dissolution rates of albite, K-feldspar and forsterite are higher than respective rates in Model B owing to the lower pH in Model A (averaged over 0. 5 m) than in model B (Figs. 6.2a and 6.2b). Quartz is less sensitive to pH at pH values below 6 (Knauss and Wolery, 1988) and thus it's dissolution rates in Model A and model B were not any different and did not seem to change from 10000 until 0 years BP.

6.3.3.2 Effect of initial texture

The effect of initial texture on silicate mineral dissolution rates for Model A and Model B is presented in Fig. 6.5. As would be expected and consistent with previous studies (e.g. Hartmann et al. 2014; Phelan et al. 2014), the mineral dissolution rates are higher for finer textures than for coarse textures because of higher mineral surface area of clay and silt sized particles compared to the sand sized particles. In model A, albite and K-feldspar dissolution rates across all initial textures, generally decrease with depth while dissolution rates of quartz generally increase with depth. In model B, albite and K-feldspar dissolution rates across all initial textures, are generally constant with depth (except for texture number 4) while dissolution rates of quartz generally follow the same trend as in Model A and increase with depth. These dissolution rate-depth trends are related to pH which is generally increasing with depth. High pH favours quartz dissolution rates and slows down albite and K-feldspar dissolution rates.

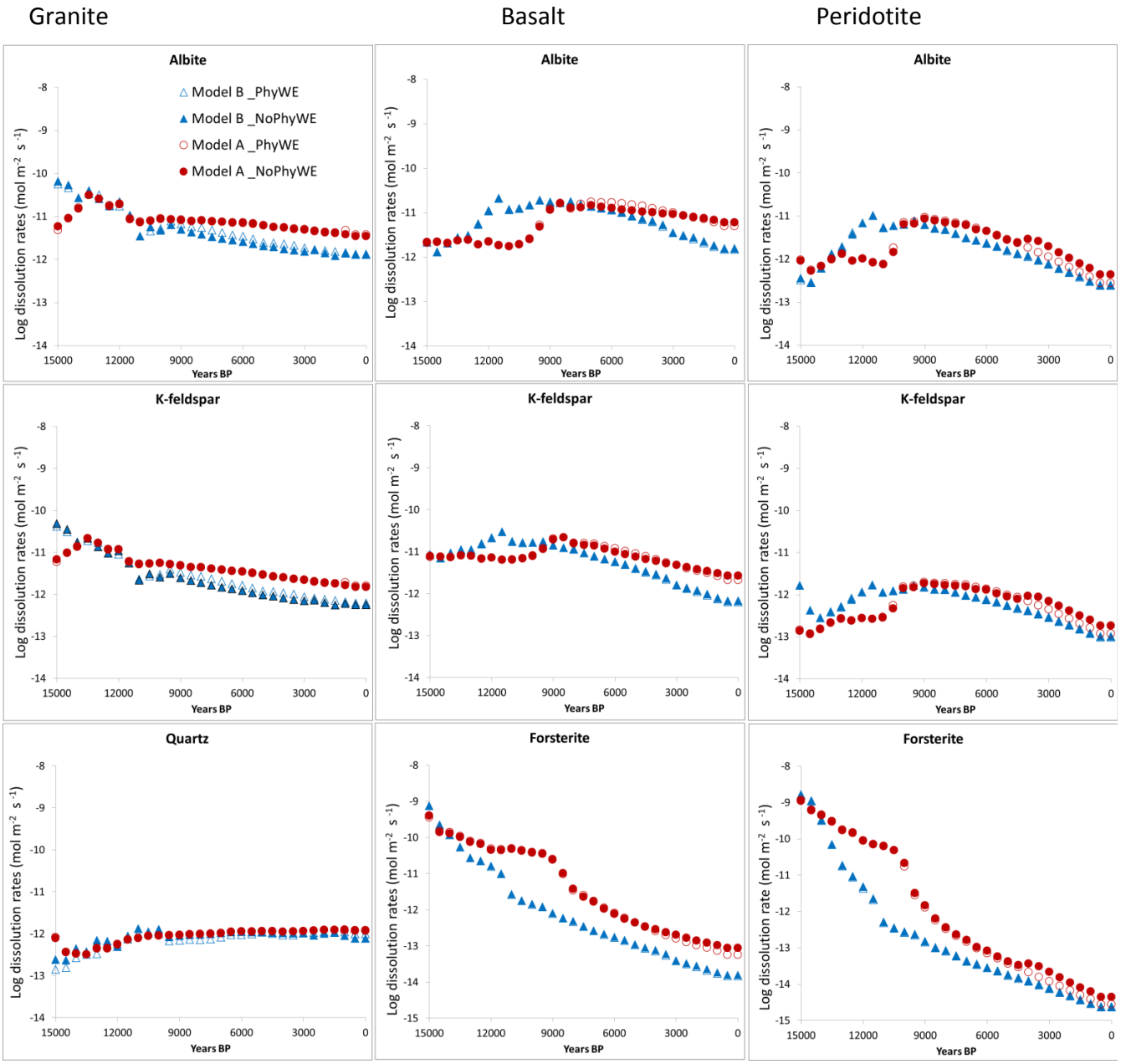

Figure 6.4. Example (based on soil texture number 5; Table 6.1) of time evolution of silicate dissolution rates in different parent materials (Granite, Basalt and Peridotite). The modelled rates are calculated for a depth of 0.5 m for every 500 years. Model A: Circles; solid (no physical weathering) open (physical weathering allowed). Model B: Triangles; solid (no physical weathering) open (physical weathering allowed).

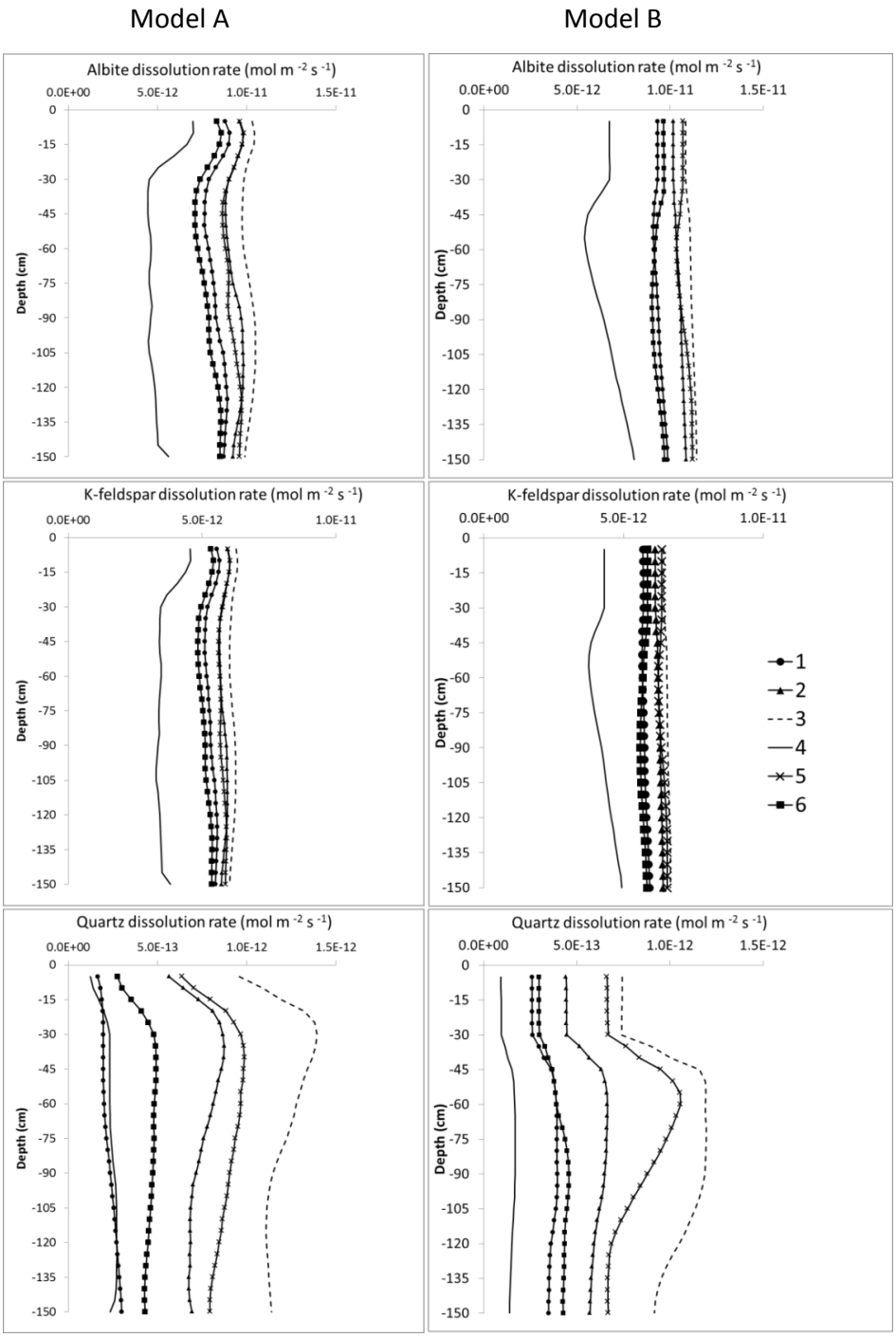

Figure 6.5. Effect of initial texture (shown in Table 6.1) on the depth distribution of silicate dissolution rates. The rates shown are taken from granite parent material and are averaged over 15000 years simulation period.

6.3.3.3 Effect of physical weathering

The effect of only physical weathering (Model A) and the integrated effect of all soil forming processes (Model B) on the average silicate dissolution rates are shown in Figs. 6.6a and 6.6b, respectively. The rates are presented as a ratio of physical weathering to no physical weathering (i.e., PhyWE / NoPhyWE) where a value greater than 1 implies higher dissolution rate due to physical weathering. The results (both in model A and B) indicate that the dissolution rates are generally higher in the top of the profile and decrease down the soil profile. Except for Forsterite, results in Model A indicate a positive effect of physical weathering on silicate dissolution rates (i.e., PhyWE / NoPhyWE > 1). Dissolution rates due to physical weathering are particularly higher in texture number 4 (solid black line) across all the minerals and parent materials with exception of Quartz mineral (in Model A) where dissolution rate due to physical weathering is highest under texture number 1. In model B however, the effect of physical weathering is almost not visible (except for the texture number 4; solid line) as indicated with unity PhyWE / NoPhyWe ratios of all minerals across the different textures. Higher dissolution rates with no physical weathering compared to with physical weathering (i.e., PhyWE / NoPhyWE < 1) were only observed for Albite and K-feldspar below 0.75 m under Model B (see Fig. 6b: granite; texture number 4).

As already mentioned in the previous section, the direct effect of texture on chemical weathering is through it's influence on the mineral surface area. Based on Eq 3.2 (Chapter 3), this would imply that the higher the number of particles moved from coarse to fine classes, the higher the mineral surface area and thus the higher the mineral dissolution rate. This seems to be the case especially for coarse texture (texture number 4) where the dissolution rates of albite and K-feldspar in basalt and peridotite (Fig. 6.6a) are up to 1.4 times higher with PhyWE compared to NoPhyWE. The effect of physical weathering on the dissolution rates of albite and K-feldspar seems to be more pronounced in basalt and peridotite where pH is relatively higher and thus imposes less dominance on the chemical dissolution rates of albite and K-feldspar. The generally lower pH under granite could explain the higher effect of physical weathering on Quartz dissolution rates under coarse textures 1, 4 and 6 (Fig. 6.6a). The effect of texture on the dissolution rates could also be indirect through it's relationship with hydrology. Our results imply that, although the physical weathering process produced more clay sized particles (Fig. 6.3, left panel) from already fine textures (i.e., 3 and 5; Table 6.1), the slowing

down of water flow by this fine texture resulted into reduced leaching and higher pH, consequently cancelling out the added effect of physical weathering. Hydrology (water flow) and fluid residence time influence leaching and saturation levels of the soil solution (Moore et al., 2012; Velbel, 1993). According to Moore et al. (2012), hydrology is a key physical extrinsic factor and perhaps one of the most important factors that could explain observed differences between laboratory and field measured rates.

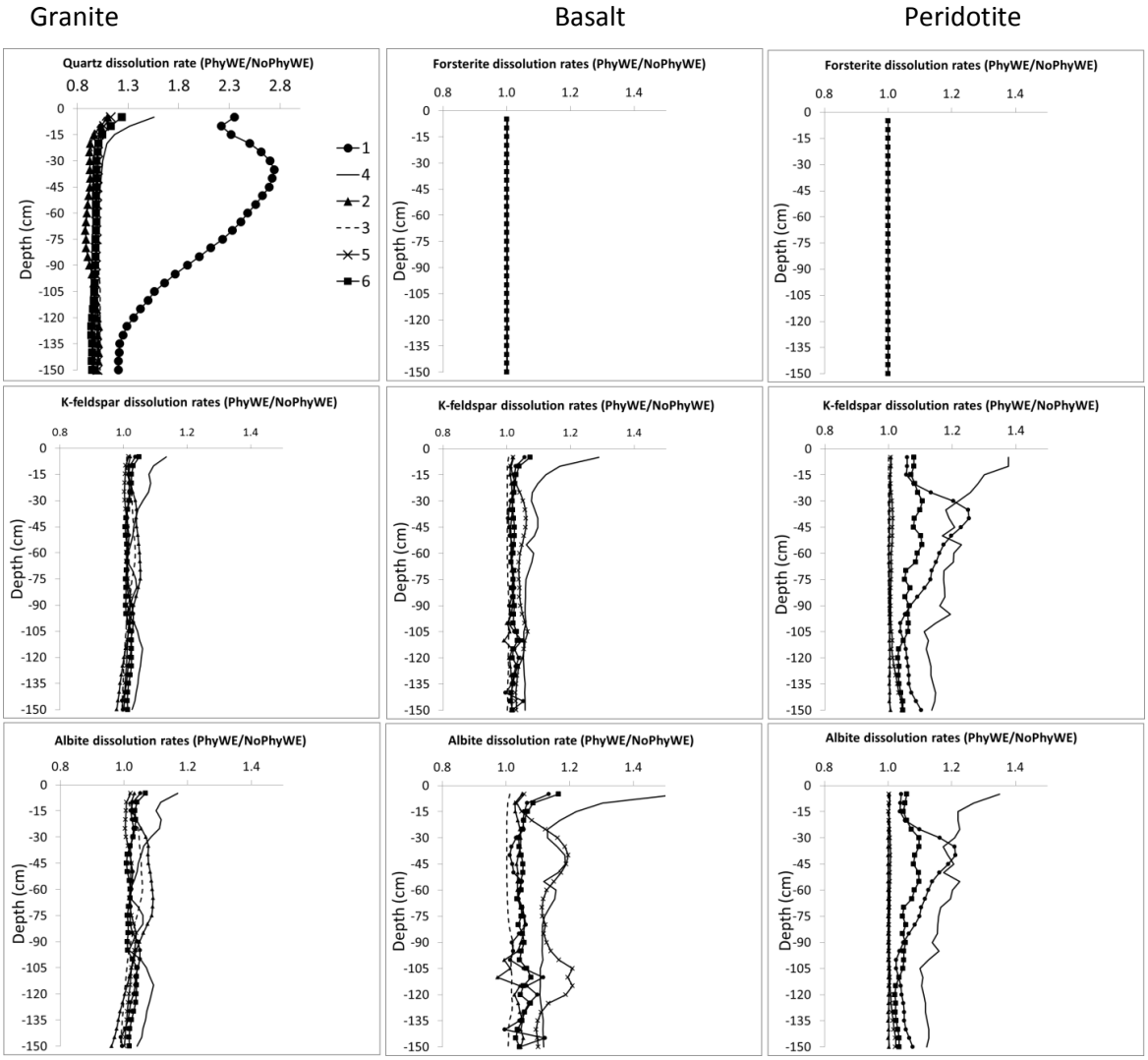

Figure 6.6a. Effect physical weathering on silicate mineral dissolution rates (Model A). Dissolution rates are presented here as a ratio of physical weathering to no physical weathering (i.e., PhyWE / NoPhyWE). Values greater than one imply that the rates are higher when physical weathering is allowed. Roman numerals 1 – 6 represent texture numbers presented in Table 6.1.

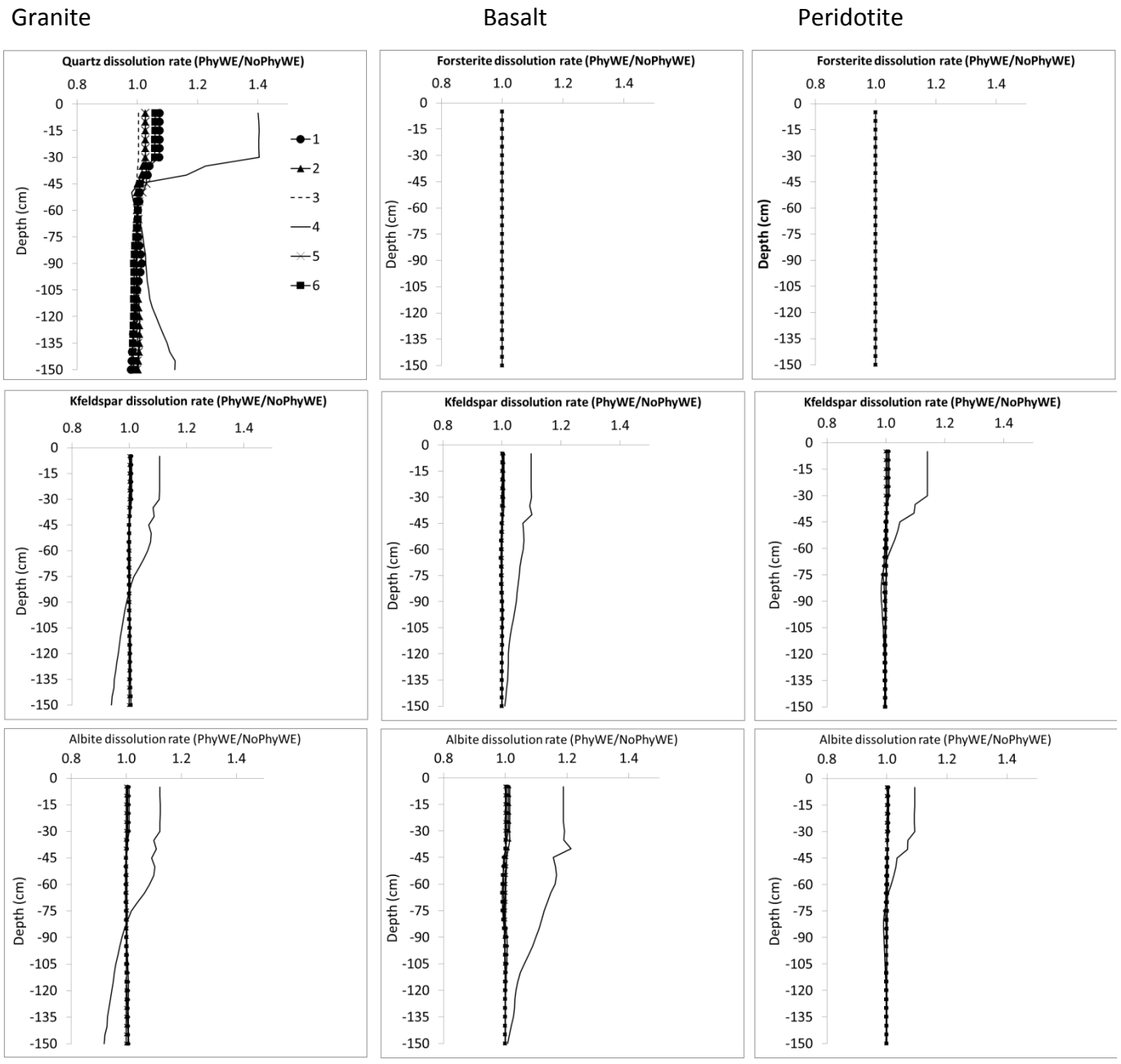

Figure 6.6b. Integrated effect of soil processes on silicate mineral dissolution rates (Model B). Dissolution rates are presented here as a ratio of physical weathering to no physical weathering (i.e., PhyWE / NoPhyWE). Values greater than one imply that the rates are higher when physical weathering is allowed. Roman numerals 1 – 6 represent texture numbers presented in Table 6.1.

6.3.3.4 Interactive effects of selected soil processes on chemical weathering rates

The interacting soil processes that affect chemical weathering and are discussed in this study include clay migration, plant uptake, carbon cycling and physical weathering. The results of these processes are presented under model B (in Figs. 6.2b, 6.3 (right panel), 6.4, 6.5, 6.6b, 6.7 and 6.8). These processes have both direct and indirect effects on chemical weathering rates (White, 2002) through their influence on texture (e.g. clay migration, physical weathering, bioturbation) and on pH (e.g. clay migration, plant uptake, CO_2 production by mineralisation of organic matter). As discussed in Finke (2012), clay migration process moves clay mass from the top part of the profile into the lower part of the profile (Fig. 6.3, right panel) leading to the formation an argillic (Bt) horizon which slows down water flow thus increasing solute concentration and lowering reaction affinity (Smeck and Ciolkosz 1989; White and Brantley 2003). The clay migration processs also has a pH buffering effect (Fig. 6.2b) through its influence on cation exchange capacity (Finke, 2012). Element cycling through plant uptake and release (through organic matter decomposition) influences the pH and consequently mineral weathering rates (Brady et al., 1999; Drever, 1994; Moulton et al., 2000; Stiillings et al. 1996). Higher pH that is visible in the top 0.25 m (Fig. 6.2b) can therefore be attributed to plant nutrient cycling process.

6.3.4 Sensitivity of mineral dissolution rates to physical weathering

Sensitivity of silicate mineral dissolution rates to texture and physical weathering are shown in Fig. 6.7. Results show low sensitivity (Model A) to no sensitivity of dissolution rates (Model B) due to differences in texture and physical weathering, across different minerals and parent materials. The pH of the soil solution seems to be a dominant factor to the chemical weathering of silicate minerals. In addition, the indirect effect of physical weathering on water flow and thus soil pH seem to oppose and cancel out the direct effects of physical weathering on the mineral surface area (as shown in Fig. 6.6b) and consequently the mineral dissolution rates.

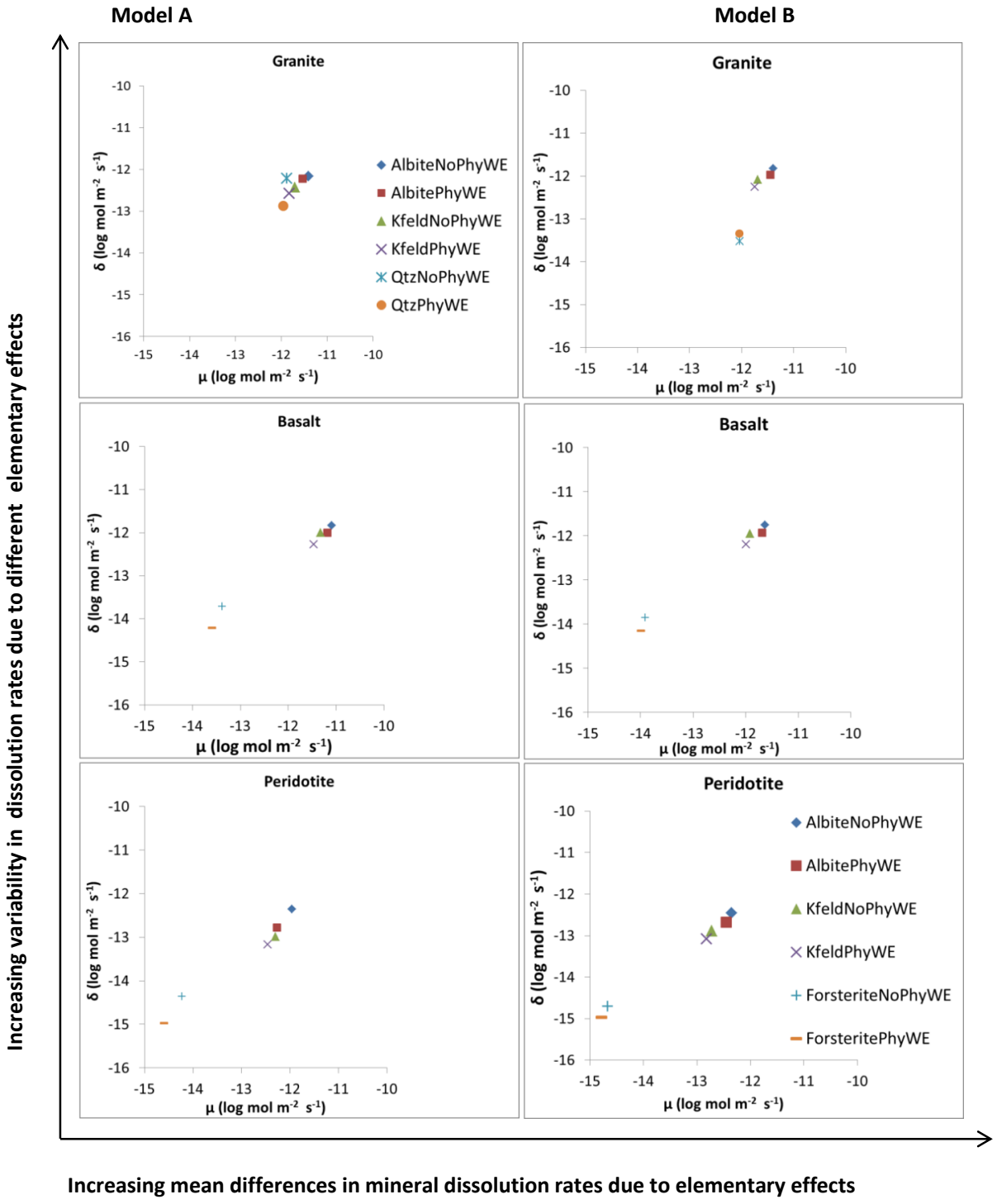

Figure 6.7. Sensitivity of mineral dissolution rates to physical weathering (Model A) and to other interactive soil processes (Model B). The data used in this sensitivity analysis was extracted from the top soil compartment (0.05 m depth). μ and δ are the mean and standard deviation, respectively of elementary effects (u_i) calculated from equation 6.2.

6.3.5 Comparison between SoilGen modelled average mineral dissolution rates with laboratory and field measured rates

SoilGen modelled silicate dissolution rates (Models A and B) were compared with rates obtained from field and laboratory experiments (Fig. 6.8). Rates plotted are for the whole profile depth (1.5 m) and for all the 6 different texture positions shown in Table 6.1. These rates are averaged for 15000 years BP and they generally fall between what is reported from field measurements and what is reported from the laboratory studies. Our results are however generally closer to the laboratory rates than the field measured rates most likely because we assumed far from equilibrium reactions.

There seems to be no difference between dissolution rates from Model A and Model B across different parent materials when looking at the average rates over the whole simulation period of 15000 years (Fig. 6.8). However, when the rates are calculated over short time intervals e.g. 500 years, there is a clear difference at some points in time between the two models and even across different parent materials (see Fig. 6.4 for example). The evolution of silicate dissolution rates with time (Fig. 6.4) is not linear and this is in line with other previous studies (e.g. Hodson and Langan, 1999; White and Brantley, 2003). Generally silicate dissolution rates decrease with time due to depletion of reactive surfaces and, the formation of leached layers and secondary minerals (Hodson and Langan, 1999; White and Brantley, 2003). The comparison of dissolution rates obtained at different time scales therefore remains a challenge and could partly explain the significant differences in silicate dissolution rates reported in literature (White and Brantley, 2003). In addition, the various definitions of chemical weathering rates used in different studies e.g. cation chemical weathering rates (CCWR), chemical silicate rock weathering rates (CSRWR) and total chemical weathering rates (TCWR) make it difficult to compare results between studies (Hartmann and Moosdorf, 2011). Interpreting and comparing results from different studies should therefore be done with utmost care.

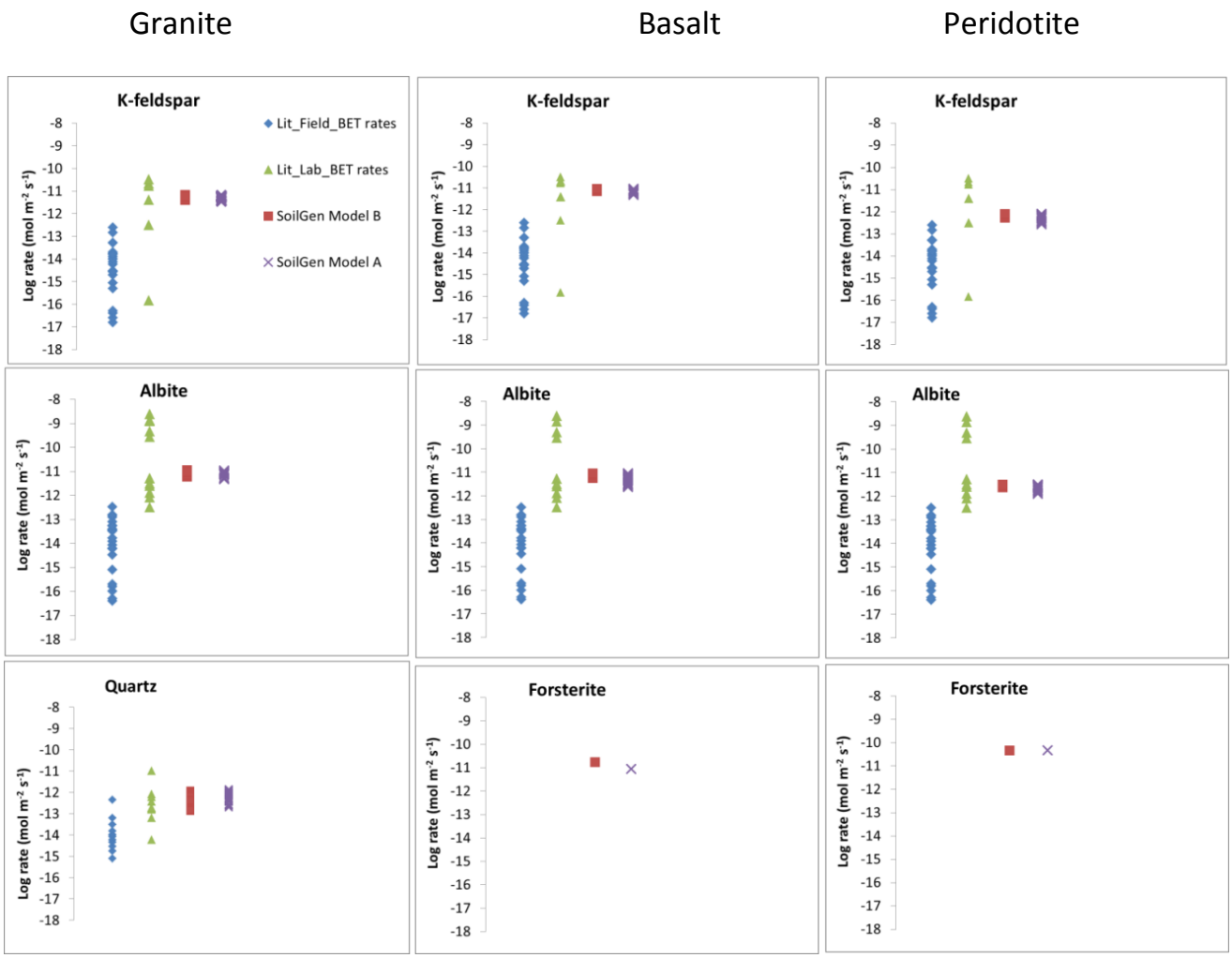

Figure 6.8. Comparison of SoilGen average mineral dissolution rates (Model A and Model B) to laboratory and field determined dissolution rates. Field rates were taken from Parry et al., 2015 and White, 2009 (Table 6.2) while lab rates were taken from : Holdren and Speyer, 1987; Siegal and Pfannkuch, 1984; Swoboda-Colberg & Drever, 1993; Blum and Stillings,1995, Lee et al., 1998 (**K-feldspar**); Stillings et al., 1996; Welch and Ullman, 1996; Oxburgh et al.,1994; Blum and Stillings, 1995, Chou and Wollast,1985; Knauss and Wolrey, 1986; Hamilton et al., 2000 (**Albite**); Brady and Walther, 1990; Dove, 1994 (Quartz). The same field and laboratory rates are repeated for different parent materials (Granite, Basalt and Peridotite). Laboratory and field dissolution rates for Forsterite are not shown.

In our comparisons (Fig. 6.8) we chose to use only field and laboratory dissolution rates normalized to BET surface areas because the texture equation (Chapter 3; Eq. 3.2) used to model mineral surface area was based on the calibration study with measured BET surface area (Sverdrup and Warfvinge,

1995). The field and laboratory rates were however not tied to the time scales or parent materials which could also limit our comparisons to some extent. There are also other questions that could be raised and that could potentially limit our comparisons with field and laboratory measurements. For example if the calibrations already done for clay migration, physical weathering and carbon cycling processes in the quartz-dominated loess sediment (Zonian forest; Finke, 2012) hold for other sites with mafic and ultramafic parent materials? and whether ignoring the differences in climate and the time scales would invalidate the comparison between the dissolution rates from this study and previous studies? To answer such questions requires a more detailed study that is specific to field sites with field data of soil age, silicate dissolution rates, climate, hydrology, mineralogy and any other important factors to enable the calibration and validation of the model. Although still challenging, such studies are already feasible on well-studied chronosequences (e.g. Moore et al., 2012). However the intention of these comparisons (Fig. 6.8) is to show the general trends of our simulations rather than the absolute values.

6.3.6 Limitations of this study

It was possible to demonstrate the interactive effects of soil processes on the silicate dissolution rates using the SoilGen2.25 model. However several assumptions and simplifications were made and should be taken into account when interpreting the findings this study. As already mentioned in the introduction section, this study was based on the assumption there was no erosion and therefore the chemical weathering rates reported here are only valid for supply-limited weathering regimes. In addition, some initial soil properties (e.g., bulk density, solution and surface chemistry, clay migration parameters) were assumed to be similar for all the three parent materials, which in reality is not the case. Particularly, we kept the clay migration parameters (e.g., %montmorillonite and %illite) constant a cross the three parent materials resulting into the unrealistic formation of Bt horizons even in the basalt and peridotite parent material scenarios, since the amount of clay migration in the model is partly influenced by the amount of the 2:1 clay minerals (see Eqs. 2.19 and 2.20, chapter 2). Furthermore, save for the limitations of normative mineralogy calculations (e.g., not all minerals are taken into account), rescaling and manipulation of mineralogy weight compositions (see Appendices 3.2 and 3.3) to suit only the minerals implemented in the model resulted into rather unrealistic input of mineral compositions of basalt and peridotite parent materials (Table 6.2). This limitation can

partly be dealt with by the flexibility now introduced into the model by adding two extra minerals "otherite" and "amorphite" (see chapter 3 for explanation on these minerals).

6.4. Conclusions and outlook

We have used a fully mechanistic soil evolution model (SoilGen) to explore the sensitivity of silicate dissolution rates to the interaction between intrinsic (mineral composition, mineral surface area) and extrinsic factors (climate, physical weathering, clay migration, plant uptake, hydrology). Results from this study have shown consistency with both theoretical understanding of the effects of these factors on chemical weathering, and with observations from experiments and some modelling studies. Our results have demonstrated that although soil solution chemistry (pH) plays a dominant role in determining the silicate dissolution rates, all processes that directly or indirectly influence the soil solution composition play a major role in driving silicate dissolution rates. For example, although the sensitivity results did not confirm sensitivity of dissolution rates to physical weathering, the effect of texture (as influenced by physical weathering) on hydrology could have a substantial effect on the water flow, element leaching and consequently the pH and silicate dissolution rates.

Our dissolution rates results were in between field and laboratory rates, however they were rather high and closer to the laboratory rates owing to the assumption of far from equilibrium reaction. This remains a limitation of this study since near-to-equilibrium conditions have mainly been reported from the field experiments. However these findings are important and challenge us to include secondary mineral precipitation mechanism in the model and perform comparative study to quantify these effects. Furthermore, calibration and validation of the model to the sites with detailed chronosequence data (soil age, silicate dissolution rates, climate, hydrology and mineralogy) is needed.

Despite the limitations identified, this study is another important step to demonstrate the critical need to couple different soil processes with chemical weathering in order to explain differences between silicate dissolution rates measured in the laboratory and in the field. In summary, results showed an inverse relationship of silicate mineral dissolution rates with time, an obvious effect of texture and, an indirect but substantial effect of physical weathering on silicate dissolution rates.

Additionally, results have shown that clay migration and plant nutrient recycling processes influence the pH and thus the silicate dissolution rates.

Author contribution

E. Opolot (first author) contributed to the model code development (weathering module), performed the simulations and prepared the manuscript with continuous and valuable contribution from Peter Finke (co-author). Peter Finke developed the SoilGen model code and contributed to the design of the research.

Acknowledgments

This work is part of the PhD project under the theme "Soils Under Global change, SOGLO" and funded by the Belgian Science Policy Office (project BELSPO/IUAP p7/24).

References

Anderson, S. P., von Blanckenburg, F. and White, a. F.: Physical and Chemical Controls on the Critical Zone, Elements, 3(5), 315–319, doi:10.2113/gselements.3.5.315, 2007.

Beaulieu, E., Goddéris, Y., Labat, D., Roelandt, C., Calmels, D. and Gaillardet, J.: Modelling of water-rock interaction in the Mackenzie basin: Competition between sulfuric and carbonic acids, Chem. Geol., 289(1-2), 114–123, doi:10.1016/j.chemgeo.2011.07.020, 2011.

Blatt, H. and Tracy R.J.: Petrology: Igneous, sedimentary and metamorphic, 2nd ed. New York, W.H. Freeman. ISBN 0-7167-2438-3, 1996.

Blum A. E. and Stillings L. L. Feldspar dissolution kinetics. In Chemical Weathering Rates of Silicate Minerals (ed. A. F. White and S. L. Brantley), Mineralogical Society of America, 31, 291-351, 1995.

Brady, P. V., Dorn, R. I., Brazel, A. J., Clark, J., Moore, R. B. and Glidewell, T.: Direct measurement of the combined effects of lichen, rainfall, and temperature onsilicate weathering, Geochim. Cosmochim. Acta, 63(19-20), 3293–3300, doi:10.1016/S0016-7037(99)00251-3, 1999.

Brady, P. V. and Walther, J.V.: Kinetics of quartz dissolution at low temperatures, Chem. Geol., 82, 253–264, 1990.

Brantley, S. L., Goldhaber, M. B. and Ragnarsdottir, K. V.: Crossing disciplines and scales to understand the Critical Zone, Elements, 3, 307–314.

Carey, A. E., Lyons, W. B. and Owen, J. S.: Significance of landscape age, uplift, and weathering rates to ecosystem development, Aquat. Geochemistry, 11(2), 215–239, doi:10.1007/s10498-004-5733-6, 2005.

Casey, W. H., Banfield, J. F., Westrich, H. R. and McLaughlin, L.: What do dissolution experiments tell us about natural weathering?, Chem. Geol., 105(1-3), 1–15, doi:10.1016/0009-2541(93)90115-Y, 1993.

Chou, L. and Wollast, R.: Steady-state kinetics and dissolution mechanism of albite. Am. J. Sci, 285, 963- 993, 1985.

Cross, W., Iddings, J.P., Pirsson, L. V., and Washington, H. S.: A quantitative chemico-mineralogical classification and nomenclature of igneous rocks: Jour. Geo, 10, 555-690, 1902.

Dixon, J. L. and von Blanckenburg, F.: Soils as pacemakers and limiters of global silicate weathering, Comptes Rendus Geosci., 344(11-12), 597–609, doi:10.1016/j.crte.2012.10.012, 2012.

Dove, P.M.: The dissolution kinetics of quartz in sodium-chloride solutions at 25 oC to 300 oC. Am. J. Sci, 294, 665–712, 1994.

Drever, J. I.: The effect of land plants on weathering rates of silicate minerals, Geochim. Cosmochim. Acta, 58(10), 2325–2332, doi:10.1016/0016-7037(94)90013-2, 1994.

Finke, P. A.: Modelling the genesis of luvisols as a function of topographic position in loess parent material, Quat. Int., 265, 3–17, doi:10.1016/j.quaint.2011.10.016, 2012.

Finke, P. A. and Hutson, J. L.: Modelling soil genesis in calcareous loess, Geoderma, 145(3-4), 462–479, doi:10.1016/j.geoderma.2008.01.017, 2008.

Finke, P. A., Vanwalleghem, T., Opolot, E., Poesen, J. and Deckers, J.: Estimating the effect of tree uprooting on variation of soil horizon depth by confronting pedogenetic simulations to measurements in a Belgian loess area, J. Geophys. Res. Earth Surf., 118(4), 2124–2139, doi:10.1002/jgrf.20153, 2013.

Finke, P. A., Samouëlian, A., Suarez-Bonnet, M., Laroche, B. and Cornu, S. S.: Assessing the usage potential of SoilGen2 to predict clay translocation under forest and agricultural land uses, Eur. J. Soil Sci., 66(1), 194–205, doi:10.1111/ejss.12190, 2015.

Gabet, E. J.: A theoretical model coupling chemical weathering and physical erosion in landslide-dominated landscapes, Earth Planet. Sci. Lett., 264(1-2), 259–265, doi:10.1016/j.epsl.2007.09.028, 2007.

Gabet, E. J. and Mudd, S. M.: A theoretical model coupling chemical weathering rates with denudation rates, Geology, 37(2), 151–154, doi:10.1130/G25270A.1, 2009.

Ganor, J., Lu, P., Zheng, Z. and Zhu, C.: Bridging the gap between laboratory measurements and field estimations of silicate weathering using simple calculations, Environ. Geol., 53(3), 599–610, doi:10.1007/s00254-007-0675-0, 2007.

Goddéris, Y., François, L. M., Probst, A., Schott, J., Moncoulon, D., Labat, D. and Viville, D.: Modelling weathering processes at the catchment scale: The WITCH numerical model, Geochim. Cosmochim.Acta, 70(5), 1128–1147, doi:10.1016/j.gca.2005.11.018, 2006.

Goddéris, Y., Brantley, S. L., François, L. M., Schott, J., Pollard, D., Déqué, M. and Dury, M.: Rates of consumption of atmospheric CO2 through the weathering of loess during the next 100 yr of climate change, Biogeosciences, 10(1), 135–148, doi:10.5194/bg-10-135-2013, 2013.

Hamilton I. P., Pantano C. G., and Brantley S. L.: Dissolution of albite glass and crystal. Geochim.Cosmochim. Acta, 64,2603-2615, 2000.

Hartmann, J. and Moosdorf, N.: Chemical weathering rates of silicate-dominated lithological classes and associated liberation rates of phosphorus on the Japanese Archipelago-Implications for global scale analysis, Chem. Geol., 287(3-4), 125–157, doi:10.1016/j.chemgeo.2010.12.004, 2011.

Hartmann, J., West, A. J., Renforth, P., Köhler, P., Rocha, C. L. D. La, Wolf-gladrow, D. A., Dürr, H. H. and Scheffran, J.: Enhanced chemical weathering as a geoengineering strategy to reduce atmospheric carbon dioxide , supply nutrients , and mitigate ocean acidification,Rev. Geophys, 51, 113–149, doi:10.1002/rog.20004.1.Institute, 2013.

Hartmann, J., Moosdorf, N., Lauerwald, R., Hinderer, M. and West, a. J.: Global chemical weathering and associated P-release — The role of lithology, temperature and soil properties, Chem. Geol., 363, 145–163, doi:10.1016/j.chemgeo.2013.10.025, 2014.

Harris, P.G., Reay, A. and White, G.I.: Chemical composition of the upper mantle, J. Geophys. Res., 72 (24), 6359–6369, doi:10.1029/JZ072i024p06359, 1967.

Hellevang, H., Pham, V. T. H. and Aagaard, P.: Kinetic modelling of CO2–water–rock interactions, Int. J. Greenh. Gas Control, 15, 3–15, doi:10.1016/j.ijggc.2013.01.027, 2013.

Hilley, G. E., Chamberlain, C. P., Moon, S., Porder, S. and Willett, S. D.: Competition between erosion and reaction kinetics in controlling silicate-weathering rates, Earth Planet. Sci. Lett., 293(1-2), 191–199, doi:10.1016/j.epsl.2010.01.008, 2010.

Hodson, M.E., Langan S.J. and Wilson, M.: A critical evaluation of the use of the PROFILE model in calculating mineral weathering rates. Water, Air, and Soil Pollution 98: 79-104, 1997.

Holdren, Jr., G.R. and Speyer, P.M.: Reaction rate surface area relationships during the early stages of weathering, II. Data on eight additional feldspars.Geochim.Cosmochim.Acta, 51, 2311-2318, 1987.

Jenny, H.: Factors of Soil Formation: A System of Quantitative Pedology. McGraw-Hill, New York. 281 pp. 1941.

Jenkinson, D.S., Coleman, K.: Calculating the annual input of organic matter to soil from measurements of total organic carbon and radiocarbon. European Journal of Soil Science, 45, 167-174. 1994.

Kelsey, C. H.: Calculation of the CIPW norm: Mineralogical Magazine, v. 34, p. 276-282. Mineralogical Magazine, v. 34, p. 276-282, 1965

Knauss, K.. G. and Wolery, T. J.: Dependence of albite dissolution kinetics on ph and time at 25°c and 70°c, Geochim. Cosmochim. Acta, 50(11), 2481–2497, doi:10.1016/0016-7037(86)90031-1, 1986.

Knauss, K. G. and Wolery, T. J.: The dissolution kinetics of quartz as a function of pH and time at 70°C, Geochim. Cosmochim. Acta, 52(1), 43–53, doi:10.1016/0016-7037(88)90055-5, 1988.

Larsen, I.J., Almond, P. C., Eger, A., Stone, J.O., Montgomery, D. R., and Malcolm, B.: Rapid soil production and weathering in the Southern Alps, New Zealand, Science, 343(6171), 637–640, 2014

Lee, M. R., Hodson, M. E. and Parsons, I.: The role of intragranular microtextures and microstructures in chemical and mechanical weathering: Direct comparisons of experimentally and naturally weathered alkali feldspars, Geochim. Cosmochim. Acta, 62(16), 2771–2788, doi:10.1016/S0016-7037(98)00200-2, 1998.

Maher, K., Steefel, C. I., White, A. F. and Stonestrom, D. a.: The role of reaction affinity and secondary minerals in regulating chemical weathering rates at the Santa Cruz Soil Chronosequence, California, Geochim. Cosmochim.Acta, 73(10), 2804–2831, doi:10.1016/j.gca.2009.01.030, 2009.

Moore, J., Lichtner, P. C., White, A. F. and Brantley, S. L.: Using a reactive transport model to elucidate differences between laboratory and field dissolution rates in regolith, Geochim. Cosmochim.Acta, 93, 235–261, doi:10.1016/j.gca.2012.03.021, 2012.

Morris, M.: Factorial sampling plans for preliminary computational experiments, Technometrics, 33(2), 161–174, 1991.

Moulton, K .L., West, J. and Berner, R.A.: Solute Flux and Mineral mass balance approaches to the quantification of plant effects on silicate weathering. American Journal of Science., 300, 539 – 570, 2000.

Navarre-Sitchler, A. and Brantley, S.: Basalt weathering across scales, Earth Planet. Sci. Lett., 261(1-2), 321–334, doi:10.1016/j.epsl.2007.07.010, 2007.

Oliva, P., Viers, J. and Dupré, B.: Chemical weathering in granitic environments, Chem. Geol., 202(3-4), 225–256, doi:10.1016/j.chemgeo.2002.08.001, 2003.

Opolot, E., Yu, Y. Y. and Finke, P. A.: Modelling soil genesis at pedon and landscape scales: Achievements and problems, Quat. Int., 376, 34–46, doi:10.1016/j.quaint.2014.02.017, 2015.

Oxburgh R., Drever 1. I., and Sun Y.: Mechanism of plagioclase dissolution in acid solution at 25° C. Geochim. Cosmochim. Acta, 58 (2), 661-669, 1994.

Parry, S. a., Hodson, M. E., Kemp, S. J. and Oelkers, E. H.: The surface area and reactivity of granitic soils: I. Dissolution rates of primary minerals as a function of depth and age deduced from field observations, Geoderma, 237-238, 21–35, doi:10.1016/j.geoderma.2014.08.004, 2015.

Pham, V. T. H., Lu, P., Aagaard, P., Zhu, C. and Hellevang, H.: On the potential of CO2–water–rock interactions for CO2 storage using a modified kinetic model, Int. J. Greenh. Gas Control, 5(4), 1002–1015, doi:10.1016/j.ijggc.2010.12.002, 2011.

Phelan, J., Belyazid, S., Kurz, D., Guthrie, S., Cajka, J., Sverdrup, H. and Waite, R.: Estimation of Soil Base Cation Weathering Rates with the PROFILE Model to Determine Critical Loads of Acidity for Forested Ecosystems in Pennsylvania, USA: Pilot Application of a Potential National Methodology, Water, Air, Soil Pollut., 225(9), 225:2109, doi:10.1007/s11270-014-2109-4, 2014.

Roelandt, C., Goddéris, Y., Bonnet, M.-P.and Sondag, F.: Coupled modelling of biospheric and chemical weathering processes at the continental scale, Global Biogeochem. Cycles, 24(2),GB2004, doi:10.1029/2008GB003420, 2010.

Saltelli, A., Ratto, M., Tarantola, S. and Campolongo, F.: Sensitivity Analysis for Chemical Models, Chem. Rev., 105, 2811–2827, 2005.

Sauer, D., Finke, P., Sørensen, R., Sperstad, R., Schülli-Maurer, I., Høeg, H. and Stahr, K.: Testing a soil development model against southern Norway soil chronosequences, Quat. Int., 265, 18–31, doi:10.1016/j.quaint.2011.12.018, 2012.

Schoonejans, J., Vanacker, V., Opfergelt, S., Ameijeiras-Mariño, Y., and M. Christl.: Kinetically limited weathering at low denudation rates in semiarid climatic conditions, J. Geophys. Res. Earth Surf., 121, 336‐350, doi:10.1002/ 2015JF003626., 2016.

Siegel, D. I. and Pfannkuch, H. O.: Silicate mineral dissolution at pH 4 and near standard temperature and pressure, Geochim. Cosmochim. Acta, 48(1), 197–201, doi:10.1016/0016-7037(84)90362-4, 1984.

Smeck, N.E. and Ciolkosz, E.J.:. Fragipans: their occurrence, classification and genesis. SSSA Spec. Publ., 24. Soil Sci. Soc. Amer., Madison. 153 pp, 1989.

Soil Survey Division Staff.: Soil survey manual. Soil Conservation Service.U.S. Department of Agriculture, Handbook 18, chapter 3, 1993.

Stendahl, J., Akselsson, C., Melkerud, P.-A. and Belyazid, S.: Pedon-scale silicate weathering: comparison of the PROFILE model and the depletion method at 16 forest sites in Sweden, Geoderma, 211-212, 65–74, doi:10.1016/j.geoderma.2013.07.005, 2013.

Stillings, L. L. and Susan, L.: Feldspar dissolution at 25°C and pH 3: Reaction stoichiometry and the effect of cations, Geochim. Cosmochim.Ac., 59, 1483–1496, 1995.

Stiillings, L. L., Drever, J. I., Brantley, S. L., Sun, Y. and Oxburgh, R.: CHEMICAL Rates of feldspar dissolution at pH 3 - 7 with 0 - 8 m M oxalic acid, Chem. Geol., 132, 79–89, 1996.

Sverdrup, H. and Warfvinge, P.: Estimating field weathering rates using laboratory kinetics. In: White, A., Brantley, S. _Eds.., Weathering Kinetics of Silicate Minerals. Reviews in Mineralogy 31. Min. Soc. of America, 485–542, 1995.

Swoboda-Colberg, N. G. and Drever, J. I.: Mineral dissolution rates in plot-scale field and laboratory experiments, Chem. Geol., 105(1-3), 51–69, doi:10.1016/0009-2541(93)90118-3, 1993.

Van Ranst, E.: Genesis and properties of silty forest soils in central Belgium and the Ardennes. Unpublished PhD-thesis, Ghent University, Belgium, 349 pp., 1981 (in Dutch).

Velbel, M. A.: Constancy of silicate-mineral weathering-rate ratios between natural and experimental weathering: implications for hydrologic control of differences in absolute rates, Chem. Geol., 105(1-3), 89–99, doi:10.1016/0009-2541(93)90120-8, 1993.

Welch S. A. and Ullman W. J.: Feldspar dissolution in acidic and organic solutions: Compositional and pH dependence of dissolution rate. Geochim.Cosmochim. Acta, 60, 2939-2948. 1996

White, A.: Natural weathering rates of silicate minerals, Treatise on geochemistry, 5.05, 133–168, 2003.

White, A. F.: Determining mineral weathering rates based on solid and solute weathering gradients and velocities: application to biotite weathering in saprolites, Chem. Geol., 190(1-4), 69–89, doi:10.1016/S0009-2541(02)00111-0, 2002.

White, A. F. and Brantley, S. L.: The effect of time on the weathering of silicate minerals: why do weathering rates differ in the laboratory and field?, Chem. Geol., 202(3-4), 479–506, doi:10.1016/j.chemgeo.2003.03.001, 2003.

White, A. R. T. F., Blum, A. E., Schulz, M. S., Bullen, T. O. M. D., Harden, J. W., Peterson, M. L., Survey, U. S. G. and Park, M.: Chemical weathering rates of a soil chronosequence on granitic alluvium : I . Quantification of mineralogical and surface area changes and calculation of primary silicate reaction rates, Geochim. Cosmochim. Ac., 60(14), 2533–2550, 1996.

Wosten, J.H.M., Lilly, A., Nemes, A. and Le Bas, C.: Development and use of a database of hydraulic properties of European soils. Geoderma, 90, 169–185, doi:10.1016/S0016-7061(98)00132-3, 1999.

Yu, Y. Y., Finke, P. a., Wu, H. B. and Guo, Z. T.: Sensitivity analysis and calibration of a soil carbon model (SoilGen2) in two contrasting loess forest soils, Geosci. Model Dev., 6(1), 29–44, doi:10.5194/gmd-6-29-2013, 2013.

Zhu, C.: In situ feldspar dissolution rates in an aquifer, Geochim. Cosmochim.Acta, 69(6), 1435–1449, doi:10.1016/j.gca.2004.09.005, 2005.

Zhu, C. and Lu, P.: Alkali feldspar dissolution and secondary mineral precipitation in batch systems: 3. Saturation states of product minerals and reaction paths, Geochim. Cosmochim.Acta, 73(11), 3171–3200, doi:10.1016/j.gca.2009.03.015, 2009.

Zhu, C., Lu, P., Zheng, Z. and Ganor, J.: Coupled alkali feldspar dissolution and secondary mineral precipitation in batch systems: 4. Numerical modelling of kinetic reaction paths, Geochim. Cosmochim.Acta, 74(14), 3963–3983, doi:10.1016/j.gca.2010.04.012, 2010.

Zwertvaegher, A., Finke, P., De Smedt, P., Gelorini, V., Van Meirvenne, M., Bats, M., De Reu, J., Antrop, M., Bourgeois, J., De Maeyer, P., Verniers, J. and Crombé, P.: Spatio-temporal modelling of soil characteristics for soilscape reconstruction, Geoderma, 207-208, 166–179, doi:10.1016/j.geoderma.2013.05.013, 2013.

Code availability

The SoilGen model is freely available. The user manual and the programs for previous versions can be downloaded at: http://users.ugent.be/~pfinke/index_bestanden/Page1167.htm. SoilGen2.25 version is not yet available on the website but can be obtained on request (by sending an email to peter.finke@ugent.be).

Chapter 7 : General Conclusions, Challenges and Areas for Future Research

"Make things as simple as possible but not simpler" **- Albert Einstein**

7.1 Summary and General Conclusions

The objectives of this thesis were (i) to contribute to the on-going discussion on process coverage of soil and landscape evolution models, which are necessary tools to assess the soil evolution under global change. As a consequence of objective (i), this study was (ii) to extend the description of the chemical weathering module and (iii) the biogeochemical module of the pedogenesis model (SoilGen). Finally, objective (iv) of this study aimed at demonstrating through case studies, the application of the SoilGen model to assess the evolution of soil properties (notably, soil horizon thickness, soil pH, texture, etc.) as a function of global change (i.e., change in climate, vegetation and or land use).

In the first objective (**Chapter 2**), the review on the soil models (particularly on the SoilGen model), their process coverage, challenges and way forward was conducted and several conclusions were reached. The development of soil and landscape evolution models has progressed quite rapidly in the last decade (see Fig 1.3; Chapter 1), and are increasingly becoming invaluable tools to provide answers to many environmental questions including soil and global change interaction and, soil and ecosystem functioning. However, most soil models either at pedon or landscape scales were still limited in soil forming processes defined in (Bockheim and Gennadiyev, 2000). Hydrological processes are hardly incorporated in most models and, most of the models have focused on individual soil forming processes rather than the integral definitions of these processes as would be the case in field situations. In addition some of soil models simulate soil evolution at short time scales. Such conclusions have also been demonstrated in review of soil models presented in Minasny et al. (2015).

Through this study, it is clear that the strengths of the SoilGen model lies in its ability to simulate the integrated effect of biological, geochemical and physical soil forming processes moreover at millennium time scale. Prior to this study, the SoilGen model had been applied in several case studies and simulated soil properties matched the measured soil properties in most cases. The mismatch between SoilGen simulated soil properties and measurements were partly attributed to the simplifications on the chemical weathering and chemical processes. In addition, the evolution of soil structure with time is not simulated, rather a constant volume of each compartment with time is assumed. The feedback between evolution of soil properties and vegetation development is equally simplified and only captured through ion uptake and annual litter input. Last but not least, being a

profile based model, the SoilGen model does not include the feedback effects between the vertical soil forming processes and the lateral soil production and redistribution processes (Vanwalleghem et al., 2013).

The objectives (ii) and (iii) are presented in **chapters 3 and 4** of this thesis. These chapters aimed at addressing some of the limitations of the SoilGen model pointed out in the first objective (chapter 2). In chapter 3, an extended chemical weathering mechanism was proposed and formulated. The extended mechanism includes the weathering of both primary and secondary minerals and allows the precipitation of secondary minerals. The mechanism of primary mineral dissolution at far from equilibrium conditions has already been implemented and the sensitivity test results are presented in chapter 6. However, the mechanism allowing the formation of secondary minerals (near-equilibrium conditions) is ready but not yet implemented. In chapter 4, the biogeochemical module of the SoilGen module was extended to include iron (Fe^{2+} and Fe^{3+}) and silica (H_4SiO_4) chemical species. These elements play a crucial role in soil formation and should be included in the soil evolution models. This new formulation is also ready and the procedure for implementation into the SoilGen model has already been presented in chapter 4. What is remaining is programming into the SoilGen language (Pascal-Lazurus), debugging and linking such a code to other SoilGen modules. This exercise is likely to take about three months and this should be feasible within the contract period of this PhD study.

The last objective of this study was to demonstrate the application of the SoilGen model to simulate evolution of soil properties under changing boundary conditions (global change). This objective was achieved using two case studies presented in chapters 5 and 6. In **chapter 5** the SoilGen model was used to estimate the effect of bioturbation (due to treefalls) on the variation of soil horizon thickness. The hypothesis was that using a soil formation model (SoilGen) would allow the estimation of profile development as a function of local variations in soil-forming factors such as relief. Measurements from 108 soil profiles covering different topographic positions in a 1329 ha area of Meerdaal forest (Belgium) were used in the model calibration and testing. For each location, two scenarios were simulated; (i) natural soil development with a parent material consisting of the C-horizon of the loess on top of Eocene marine sand and (ii) natural soil development as in scenario (i) but including disturbance by treefalls. The average wind exposure map was generated based on the digital

elevation model of the study area and all the associated wind speeds. The wind exposure factor was used to modify the disturbance cycle which was then used to calculate the probability of treefall at each of the 108 locations. Prior to the comparison between measured horizon thicknesses reported in (Vanwalleghem et al., 2010) and the simulations, the SoilGen simulated soil properties such as OC, clay content, a clay dispersion indicator, and calcite content were first converted into soil horizon depths following the horizon classification algorithm developed there in. Results indicated that including treefall events changed the model predictions especially for the superficial horizons. Consequently, soil horizon thicknesses simulated in scenario 2 (soil development with treefalls) exhibited similar trends as the observed data. The correlation with landscape variables for the Bt horizon disappeared as a result of the homogenizing effect of treefalls, as was observed in the field. The conclusion was therefore drawn that the occurrence of bioturbation due to tree falls is an important process in soil formation and could be an explanation for the lack of spatial structure observed in the field measurements.

Finally, in **chapter 6** the SoilGen model was applied to estimate the sensitivity of silicate dissolution rates to physical weathering. Our hypothesis was that physical weathering affects the magnitude of chemical weathering and this could partly explain the systematic deviations between laboratory and field approaches to estimate silicate mineral dissolution rates. Specific objectives were (i) to asses the effects of parent material composition on the silicate mineral dissolution rates, (ii) to asses model sensitivity of chemical silicate mineral dissolution rates to change in soil texture, (iii) to assess the effect of physical weathering of primary minerals on their dissolution rates, (iv) to assess the effect of interactive soil processes on silicate mineral dissolution rates and (v) to compare our modelled silicate mineral dissolution rates to rates reported in literature. We tested the hypothesis on the forested loess soils, in the Zonian forest, Belgium (50°46’31”N, 4°24’9”E) where most soil-forming processes in the SoilGen model had already been calibrated to (Finke and Hutson, 2008; Finke, 2012; Opolot et al., 2015; Yu et al., 2013) and the reconstructed model boundary conditions (climate, vegetation, bioturbation) in the last 15000 years input data were readily available for this site. Six different texture points were randomly selected from the USDA textural triangle to represent the initial soil texture and 3 different parent materials (granite, basalt and peridotite) were selected to capture slow, moderate and fast chemical weathering parent materials. Two scenarios were defined: (i) to

assess the effect of only physical weathering on silicate mineral dissolution rates and (ii) to assess the integrated effect of all soil processes defined in the SoilGen model on the silicate mineral dissolution rates. We calculated the average silicate dissolution rates for each scenario and calculated the sensitivity of silicate dissolution rates to change in particle size (due to physical weathering) following a method described in (Morris, 1991). Our results showed a dominant role of pH and an indirect but substantial effect of soil texture on dissolution rates. Clay migration and plant nutrient recycling influenced the pH and thus the dissolution rates. SoilGen simulated silicate dissolution rates were between laboratory and field measured rates. Results from this study demonstrated the necessity to couple different soil-forming processes in mechanistic soil models in order to explain the differences between lab and field dissolution rates.

7.2 General challenges and recommendations

As already mentioned in the earlier chapters of this thesis, soil evolution models are essential tools for answering many environmental questions. However like in any other field, there are associated challenges. While there are challenges that are specific to the spatial scale of modelling i.e., if it is a landscape model or it is a pedon scale model, most of these challenges cut across all soil evolution mechanistic models. In any case, these challenges can be grouped into five main categories i.e., (i) computation time, (ii) process coverage, (iii) input data, (iv) model calibration and verification and, (v) quality and usability of the model results. The subsequent discussion under this section will be limited to the challenges related to the use of the SoilGen model unless otherwise mentioned

7.2.1 Computation time versus model process coverage

Like most mechanistic models, the computation time is a challenge in the SoilGen model. Finke (2012) for example calculated 13 days and 22 hours runtime to simulate a soil profile with 5 cm compartments and 4.25 m deep for 15000 years. Such long runtimes limits the use of multiple-run calibration methods and calls for the use of simple thematic approach to calibrate only the most sensitive parameters (Yu et al., 2012). The long runtime is a result of certain processes majorly water flow driven processes (Minasny et al., 2015). To reduce runtime may therefore involve simplifying some process definitions in the model while keeping in mind the critical issue of the balance between

complexity and simplicity. Nevertheless with the on-going development of high performance computers, the issue of long runtimes may soon pose little challenge.

7.2.2 Model process coverage, model complexity and input data

Regarding the model process coverage, the question of how complex the model should be remains difficult to answer. Albert Einstein once said *"make things as simple as possible but not simpler"*. Essentially, the process coverage in the model should be in such a way that the model representation of reality is not oversimplified. At the same time, so many complex processes may limit the use of the model due to high input data requirement and the need for deep understanding (by the model users) of the processes defined in the model. In addition, the more complex the processes defined in the model are, the more it becomes difficult to verify such models thus questioning the consistency of such model simulations with observations (Holmqvist, 2002). At its current state, the SoilGen model though it looks complex, is in reality still easily verifiable with field and laboratory measurements (e.g.,Finke and Hutson, 2008; Finke, 2012; Finke et al., 2015; Sauer et al., 2012). However, some critical soil-forming processes such as soil structure and vegetation development remain undefined. In addition, there is a challenge of high input data requirement (Johnson et al., 2014) which is certainly one of the main challenges in almost all mechanistic models. The input data for model calibration and validation needs to be free of uncertainty, yet such data is often scarce. Uncertain input data especially boundary conditions is one source of uncertainty in the simulation results (Finke et al., 2015). In the SoilGen model, the initial data may not be that of a problem when the run covers a long period, at least for many soil parameters, because the sensitivity of the model to initial soil data may be limited. However this is not always the case and therefore realistic reconstructions of the initial situation are always important. It goes without saying that the model is as good as the input data!

7.2.3. Model calibration and validation

Calibration and validation of mechanistic models especially those covering a long temporal scale remain challenging (Finke and Hutson, 2008; Minasny et al., 2015). For example, for the SoilGen, only two data points along the temporal scale are usually available i.e., initial state (15000 years BP) and final state (0 years BP). There is limited information along the time scale and thus during the calibration of the model, parameters are usually tuned to arrive at the final (present) observations

(Finke and Hutson, 2008). These parameter estimates do not therefore necessarily represent the intermediate stages of the soil development leading to uncertainties in the model final simulations. Putting emphasis on applying the models on chrono-sequence sites is one way to address this challenge. Minasny et al. (2015) have for example, suggested utilizing micromorphological observations, luminescence and radioactive nuclide data to calibrate some pedogenetic processes such as bioturbation and clay migration.

7.2.4 Model results: Quality and Usability

Finally, while the quality of the process definitions in the model is the major concern of the model developer, the usability of the model results is of interest to the model end-user. Translating model outputs into for example usable and quantifiable soil ecosystem services remains a challenge to most soil modellers. Going by the words of Manfred Eigen that: *"a theory has only the alternative of being right or wrong. A model has a third possibility: it may be right, but irrelevant."* Therefore, the quality and the relevance of the model outputs need to be given equal attention when designing modelling studies. Having the soil model outputs inform of quantifiable soil ecosystem services will not only make it easily usable by non-model experts but also make it easy to communicate results to the non-scientific community. Consequently, there is need for soil modellers to work with other relevant groups such as ecosystem service experts.

7.3 Areas for future research

The future of soil models depends on the ability of such models to provide answers to issues of critical interest to the society. In principle, emphasis of soil modelling should be on integrating soil science knowledge with other scientific fields such that the outputs from such soil models are usable by interdisciplinary models (Brevik et al., 2016). In addition, future perspectives on soil models should focus on increasing model quality since this would widen their use in overall policy and decision making (Brevik et al., 2016). For all mechanistic models and for the SoilGen model in particular, future work should focus on addressing the aforementioned challenges in the preceding section. The discussion below will be focusing on the future research regarding the SoilGen model, unless otherwise mentioned.

7.3.1. Calibrating the chemical weathering module of the SoilGen model

Except for the sensitivity study performed and presented in chapter 6 of this thesis, the chemical weathering mechanism in the SoilGen model is yet to be calibrated and verified. Calibration of this process has not been performed partly because the parameters for the previous weathering mechanism, had already been constrained from the acidification model from which it was taken (Finke, 2012) and partly due to limited quality dataset to allow the calibration of the mechanism. As stated in Opolot and Finke (2015), future work should focus on calibrating and verifying the weathering part of the model (presented in chapter 3) to the sites with detailed chrono-sequence data (soil age, silicate dissolution rates, climate, hydrology and mineralogy).

7.3.2. Testing the SoilGen model in different environmental settings using the world soil dataset

The SoilGen model has already been tested and applied to answer many research questions (e.g., Finke and Hutson, 2008; Finke, 2012; Finke et al., 2013, 2015, in preparion; Sauer et al., 2012; Yu et al., 2013; Opolot and Finke, 2015; Zwertvaegher et al., 2013). However, most of these test studies have been restricted to some environments (particularly loess soils and mostly under temperate climate) and therefore its applicability in other environments is yet to be tested. Opolot et al. (2015) have shown that the current functionality of the SoilGen model allows the simulation of the soil forming processes in 15 out of the 32 “Reference Soil Groups” that are defined in the World Reference Base (WRB) for soil resources (IUSS Working Group WRB, 2006). Implementation of the weathering mechanism proposed in chapter 3 will increase this process coverage to 24 Reference Soil Groups. This means that, the SoilGen could be applied to simulate the future development of up to an estimated 84 % of the WRB-RSG groups (IUSS Working Group WRB, 2015). The available world soil data set at the International Soil Reference and Information Centre (ISRIC) and the Harmonized World Soil Database (FAO/IIASA/ISRIC/ISS-CAS/JRC, 2012) should allow such test studies.

7.3.3. Including the vegetation development mechanism in the SoilGen model

Vegetation development is an important process in soil formation as it influences several soil processes including the water balance, nutrient balance and the development of soil structure. In the current status of the SoilGen model, the feedback between the evolution of soil properties and vegetation development is simplified and the effect of vegetation on soil properties is captured only

through annual litter input and ion uptake. The effect of the evolving soil properties (e.g., pH, soil moisture) on the vegetation development is therefore not taken into account. Future focus should therefore involve defining such an interactive mechanism between the soil system and vegetation growth. Such a process definition will improve the model abilities to simulate the effect of climate and land use changes on both soil formation and vegetation development. Implementing such mechanism will certainly include working and collaborating with the vegetation and climate modellers.

7.3.4 Improving the process definition of soil structure development

Soil structure is one of the most important soil physical properties and it influences many soil-forming processes such as water and solute transport, plant root growth and organic matter decomposition rates. However, soil structure development mechanism in the soil has hardly been modelled. Until now, no model (or at least no soil model) explicitly simulates soil structure due to associated complexity in mechanically defining this property. However, there is need to incorporate such a mechanism in the soil models. Therefore, future research involving the SoilGen model could also take into account the possibility to simulate the evolution soil structure as a function of related soil-forming processes such as clay migration and organic matter decomposition.

7.3.5. Improving the runtime of the SoilGen model

The challenge of long runtime needs to be dealt with if pedogenetic models (e.g., the SoilGen model) are to benefit from advanced sensitivity and calibration techniques such as such as Bayesian sensitivity analysis method. In addition, integrating these models into the landscape models is only computationally feasible with short runtime scales. As mentioned earlier, this long runtime challenge may become less of a problem as high performance computers become affordable. However, it might even be faster to identify, evaluate and implement options that may reduce the long runtime of such models. Such options may include simplifying and or redefining specific processes notably water flow processes (Minasny et al., 2015).

7.3.6. Integrating the SoilGen model into landscape models

Models operating at pedon scales face a critical challenge of incorporating the spatial heterogeneity exhibited by soils (Minasny et al., 2015). While landscape models lack detailed vertical soil-forming

processes defined in profile scale models such as the SoilGen model, the profile models lack detailed description of lateral soil-production and redistribution processes such as soil erosion, mass wasting and sedimentation processes (Minasny et al., 2015). Consequently, the feedback between the soil profile development and such processes is often missing in the profile models (Vanwalleghem et al., 2013). Working towards an integration or coupling of soil and landscape evolution models in what is termed as "soil-scape genesis" has become inevitable especially at unstable landscapes (Minasny et al., 2015; Opolot et al., 2015). Until now, only a handful of studies (Temme and Vanwalleghem, 2015; Vanwalleghem et al., 2013) have attempted to model soil-scape evolution. Preceded by computation time improvement, it should be possible to design modelling scenarios that integrate the SoilGen model into landscape models.

Author contribution

This chapter was fully synthesised and written by E. Opolot.

References

Bockheim, J. G. and Gennadiyev, A. N.: The role of soil-forming processes in the definition of taxa in Soil Taxonomy and the World Soil Reference Base, Geoderma, 95(1-2), 53–72, doi:10.1016/S0016-7061(99)00083-X, 2000.

Brevik, E. C., Calzolari, C., Miller, B. A., Pereira, P., Kabala, C., Baumgarten, A. and Jordán, A.: Soil mapping, classification, and pedologic modelling: History and future directions, Geoderma, 264, 256–274, doi:10.1016/j.geoderma.2015.05.017, 2016.

Finke, P. A.: Modeling the genesis of luvisols as a function of topographic position in loess parent material, Quat. Int., 265, 3–17, doi:10.1016/j.quaint.2011.10.016, 2012.

Finke, P. A. and Hutson, J. L.: Modelling soil genesis in calcareous loess, Geoderma, 145(3-4), 462–479, doi:10.1016/j.geoderma.2008.01.017, 2008.

Finke, P. A., Vanwalleghem, T., Opolot, E., Poesen, J. and Deckers, J.: Estimating the effect of tree uprooting on variation of soil horizon depth by confronting pedogenetic simulations to measurements in a Belgian loess area, J. Geophys. Res. Earth Surf., 118(4), 2124–2139, doi:10.1002/jgrf.20153, 2013.

Finke, P. A., Samouëlian, A., Suarez-Bonnet, M., Laroche, B. and Cornu, S. S.: Assessing the usage potential of SoilGen2 to predict clay translocation under forest and agricultural land uses, Eur. J. Soil Sci., 66(1), 194–205, doi:10.1111/ejss.12190, 2015.

Finke, P. A., Vanwalleghem, T., Opolot, E., Poesen, J. and Deckers, J.: Using a soil formation model to identify causes of observed soil variability patterns, In preparation.

Holmqvist, J.: Modelling Chemical Weathering in Different Scales. Doctoral thesis, Lund University, Sweden, 98p, 2001.

IUSS Working Group WRB.: World reference Base for soil resources 2006, 2nd edition. World Soil Resources Reports No. 103. FAO, Rome, 2006.

IUSS Working Group WRB.: World Reference Base for Soil Resources 2014, update 2015. International soil classification system for naming soils and creating legends for soil maps. World Soil Resources Reports No. 106. FAO, Rome, 2015.

Johnson, M. O., Gloor, M., Kirkby, M. J. and Lloyd, J.: Insights into biogeochemical cycling from soil evolution model and long-term chronosequences, Biogeosciences Discuss., 11(4), 5811–5868, doi:10.5194/bgd-11-5811-2014, 2014.

Minasny, B., Finke, P., Stockmann, U., Vanwalleghem, T. and McBratney, A. B.: Resolving the integral connection between pedogenesis and landscape evolution, Earth-Science Rev., 150, 102–120, doi:10.1016/j.earscirev.2015.07.004, 2015.

Morris, M.: Factorial sampling plans for preliminary computational experiments, Technometrics, 33(2), 161–174, 1991.

Opolot, E. and Finke, P. A.: Evaluating sensitivity of silicate mineral dissolution rates to physical weathering using a soil evolution model (SoilGen2.25), Biogeosciences, 12, 6791-6808, doi: 10.5194/bg-12-6791-2015, 2015.

Opolot, E., Yu, Y. Y. and Finke, P. A.: Modelling soil genesis at pedon and landscape scales: Achievements and problems, Quat. Int., 34–46, doi:10.1016/j.quaint.2014.02.017, 2015.

Sauer, D., Finke, P., Sørensen, R., Sperstad, R., Schülli-Maurer, I., Høeg, H. and Stahr, K.: Testing a soil development model against southern Norway soil chronosequences, Quat. Int., 265, 18–31, doi:10.1016/j.quaint.2011.12.018, 2012.

Temme, A. J. A. M. and Vanwalleghem, T.: LORICA – A new model for linking landscape and soil profile evolution: Development and sensitivity analysis, Comput. Geosci., doi:10.1016/j.cageo.2015.08.004, 2015.

Vanwalleghem, T., Poesen, J., McBratney,A. and Deckers, J.: Spatial variability of soil horizon depth in natural loess-derived soils, Geoderma, 157(1-2), 37–45, doi:10.1016/j.geoderma.2010.03.013, 2010.

Vanwalleghem, T., Stockmann, U., Minasny, B. and McBratney, A. B.: A quantitative model for integrating landscape evolution and soil formation, J. Geophys. Res. Earth Surf., 118(2), 331–347, doi:10.1029/2011JF002296, 2013.

Yu, Y. Y., Finke, P. A., Wu, H. B. and Guo, Z. T.: Sensitivity analysis and calibration of a soil carbon model (SoilGen2) in two contrasting loess forest soils, Geosci. Model Dev., 6(1), 29–44, doi:10.5194/gmd-6-29-2013, 2013.

Zwertvaegher, A., Finke, P., De Smedt, P., Gelorini, V., Van Meirvenne, M., Bats, M., De Reu, J., Antrop, M., Bourgeois, J., De Maeyer, P., Verniers, J. and Crombé, P.: Spatio-temporal modelling of soil characteristics for soilscape reconstruction, Geoderma, 207-208, 166–179, doi:10.1016/j.geoderma.2013.05.013, 2013.

Curriculum Vitae

Name	**Emmanuel Opolot**
Date of Birth	8th / 07 / 1985
Place of Birth	Bukedea, Uganda
Nationality	Ugandan
Email	***oplote@yahoo.com***

Emmanuel started his primary education at the age of 5 years, at Kapaang primary school and attended his secondary school education between 1999 and 2002 at Bukedea secondary school, Bukedea district. He then joined St Peter's College Tororo, for his advanced secondary education taking Physics, Chemistry and Mathematics as principal subjects. In August 2005 he obtained a government scholarship to pursue Bachelor of Science in Agricultural Land Use and Mangement at Makerere University, Kampala. He graduated on 19th / 01 / 2009 with a first class degree and was retained as teaching assistant (on part-time basis) at then the department of Soil Science, Faculty of Agriculture, Makerere University. In the same period, he worked as a research assistant under Dr. Dick Sserunkuuma, in the department of Agricultural Economics.

In September 2010, Emmanuel obtained a VLIR-UOS scholarship to pursue MSc. Physical Land Resources (Majoring in Land Resources Engineering) co-organised by Free University of Brussels and Ghent University, Belgium. Two years later, he graduated with a Great Distinction and his MSc thesis that focused on "improving the design of local in-situ soil water conservation practices in Ethiopia, using a physically based hydrological model" was ranked as the best within the program. Consequently, he received the "De Boodt-Maselis" award for being an outstanding student both academically and socially during the official graduation ceremony, held on 20th / 09 / 2012 at the University Forum (UFO), Ghent University.

Following his successful oral interview with Prof. Dr. Peter Finke, Emmanuel was selected for the PhD research position specialising in modelling soil development. His PhD was under the big research consortium "Soils under Global Change, SOGLO" and was funded by the Belgian Science Policy Office (BELSPO). He enrolled for his PhD program on the 24th / 09 / 2012 in Faculty of Sciences, Ghent University under the supervision of Prof. Dr. Peter Finke. Emmanuel's PhD research focused on improving the definition of biogeochemical processes in the soil model (SoilGen), and using this model to quantify the impact of external forcing's such as climate and land use changes on the evolution of soil properties. The results have been published in 3 high impact peer-reviewed journals and have also been presented at several national and international conferences. Overall, Emmanuel Opolot is (co) author of 5 scientific papers. Outside the academic scene, Emmanuel is married to Suzan Aede Amucu and they are blessed with two sons; Benjamin and Ethan.

Publications and International Conferences

-Scientific papers which are part of this PhD thesis

Opolot, E. and Finke, P. A.: Evaluating sensitivity of silicate mineral dissolution rates to physical weathering using a soil evolution model (SoilGen2.25), Biogeosciences, 12, 6791-6808, doi: 10.5194/bg-12-6791-2015, 2015.

Opolot, E., Yu, Y. Y. and Finke, P. A.: Modelling soil genesis at pedon and landscape scales: Achievements and problems, Quat. Int., 376, 34–46, doi:10.1016/j.quaint.2014.02.017, 2015.

Finke, P. A., Vanwalleghem, T., **Opolot, E.,** Poesen, J. and Deckers, J.: Estimating the effect of tree uprooting on variation of soil horizon depth by confronting pedogenetic simulations to measurements in a Belgian loess area, J. Geophys. Res. Earth Surf., 118(4), 2124–2139, doi:10.1002/jgrf.20153, 2013.

-Other scientific papers

Opolot, E.,Tesfay Araya, W.,Nyssen, J., Bashar, A.,Verbist, K. and Cornelis, W.: Evaluating in situ water and soil conservation practices with a fully coupled, surface/subsurface process-based hydrological model in Tigray, Ethiopia,Land Degradation & Development, 2014.

Opolot, E.: Application of remote sensing and geographical information systems in flood management: A review, Res. J. Appl. Sci. Eng. Technol. vol.: 6 issue: 10 pag.: 1884 – 1894, 2013.

-International Conferences

Opolot, E. and Finke, P. A.: SoilGen model Demo: Scenario definition and example output. In: Soil landscape modelling (hands-on modelling workshop comparing and bench-marking soil formation models), Pedometrics 2015, Cordoba, Spain, 2015

Opolot, E. and Finke, P. A.: Sensitivity of mineral dissolution rates to physical weathering: A modelling approach, Geophysical Research Abstracts, vol.: 17, EGU2015-1807, Vienna, Austria, 2015

Finke, P. A., Vanwalleghem, T., **Opolot, E**., Poesen, J. and Deckers, J.: Using a soil formation model to identify causes of observed soil variability patterns in a forested loess area in Belgium.In Soil Forming Processes and their Rates: RAISIN Workshop,Las Vegas and Los Angeles (26-31 Oct 2014), Program and Abstracts, 17 pp, 2014

Opolot, E. and Finke, P. A.: Towards an improved modeling of chemical weathering in the SoilGen soil evolution model, Geophysical Research Abstracts, vol.: 16, EGU2014-350, Vienna, Austria, 2014

Finke, P. A., **Opolot, E**., Poesen, J. and Deckers, J., Vanwalleghem, T.: The effect of bioturbation on soil formation; Simulations and measurement in a Belgian loess area, Geophysical Research Abstracts , Vol. 16, EGU2014-14053, Vienna, Austria, 2014.

Opolot, E., Finke, P. A. and Van Ranst, E.: Modelling evolution of weathering indices with SoilGen: preliminary results and perspectives, RAISIN workshop, Abstracts, pag.: 22 – 22, Calabria, Italy

Opolot, E., Tesfay Araya, W., Nyssen, J., Bashar, A., Verbist, K. and Cornelis, W.: Evaluating in situ water and soil conservation practices with a fully-coupled surface-subsurface hydrological model in Tigray, Ethiopia" DesertLand, Abstracts pag.: 56 – 56, 2013.

Appendix 1: List of Tables

Appendix 2: List of Figures

Appendix 3: Data of Oxide and mineral weight composition used in Chapter 6

Appendix 3.1: Oxide weight composition of Basalt, Peridotite and Granite parent materials

Oxide	Parent material		
	Basalt[1,3]	Peridotite[1,2]	Granite[2,3]
	Weight (%)		
SiO2	49.11	44.18	72.04
TiO2	1.84	0.09	0.300
Al2O3	15.71	2.81	14.42
Fe2O3	3.78	1.16	1.22
FeO	7.12	7.34	1.68
MnO	0.20	0.14	0.05
MgO	6.72	40.95	0.71
CaO	9.45	2.49	1.82
Na2O	2.90	0.22	3.69
K2O	1.10	0.04	4.12
P2O5	0.35	-	0.12
Total	98.28	99.42	100.17

[1]Blatt, H. and Tracy R.J.: Petrology: Igneous, sedimentary and metamorphic, 2nd ed. New York, W.H. Freeman. ISBN 0-7167-2438-3, 1996.

[2]Harris, P.G., Reay, A. and White, G.I.: Chemical composition of the upper mantle, J. Geophys. Res., 72 (24), 6359–6369, doi:10.1029/JZ072i024p06359, 1967.

[3]Hartmann, J., West, A. J., Renforth, P., Köhler, P., Rocha, C. L. D. La, Wolf-gladrow, D. A., Dürr, H. H. and Scheffran, J.: Enhanced chemical weathering as a geoengineering strategy to reduce atmospheric carbon dioxide, supply nutrients, and mitigate ocean acidification,Rev. Geophys, 51, 113–149, doi:10.1002/rog.20004.1.Institute, 2013.

Appendix 3.2: Normative mineralogy output showing mineralogy weight composition of three parent materials. This output is based on the individual parent material oxide weight composition shown in appendix 3.1

Normative minerals	Parent material		
	Basalt	Peridotite	Granite
	Mineral weight %		
Quartz	0.00	0.00	29.43
Plagioclase	20.96	8.42	39.47
Orthoclase	23.52	0.24	24.35
Nepheline	7.14	0.00	0.00
Leucite	0.00	0.00	0.00
Kalsilite	0.00	0.00	0.00
Corundum	0.00	0.00	0.87
Diopside	13.52	4.56	0.00
Hypersthene	0.00	15.91	3.44
Wollastonite	0.00	0.00	0.00
Olivine	21.74	68.43	0.00
Larnite	0.00	0.00	0.00
Acmite	0.00	0.00	0.00
K2SiO3	0.00	0.00	0.00
Na2SiO3	0.00	0.00	0.00
Rutile	0.00	0.00	0.00
Ilmenite	2.36	0.17	0.57
Magnetite	7.61	1.68	1.77
Hematite	0.00	0.00	0.00
Apatite	0.00	0.00	0.28
Zircon	0.00	0.00	0.00
Perovskite	0.00	0.00	0.00
Chromite	0.00	0.00	0.00
Sphene	0.00	0.00	0.00
Pyrite	0.00	0.00	0.00
Halite	0.00	0.00	0.00
Fluorite	0.00	0.00	0.00
Anhydrite	0.00	0.00	0.00
Na2SO4	0.00	0.00	0.00
Calcite	0.00	0.00	0.00
Na2CO3	0.00	0.00	0.00
Total	96.85	99.41	100.18

Appendix 3.3: Mineral weight composition extracted from normative mineralogy output shown in Appendix 3.2 (Not rescaled) and rescaled to constitute minerals already defined in the SoilGen2.25 model version (Rescaled)

	Parent material	Silicate Mineral (% wt)				
		Albite[1]	K-feldspar[2]	Quartz	Forsterite[3]	Total
Not rescaled	Granite	39.5	24.4	29.4	-	93.3
	Basalt	21.0	23.5	-	21.7	66.2
	Peridotite	8.4	0.2	-	68.4	77.1
Rescaled	Granite	42.3	26.2	31.5	-	100.0
	Basalt	31.7	35.5	-	32.8	100.0
	Peridotite	10.9	0.3	0.0	88.8	100.0

[1] All plagioclase (in Appendix 3.2) was allocated to albite; [2] orthoclase (in Appendix 3.2) was taken as K-feldspar in the model and [3] all olivine (in Appendix 3.2) was allocated to forsterite since Iron cycling was not yet implemented in the model.